

AD-A267 490

DOCUMENTATION PAGE

Form Approved
OMB No. 0704-0188



Time is estimated to average 10 minutes per page, including the time for reviewing instructions, searching existing data sources, gathering and reviewing the collection of information, sending comments regarding this burden estimate or any other aspect of this collection of information, including this burden estimate, Washington Headquarters Services, Directorate for Information Operations and Reports, 1215 Jefferson Davis Highway, Suite 1204, Arlington, VA 22202-4302, and to the Office of Management and Budget, Paperwork Reduction Project (0704-0188), Washington, DC 20503.

2. REPORT DATE
MAY 1993

3. REPORT TYPE AND DATES COVERED
~~XX~~ THESIS/DISSERTATION

4. TITLE AND SUBTITLE
Digital Tracking and Control of Retinal Images

5. FUNDING NUMBERS

6. AUTHOR(S)
Steven Frank Barrett

7. PERFORMING ORGANIZATION NAME(S) AND ADDRESS(ES)
AFIT Student Attending: The Univ of Texas at Austin

8. PERFORMING ORGANIZATION
REPORT NUMBER
AFIT/CI/CIA- 93-010D

9. SPONSORING MONITORING AGENCY NAME(S) AND ADDRESS(ES)
DEPARTMENT OF THE AIR FORCE
AFIT/CI
2950 P STREET
WRIGHT-PATTERSON AFB OH 45433-7765

10. SPONSORING MONITORING
AGENCY REPORT NUMBER

DTIC
SELECTE
AUG 6 1993
S c D

11. SUPPLEMENTARY NOTES

12a. DISTRIBUTION AVAILABILITY STATEMENT
Approved for Public Release IAW 190-1
Distribution Unlimited
MICHAEL M. BRICKER, SMSgt, USAF
Chief Administration

12b. DISTRIBUTION CODE

13. ABSTRACT (Maximum 200 words)

93-18102



14. SUBJECT TERMS

15. NUMBER OF PAGES
277

16. PRICE CODE

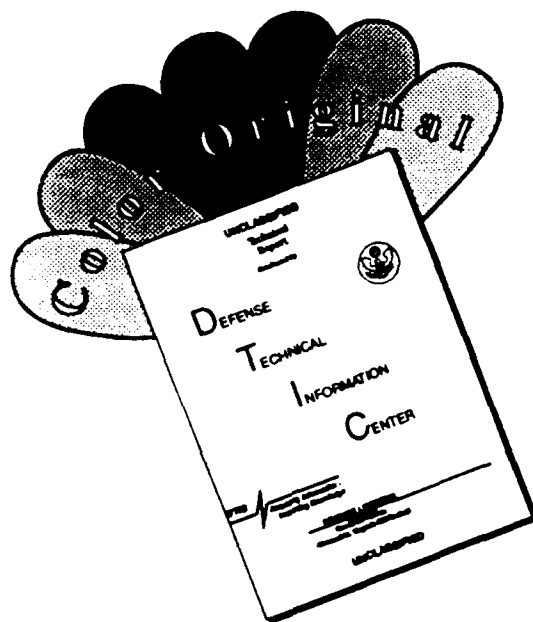
17. SECURITY CLASSIFICATION
OF REPORT

18. SECURITY CLASSIFICATION
OF THIS PAGE

19. SECURITY CLASSIFICATION
OF ABSTRACT

20. LIMITATION OF ABSTRACT

DISCLAIMER NOTICE



THIS DOCUMENT IS BEST QUALITY AVAILABLE. THE COPY FURNISHED TO DTIC CONTAINED A SIGNIFICANT NUMBER OF COLOR PAGES WHICH DO NOT REPRODUCE LEGIBLY ON BLACK AND WHITE MICROFICHE.

02-1075

DIGITAL TRACKING AND CONTROL OF RETINAL IMAGES

Accession For	
NTIS CRA&I	<input checked="" type="checkbox"/>
DTIC TAB	<input type="checkbox"/>
Unannounced	<input type="checkbox"/>
Justification:	
By _____	
Distribution/ _____	
Availability Codes	
Dist	Avail and/or Special
A-1	

APPROVED BY
DISSERTATION COMMITTEE:

Supervisor: *A. J. Welch* DTIC QUALITY INSPECTED 3

Rebecca Richards K DTIC QUALITY INSPECTED 3

William P. Guder

[Signature]

John A. Pearce

JAC [Signature]

To Cindy, thanks for being you.

**DIGITAL TRACKING AND CONTROL
OF RETINAL IMAGES**

by

STEVEN FRANK BARRETT, B.S., M.E.

DISSERTATION

Presented to the Faculty of the Graduate School of
The University of Texas at Austin
in Partial Fulfillment
of the Requirements
for the Degree of

DOCTOR OF PHILOSOPHY

THE UNIVERSITY OF TEXAS AT AUSTIN

May 1993

Acknowledgements

I only wish I could put into words the truly heart felt thanks to all of the friends and family who made this adventure possible.

I would like to begin by thanking my committee members: Dr. A.J. Welch, Dr. Alan Bovik, Dr. Wilson Geisler, Dr. John Pearce, Dr. Rebecca Richards-Kortum, and Dr. Grady Rylander. I appreciate the well prepared lessons, the stimulating ideas, and your willing assistance on many occasions. A special thanks to Dr. Welch for your always open door and unassuming leadership. You are a great role model.

I would also like to thank Brigadier General Erlind Royer, Colonel Alan Klayton, and Lieutenant Colonel Harry Bare for making this all possible. I have dedicated myself to apply what I've learned to being a better teacher and officer in service to the cadets at the United States Air Force Academy. I would also like to thank Major Mike Markow who told me about UT and this exciting project. Your work has formed the basis for this research and many others.

At UT I have made many friends. I would like to thank Chris Humphrey for her expert photography advice and Arthur Birdwell for his technical advice. A special thank you to Dr. Maya Jerath. I really appreciate your insight and friendship. I would also like to thank Dr. Jerry Fenig, DVM, and staff at the Animal Resource Center for the expert animal care and assistance. You were instrumental in successful *in vivo* testing.

To my family ... you've been wonderful! Thanks mom and dad for teaching me anything is possible if you work hard and believe in yourself. Thank you Jackie and Ray for making me a part of your family. You showed me hard work is important but so is having fun. I wish you were here Ray to share this with me. Thank you Heather, Jonathan, and Graham for your understanding and patience. The little time we were able to spend together made the long work hours worthwhile. I love you three with all my heart. Cindy, thank you for the best 17 years of my life. You worked harder than I did these past three years keeping everybody happy. I love you.

This research was sponsored in part by the Texas Coordinating Board and in part by the Office of Naval Research under grant N00014-91-J-1564.

DIGITAL TRACKING AND CONTROL OF RETINAL IMAGES

Publication No. _____

Steven Frank Barrett, Ph.D.
The University of Texas at Austin, 1993

Supervisor: Ashley J. Welch

Laser induced retinal lesions are used to treat a variety of eye diseases such as diabetic retinopathy and retinal detachment. Both the location and size of the retinal lesions are critical for effective treatment and minimal complications. Currently, once an irradiation is begun, no attempt is made to alter the laser beam location on the retina. However, adjustments are desirable to correct for patient eye movements. Lesions form in much less than one second and typical treatment for a disease such as diabetic retinopathy requires as many as 2000 lesions per eye. This type of tedious task is ideally suited for computer implementation.

A system has been developed to track a specific lesion coordinate on the retinal surface and provide corrective signals to maintain laser position on the coordinate. Six distinct retinal landmarks are tracked on a high contrast retinal image using two-dimensional blood vessel templates. Use of therapeutic lesions as tracking algorithm landmarks is also investigated. An X and Y laser correction signal is derived from the landmark tracking information and

provided to a pair of galvanometer steered mirrors to maintain the laser on a prescribed location. Once the laser position has been corrected, a function checks the terminal laser position for minor corrections.

A development speed tracking algorithm has been implemented and tested using both vessel and lesion templates. Closed loop feedback control of laser position is demonstrated with calibrated retinal velocities and *in vivo* testing of the development system.

Trade off analysis of parameters affecting tracking system performance is provided. The analysis is used to specify requirements and implementation details for a real time system.

Table of Contents

Acknowledgements	iv
Abstract	vi
List of Figures	xiv
Chapter 1. Introduction	1
1.1 Overview	1
1.2 Treatment Protocol	3
1.3 System Description	6
1.3.1 Reflectance Based Feedback Control System	6
1.3.2 Retinal Observation and Tracking System	7
1.4 Other Applications	8
1.5 Preview	8
Chapter 2. The Eye	10
2.1 Eye Anatomy	10
2.1.1 Gross Anatomical Structure	10
2.1.2 Visible Retinal Features	11
2.1.3 Eye Movements	14
2.1.4 Retinal Tracking System requirements	16
2.1.5 Eye Fixation Capability	16
2.2 Diabetic Retinopathy and Other Retinal Diseases	18
2.2.1 Diabetic Retinopathy	18
2.2.2 Macular Degeneration	20
2.2.3 Retinal Breaks and Tears	21
2.3 The Aging Eye	21

Chapter 3. The Retinal Observation Subsystem	23
3.1 Objective	23
3.2 Previous Work on Retinal Imaging	23
3.2.1 Television Ophthalmoscopy	23
3.2.2 Fundus Chromatic Studies	24
3.3 Retinal Imaging	27
3.3.1 Fluorescein Angiogram Retinal Imaging	27
3.3.2 Scanning Laser Ophthalmoscope (SLO) Imaging	30
3.3.3 Silicon Intensified Tube (SIT) Cameras	33
3.3.4 Charge Coupled Device (CCD) Cameras	34
3.3.5 Retinal Image Enhancement	35
3.3.6 Imaging Technique Comparison	39
3.4 Storage Media	41
3.4.1 Video Tape	42
3.4.2 Diskette	42
3.4.3 Optical Disk Storage	42
3.4.4 Digital Audio Tape	43
3.4.5 Storage Medium of Choice	43
3.5 Retinal Observation Software	43
3.5.1 Previous Work	44
3.5.2 RETINA Software	44
Chapter 4. The Retinal Tracking Subsystem	46
4.1 Objective	46
4.1.1 Theoretical Basis	46
4.1.2 The Ideal Tracking Algorithm	49
4.1.3 Overview	50
4.2 Lesion Data Base	51
4.2.1 Panretinal Photocoagulation Treatment	62
4.2.2 Treatment for Retinal Breaks or Tears	62
4.3 Template Building	65
4.3.1 Template Theory	65
4.4 The Tracking Algorithm	72

4.4.1	Previous Work	73
4.5	The Algorithm	84
4.5.1	Assumptions and Validity of Assumptions	85
4.5.2	Geographic Distributed Normalized Templates	91
4.5.3	The tracking algorithm	96
 Chapter 5. The Laser Pointing Subsystem		107
5.1	Objective	107
5.2	Ideal Laser Pointing Subsystem Characteristics	107
5.3	Previous Work	108
5.4	Galvanometers	109
5.4.1	Theory of Operation	110
5.4.2	Characteristics	111
5.4.3	Scan Heads	113
5.5	X-Y Scanning Systems	114
5.5.1	Drive Signals	115
5.5.2	Sources of Error	116
5.6	<i>Retinal Tracking Subsystem Requirements</i>	117
5.6.1	Response Time	118
5.6.2	Position Resolution	118
5.6.3	Maximum Displacement	118
5.6.4	Closed Loop Control	119
5.6.5	Scan Type Employed	119
5.7	System Design	119
5.8	Development System Implementation	119
5.8.1	System Alignment	121
5.9	Laser Pointing Subsystem Testing	122
 Chapter 6. Tracking on a Featureless Retina		123
6.1	Alternate tracking mechanism requirement	123
6.2	Overview	123
6.3	The Lesion Template	124
6.4	Two-dimensional lesion templates	126

6.5	Testing on ideal lesions	127
6.6	Testing lesion templates on a rabbit retina	128
6.7	Template tracking methods	132
6.7.1	The Unique Template tracking method	132
6.7.2	The Adaptive Template tracking method	135
6.8	Lesion Tracking and Image Analyzer software	143
Chapter 7. Development System Instrumentation		148
7.1	Overview	148
7.2	The Fundus Camera	150
7.2.1	Fundus Camera Filters	152
7.3	The CCD Video Camera	153
7.4	The Video Frame Grabber	153
7.4.1	Theory of Operation	153
7.5	Laser Pointing Hardware	155
7.5.1	Driver Amplifiers	155
7.5.2	Optical Scanners	156
7.6	The Laser Shutter	156
7.7	The Computer	157
7.7.1	Specifications	157
7.7.2	Specifications	157
7.8	Data Acquisition and Control Hardware	158
7.9	The RETINA HW/SW Interface	159
7.9.1	The Fixation Device	162
Chapter 8. Development System Testing		165
8.1	Retinal Tracking Subsystem testing using blood vessel templates . .	165
8.1.1	Test system configuration	165
8.1.2	Test description	166
8.1.3	Test results	171
8.1.4	Analysis of test results	171
8.2	Laser Pointing Subsystem testing	183
8.2.1	Testing the Laser Pointing Subsystem with simulated retinal movement	183

8.2.2	Testing the Laser Pointing Subsystem with lesion templates .	186
8.2.3	Analysis of results	192
Chapter 9. In vivo Development System Testing		195
9.1	Overview	195
9.2	Optical configuration for <i>in vivo</i> testing	195
9.3	Safety considerations for <i>in vivo</i> testing	196
9.4	<i>In vivo</i> experimental method	199
9.5	<i>In vivo</i> experimental results	206
9.6	<i>In vivo</i> panretinal photocoagulation and retinal tear demonstration	207
9.6.1	Objectives	207
9.6.2	Equipment Configuration	208
9.6.3	Preliminary Testing	211
9.6.4	<i>In vivo</i> demonstrations	215
Chapter 10. The Real Time System		232
10.1	Overview	232
10.2	Sensitivity Analysis	232
10.2.1	Factors influencing Retinal Tracking Subsystem performance	233
10.2.2	System specification trade-offs	235
10.2.3	Interpretation and analysis of results	236
10.3	Real Time Equipment Specification	241
10.3.1	Real time system parameters	241
10.3.2	The camera	243
10.3.3	The frame grabber	244
10.3.4	The Computer	245
10.3.5	Galvanometers and driver amplifiers	245
10.3.6	Data acquisition system	246
10.3.7	Laser Shutter	246
10.3.8	System Description	246
10.3.9	Real time system cost	246
10.3.10	Technical concerns	248

Chapter 11. Conclusions	249
11.1 Conclusions	249
11.2 Future Improvements and Further Research	250
11.2.1 <i>In vivo</i> testing on <i>Macaca mulatta</i> monkeys	250
11.2.2 Solid-state laser diode therapeutic laser	252
11.2.3 System integration study	255
11.2.4 Neural nets to learn match conditions	259
11.3 Summary of significant findings	260
11.3.1 Application of tracking algorithm to other laser stabilization systems	261
11.4 Acknowledgements	262
 Bibliography	 263
 Vita	 278

List of Figures

1.1	The retinal mosaic	4
1.2	The conceptual Robotic Laser System.	5
1.3	The Robotic Laser System.	6
2.1	Horizontal section of the eye	11
2.2	Retinal components	12
2.3	The visible retinal surface	13
2.4	Factors influencing the Retinal Tracking Subsystem	17
3.1	Hemoglobin absorption characteristics	25
3.2	Retinal imaging with optical filters	26
3.3	Fluorescein enhanced retinal image	29
3.4	Scanning Laser Ophthalmoscope	30
3.5	SLO image at a 50 degree field of view	31
3.6	Filter characteristics	36
3.7	RETINA Software.	37
3.8	Histogram modification mod_his1	39
3.9	Real time histogram modification with function mod_his1	40
4.1	Translation, rotation, and scale	48
4.2	The RETINA Tracking Algorithm.	50
4.3	The field of view numbering system.	52
4.4	The patient file.	53
4.5	Modified Markow vessel enhancement templates	54
4.6	Lesion Data Base building	56
4.7	Enhance horizontal vessels, median filter, enhance vertical vessels	57
4.8	Median filter, reduce bar noise, median filter	58
4.9	Combine enhancements, remove edge effects, binary image . . .	59
4.10	Examine neighborhood, protect anatomy, plot coordinates . . .	60

4.11	The final result	61
4.12	Retinal break or tear data base building.	63
4.13	Retinal break or tear treatment	66
4.14	Retinal break or tear treatment	67
4.15	Retinal break or tear treatment	68
4.16	The image I and the template T	69
4.17	One dimensional template orientation	77
4.18	The 1D template	78
4.19	Using expansion in the search pattern	79
4.20	Response of the Markow template in the vicinity of a blood vessel	82
4.21	Scattergram of retinal movement	88
4.22	Time record of the 40 x 40 pixel search area	89
4.23	Average fundus reflectance versus illumination	90
4.24	The tracking template	92
4.25	Normalized template response	93
4.26	Theoretical template response	94
4.27	The template array.	95
4.28	The limited exhaustive search	97
4.29	The tracking algorithm.	99
4.30	Patient data availability matrix	100
4.31	Laser position check	105
5.1	The Fundus Field of View Cartesian Coordinate System	108
5.2	The galvanometer	110
5.3	Scan head geometries	113
5.4	X-Y scanning system	114
5.5	The developmental Laser Positioning Subsystem	120
6.1	The lesion template.	125
6.2	The lesion template search	126
6.3	The two-dimensional lesion template	127
6.4	The template array	128
6.5	Lesion template building with ideal lesions	129
6.6	Results of lesion tracking experiments	131

6.7	The lesion triad template	133
6.8	Interlocking triad lesion templates	134
6.9	Results of adding interlocking lesion triad templates to the function build_lesion_data_base	135
6.10	Therapeutic lesion formation using Adaptive Templates	137
6.11	Complete pattern of 61 therapeutic lesions	138
6.12	Random lesion type assignment	141
6.13	Results of distinct lesion type selection	141
6.14	The pixel coordinate shift	142
6.15	Adaptive Template results	143
6.16	Lesion Tracking and Image Analyzer (LETINA) software	145
6.17	Program RANDOM	146
6.18	The limited exhaustive search using lesion templates	147
7.1	Developmental system instrumentation	149
7.2	Noncontact fundus camera optics	151
7.3	The Matrox PIP-1024 video frame grabber	154
7.4	Data Translation DT2801A	158
7.5	The RETINA HW/SW Interface	160
7.6	The fixation device	164
8.1	Tracking algorithm test configuration	167
8.2	Results of testing subject RCL	172
8.3	Results of testing subject CSL	173
8.4	Results of testing subject SBR	174
8.5	Results of testing subject ICR	175
8.6	Summary of results for tracking tests	176
8.7	Reflectance of a 0.5 standard	179
8.8	Position update timing distribution	181
8.9	Laser Pointing Subsystem test configuration	184
8.10	Subject RCL without laser position check at 12.8 dgs	185
8.11	Subject RCL without laser position check at 16.0 dgs	186
8.12	Subject RCL with laser position check at 12.8 dgs	187
8.13	Subject RCL with laser position check at 16.0 dgs	187

8.14 Subject CSL with laser position check at 12.8 dgs	188
8.15 Subject CSL with laser position check at 16.0 dgs	188
8.16 Subject SBR with laser position check at 12.8 dgs	189
8.17 Subject SBR with laser position check at 14.0 dgs	189
8.18 Subject DL	190
8.19 Human retina testing at 6.7 dgs	191
8.20 Laser Position Subsystem lag versus retinal velocity	193
9.1 <i>In vivo</i> optics	197
9.2 <i>In vivo</i> experimental configuration	200
9.3 Equipment configuration for <i>in vivo</i> tracking	201
9.4 Rabbit preparation for <i>in vivo</i> experiments	202
9.5 Rectangular laser pattern on the retina	203
9.6 <i>In vivo</i> alignment of the Laser Pointing Subsystem	204
9.7 Preparation for the <i>in vivo</i> experiment	205
9.8 Plot of laser position during <i>in vivo</i> tracking	206
9.9 Video results of <i>in vivo</i> tracking	207
9.10 Laser Positioning Subsystem modifications for argon laser delivery	209
9.11 Modifications for the Innova 100 Argon Ion Laser	211
9.12 Panretinal photocoagulation simulation	212
9.13 Results of photocoagulation on paper retina targets	214
9.14 Transmission characteristics of an OG-550 filter	216
9.15 <i>In vivo</i> experimental configuration	217
9.16 <i>In vivo</i> tests results for diabetic retinopathy treatment	219
9.17 <i>In vivo</i> tests results for retinal tear repair treatment	221
9.18 Retinal hemorrhage	223
9.19 First matrix experiment results	225
9.20 Second matrix experiment results	226
9.21 Third matrix experiment results	228
9.22 Summary of <i>in vivo</i> experiments	229
9.23 <i>In vivo</i> lesion template tracking	231
10.1 Target radius of the laser	234

10.2 Relationship between parameters influencing tracking algorithm performance	237
10.3 Trade-off analysis results	238
10.4 Results using an Intel 33 MHz 80486DX processor	239
10.5 Resolution of adjacent lesions	242
10.6 The real time system configuration	247
11.1 Equipment configuration for <i>in vivo Macaca mulatta</i> experiments	251

Chapter 1

Introduction

1.1 Overview

Dr. A.J. Welch, Dr. H. Grady Rylander III M.D., and associated researchers have worked toward the development and system specification for a Robotic Laser System. The overall goal of this ongoing project is development of an automated surgical laser system for placing laser lesions on the human retina for the treatment of retinal diseases.

Laser induced lesions are used to treat a variety of retinal diseases including diabetic retinopathy, macular degeneration, and retinal breaks and tears. During treatment for these diseases an argon laser beam is directed into the eye via the cornea. Due to the optical characteristics of the cornea, the aqueous humor, lens, and the vitreous humor; the argon laser light passes through these media to the retina. The argon laser light is absorbed and converted to heat in the pigment epithelium. Heat conducted from the pigment epithelium coagulates the retinal tissue. The thermally damaged retinal tissue results in therapeutic lesions useful for the treatment of retinal disease. The size of the retinal lesion is critical for the treatment of the diseases and minimization of complications.

Laser treatment is currently performed in a ballistic manner. The oph-

thalmologist aims the laser at the prescribed retinal lesion site and then fires the laser. The laser has a preset power, spot size, and exposure time. Once the laser is fired, no attempt is made to compensate for variability in retinal tissue absorbance or for retinal movement. Placing lesions in this manner in the correct location and of the correct size is an acquired art [1]. Furthermore, treatment protocol for diabetic retinopathy requires up to 2,000 laser lesions per retina. This tedious, yet critical task is ideally suited for computer implementation.

Markow [2] studied the feasibility of a Robotic Laser System. His intent was to "develop an automated laser delivery system and retinal observation system that is capable of placing multiple lesions of predetermined sizes into known locations in the retina". Markow demonstrated the concept of such a system. However, considerable research was required to advance the concept to a realizable system.

The intent of my research is the development of a software algorithm to track and correct for human retinal movement during robotic controlled laser treatment of various retinal diseases. From this general statement an entire research effort has grown to encompass retinal tracking, Lesion Data Base building for the treatment of diabetic retinopathy and retinal breaks and tears, a laser pointing subsystem, work on adaptive template mechanisms to track movements when visible retinal features are not available to serve as landmarks, trade off analysis of factors affecting tracking algorithm performance, and specification of a real time system.

This chapter begins with a description of the treatment protocol envisioned for using a Robotic Laser System. This is followed by a general de-

scription of the two main systems that work concurrently to produce controlled lesions: a Reflectance Based Feedback Control System and a Retinal Observation and Tracking System. A brief review is provided on the work of my colleague Dr. Maya Jerath on the former system. The remainder of this document details my research on the latter system. The chapter concludes with an overview of this research effort.

1.2 Treatment Protocol

The following paragraphs describe the treatment protocol envisioned for using a Robotic Laser System. This protocol combines treatment methods currently used in retinal photocoagulative therapy with Robotic Laser System capabilities.

To treat a patient with the Robotic Laser System requires a series of appointments. During the first appointment the patient has their retina mapped using the Retinal Observation Subsystem. This system uses a standard fundus camera connected to a video charge coupled device (CCD) camera and a video frame grabber to map the visible surface of the retina. The video frame grabber provides still 'snapshots' of retinal movements. Mapping of the retina is subdivided into separate fundus camera fields of view or the individual fields of view may be mosaiced into a single retinal map as illustrated in Figure 1.1. After the retinal map is complete the patient will be allowed to return home.

From the retinal map the ophthalmologist diagnoses the retinal disease and prescribes required treatment. A Lesion Data Base for the treatment is then built along with any required tracking templates. The lesion data and the templates are then stored in the patient's data file until the follow-up



Figure 1.1: The retinal map formed by a mosaic of individual fundus camera field of view images. Seven separate images were used to form this image.

appointments.

During the follow-up visit(s), the patient receives laser treatment. The patient is placed in a supine position with his head stabilized to prevent movement. Reference Figure 1.2. The ophthalmologist may space out the treatment sessions to evaluate the effectiveness of the treatment.

After the patient is comfortable, the fundus camera is aligned and focused on the patient's retina. Use of a visual fixation device on the conjugate eye assists in the initial field of view alignment and also minimizes retinal movement during the treatment session.

After initial alignment is complete, the tracking algorithm establishes lock using a set of blood vessel templates. Therapeutic lesions are then placed on the retina in the precise location and size as previously prescribed by the

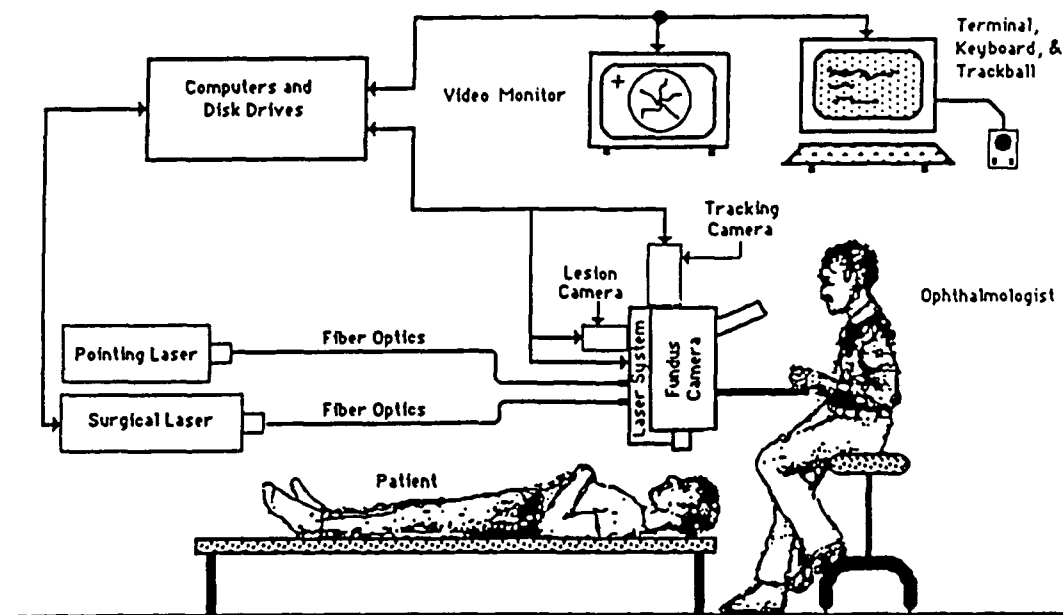


Figure 1.2: The conceptual Robotic Laser System [2].

ophthalmologist. A single lesion may take up to 200 ms to form [4]. Therefore, treatment for a single field of view is accomplished in approximately 45 seconds. When a lesion reaches its prescribed size, the system issues the necessary commands to close the laser shutter and move the laser position to the next prescribed lesion site [adapted from [2, 3]].

During the treatment session the eye may move, the patient may blink, the tracker may lose lock, the patient may panic, or some critical portion of the system might fail. The system must have the capability to respond to these different contingencies.

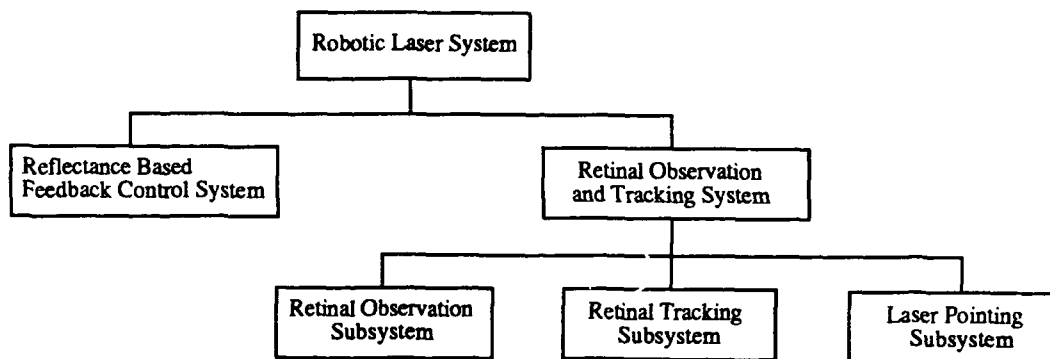


Figure 1.3: The Robotic Laser System.

1.3 System Description

The Robotic Laser System has two main systems: the Reflectance Based Feedback Control System and the Retinal Observation and Tracking System. A system organizational chart is provided in Figure 1.3.

1.3.1 Reflectance Based Feedback Control System

The Reflectance Based Feedback Control System is a real time system to monitor lesion growth. It uses a two-dimensional reflectance image acquired via a CCD camera which views lesion formation on axis with the argon coagulating laser. Reflectance images are acquired and processed as the lesion forms. When parameters of the reflectance images meet certain preset thresholds, the laser shutter is closed. A signal is then issued to the Retinal Observation and Tracking System to load the next lesion coordinate and redirect the laser to the new lesion site. Jerath has demonstrated real time lesion parameter control in an egg white model medium and *in vivo* using cross bred pigmented rabbits [4, 5, 6, 7, 8].

1.3.2 Retinal Observation and Tracking System

The Retinal Observation and Tracking (OT) System tracks a specific lesion coordinate on the retinal surface. The system also provides corrective signals to maintain the laser position on the retina and assists the ophthalmologist in building a Lesion Data Base.

The OT system has been subdivided by function into the following subsystems: Retinal Observation Subsystem (ROS), Retinal Tracking Subsystem (RTS), and Laser Pointing Subsystem (LPS).

Retinal Observation Subsystem

ROS provides a digitized map of the retina for use in diagnosis and tracking. Software to automatically build a Lesion Data Base for treatment of diabetic retinopathy and retinal breaks and tears resides in this subsystem. Also, special functions to enhance the retinal image, calculate statistics, and build a mosaic image are all encompassed within this subsystem.

Retinal Tracking Subsystem

RTS tracks retinal movement during photocoagulation and provides corrective signals to the Laser Pointing Subsystem to maintain the laser on a prescribed coordinate. The tracking subsystem responds to inputs from the patient and the Reflectance Based Feedback Control System.

Laser Pointing Subsystem

LPS accurately points the laser at the coordinate provided by the Retinal Tracking System. The pointing system must have the capability to direct the laser to any specified coordinate within the fundus camera retinal field of view.

1.4 Other Applications

The Retinal Observation and Tracking System has been specifically designed for the treatment of various retinal diseases. However, with slight modifications this system may be used to stabilize a laser during corneal thermal keratoplasty, laser vessel welding, and other applications requiring stabilized laser delivery. The system may also be used to document the movement of the retina for physiological and psychological studies. This capability will be demonstrated later in this document.

1.5 Preview

This document begins with a brief review of the anatomy and physiology of the eye and retina pertinent to this research effort. Information is also provided on eye movements, disease, and aging. Each of the different subsystem's design and theory of operation is then provided followed by a discussion of the instrumentation used to implement the subsystems. A chapter is also devoted to the special case of tracking on a featureless retina. System testing methodology and results then follow. A detailed trade off analysis of parameters affecting tracking system performance is then provided. This analysis is used to discuss the equipment and costs required to convert the development system into a real time clinical system. This document concludes with a review of major

accomplishments and suggested areas of further research.

Chapter 2

The Eye

2.1 Eye Anatomy

In this chapter a brief review is provided on eye anatomy, principal retinal features, eye movements, and fixation capability. This review is followed by a discussion of various retinal diseases and injuries potentially treatable by the Robotic Laser System and aging mechanisms with the eye.

2.1.1 Gross Anatomical Structure

The eyes are the complex sense organs of the visual system. The principal anatomical structures are provided in Figure 2.1 [9].

The eye is approximately spherical (24 mm long by 22 mm across) [10]. It is encased in a tough, protective outer layer called the sclera. The anterior portion of the sclera is clear and allows light to enter the interior portion of the eye. The clear scleral section is called the cornea. Light initially enters the eye via the cornea and then passes in turn through the anterior chamber, the lens, and the vitreous chamber. Light then strikes the retina.

The retina consists of ten layers. Within these layers are the visual receptors: the rods and the cones. There are also four types of neurons in the

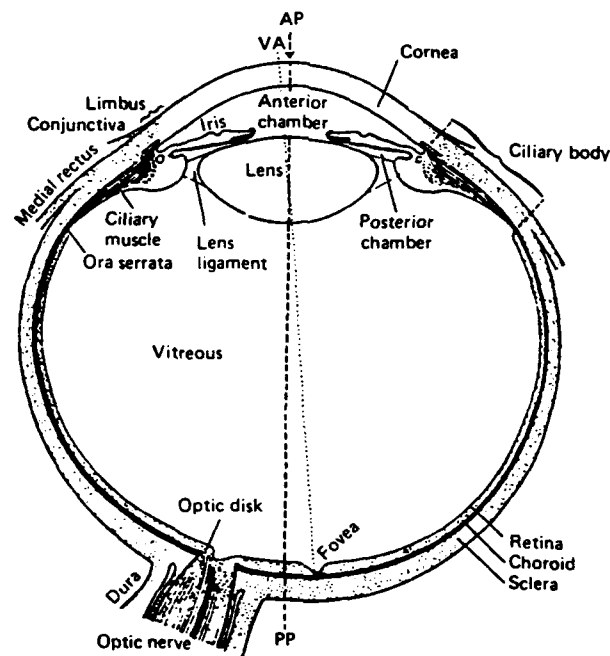


Figure 2.1: Horizontal section of the right eye [9]

retinal layers: bipolar cells, ganglion cells, horizontal cells, and the amacrine cells. The different layers of the retina are illustrated in Figure 2.2 [9].

The rods and cones coupled with the neurons provide a matrix of receptors with converging links to the optic nerve. The rods and cones synapse with the bipolar cells, the bipolar cells synapse with the ganglion cells, and the ganglion cells converge to form the optic nerve. The optic nerve routes the visual information from the eye to the occipital cortex of the brain [9].

2.1.2 Visible Retinal Features

The retinal features visible by a fundus camera form distinct landmarks important to the tracking task. The most visible feature on the retinal surface is

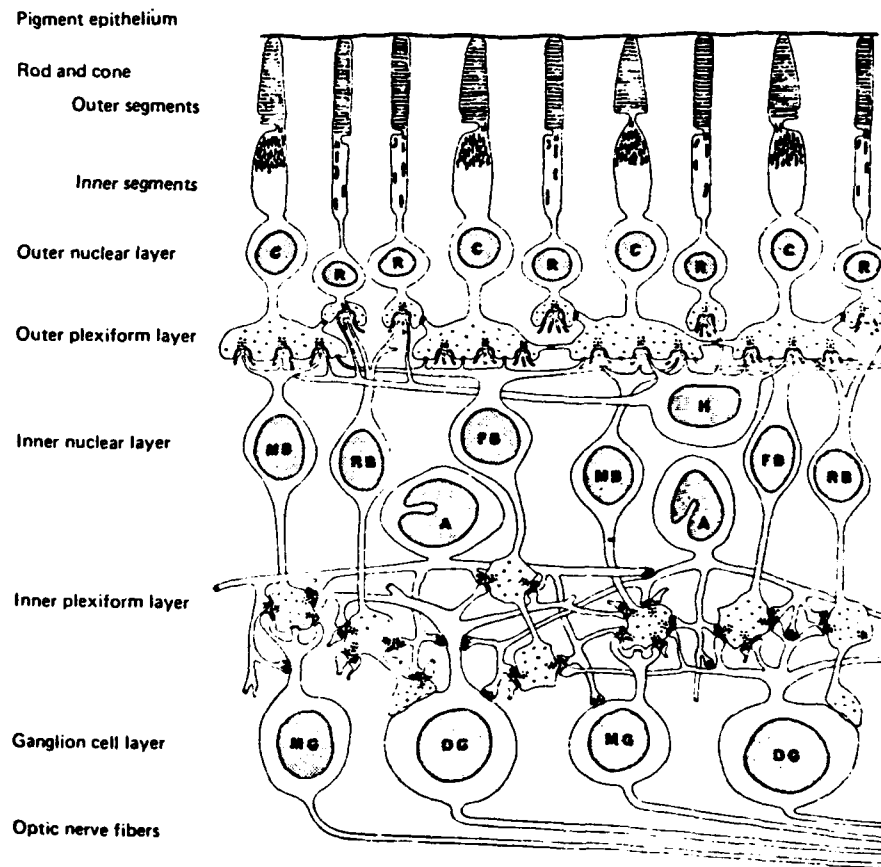


Figure 2.2: Components of the retina. C: cones, R: rods, H: horizontal cells, and A: amacrine cells [9]

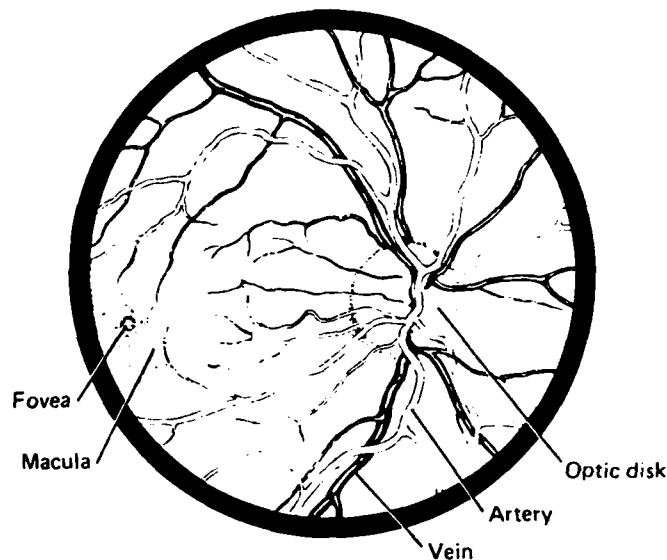


Figure 2.3: The visible retinal surface [9]

the optic disk as illustrated in Figure 2.3 [9].

The optic disk is the point at which blood vessels enter the eye and spread over the surface of the retina. It is also the point where nerves from the retina meet and exit the eye as the optic nerve as discussed above. The exact dimensions of the optic disk vary slightly by race, eye, and sex. The mean horizontal axis of the left optic disk is 1.88 mm (standard deviation 0.18) with a mean vertical axis of 1.77 mm (standard deviation 0.19) [11]. The right optic disk has similar dimensions. Similar values are reported by Mansour [12]. Optic disk measurements are used as a calibration tool to measure the dimensions of other retinal features in the software developed for this project.

Near the optic disk is the fovea which is the area of acute vision due to its high concentration of cone photoreceptors. The fovea is approximately 300 microns in diameter and it must be protected from damage. A single laser

pulse to the fovea can result in permanent degradation of acute vision [1]. The center of the fovea, the foveola, is located 3.42 mm (\pm .34 mm) temporally and inferiorly to the horizontal axis of the optic disk [13]. This dimension is used in the Lesion Data Base building algorithm. The macula with a 5000 micron diameter surrounds the fovea.

The retinal vessel network surrounding the optic disk and fovea is called the arcades. It is also visible from the retinal surface. Retinal vessels range in size from 50 microns to 250 microns [14].

2.1.3 Eye Movements

Eye movement is controlled by the external ocular muscles. These muscles include the lateral rectus muscles for looking to the side, the medial rectus muscles for looking toward the nose, the superior rectus muscle for looking up, the inferior rectus muscle for looking down and the superior and inferior oblique muscle for depressing and elevating the gaze respectively [9]. These muscles act in a coordinated fashion to affect the different types of eye movement. Certain eye movements suffer age related degradation. Generally, eye movements slow with advancing age. The following paragraphs detail the different types of eye movements important to this study.

Saccades

Saccadic eye movements are rapid with velocities of up to 800 degrees per second for visual target acquisition. These movements rapidly propel the point of visual fixation from one target to another in the visual field. They are typically of short duration, lasting from 20 to 200 milliseconds, and are ballistic

in nature. Most naturally occurring saccades are less than 15 degrees. For larger saccadic eye movements the head may be moved [15].

Smooth Pursuit and Vergence Movements

Smooth pursuit and vergence movements are for tracking movements to follow a slowly moving object. These movements maintain the image of the moving object on the fovea of each eye. The vergence system maintains the image on the fovea as an object moves toward or away from the observer and the smooth pursuit system tracks objects with horizontal or vertical movement. Both of these systems are slow compared to the saccadic system. The smooth pursuit system can accurately track up to approximately 50 degrees per second [15].

Optokinetic and Vestibular-Ocular Movements

The optokinetic and the vestibular-ocular systems are used to compensate for observer motion. These systems maintain stable vision as a person moves. These systems work together to provide accurate compensation for head movement over a wide range [15].

Micro-saccades and Micronystagmus Movements

Micro-saccadic movements are required to maintain visibility of stationary objects due to image fading. These small movements occur approximately every second and shift the gaze by 5 to 10 minutes of arc. These movements are difficult to suppress. Micronystagmus are oscillatory movements at rates of approximately 0.02 Hertz and amplitudes up to approximately 1 minute of arc. From an engineering point of view these movements may be regarded as system

noise [16].

2.1.4 Retinal Tracking System requirements with reference to retinal movement

There are many factors which affect the Retinal Tracking Subsystem's capability to maintain 'lock' during retinal movement. These factors are discussed in Chapter 8. The two most important factors are retinal velocity and desired Laser Pointing Subsystem target radius. Target radius is defined as the radius of a circle which contains laser spot centroid movement. Figure 2.4 illustrates the number of position updates required per second for a given retinal velocity to achieve a desired target radius.

2.1.5 Eye Fixation Capability

Different fixation methods may be used to minimize eye movements. These include: bite bars, stabilizing cushions, chin or head stabilizers, or a visual fixation device. These methods may be used separately or in combination. For this study a visual fixation array of light emitting diodes has been used in combination with a chin and forehead stabilizer to minimize patient eye movements. A detailed description of the visual fixation device design is provided later in this document.

Human visual fixation is provided by a negative feedback mechanism. This mechanism prevents the point of visual fixation from leaving the area of the fovea on the retinal surface. When a spot of light is focused on the fovea microneystagmus movements cause the spot to move back and forth across the

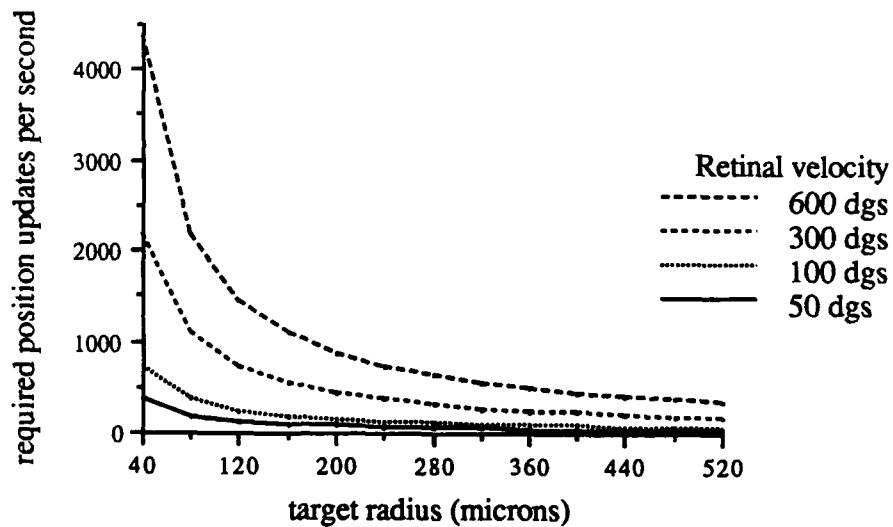


Figure 2.4: Factors influencing the Retinal Tracking Subsystem's 'lock' capability. The number of position updates required per second are provided as a function of retinal velocity in degrees per second and desired Laser Pointing Subsystem target radius.

cones. Each time the spot reaches the edge of the fovea a micro-saccade occurs bringing the spot back to the central foveal region [17]. Many movements of these types have been observed during the course of this study. Studies conducted by Kosnik, Fikre, and Sekuler with untrained psychophysical observers indicate that fixation stability does not degrade significantly with age. They define fixation stability using a contour ellipse of the scatter of eye positions about its mean position. The area of the ellipses is expressed in minutes of squared. The young group (mean age = 22 years) have a mean ellipse area of 165 min of arc (S.D. 90.2) while the older group (mean age = 70 years) have a mean ellipse area of 198 min of arc (S.D. 90.4) [18].

2.2 Diabetic Retinopathy and Other Retinal Diseases

The Robotic Laser System will have the capability to treat various eye diseases and injuries. Some of the more common maladies treatable by the Robotic Laser System are described in this section.

2.2.1 Diabetic Retinopathy

Diabetic retinopathy is a disease of the retina that begins in a non-inflammatory role and progresses through increasingly severe stages. The non-inflammatory stage is characterized by small aneurysms and hemorrhages along the retinal surface. The preproliferative stage is characterized by blood vessel obstruction. The final and most severe stage is called the proliferative stage. The key feature of the proliferative stage is the rapid formation of new, poor quality blood vessels. This characteristic is called neovascularization. These new vessels grow into the vitreous portion of the eye and may obstruct the visual path.

Also, these poorly formed vessels leak blood into the vitreous chamber further obstructing vision [1].

The precise stimulus for neovascularization is unknown. In 1956 Wise [19] hypothesized a retinal hypoxic condition stimulated the new vessel growth. His hypothesis has yet to be confirmed. However, recent work by Stefansson et al. support Wise's hypothesis. Their experiments demonstrate that oxygen tension was significantly higher over retinal areas treated with panretinal photocoagulation than other untreated areas of the same retina [20].

To better understand the treatment protocol for diabetic retinopathy a closer examination of the retinal oxygen supply is required. The retinal oxygen supply is provided by two separate systems: 1) the inner retinal supply providing oxygen from the vitreous to the outer plexiform layer and 2) the outer retinal supply providing the needs of the avascular photoreceptors (the rod and cones). The inner retinal supply is provided by the retinal circulatory system while the outer retinal supply is provided by diffusion from the choroidal circulation.

The retinal circulatory system is sensitive to changes in the oxygen supply. A hypoxic condition induces an autoregulatory vasodilation response. The retinal vessels adjust their flow to maintain the tissue oxygen level at a constant level. The retinal circulatory system provides 50 percent of its oxygen to the tissue. The choroidal system does not autoregulate significantly. Only 4 percent of its oxygen supply is provided to the retinal tissue [21].

Homeostasis of oxygen availability in the retina provides a sufficient mechanism to initiate or inhibit vessel growth. Dilation of retinal vessels for any length of time initiates new vessel growth. The rate of new vessel growth

is proportional to the amount of dilation of retinal vessels. The loss in diabetes of the sphincter-like mural cells may facilitate retinal vessel dilation [21].

Diabetic retinopathy is treated with panretinal photocoagulation. An argon laser at a wavelength of 488 nanometers and 514 nanometers is used to selectively denature peripheral portions of the retina while sparing critical vision anatomy about the fovea and optic disk. The retinal vessel network is also spared. Many different lesion patterns may be used. A pattern of two concentric rings of 200 micron lesions about the critical vision anatomy surrounded by concentric rings of 500 micron lesions out to the far retinal periphery is common [1]. This technique preserves acute vision about the macula at the expense of the peripheral vision. This treatment is based on the hypothesis that the lesions selectively destroy rods and cones by photocoagulation to allow more choroidal oxygen to reach the inner retina and constrict retinal vessels. This selective denaturation improves the oxygen supply to the retina by increasing the oxygen tension. This has recently been verified in human patients [20]. The improved oxygen tension suppresses the neovascularization response. The success of argon laser treatment is roughly proportional to the amount of retinal tissue photocoagulated [21].

2.2.2 Macular Degeneration

Macular degeneration is also called senile macular degeneration because it is most common in the elderly population. This disease is the leading cause of blindness in people over 65 years of age. However, the disease may also affect younger people. This disease occurs in two forms: the more common drusenoid or dry form and the neovascularization or exudative form. The neovascular-

ization form occurs in approximately 20 percent of the macular degenerative cases. This is the more active of the two forms. This form can be treated via argon laser photocoagulation techniques while the drusenoid form can not. The neovascularized form is typified by leaky blood vessels and hemorrhaging into the macula and the fovea. Treatment is similar to that prescribed for diabetic retinopathy. In about 10 percent of the neovascularized cases, the bleeding is so close to the fovea that treatment is not currently possible. If untreated, the fovea may become obliterated and destroyed within a month or two resulting in loss of acute vision [22].

2.2.3 Retinal Breaks and Tears

The retina may be subdivided into two main layers: the neural retina and the retinal pigment epithelium. The pigment epithelium provides a nursing role to the rods and the cones. Certain traumatic injuries result in retinal breaks and tears. If left untreated the two layers may separate. This separation is called retinal detachment. If the layer separation is not repaired blindness will result. The retinal breaks and tears may be repaired using photocoagulation to seal the break. The rods and cones within the traumatic site are no longer functional [1, 53]. A common technique is to surround the torn area with two continuous, concentric rings of 200 micron lesions.

2.3 The Aging Eye

It is important to review the effects of aging on the eye since many patients treatable by the Robotic Laser System will be elderly. Weale [23] has carefully documented the effects of aging on different eye structures. The effects include:

- The cornea yellows in advanced age. Also, the older cornea tends to scatter more light [23].
- There is a marked decrease in pupil area. Weale notes the ratio of maximum to minimum pupillary area slowly decreases with age [23].
- The crystalline lens tends to scatter more light [23].
- The vitreous body usually has a clear, gel consistency. With advanced age the collagen fibrillar network within the gel tends to agglomerate and form a floating 'powder' [23].
- The retina may experience the appearance of blood vessels, yellowish-white spots, and drusen [23]. Drusen is hyaline excrescences in the eye due to aging [24].

Chapter 3

The Retinal Observation Subsystem

3.1 Objective

The Retinal Observation Subsystem provides a digitized map of the patient's retina for use by the ophthalmologist to diagnose different retinal diseases or injury and plan required treatment. The tracking algorithm also requires a high contrast digitized image of the retina where features are clearly discernible against the retinal background. This chapter provides a brief review of research activity in the area of retinal imaging followed by a comparative study of different imaging systems considered. This chapter concludes with a description of software written to capture, enhance, and store the digitized retinal map.

3.2 Previous Work on Retinal Imaging

This section provides a review of techniques used to image and enhance the retinal image via optical filters and video frame grabber input look up table manipulations.

3.2.1 Television Ophthalmoscopy

Video funduscopy is the use of video camera equipment to film the fundus - "the back portion of the interior of the eye visible through the pupil [24]".

This technique, also known as television ophthalmoscopy, is not new. In 1962 West et al. claimed "The idea of television ophthalmoscopy is not a new one. Ridley demonstrated such a device ten years ago." Early development of this technique was hindered by video camera imaging technology [25]. Even with these limitations, retinal studies using monochromatic illumination at different wavelengths were accomplished.

3.2.2 Fundus Chromatic Studies

A detailed analysis of retinal monochromatic response was conducted by Delori et al. in 1976. Delori found that specific features of the fundus could be imaged with increased contrast when appropriate monochromatic illumination was used. Delori concluded monochromatic studies permit more accurate visualization than can be achieved with white light. Important to this investigation was the conclusion: "The optical wavelength for observing large retinal vessels is 570 nanometers, but their visibility is generally excellent between 540 and 580 nanometers. The vessels appear dark and well defined with a central irregular streak of light along the larger vessels[26]". The improved visibility of vessels in this region is due to the peak of hemoglobin absorption near 570 nm. Reference Figure 3.1 [27].

Based on this conclusion a 568 nm interference filter was chosen to enhance the retinal vessel contrast. The results of using this filter compared to a white light source and a 530 nm bandpass filter is illustrated in 3.2. The 530 nm filter was provided as an option with the fundus camera.

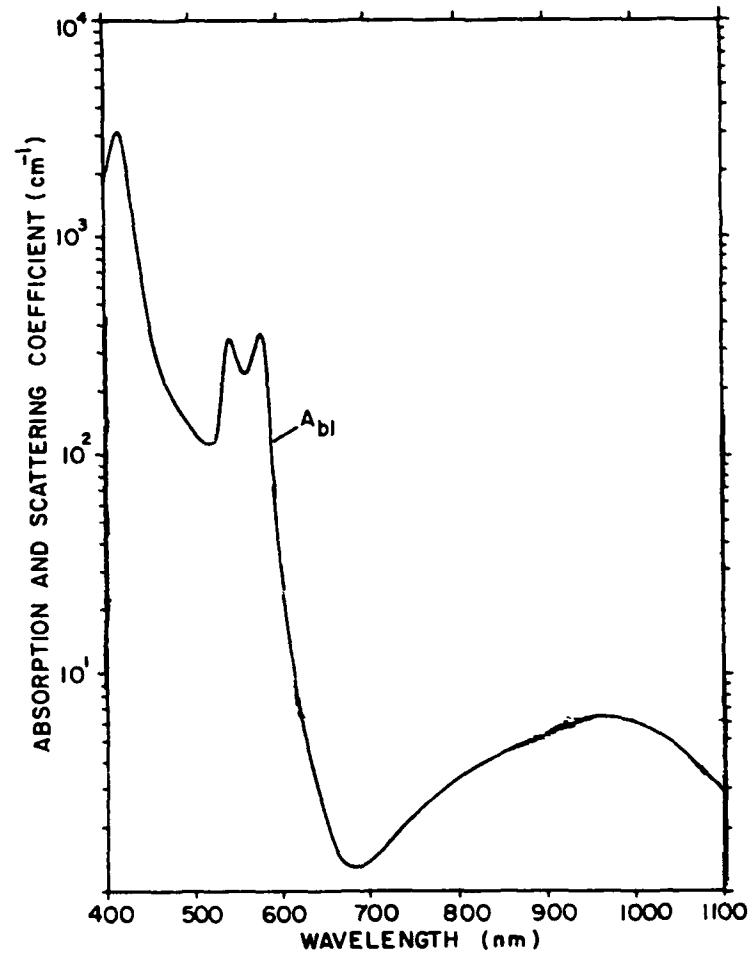


Figure 3.1: Absorption characteristics of blood assumed to be represented by oxy-hemoglobin[27]

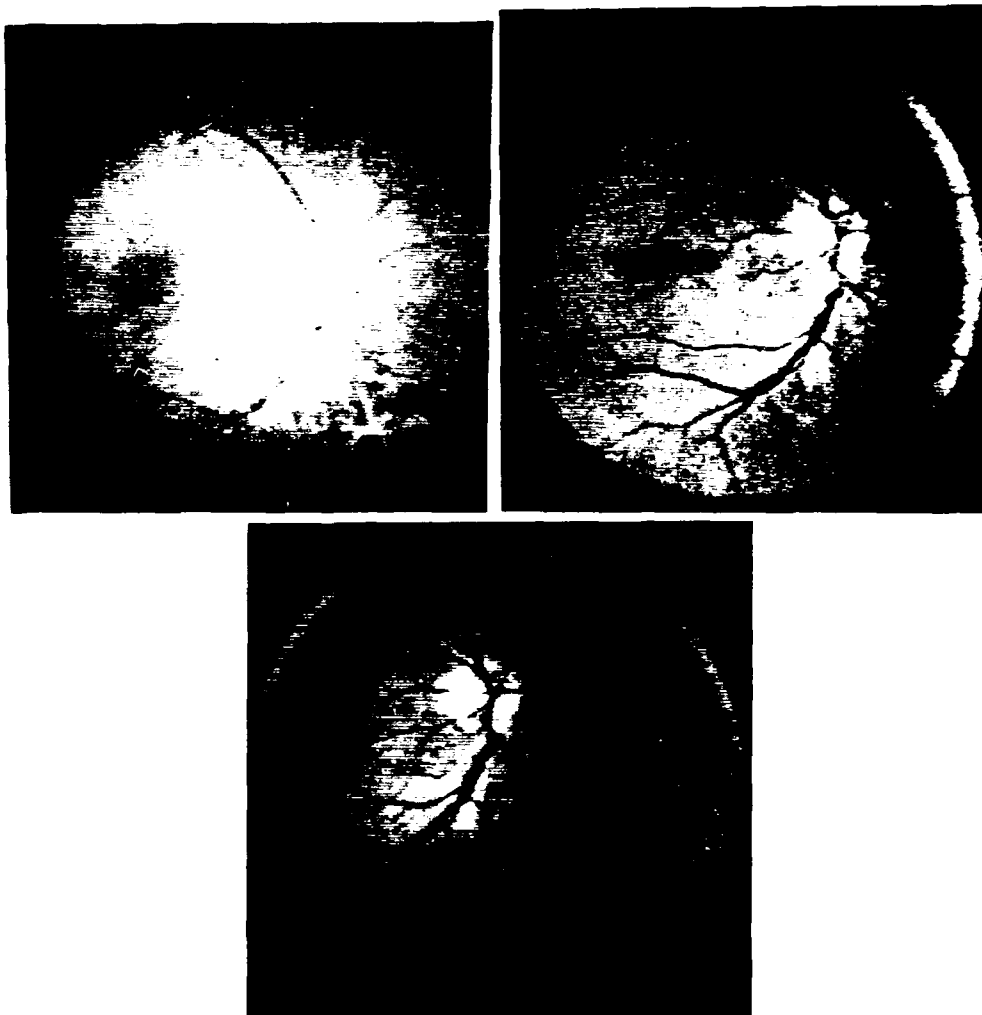


Figure 3.2: Retinal imaging with optical filters. Left to right: white light source, 530 nm bandpass filter, 568 nm interference filter

3.3 Retinal Imaging

This section contains a description of different imaging technologies considered for this project. A brief theory of operation is provided with each technique along with inherent advantages and disadvantages. This section concludes with a comparative analysis and a selection of an imaging system for the remainder of the study.

3.3.1 Fluorescein Angiogram Retinal Imaging

Fluorescein angiogram retinal imaging is a clinical tool used by ophthalmologists to obtain a high contrast image of the retina. Specifically, it is used to image microaneurysms associated with critical retinal diseases long before the disease becomes acute. This technique may also be used to examine retinal vessel disorders such as blockages and leaking. The literature further indicates this technique may be used to quantify blood flow parameters within the retina. The motivation for studying this technique was to improve the gray level contrast between the retinal vessels and background [28].

Fluorescein Angiogram Development

The fluorescein angiogram technique is not new. It was originally introduced to clinical practice by Novotny and Alvis in 1961. Their objective was to develop a technique to observe retinal blood flow with increased visibility and definition. They originally determined both the excitation and emission wavelengths of blood fluorescein mixtures spectrofluorometrically. The optimal excitation wavelength was found to be 490 nm and the maximal emission wavelength was 520 nm. Blue and green filters were used to modify the excitation and emission

paths respectively [29].

Fluorescein Angiogram Current Techniques

Currently, fluorescein imaging is accomplished by injecting fluorescein sodium 10 percent in a dose of 10 mg per kg body weight as a bolus into a cubital vein. The time from injection into the vein until fluorescence visualization varies from 12 to 30 seconds. The fluorescence lasts for approximately 3.5 minutes. The fluorescein sodium eventually appears in the aqueous humor which contributes to the loss of image clarity [29, 28].

A fundus camera equipped with a standard 35 mm camera is typically used to film the progress of the fluorescein sodium in the retinal vessels. A blue filter with a passband similar to the fluorescein sodium excitation band is placed in the illuminating source's path. Ideally, this excitation filter should have a passband from 400 to 500 nm. However, the absorption characteristics of the human eye from 400 to 450 nm severely limit excitation at these wavelengths. A barrier filter with a passband similar to the emission band is placed before the camera's objective lens. Ideally, this is a highpass filter which blocks wavelengths below 500 nm [28].

Advantages of the Fluorescein Angiogram

The fluorescein angiogram allows the discernment of small structures and temporal studies of the retinal vessels not possible with other imaging techniques. In fact, Nielsen noted that fluorescein sodium is the most employed dye in ophthalmology for diagnostic purposes [28]. A sample of a fluorescein enhanced retinal image is provided in Figure 3.3. The image was provided by Dr. H.



Figure 3.3: Fluorescein enhanced retinal image

Grady Rylander.

The Disadvantages of Fluorescein Sodium

The adverse effects of using fluorescein sodium imaging are well documented. Thorough studies accomplished in 1982 and 1983 on several thousand patients indicated complications occur in 5.4 percent of cases. The study indicated that complications tend to occur more frequently in male patients who have had multiple angiographies. The most common adverse effect was transient nausea. The study estimated that life threatening circulatory reactions occur in 5 out of 10,000 angiographies. However, it was noted that serious cardiopulmonary complications may be coincidental only as a reflex mechanism associated with venipuncture and not with the injected dye. The study concluded that "despite the low incidence of life threatening reactions fluorescein angiography of the retina should be performed only when the indication is justified and then only

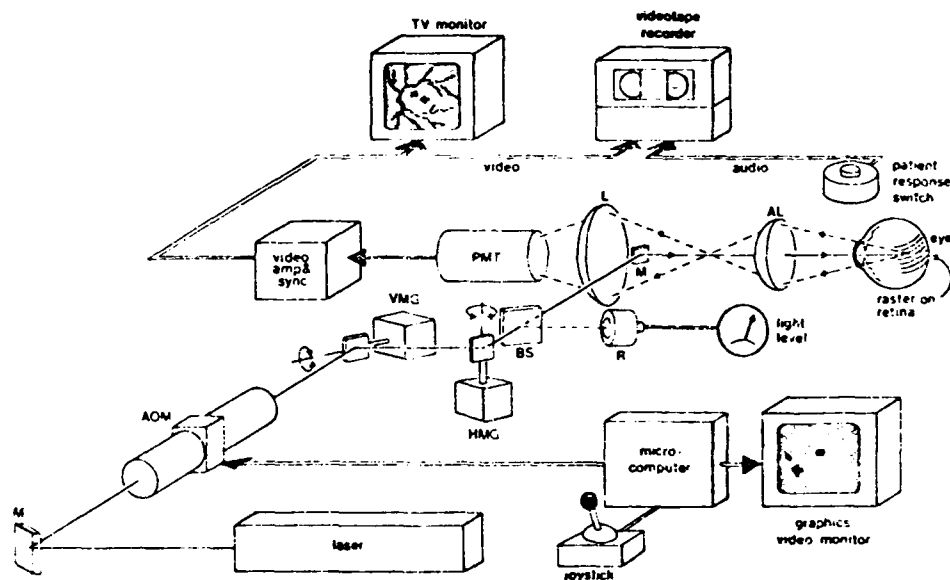


Figure 3.4: Scanning Laser Ophthalmoscope [31]

if it provides a guideline for treatment [28]".

3.3.2 Scanning Laser Ophthalmoscope (SLO) Imaging

The SLO technique of retinal imaging uses a dim 568.2 nm krypton laser beam to scan the retina. Recall from Delori's study that 568.2 nm is close to the peak absorption of hemoglobin.

There are two main optical paths in the SLO system: 1) the raster path, and 2) the light collection path. The raster optical path provides the vertical and horizontal sweeps of the laser light source. The sweeps are accomplished using acousto-optical modulators (AOM) and mirrors connected to galvanometers. Basically, the intensity modulated beam from the AOM is swept vertically in a sawtooth waveform by a mirror mounted on a galvanome-

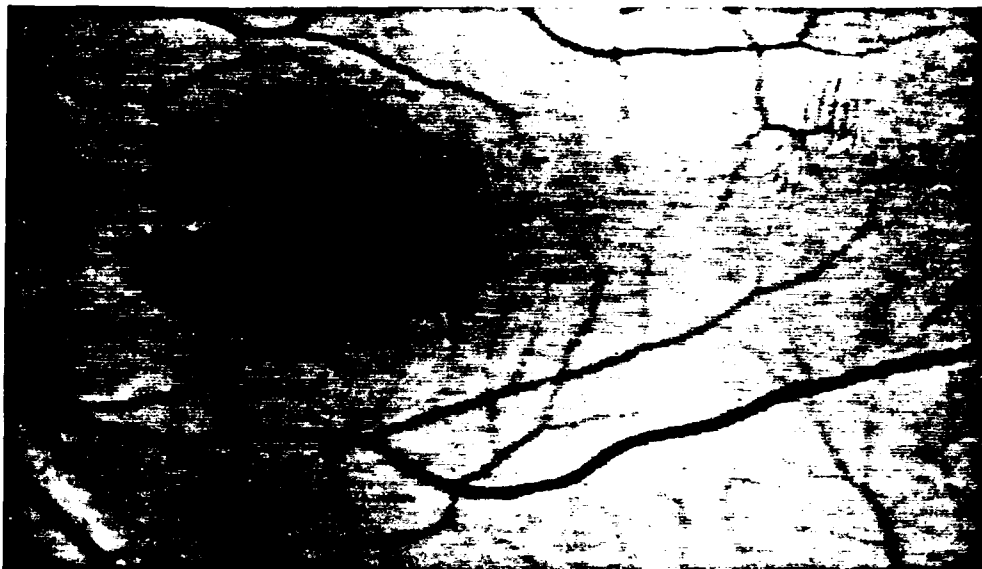


Figure 3.5: SLO image at a 50 degree field of view

ter (VMG). Reference Figure 3.4 [31]. A second mirror mounted to a tuned resonant galvanometer (HMG) sweeps the beam horizontally with a sinusoidal waveform. The vertical and the horizontal sweeps of the beam by the mirror galvanometers produce a raster pattern of parallel horizontal lines directly on the retina. The returned light from a specific point on the retina is captured by a photomultiplier tube (PMT) and displayed as the intensity of the spot on a television monitor. This is accomplished via a small mirror (M) optically conjugate with the eye's pupil and brought to a focus on the retina by an aspheric ophthalmoscopic lens (AL). The laser moves over the retina synchronously with the spot on the monitor such that there is a one-to-one correspondence between a specific point on the retina and a specific point on the television screen. Thus, a video image is built up point-by-point [30, 31]. Figure 3.5 provides a sample of the fine resolution available with the SLO technique. This image was provided by Dr. Ann Elsner of the Boston Eye Research Institute.

Advantages of the SLO

The SLO imaging technique has many advantages. The advantages include:

1. The retinal illumination required for SLO imaging is on the order of 1000 times less than standard fundus imaging and 10,000 times less than the fluorescein angiogram [32].
2. The SLO uses only a 0.9 millimeter diameter entrance pupil leaving the rest of the pupil for the image. Since a small entrance pupil is required pupil dilation is not required [32, 33].
3. The laser source may be steered around opacities such as cataracts [32].
4. The SLO allows fluorescein angiography with many orders of magnitude less light and one-tenth the dye dosage. This allows the examination of both eyes and repetitive examinations during a single clinical visit [32].
5. As a patient ages, the lens and the vitreous humor tend to scatter and absorb light in greater quantities. The scattering is seen as a glare by the patient and as a cloudiness by the clinician. The cloudiness reduces image contrast. Increasing the level of retinal illumination in a standard fundus camera further increases the scattering and degrades image contrast. SLO reduces these scattering effects since retinal illumination is provided through a smaller portion of the scattering medium [32].
6. Color images are possible by using the illuminating laser in a "white light mode". In this case there is simultaneous emission of 647, 568, and 502 or 496 nm light. Three separate detectors are required [32, 33].

7. Any graphical material that can be displayed on a computer monitor can also be impressed on the retinal pattern formed by the sweeping laser beam. This capability would allow an adaptive feedback patient fixation device. This technique has been used to investigate how patients with macular scotomas (area of depressed vision [24]) use residual functional retinal areas to inspect visual detail [32].
8. The SLO imaging system has a large depth of field which permits the iris, vitreous humor structures, and the retinal surface to be in focus simultaneously. It also has the capability to be used in the confocal mode where a single retinal plane is in focus [32, 33].

Disadvantages of the SLO Technique

The disadvantage with the SLO is limited availability due to high cost.

3.3.3 Silicon Intensified Tube (SIT) Cameras

Silicon intensified tube type cameras are designed specifically for low light, low contrast imaging environments [35]. The camera's lens forms an image on the tube's photosensitive element. The charge density at a specific point on the element is proportional to the incident light flux at that point. An electrical analog of the image is thus formed on the photosensitive element. The photosensitive element is scanned with an electron beam to convert the charge distribution into a voltage [36].

Although these cameras work very well in a low light, low contrast environment they are heavy, susceptible to damage from image burn, and expensive

(10,000 dollars) relative to some of the other camera technologies discussed. A SIT camera was tested early in this study. Due to the disadvantages listed above and the small image obtained when coupled with a fundus camera, the SIT technology was eliminated from further consideration.

3.3.4 Charge Coupled Device (CCD) Cameras

A charge coupled device camera has a single integrated circuit for the active camera element. This 'chip' consists of a two-dimensional array of metal-oxide-semiconductor (MOS) capacitors operating in the deep depletion mode. The capacitor is biased such that impinging light generates electron-hole pairs that are trapped in potential wells within the MOS structure. The number of pairs generated is proportional to the amount of light impinging on a given MOS capacitor [37]. Ideally, each MOS device in the array should have a linear response and be identical to other MOS devices in the array. This is not the case.

A charge coupled device generated image consists of the entire array of separate point charges. Each separate point charge forms a picture element or pixel. To convert the charge into a useable signal it must be shifted out a line at a time. Once shifted out of the array the charge is converted to a voltage signal a pixel at a time until all pixels in an image have been converted. When the shifting operation is complete, a new image can be formed [37].

High performance CCD cameras are available with dynamic range extending over twelve orders of magnitude, high sensitivity down to 10 micro-foot-candles, and resolutions of 750 by 500 pixels or more. To achieve this dynamic range capability image intensifiers, and specialized iris and gating cir-

uits must be employed [38]. The dynamic range of the CCD camera is limited by generation and recombination noise on the low intensity end and potential well overload (or saturation) on the high end. The CCD camera used in this study had sensitivity of 70 milli-foot-candles, resolution of 510 x 492 pixels and operated at a standard frame rate of 30 frames per second. The camera costs under one thousand dollars.

3.3.5 Retinal Image Enhancement

There are a number of image processing techniques that may be employed to enhance the contrast of an image or enhance certain features within an image. These include various filtering schemes and gray scale histogram modification. In this study these techniques were used with the CCD camera to enhance the retinal image for tracking.

Optical Filtering

Ideas presented in Delori's work on fundus chromatic studies were used to enhance the retinal image contrast. A 568 nm (Edmund Scientific J43,127) interference filter was used inline with the fundus camera halogen illumination lamp to bathe the interior of the eye in green light. The result of this filter employment is provided in Figure 3.2 and characteristics of this filter are provided in Figure 3.6. These characteristics were measured with a Varian 2300 spectrophotometer.

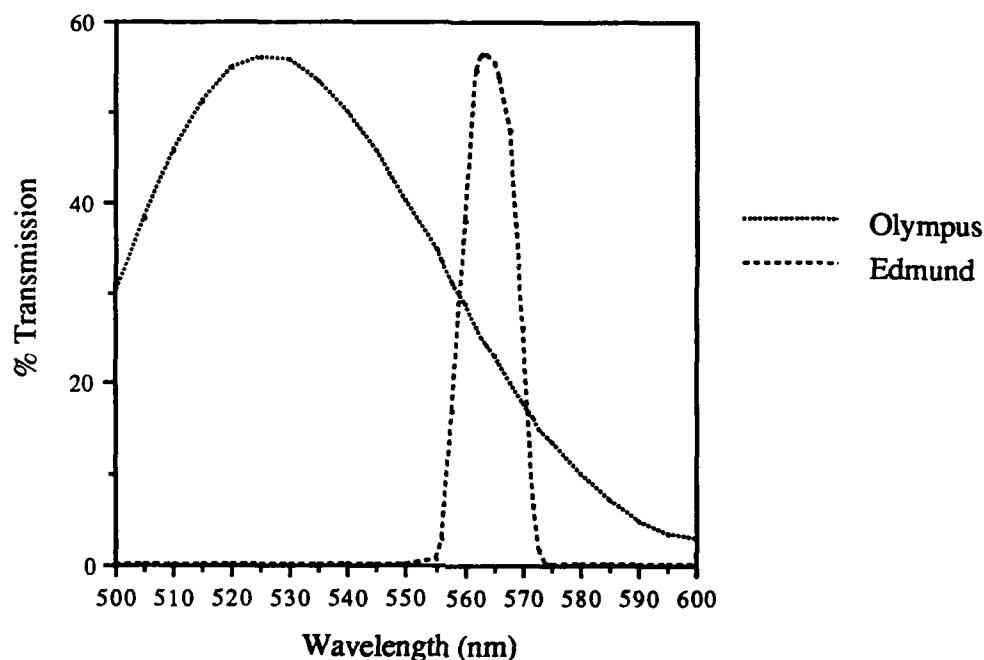


Figure 3.6: J43,127 568 nm interference filter characteristics contrasted with the Olympus 530 nm bandpass filter

Real Time Histogram Modification

The RETINA Tracking and Image Analyzer software developed for this project has many capabilities to enhance an image. The specific method used in this study for contrast enhancement is histogram modification using function `mod_his` (modify histogram) under the Image Statistics Menu. Reference Figure 3.7.

There are three different options for histogram modification within function `mod_his`. These functions have been developed from Rosenfeld and Kak's general description of histogram modification techniques [34]. The `mod_his1` function examines the gray level histogram of a reference image. The reference image is a randomly chosen image of the patient's retina under treatment. The function maps each current gray level in the reference histogram to a new

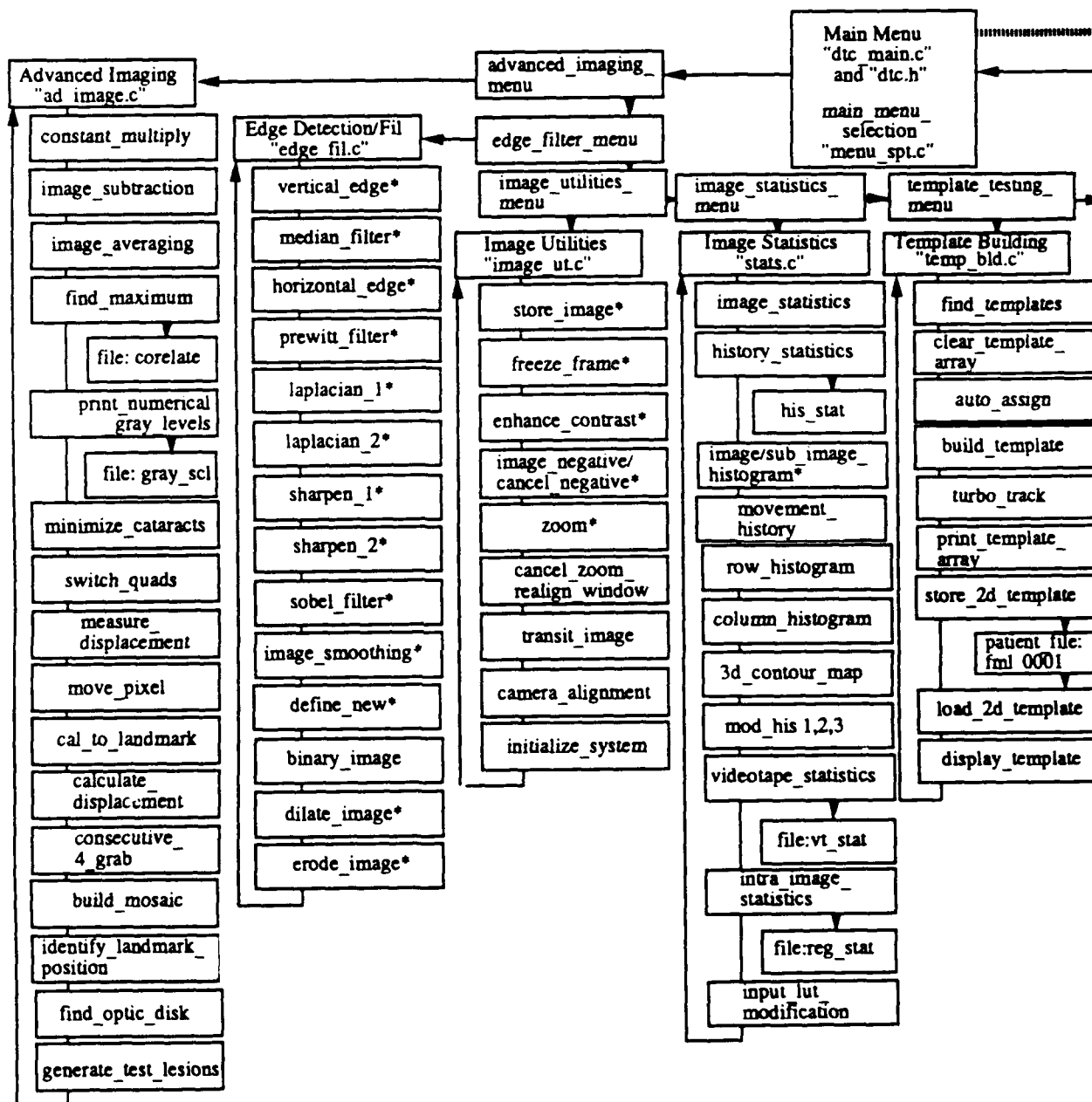
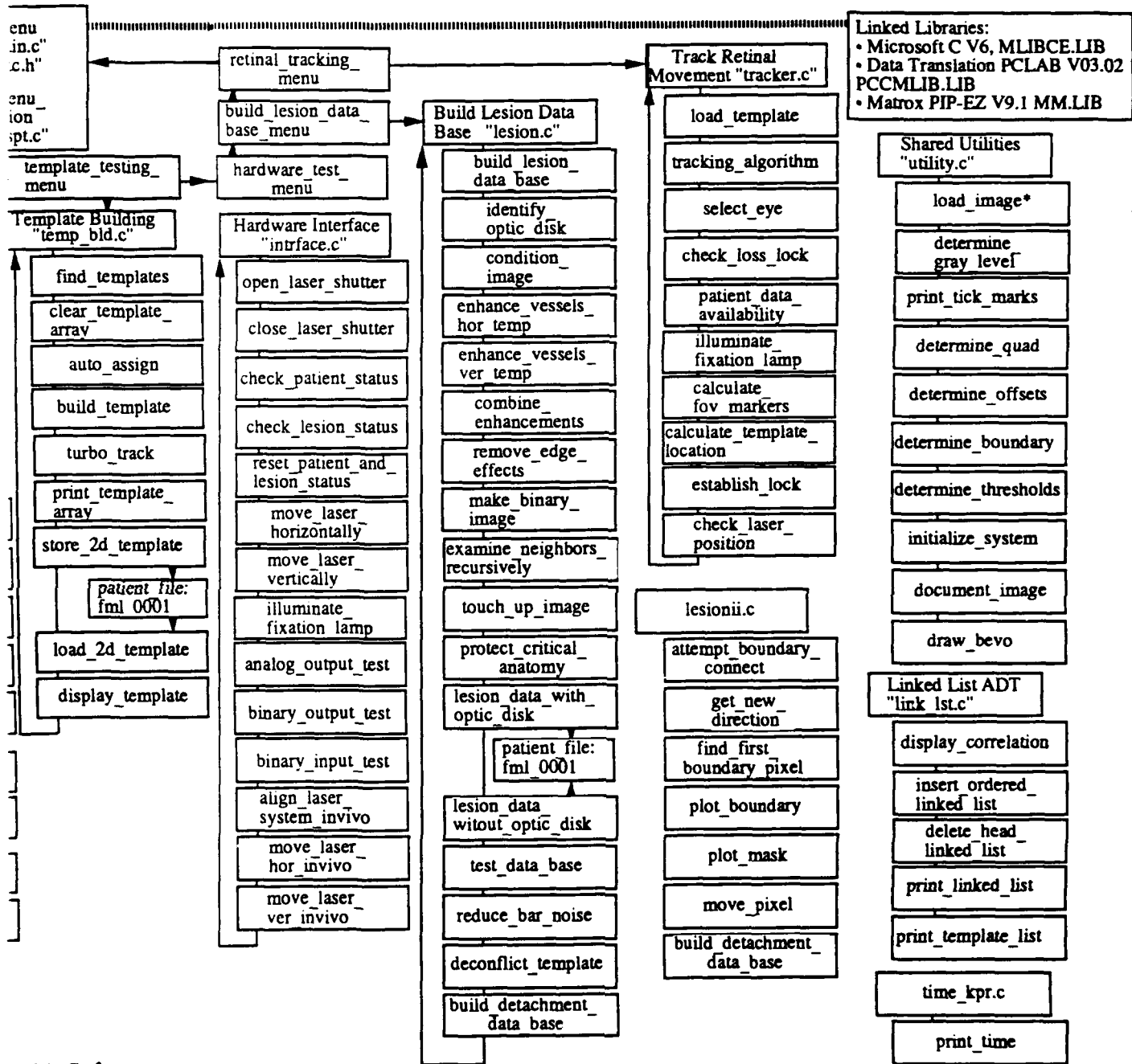


Figure 3.7: RETINA Software.



INA Software.

(2)

single unique gray level. The new gray level values are equally spaced across the gray level spectrum from 0 to 255. The gray levels between the new gray level values are not used. This technique is known as 'global linear min-max windowing' [39]. The gray scale modification performed by function `mod_his1` may be described by:

$$g' = \begin{cases} t_{L'}; & g < t_L \\ t_{L'} + ((g - t_L) * (t_{H'} - t_{L'}) / (t_H - t_L)); & t_L \leq g \leq t_H \\ t_{H'}; & g > t_H \end{cases} \quad (3.1)$$

where:

- g' : modified gray level
- g : premodified gray level
- $t_{L'}$: lower bound of expanded histogram (usually 0)
- $t_{H'}$: upper bound of expanded histogram (usually 255)
- t_L : lower bound of image histogram
- t_H : upper bound of image histogram

An illustration of this histogram modification is provided in Figure 3.8.

This method was chosen because it can be implemented on the Matrox PIP-1024 frame grabber without a time penalty. This is accomplished by loading the gray level mapping obtained from function `mod_his1` into the input look up table (ILUT) of the frame grabber. All incoming video images are processed through the ILUT. The ILUT normally has a one-to-one mapping

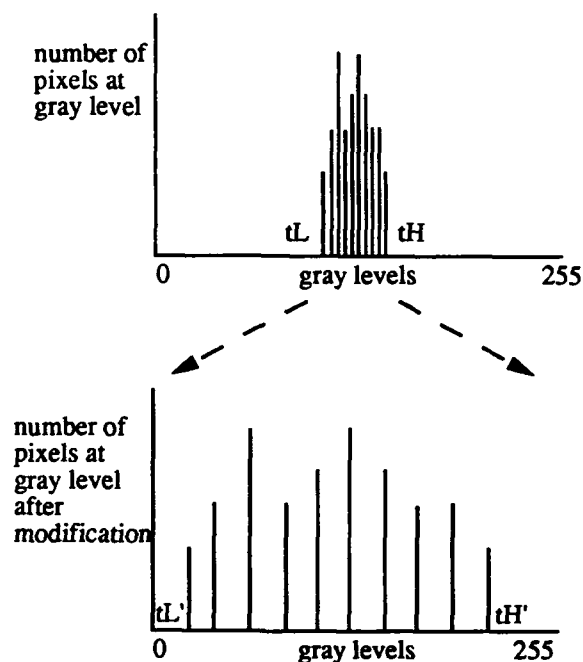


Figure 3.8: Histogram modification mod_his1

between gray levels of the incoming image and the gray levels presented to the frame grabber. However, this mapping function may be modified to any desired map without incurring an additional time penalty. A sample obtained from the histogram modification mod_his1 is provided in Figure 3.9. Functions mod_his2 and mod_his3 provide even more dramatic results but they can not be implemented without a time penalty. Many frame grabbers have the capability to modify the input look up table.

3.3.6 Imaging Technique Comparison

To compare different imaging technologies I obtained sample images of the human retina using 1) a CCD camera equipped with a 568 nm filter and histogram modification, 2) fluorescein angiogram images provided by Dr. H. Grady Ry-

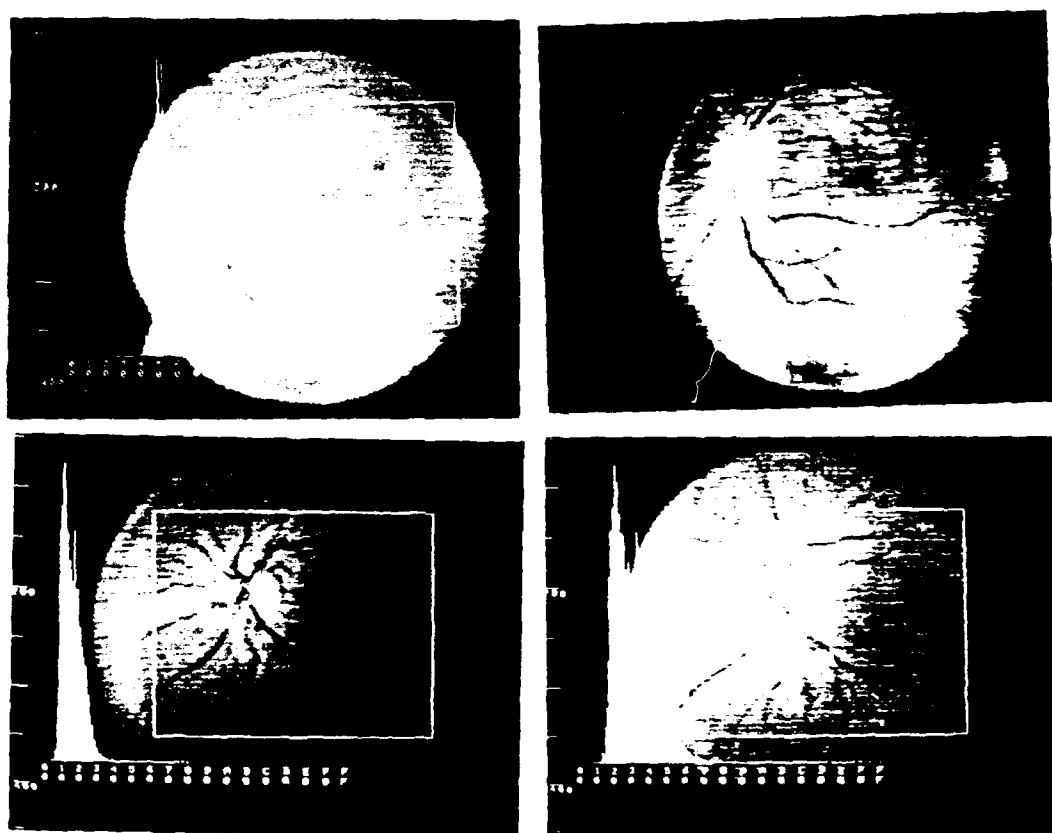


Figure 3.9: Real time histogram modification with function `mod_his1`

lander, and 3) SLO images provided by Dr. Ann Elsner of the Boston Eye Research Institute. The imaging technologies were compared on the basis of contrast delta which is the difference in average gray level between a vessel central to the image and the adjoining retinal background. The fluorescein angiogram images were found to have the highest contrast delta (34.5) followed by SLO (28.5) and the CCD with contrast enhancement (23.4). The CCD camera image without contrast enhancement had a contrast delta of 5.2.

I am reluctant to draw quantitative conclusions from such a small number of samples (12). Furthermore, a direct comparison between imaging types was not possible since the same subject eye was not compared under similar conditions. Due to the availability of the CCD camera and the contrast enhancement provided by optical filtering and histogram modification, the CCD technology was used for the remainder of the study. The cost of the SLO and the concerns related to fluorescein sodium limited further consideration of these technologies. However, the tracking algorithm may be easily adapted for use with either technology.

3.4 Storage Media

Since the Retinal Observation Subsystem will be used in clinical practice it is important that pertinent patient information such as key diagnostic and treatment images be retained for future reference. A single image of 512 x 512 pixel spatial resolution by 256 gray scale resolution requires 256 kilobytes for storage. A single retina may require more than sixteen of these images. A record of both eyes would thus require at a minimum 8 megabytes of data. Additional data storage requirements which will be discussed later in this document account

for another 128 kilobytes per patient. Different media may be chosen to store patient data.

3.4.1 Video Tape

Standard video tape cartridges have the advantage of high data capacity. A single video tape could store a single patient's data file in a fraction of a second of video tape. However, the video tape is bulky to store and suffers age related degradation. Furthermore, data requires sequential access.

3.4.2 Diskette

Currently, storage on standard computer 'floppy' disks is feasible. The maximum disk capacity is currently limited to 1.44 megabytes per disk. Thus a single patient's data file would require 6 diskettes for storage. Although these disks are small, 6 disks per patient would become cost and storage space prohibitive. A more realistic alternative would be a hard disk drive for patient files. Disk drives with capacities in excess of a gigabyte are now common.

3.4.3 Optical Disk Storage

Optical disk technology is now available for image storage. Re-writeable optical disks are available in 400 megabyte capacities. Disks cost approximately 200 dollars each. Optical disk drives for image or data storage cost approximately 5,000 dollars. The data transfer speed for optical disks are 200 kilobytes per second [40].

3.4.4 Digital Audio Tape

Digital audio tape (DAT) technology shows promise for image storage. These tape cartridges are approximately three inches long by two inches wide. Cartridges are now available with capacities to 1.2 gigabytes at a cost of 30 dollars. Although the tape is accessed sequentially, a file can be found in less than 20 seconds. The data transfer rate for the DAT is 192 kilobytes per second. Reed-Solomon error correcting techniques are used for data reliability [40]. Digital audio tape drives are now available as options on personal computers for under 400 dollars.

3.4.5 Storage Medium of Choice

The storage medium of choice for this subsystem is the standard hard disk due to its ready availability. However, the DAT system is also desired as an archival system for clinics with a large patient base.

3.5 Retinal Observation Software

Retinal observation software was written to support the need for image acquisition, storage, and enhancement. A structure chart of the RETINA software was provided earlier in this chapter. This section provides a brief review of similar software that is available and highlights the capabilities of the RETINA software.

3.5.1 Previous Work

There are many software packages that have been developed to image the retina and its specific features. Also packages have been developed to provide specialized functions such as measure cup to disc ratios and create a mosaic map of the retina. These packages are too numerous to separately detail here. The interested reader is referred to the bibliography [41, 42, 43, 44, 45, 46, 47]. Some of these ideas were adapted for use in the RETINA software.

3.5.2 RETINA Software

Program RETINA (Retinal Tracking and Image Analyzer) is a user friendly, menu driven program developed to image and track the retina. The program is written in Microsoft C version 6.0. It requires approximately 4 megabytes of random access memory and a runtime stack size of 24,000 bytes. The program requires a Matrox PIP-1024 frame grabber with its accompanying software library PIP-EZ and a Data Translation DT-2801A data acquisition system and its accompanying library PC LAB.

Top down software design techniques were used in software development. Also, the Air Force's Reliability and Maintainability 2000 (R&M 2000) software design techniques were applied in development [48]. The program is completely modular for ease of modification and update.

The program is centered about a main menu from which the user can call specific submenus. These main menu selections include: image utilities, advanced imaging functions, edge detection algorithms, image statistical functions, template and lesion data base building functions, and the actual tracking

algorithm. There are also numerous support functions to interface the software to the Hardware/Software Interface, a linked list abstract data type, and functions to time code execution. Specific functions will be detailed throughout this document. Functions identified with an asterisk (*) on the structure chart are library functions provided with the PIP-EZ or the PCLAB software libraries.

Chapter 4

The Retinal Tracking Subsystem

4.1 Objective

The purpose of the Retinal Tracking Subsystem is to measure and compensate for eye movements during laser treatment for diabetic retinopathy and other retinal diseases treatable by photocoagulation. The system designed and implemented in this project uses digital video picture registration to accomplish this task. This chapter reviews the theoretical basis of picture registration followed by a discussion of the ideal tracking algorithm. The ideal algorithm will be used as a benchmark to measure the effectiveness of existing tracking algorithms. This is followed by a short overview of the tracking algorithm. The remainder of the chapter details the tracking algorithm. Testing and timing of the tracking algorithm is detailed in a separate chapter.

4.1.1 Theoretical Basis

Conceptually, digital video picture registration uses digitized video images to determine the amount of object movement that has occurred. A reference image of the object is first obtained. Subsequent images of the object are compared to the reference image to determine the amount of object movement. If information on object movement is provided to a system for adjustment,

object tracking has occurred.

The object in our discussion is the retina. Ghaffari has conceptualized the steps required to track the retina [49].

1. Store a retinal video image as the reference image.
2. Find the position of the best match between the reference image and the present image.
3. Calculate the amount of movement.
4. Update the system with the amount of movement that has occurred.
5. Repeat steps 2 through 4.

Intuitively, the amount of time required to accomplish step 2 is directly related to the size of the search area and the complexity of the algorithm to match the images. Furthermore, step 2 is complicated by complex retinal movements involving rotation about 3 axes of rotation. These axes, called the X, Y, and Z axis of Fick, rotate about the eye's center of rotation. Listing's plane passes through the center of eye rotation and contains the X and Z axes of Fick. Video imaging describes movement relative to the imaging plane as translation, rotation, and scale. Translation is object displacement along the image abscissa, ordinate, or both. Rotation is an angular displacement about a specific axis. Scale is an object's increase or decrease relative to a fixed ratio within an image. These terms are illustrated in Figure 4.1. Methods to measure, minimize, and compensate for these movements are provided later in this document.

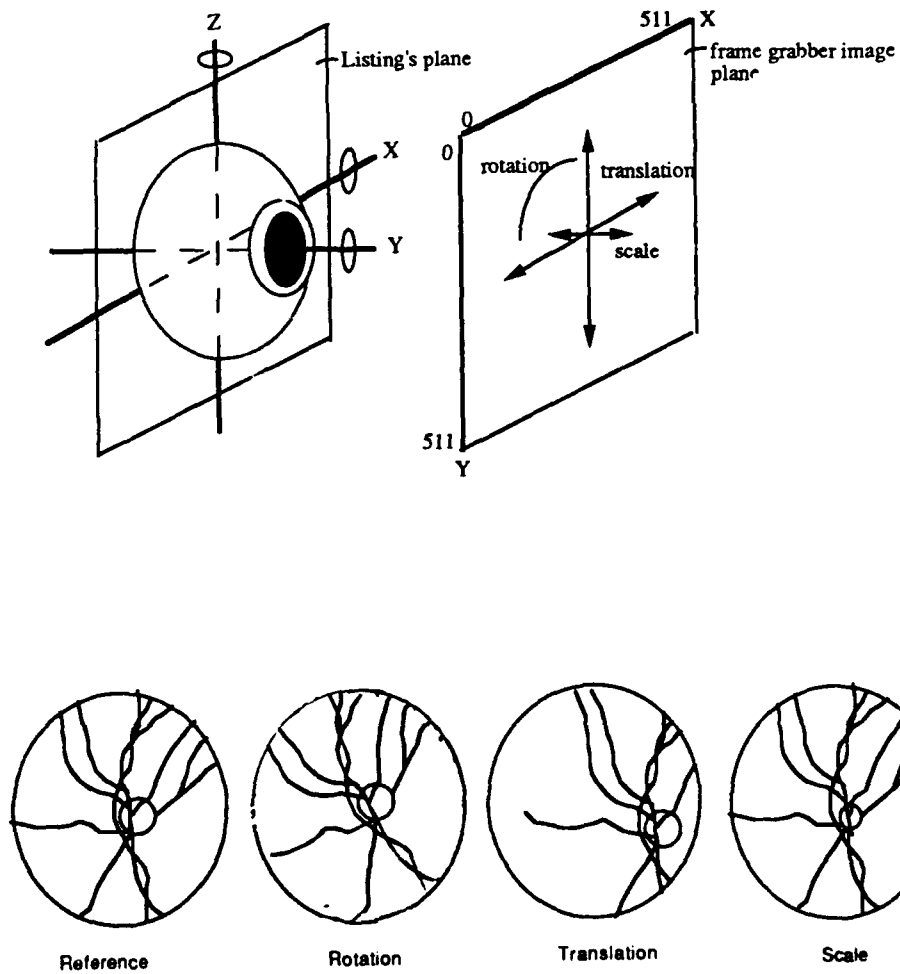


Figure 4.1: Top: the X, Y, and Z axes of Fick rotation as related to the image plane frame of reference [adapted from [50]]. Bottom, left to right: reference image, translation, rotation, and scale movements related to a retinal image.

4.1.2 The Ideal Tracking Algorithm

To design an effective tracking algorithm a description of an ideal algorithm is useful as a guide for development, as a benchmark for evaluation, and as a planning aid for future algorithm improvements. This section provides a list of requirements for an ideal retinal tracking system. Such a system should have the following capabilities:

1. Track all retinal movements and provide the necessary corrective signals to compensate for the movement.
2. Have zero response time.
3. Be impervious to changes in retinal illumination.
4. Track effectively in all retinal fields of view.
5. Track effectively in pathological degraded conditions such as cataracts and vitreous opacities.
6. Protect the critical vision anatomy (the fovea and optic disk) and the retinal vessels from laser irradiation.
7. Respond to patient input (panic, blinks, etc.).
8. Have control over the laser positioning system and the laser shutter.
9. Track in the absence of visible retinal features.
10. Incorporate or not be affected by newly developed retinal lesions.

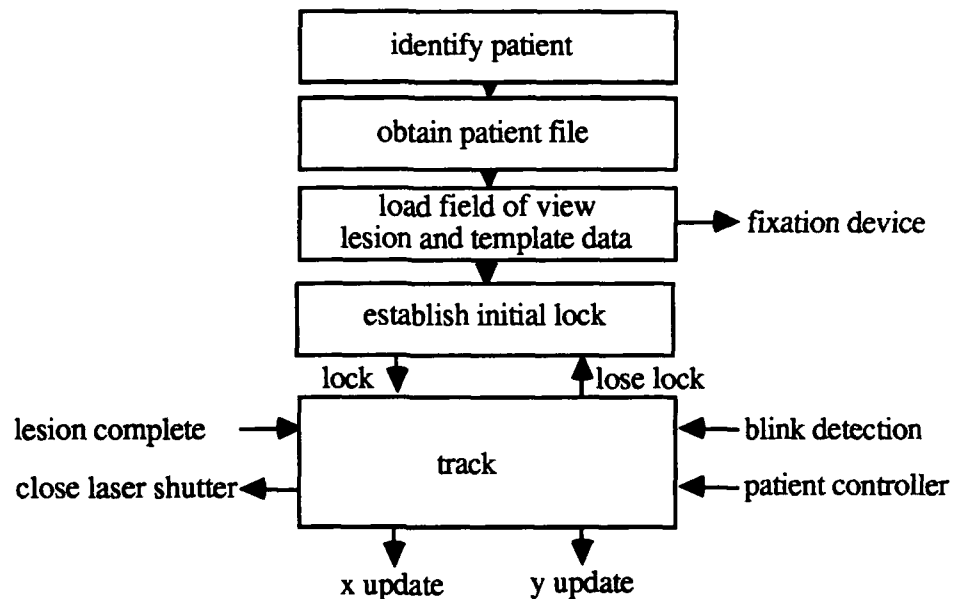


Figure 4.2: The RETINA Tracking Algorithm.

4.1.3 Overview

The flow chart for the tracking algorithm designed for this project is provided in Figure 4.2. This algorithm has been given the name Retinal Tracking and Image Analyzer (RETINA).

The tracking algorithm must attend to many tasks. These include: identifying the patient, retrieving the patient file from the data base, loading data for the retinal field of view for treatment from the patient's file, controlling the fixation device to minimize eye movement, establishing tracker initial lock on the retina, performing tracking, and responding to different contingencies such as loss of tracker lock, patient blink, and patient panic. Furthermore, the tracking algorithm must respond to inputs from the Reflectance Based Feedback Control System and provide inputs to the Laser Pointing Subsystem. Each one of these tasks will now be discussed.

4.2 Lesion Data Base

The Lesion Data Base (LDB) is a data bank that contains the information for lesion placement and size for the treatment of diabetic retinopathy or retinal breaks and tears. The construction of a data base for treatment of macular degeneration is not presented since treatment protocol for this disease is similar to diabetic retinopathy treatment.

Development of an LDB is complicated by the following factors:

1. Standard fundus cameras for imaging the retina have a maximum field of view of 60 degrees [51]. The fundus camera used in this study had a maximum field of view of 50 degrees. This limitation requires a separate data base for each of the retinal field of views requiring treatment. These field of view data bases must be independently retrieveable and be deconflicted from adjoining field of view data bases. Deconfliction prevents multiple treatment of a given retinal area. Furthermore, it would be very convenient if all data for a given patient could be stored in a single file.
2. Critical vision anatomy should be spared from laser irradiation. This anatomy includes the optic disk, the fovea and macula, and the retinal vessels [1, 21].
3. Minimal user input should be necessary for effective use of the clinician's time.

The LDB methodology developed for this research minimizes these complications. The following description details the multiple stages of image processing required to develop a complete patient LDB.

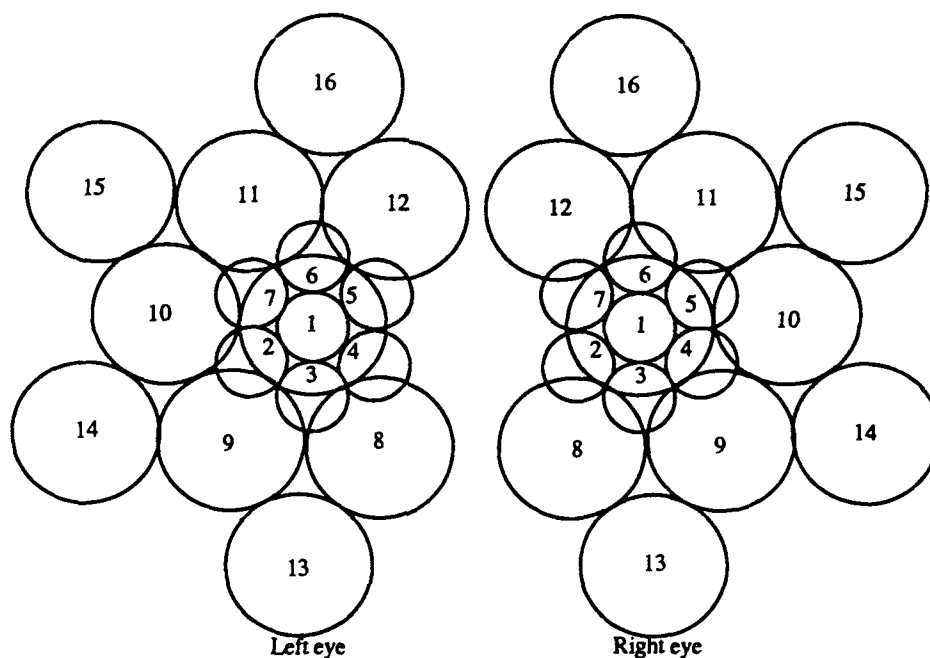


Figure 4.3: The field of view numbering system.

The first step in developing an LDB for a given retinal field of view is to identify the patient and the field of view. The patient file is identified by the patient's initials followed by an underscore and the patient's last four digits of their social security number (for example: sfb_8253). This file designator provides a short, descriptive, unique file label. Fields of view are identified using a single letter ('l' or 'r') to identify the eye and integers (1 to 16) to identify the field of view for treatment. Fields of view are numbered as illustrated in Figure 4.3. Only 16 fields of view are currently programmed for each eye. This is a sufficient number for proof of design. The design can be easily extended to any number of field of views.

The individual field of view data bases are kept separate within a patient's file using a hashing function. The hashing function provides unique

Patient Data File
File Designator: fml_0001

Left Eye Template Data

.
.
.

Right Eye Template Data

.
.
.

Left Eye Lesion Data

.
.
.

Right Eye Lesion Data

.
.
.

Figure 4.4: The patient file.

header and trailer data words which signal the beginning and end of a field of view's lesion data [52]. A similar hashing function is used to store the field of view template data in the patient's file. A sample diagram of the patient's file is provided in Figure 4.4.

After the patient file has been specified and opened for writing and the appropriate field of view hashing header has been generated the LDB building function prompts the user for the location of the optic disk on the image. A cursor is provided for the user to align with the center of the optic disk (if required). The function then initiates 12 steps of image processing to build the LDB. The steps include functions to enhance the retinal vessels via edge detection followed by filtering steps to remove noise. The retinal vessel map

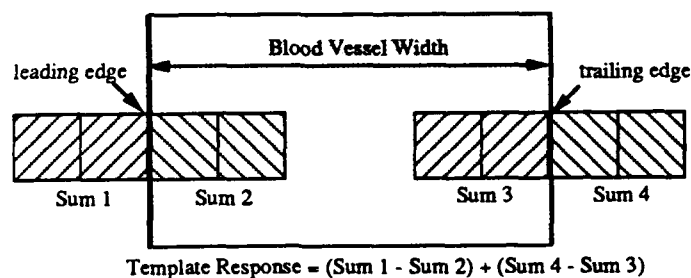


Figure 4.5: Modified Markow vessel enhancement templates

generated is then converted to a binary image. The critical vision anatomy is then masked from lesion placement. Lesion coordinates are then plotted and stored in the patient file. The user may then test the LDB for a visual demonstration of lesion placement. Additional details on the LDB process are now provided.

The reference retinal image is first scanned with horizontal and vertical templates of five pixel width to emphasize the vessel network. This template width equates to a vertical blood vessel width of 175 microns and a horizontal vessel width of 145 microns (for development system configuration). Additional vessel widths were tested but did not significantly add to the enhancement provided by the 5 pixel width template. Figure 4.5 provides a diagram of this modified Markow template operation. A detailed discussion of the Markow template is contained later in this chapter.

The results of the horizontal and vertical vessel enhancement steps are then combined after median filtering. A median filter provides image smoothing

but does not blur edges [34]. Horizontal and vertical vessels enhancement steps are combined by choosing the highest template response from the two steps at a given image coordinate.

The surrounding image edge effects are then 'trimmed off' since they are an artifact from the fundus camera. The binary vessel map is then formed by allowing the user to determine the thresholds for the binary function. The result is a white (255) vessel map on a black (0) background. The user is allowed to iterate as required to obtain the desired vessel map. To remove spot noise from the binary vessel map, each white (255) pixel is examined for connectivity. If a white pixel is found to have an adjoining white neighbor it is considered to be an information pixel otherwise it is considered spot noise. The spot noise identified pixels are immediately mapped to black (0). This results in a significant decrease in image spot noise.

After the binary vessel map is complete, the critical anatomy is protected by masking the critical area of the fovea and optic disk. The area surrounding the tracking templates is also protected to prevent irradiation and modification of these tracking landmarks. Lesion coordinates are then generated and stored in the patient's file.

Lesions are placed as prescribed for the treatment of diabetic retinopathy or retinal breaks or tears. The individual field of view data bases do not overlap. The LDB building process is summarized in Figure 4.6. The optic disk is visible in fields of view one through seven. Therefore, the optic disk and other vision critical anatomy must be identified and protected from lesion placement. Results are provided in Figures 4.7 through 4.11.

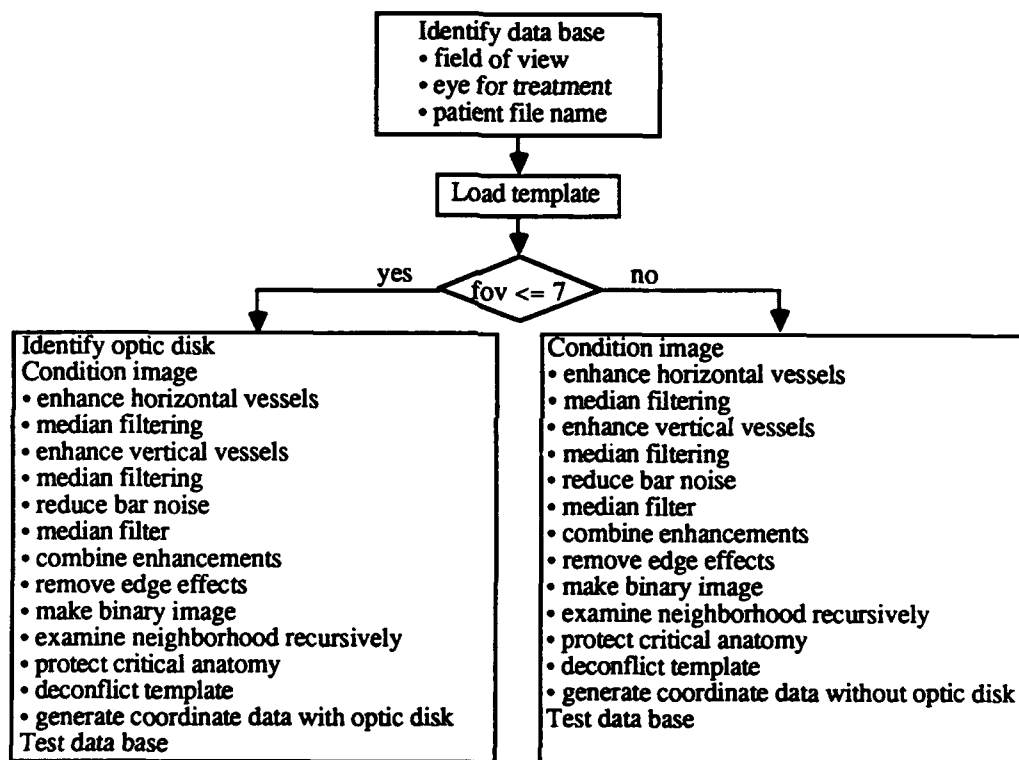


Figure 4.6: Lesion Data Base building

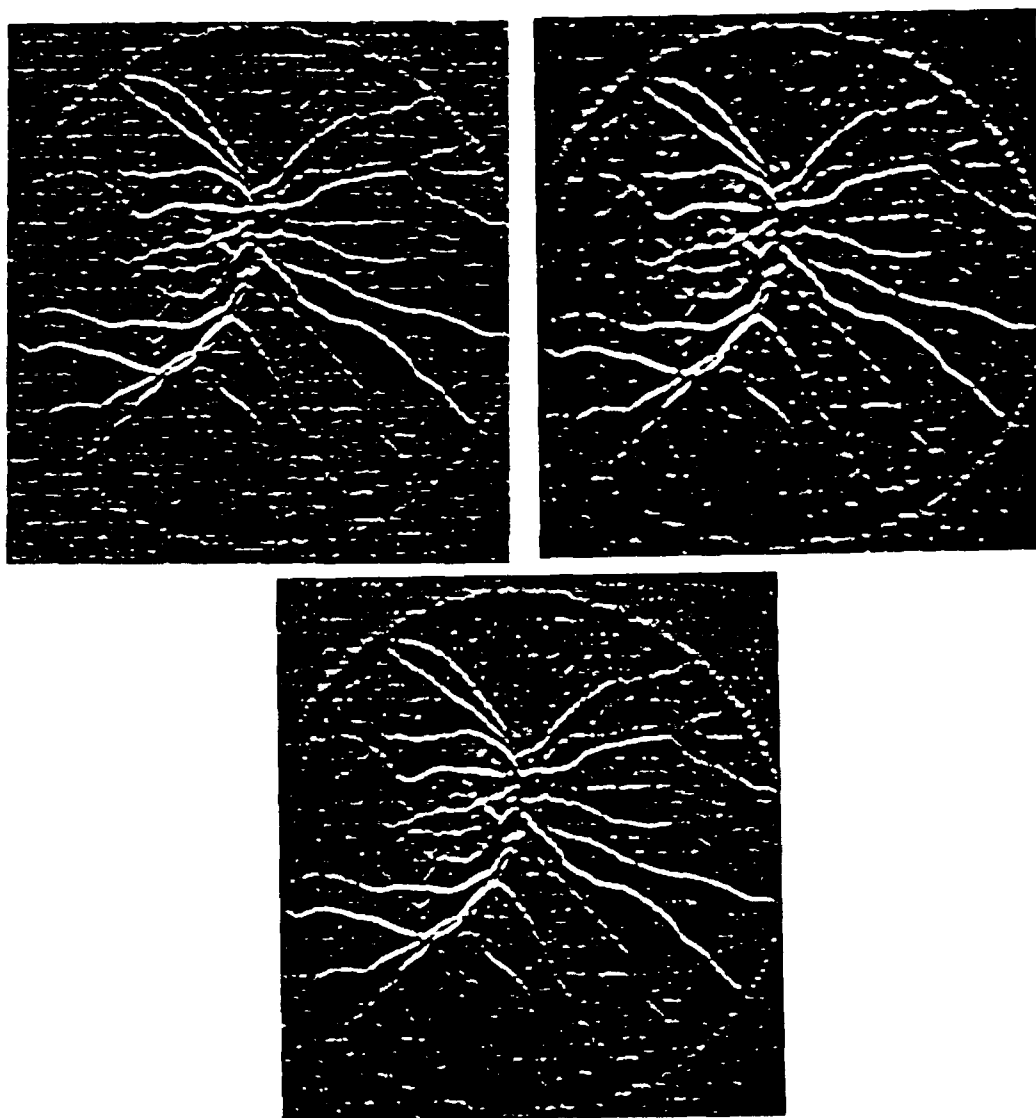


Figure 4.7: Left to right: enhance horizontal vessels, median filter, enhance vertical vessels

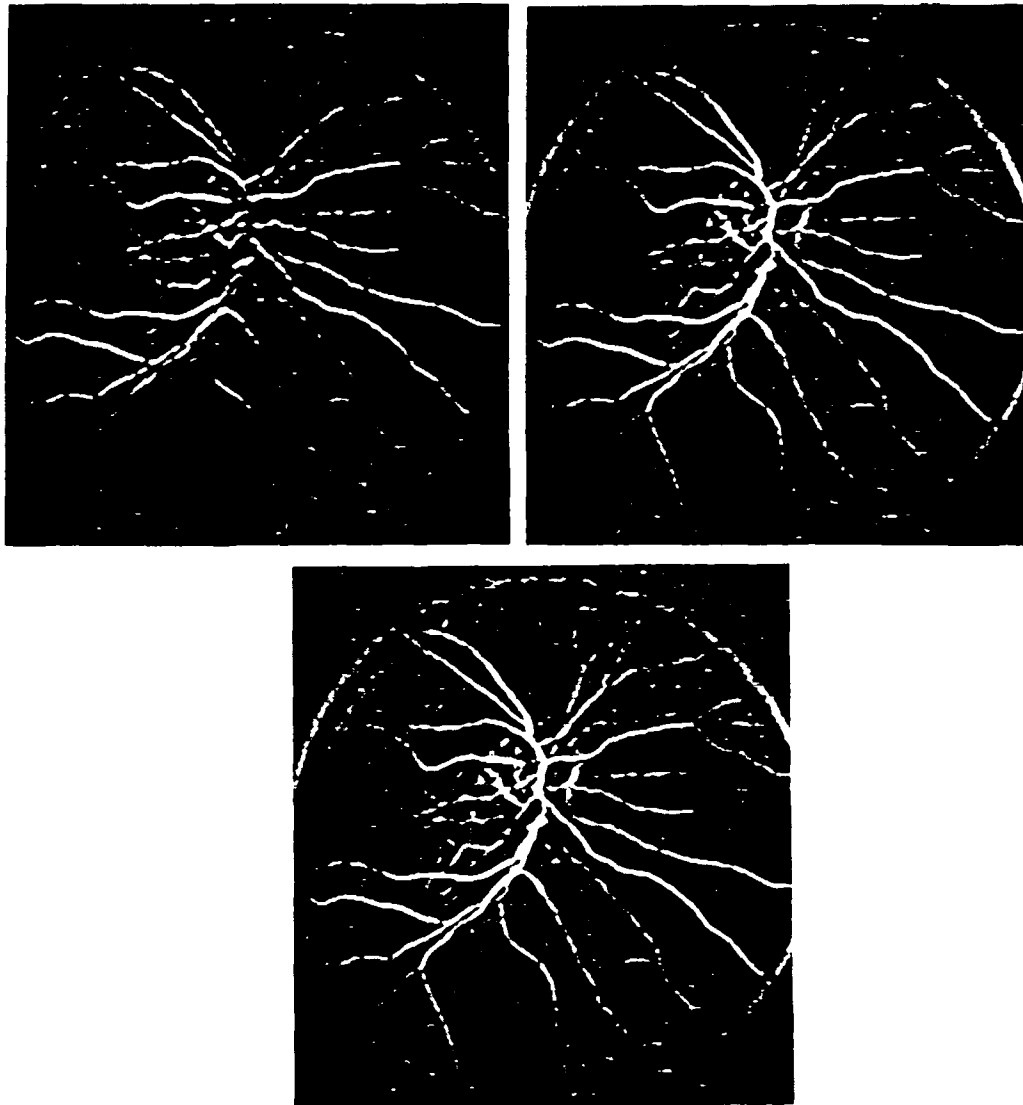


Figure 4.8: Left to right: median filter, reduce bar noise, median filter

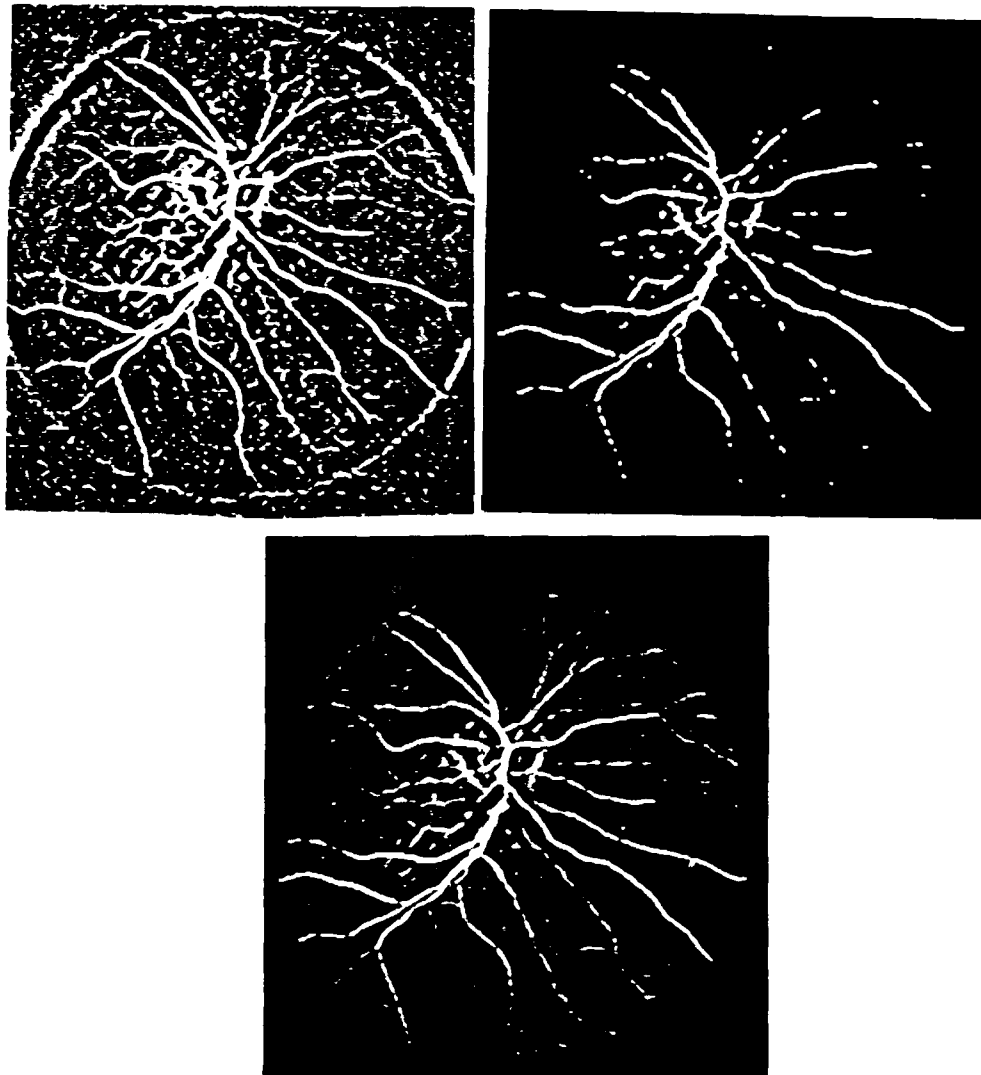


Figure 4.9: Left to right: combine horizontal and vertical enhancements, remove edge effects, binary image

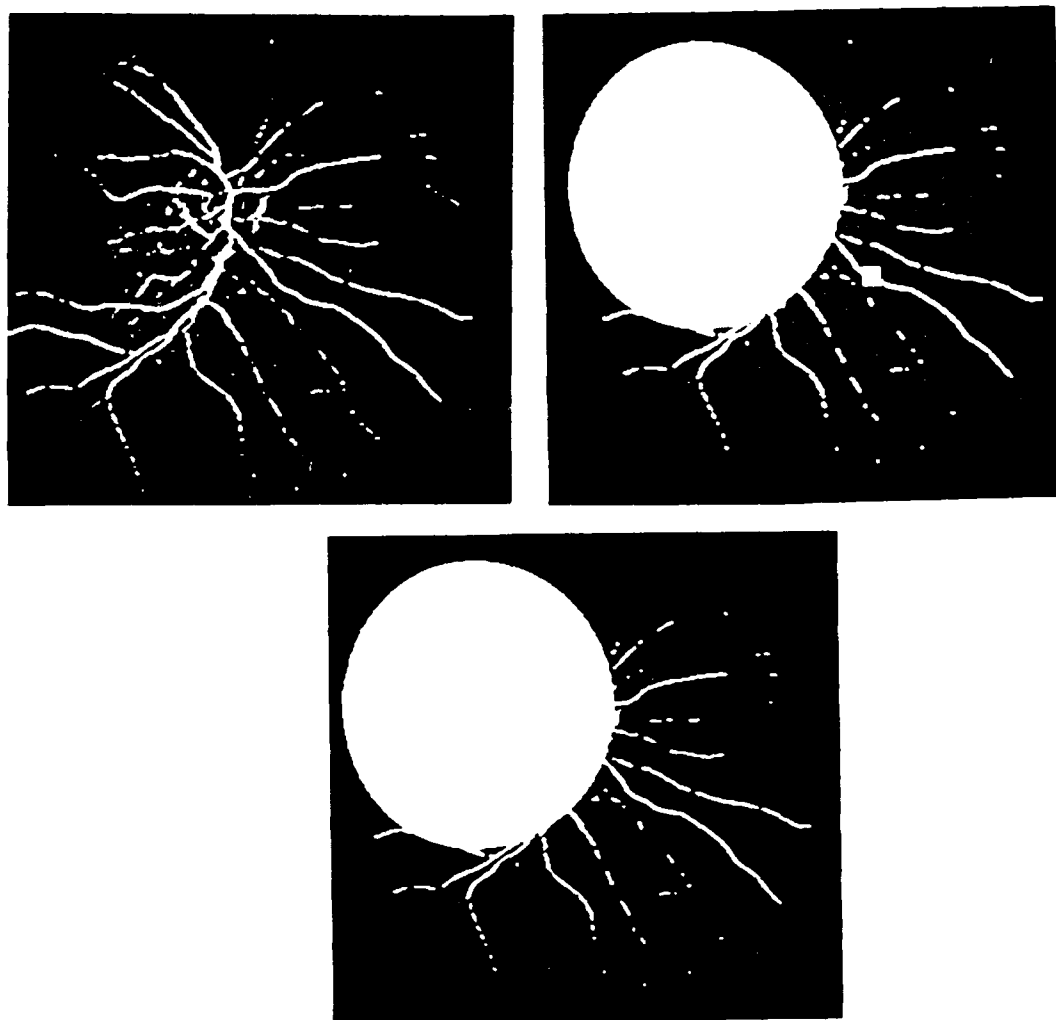


Figure 4.10: Left to right: examine neighborhood for connectivity, protect critical anatomy, plot coordinates

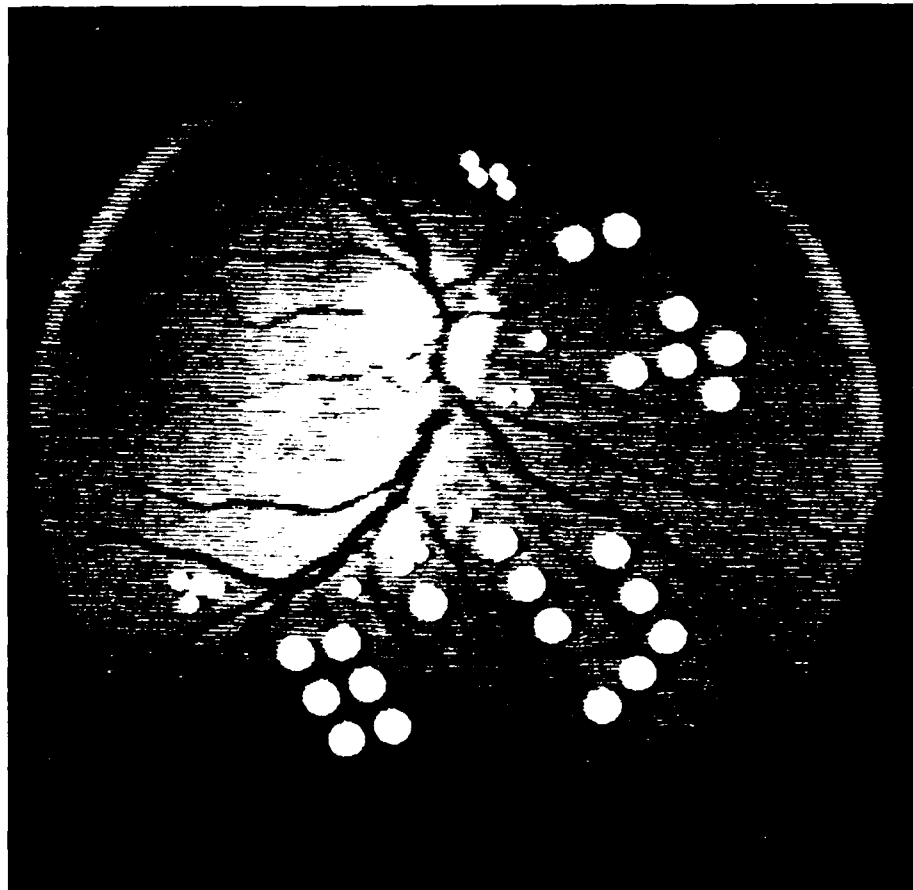


Figure 4.11: The final result

4.2.1 Panretinal Photocoagulation Treatment for Diabetic Retinopathy

As discussed earlier in this document treatment for diabetic retinopathy consists of placing laser lesions on the retina in a circular pattern about the region of critical vision anatomy. The lesion pattern consists of two rings of 200 micron lesions spaced 300 microns from center to center. The outer rings are 500 micron lesions spaced 750 microns center to center. The lesions are no closer than one-half of a lesion diameter from the nearest adjoining retinal vessel.

4.2.2 Treatment for Retinal Breaks or Tears

The treatment for retinal breaks or tears consists of placing two rings of 200 micron lesions about the damaged area. These lesions are placed 200 microns from center to center to form a continuous ring. The spacing between adjacent rings is 300 microns center to center [1, 53]. A separate imaging process is required to develop a LDB for treatment of retinal breaks or tears. This process must have the capability and flexibility to place lesions around retinal tears of irregular size and shape.

A flow chart for the algorithm developed to build a retinal break or tear data base is provided in Figure 4.12.

The initialization steps are similar to those for building a diabetic retinopathy treatment data base. These steps identify the field of view for treatment and generate hash markers for data storage in the patient's file. The boundaries of the treatment area are also defined to reduce the amount of processing time required to build the break or tear data base.

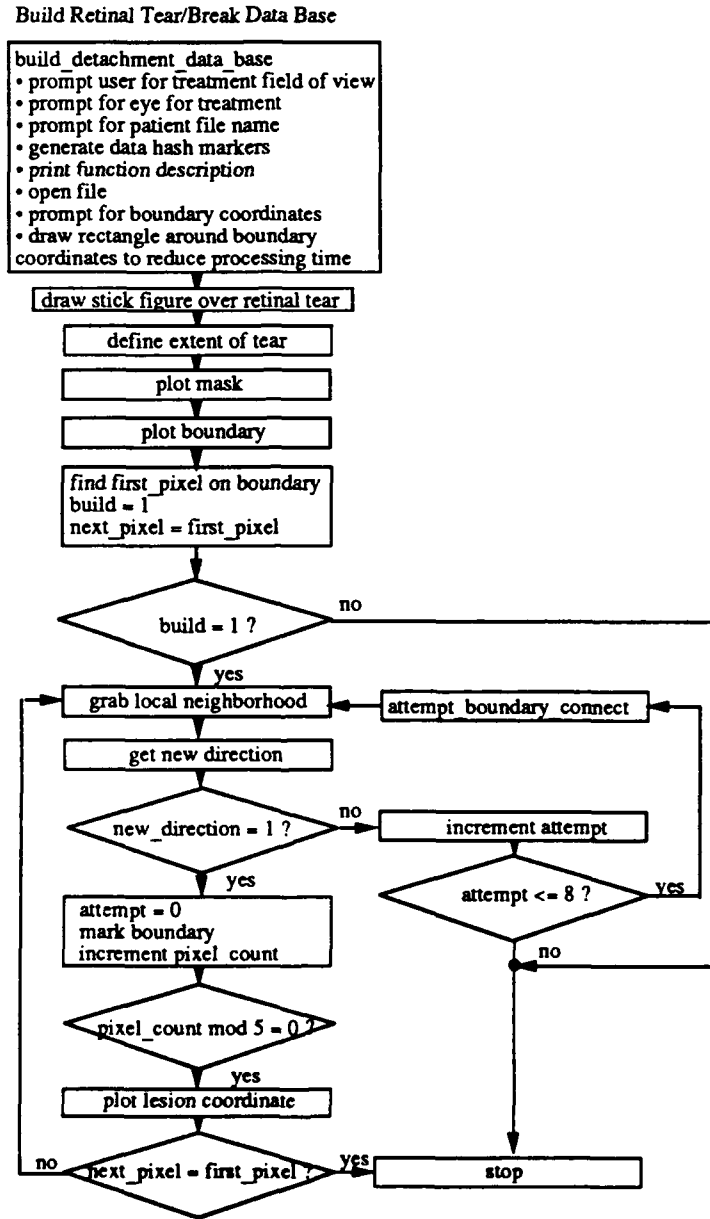


Figure 4.12: Retinal break or tear data base building.

The treatment data base is formed by drawing a white (255) 'stick figure' over the retinal tear. This figure may be any shape. However, the figure must be continuous. After the user draws the stick figure using the cursor control, a line is drawn from the stick figure to the edge of the detached area. This line defines the extent of the treatment area. The algorithm then masks the area over the stick figure. This is done by detecting the presence of the stick figure by searching for white pixels (255) in the treatment area. If a white pixel is found a circular mask is plotted at the white pixel coordinate with a radius equal to the extent of the the damaged area. This process continues over the entire stick figure. The result is a masked area about the detached area. A single pixel boundary is then plotted about the mask area by detecting the mask's edge.

Data base development continues by searching for a white boundary pixel within the defined treatment area. When a boundary pixel is found it is designated as the first boundary pixel. The boundary is then traced by examining the neighborhood of pixels about the first boundary pixel for another boundary pixel. If another white boundary pixel is found the new_direction flag is set. This process continues around the boundary until the boundary tracing operation returns to the first boundary pixel. At every fifth pixel (\approx 200 microns) around the boundary a lesion coordinate is plotted. The entire process is repeated with a larger mask to provide the second ring of 200 micron pixels.

If during the boundary tracing operation another boundary pixel is not found, the function `attempt_boundary_connect` tries to re-establish boundary contact about the last known boundary pixel. Up to eight attempts are allowed

in all directions from the last known pixel to re-establish the boundary tracing operation. The development of the retinal break or tear data base is illustrated in Figures 4.13 through 4.15.

4.3 Template Building

The next step after building the LDB is to construct a template for tracking retinal movement. In the actual software steps, template building precedes LDB building. This is required to protect the template tracking landmarks from lesion modification or destruction. This section details the construction of the tracking template. Template theory is reviewed followed by a review of previous work in this area. A detailed description of template selection follows.

4.3.1 Template Theory

Digital picture registration uses the technique of template matching [54]. Bovik provides a good review of the template matching theory [55]. The discussion below is based on his coverage of the topic.

Template matching is based on having a reference image of an object. For this discussion, this reference image will be designated as **I**. In the retinal tracker, **I** will be a 512 x 512 digitized image of the retina with 256 different gray levels of contrast. Multiple images of this type are required to map the retina. Only a single field of view will be considered at a time with the retinal tracker. Within the reference image **I** are distinct features. In the retina these features are the retinal vessels and photocoagulation lesions. The movement of these features between the reference image and subsequent images are used to determine overall retinal movement.

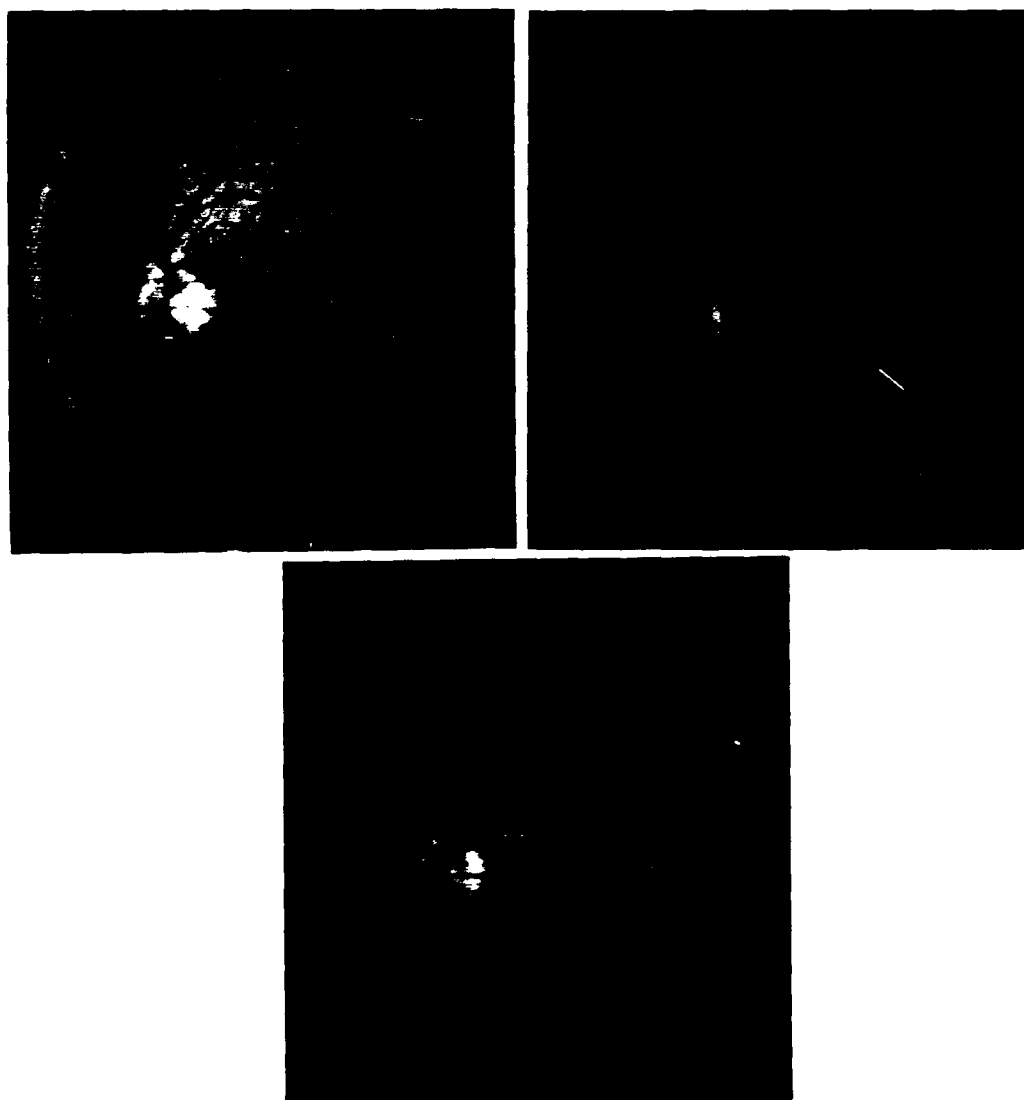


Figure 4.13: Left to right: simulated retinal tear, treatment area definition, drawing the 'stick figure'

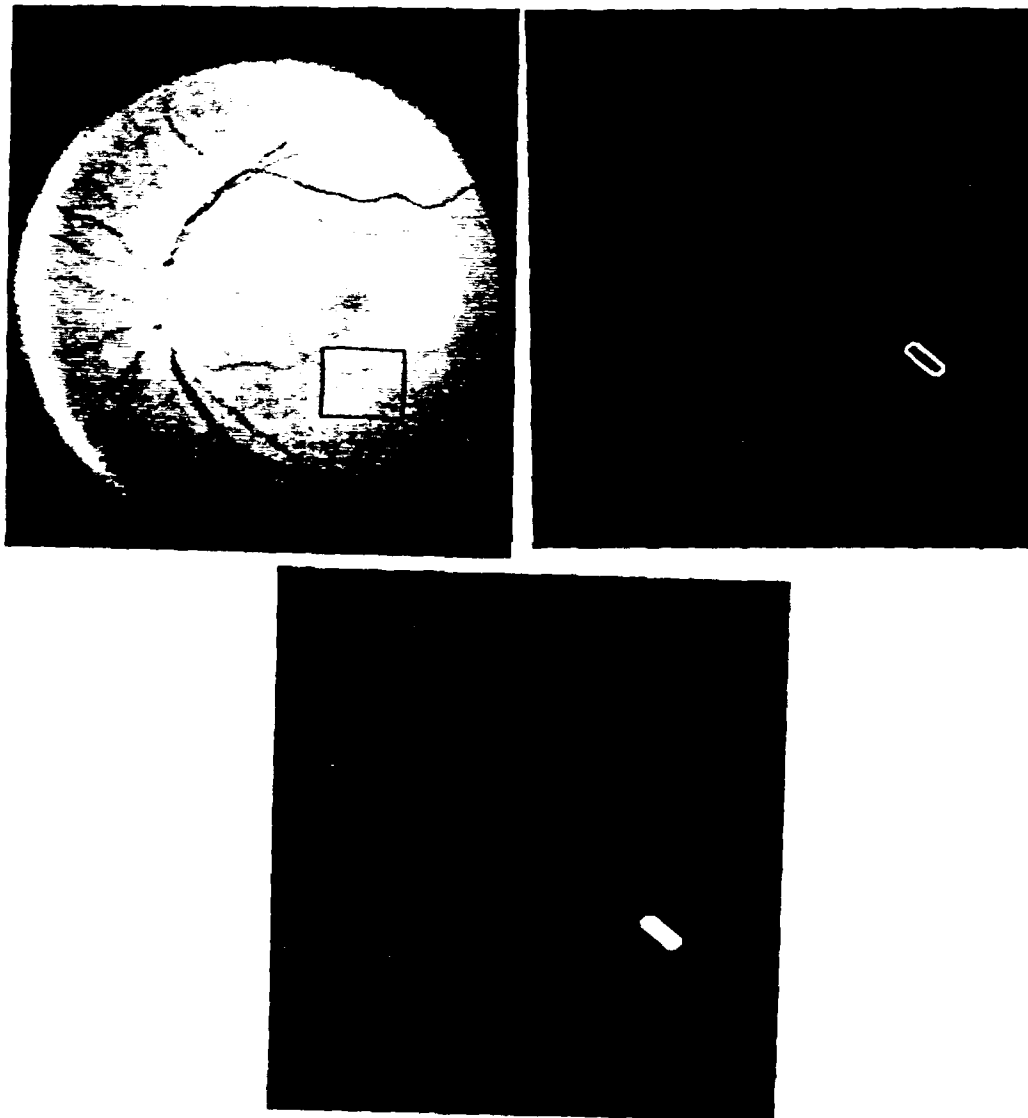


Figure 4.14: Left to right: defining extent of tear, the inner lesion ring mask, inner boundary

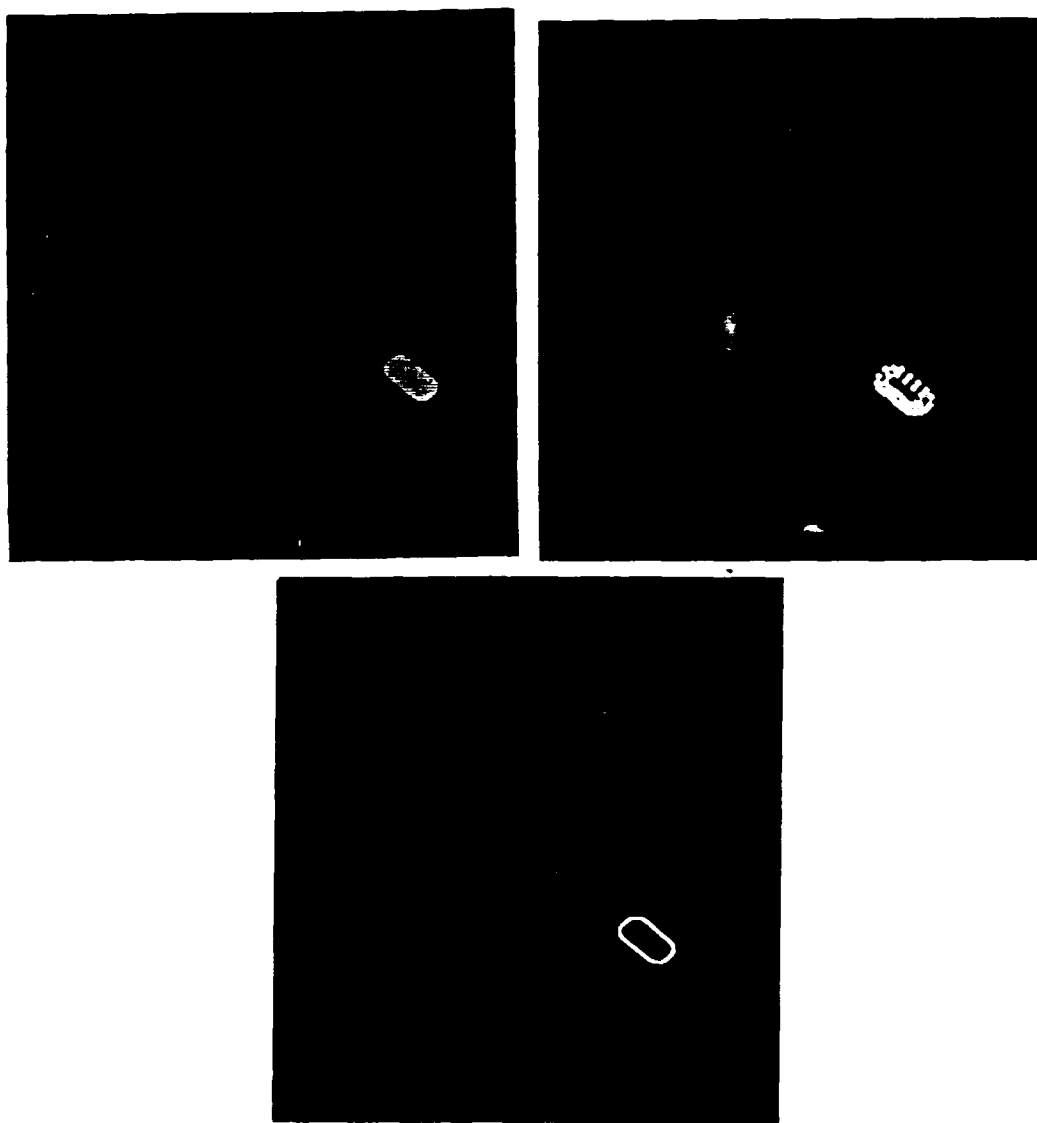


Figure 4.15: Left to right: the outer mask, outer boundary, final result

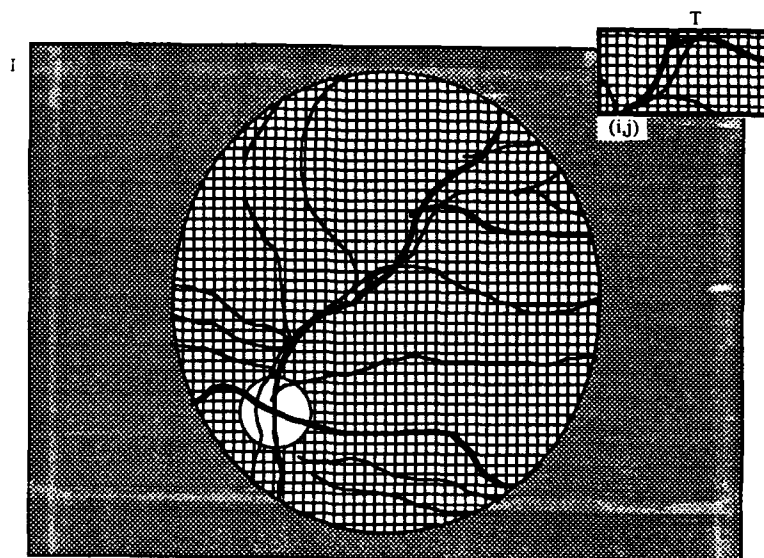


Figure 4.16: The image **I** and the template **T**.

A window may be constructed that contains one or more of the distinct vessel features. This window is a sub-image of **I**. This window designated as the template **T** is a sub-image of **I**. The $m \times n$ dimension of **T** is much less than the dimension of **I**. The relationship between **I** and **T** is diagrammed in Figure 4.16.

The template **T** will overlay the image **I**. The set of pixels covered by the template **T** when it overlays **I** at coordinate (i,j) is given by:

$$\mathbf{T} \cdot \mathbf{I}(i, j) = \mathbf{I}(i + m, j + n); (m, n) \in \mathbf{T} \quad (4.1)$$

There are several different 'match' measures that may be defined to determine the best match between template **T** and $\mathbf{T} \cdot \mathbf{I}(i, j)$. When **T** is placed at different coordinates on **I** and a measure is applied to each of these coordinates where **T** can be placed a match image **J** results. The match image

J will have a maximum (or minimum depending on the measure) at positions where a good match occurs.

Some measures are more appropriately designated as mismatch measures since they provide a small numerical value when gray levels in **T** and **T · I(i, j)** are similar. Different methods of measuring mismatch include maximum absolute error, mean absolute error, and mean-square error. The mean-square error technique can be dissected and modified to form a good match measure.

The mean-square error mismatch measure is given by:

$$MSE \mathbf{T} \cdot \mathbf{I}(i, j), \mathbf{T} = \sum_{m,n \in \mathbf{T}} [\mathbf{I}(i+m, j+n) - \mathbf{T}(m, n)]^2 \quad (4.2)$$

This measure can be decomposed into three separate parts including: a total template energy term $E_{\mathbf{T}}$ which is constant with respect to (i, j) , a local image energy term $E_{\mathbf{T} \cdot \mathbf{I}(i, j)}$ at (i, j) which provides no information on a specific **T** and a cross-correlation term of **I** and **T**.

The cross-correlation term is given by:

$$C_{\mathbf{I}, \mathbf{T}}(i, j) = \sum_{m,n \in \mathbf{T}} \mathbf{I}(i+m, j+n) \mathbf{T}(m, n) \quad (4.3)$$

The mean-square error with this terminology may be written as:

$$MSE \mathbf{T} \cdot \mathbf{I}(i, j), \mathbf{T} = E_{\mathbf{T}} + E_{\mathbf{T} \cdot \mathbf{I}(i, j)} - 2C_{\mathbf{I}, \mathbf{T}}(i, j) \quad (4.4)$$

Since the mean-square error is quantitatively small when there is a good match, $C_{\mathbf{I},\mathbf{T}(i,j)}$ must increase at this match location. Recall, $E_{\mathbf{T}}$ and $E_{\mathbf{T},\mathbf{I}(i,j)}$ are not affected by match conditions.

The Schwarz Inequality provides an upper bound on the size of the cross-correlation $C_{\mathbf{I},\mathbf{T}(i,j)}$.

$$C_{\mathbf{I},\mathbf{T}(i,j)} \leq \sqrt{E_{\mathbf{T},\mathbf{I}(i,j)} \cdot E_{\mathbf{T}}} \quad (4.5)$$

To determine the relative goodness of the match, the cross-correlation must be compared to this upper bound. This can be accomplished by defining the normalized cross-correlation $C'_{\mathbf{I},\mathbf{T}(i,j)}$ as:

$$C'_{\mathbf{I},\mathbf{T}(i,j)} = C_{\mathbf{I},\mathbf{T}(i,j)} / \sqrt{E_{\mathbf{T},\mathbf{I}(i,j)} \cdot E_{\mathbf{T}}} \quad (4.6)$$

Then:

$$C'_{\mathbf{I},\mathbf{T}(i,j)} \leq C_{\mathbf{I},\mathbf{T}(i,j)} \leq 1 \text{ for every } (i,j) \quad (4.7)$$

The normalized cross-correlation may then be thresholded by:

$$K(i,j) = 1 \text{ if } C'_{\mathbf{I},\mathbf{T}(i,j)} \leq t \quad (4.8)$$

to identify a point having a good match [55]. The threshold must distinguish between the single correct match and other potential match locations.

Once a match is determined, movement may be calculated. The difference in position between the template position on the **reference image** and

the template position on **subsequent images** provides a quantitative measure of retinal movement. This information may be provided as feedback to reorient the laser positioning mirrors to an updated position. The overall effect is to maintain the position of the laser on the same lesion location. The Retinal Tracking Subsystem must be able to resolve within the laser spot size to compensate for movement during irradiation. The response time of this system must be faster than typical eye movements - maximum velocity of up to 800 degrees per second and maximum acceleration of 40,000 degrees per second [2].

4.4 The Tracking Algorithm

Tracking the movement of the human retina is not a new idea. As early as 1968 West described a system for laser position control near the fovea [56]. According to Timberlake the system was probably not built [57]. Kelly and Crane completed a detailed study in 1968 for the National Aeronautics and Space Administration (NASA) for a fundus tracker. Their method involved "projecting a scanning pattern onto the retina, and detecting the translational and rotational movements of the reflected pattern by means of a certain type of high-speed correlation processing of the video signal." They visualized the real system operating at a rate from 200 to 1000 updates per second. Due to equipment limitations they tested their apparatus with video updates every few seconds [58].

Since that initial work many researchers have attempted to track the movement of the human retina using various technologies. This section begins with a review of previous tracking technologies and algorithms and concludes with a detailed description of the tracking algorithm developed for this project.

4.4.1 Previous Work

Double-Purkinje Image Eyetracker

A decade after the work of Kelly and Crane, Crane and Steele developed an optical system to track the movement of the retina using a double-Purkinje image method. This system, called the Double-Purkinje Image eyetracker, detected the reflection of a near infrared (0.93 microns) beam projected into the eye. The beam was reflected from the four optical surfaces of the eye: the anterior and posterior surfaces of the cornea and the anterior and posterior surfaces of the crystalline lens. These four reflected images are called the Purkinje-Sanson images I, II, III, and IV [16]. The tracker monitored the movement of the I and IV images to derive information on retinal rotation and translation. This system required a dental-impression bite board and a 2-point forehead rest to stabilize the patient's head against movement [59, 60]. Recent improvements in this design have resulted in tracking capability to a maximum of 100 degrees per second with a response time of 0.13 seconds [61].

Feature-Based Registration of Retinal Images

Several researchers have used the natural features of the retina, most notably the optic disk and the retinal vessels, to track retinal eye movement. Barnea and Silverman developed a sequential similarity detection (SSD) technique to measure eye movement. This technique reduced the computation time by a factor of 100 over then current cross-correlation techniques. The SSD technique uses the sum of the absolute values of the differences (SAVD) to measure the similarity of a reference template to an image. The similarity measure is defined by:

$$SAVD(m, n) = \sum_{j=1}^J \sum_{k=1}^K | F_1(j, k) - F_2(j - m, k - n) | \quad (4.9)$$

where:

- $F_1(j, k)$ is a $J \times K$ pixel template.
- $F_2(j, k)$ is a $M \times N$ pixel search area.

This technique provided normalization to account for illumination differences between the template and the search area and implemented a thresholding technique to reduce computation time. The thresholding technique was implemented by first examining similarity at only randomly selected points within the template. During the examination of similarity a running total of accumulated error was compared to the pre-established threshold. When the threshold was exceeded the similarity calculation for the template at the present search area location was aborted. Additional points of the template were compared with the search area if the threshold was not exceeded. The coordinate of the search area that allowed the most similarity point calculations prior to exceeding the threshold was declared the match [62].

Peli et al. [63] improved on the Barnea and Silverman algorithm by selecting template points for calculating SAVD from the positions of the vessels in the template. This modification reduced the computation time of the similarity measure. To further reduce processing time a two-stage template matching algorithm was also implemented. The two-stage process used a coarse search to determine the most likely area of the match. This was accomplished by skipping over rows and columns in the search area. The coarse search was followed

by a fine search about the coarse search match point. Although this technique reduced processing time, Peli noted the following: "The most important difficulty encountered with this coarse-fine approach is that coarse subsampling may actually skip the important points in the search area, resulting in erroneous determination in the first stage. This is especially true for a pattern with small, sharp details such as that seen in retinal vessels".

Acousto-Optical Cells

Ghaffari investigated using the optical image correlation technique for retinal tracking. In this technique, acousto-optical (A-O) cells performed the fine image matching operation. The cells "convert the real-time one-dimensional video information into a spatial light intensity controller system." Specifically, a two-dimensional template was generated to store a reference image. This image was then correlated to the real-time video frames. The results of this correlation was a new light distribution with a relative maximum located at the center of the best match. Retinal movement was calculated by measuring the movement of the relative correlation image maximum from one frame to the next. Ghaffari tested this system by tracking several different character symbols and simulated blood vessels. He reported "a $\pm 2.0\%$ linearity in the horizontal and $\pm 1.8\%$ linearity in the vertical directions. The tracking system can handle speed and acceleration of 656 degrees per second and 19,687 degrees per second² for 30 frames per second video rate. The accuracy of tracking is within ± 5 pixels in a 275 pixel square area" [49].

Scanning Laser Ophthalmology

Several researchers have used the scanning laser ophthalmoscope to track the movement of the retina. The algorithm developed calculates the cross-correlation between preselected binary templates with binary retinal images. The binary images are coded with +1 = white and -1 = black. This coding scheme allows the calculation of the Hamming distance as a mismatch measure between the template and the image under search. The researchers indicate that computation time may be reduced by performing the cross-correlation in the frequency domain using standard Fast Fourier Transform (FFT) techniques. This reduces the computation time to 2 seconds for a 512 x 512 pixel image. The tracker is able to compute the match position within 2 pixels of a 512 x 512 pixel image [64, 65].

Markow's Blood Vessel Tracking

Markow studied the digital retinal tracking problem in some detail. After reviewing many different tracking techniques he concluded that they were computationally exorbitant. However, he borrowed portions from these techniques to develop a tracking algorithm using blood vessel templates.

This tracking algorithm uses two one-dimensional (1D) blood vessel templates normally oriented to one another. One template is horizontal and the other is vertical. These two templates are bounded by the template window T discussed earlier in this chapter. The 1D templates' orientation is illustrated in Figure 4.17 [2].

The horizontal 1D template H_t and the vertical 1D template V_t are each a set of pixels. Each of the small squares within Figure 4.18 represents

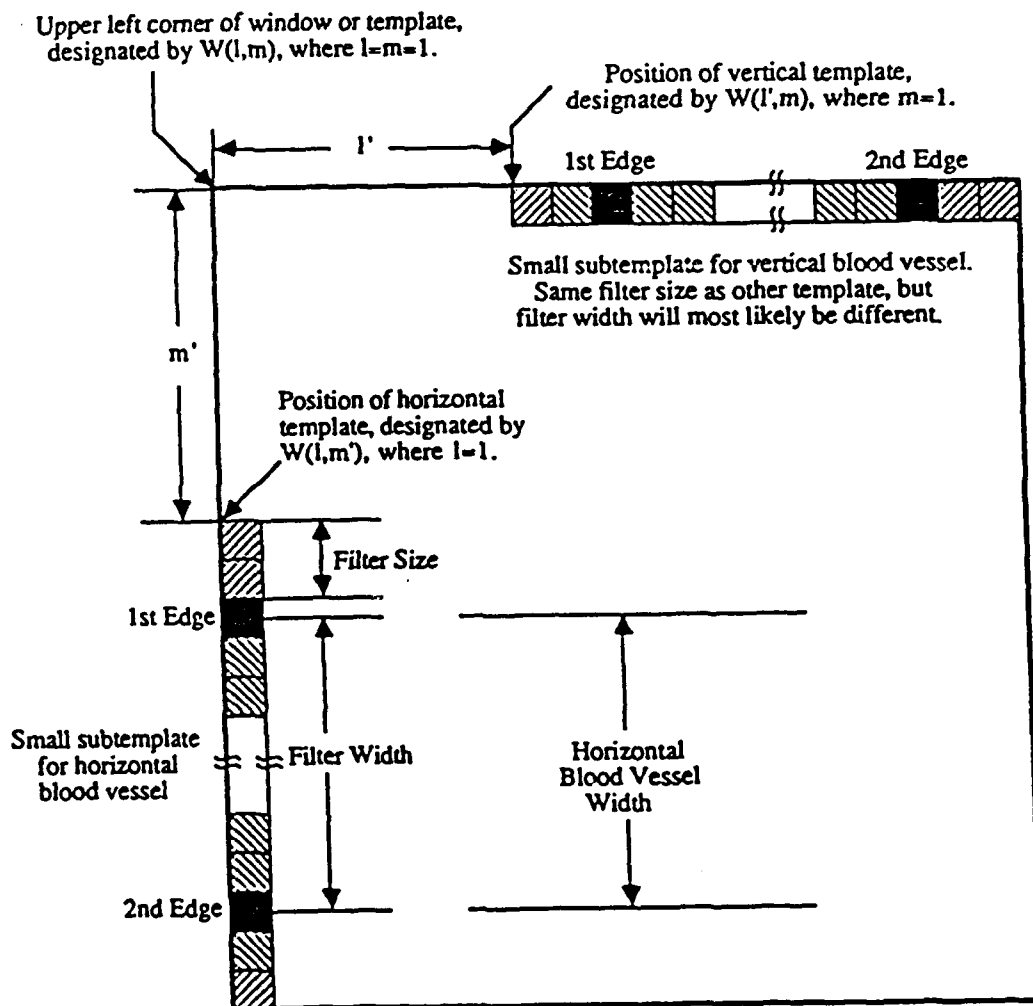


Figure 4.17: One dimensional template orientation [2]

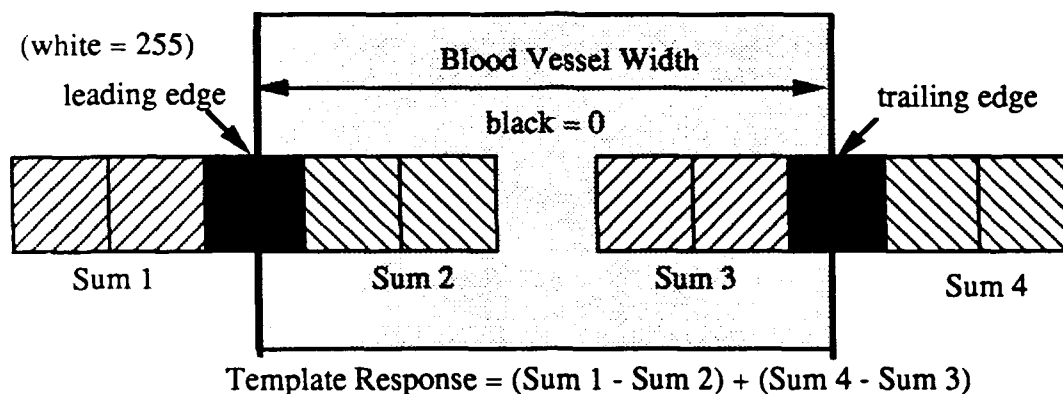


Figure 4.18: The 1D template. For an ideal image (a black (0) vessel on a white (255) retina) Sum 1 is 510, Sum 2 is 0, Sum 3 is 0, and Sum 4 is 510. The overall template response is 1020.

a single pixel. The small black squares represent where the edges of a blood vessel would occur. To search for a blood vessel of a specific width, pixels are inserted between the blood vessel edge pixels. The number of pixels inserted corresponds to the width of the blood vessel desired. Markow limited the number of pixels for insertion from 2 to 9 [2].

The 1D templates measure the template response to determine where a blood vessel's leading edge exists. To detect a blood vessel edge, the gray level values of the two pixels to the right of the small black squared are summed (Sum 2). Also the gray level values of the two pixels to the left of the black square are summed (Sum 1). Sum 2 is then subtracted from Sum 1. If a leading edge exists at the location of the small black square, a large number will result. For an ideal vessel edge (a black (0) vessel on a white (255) retina) the response is 510. The trailing edge of the vessel is found in a similar manner. The overall template response is the sum of the results from the leading edge

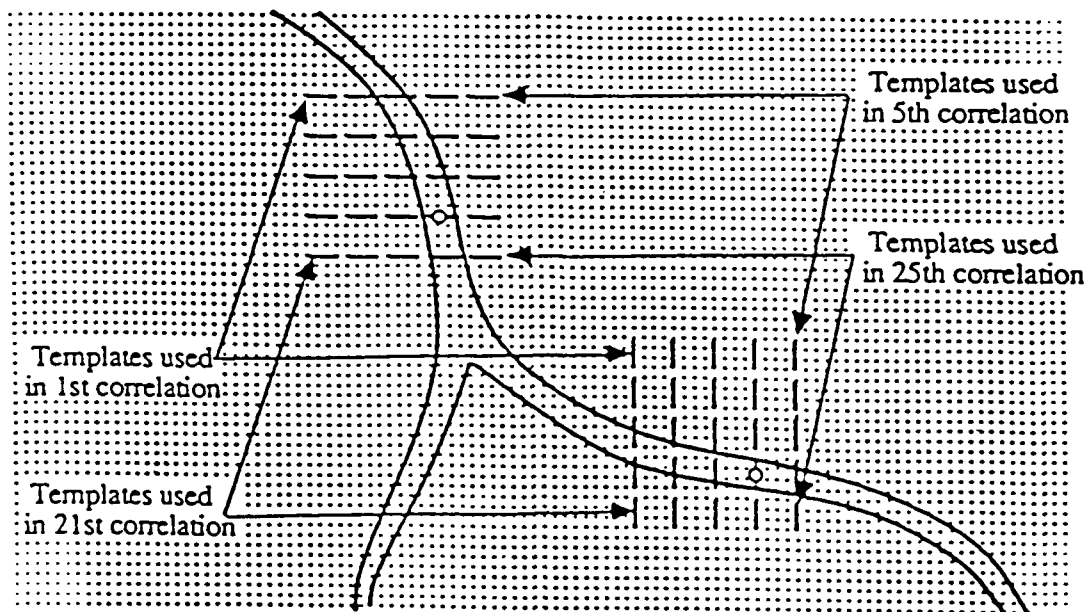


Figure 4.19: Using expansion in a 5 x 5 search pattern [2]

and trailing edge templates. If a blood vessel's edges align with the template, a large correlation value will result [2].

Templates H_t and V_t are initially selected by scanning the templates of various widths over the reference image. The 1D templates with the highest correlation are retained to construct the two-dimensional (2D) template. The 2D template consists of a horizontal and a vertical template pair locked together in a known orientation. The 2D template is used for retinal tracking [2].

In an effort to speed up the template searching process, Markow implemented expansion techniques. Rather than shifting the template a pixel at a time during the search, it was shifted over every fourth pixel in a 5 x 5 pattern. This was followed by a fine search about the maximum point determined by the coarse search. Reference Figure 4.19 [2].

Markow initially tested this blood vessel template algorithm on a sim-

ulated blood vessel. Qualitatively, he demonstrated the capability of the algorithm to distinguish between the correct match and false positives. In all test cases, the correct match had the highest value of correlation. The ratio of the largest possible false positive to the true match decreased as the template used more 1D templates and wider filter widths. The results were inconclusive concerning the optimum filter configuration. Markow tested the algorithm on a slowly rotating fundus photograph. The tracker was able to maintain lock on retinal images rotating at 0 Hz, 1/3 Hz, 1-1/2 Hz and 5 Hz. At higher frequencies, the tracker could not establish initial lock. Markow also noted that in all test cases the precalculated expected value of template correlation was much higher than the actual correlation value obtained with the tracking system [2].

Concerns for the Markow Tracking Algorithm The Markow Tracking Algorithm was investigated in detail as a starting point for this research effort. Markow did an **excellent** job documenting his successes and areas of further research [2]. After spending several months testing the algorithm and attempting to optimize template selection for accuracy and speed, the following areas of concern were identified:

- Markow employed a coarse-fine search technique to reduce computation time in the searching process. As Peli [63] described "coarse subsampling may actually skip the important points in the search area". I rewrote Markow's tracking algorithm in C and attempted to maximize the accuracy of the algorithm using his template scheme. The algorithm was then tested on actual human retinal images in which movement was simulated by picking different search initialization coordinates. A success rate of

approximately 58% (the success rate is defined as correct match coordinate found/total number of searches) was obtained at a skip increment of four pixels. The major cause of the inaccuracy was the coarse search skipping over the correct coarse search pivot point.

- Since a coarse-fine search technique was used it was doubtful that a 100% accuracy rate could be obtained.
- The template Markow employed was not normalized. Therefore, any variation in retinal image intensity and nonlinear imaging device response could result in an erroneous determination of the template match.
- The template developed by Markow provided a positive response over a multi-pixel region as illustrated in Figure 4.20. This is a sound idea for a coarse-fine based tracking algorithm; however, it could result in false positives.
- As cited by Markow, the algorithm could not determine a loss of lock condition [2].
- The algorithm did not provide for the patient to halt the tracking and laser irradiation process.

Due to these areas of concern, a different method of tracking the movement of blood vessels was required to improve the accuracy and speed of the algorithm.

Mayan Templates My colleague, Dr. Maya Jerath, suggested using a 'spatially tuned' skip increment to increase the success rate of the coarse-fine search

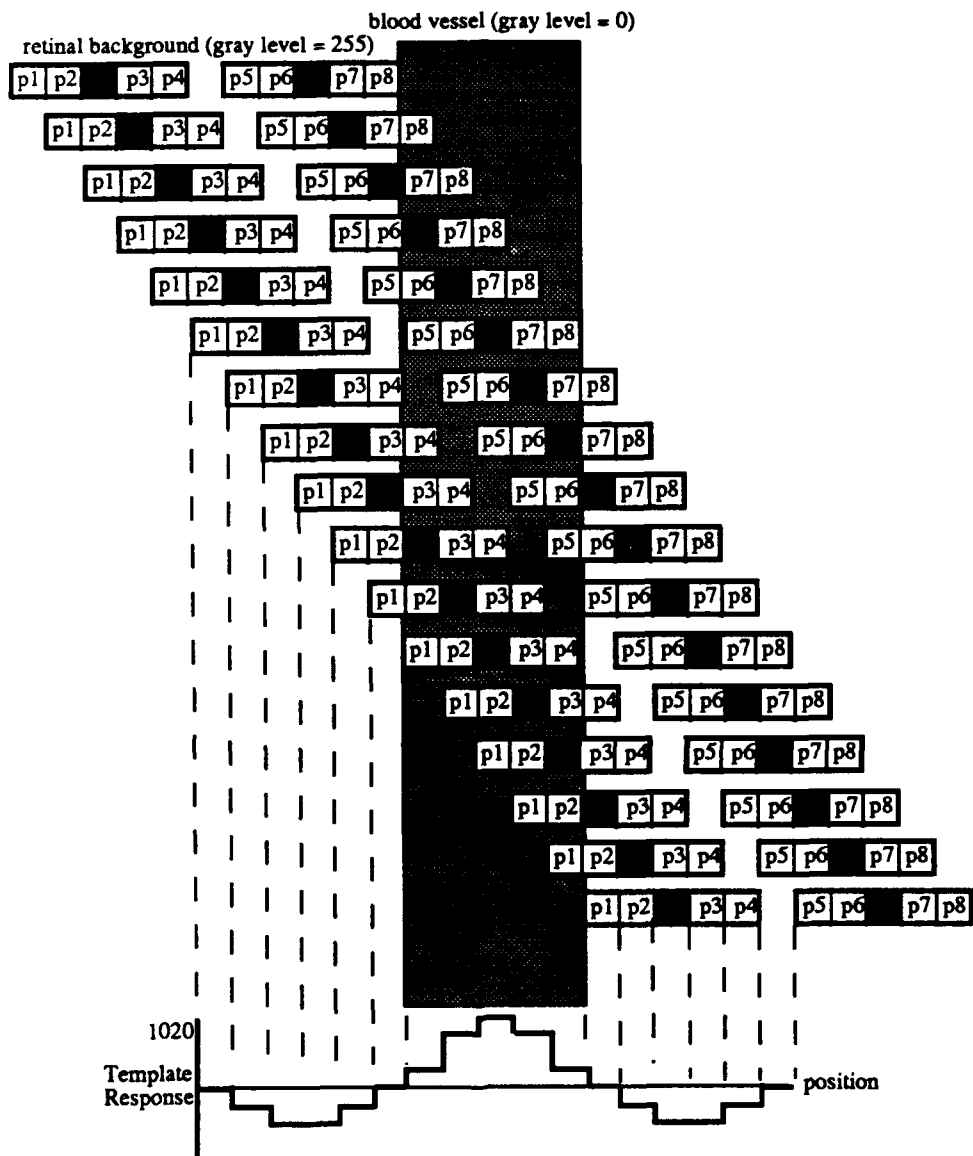


Figure 4.20: Response of the Markow template in the vicinity of a blood vessel. This figure illustrates the response from a single template in the vicinity of a vertical blood vessel. The template is swept horizontally across the vessel. Different horizontal template positions are illustrated. The template response for an ideal vessel (a black (0) vessel on a white (255) retina) at each template position is provided on the template response plot.

technique. Her idea, which I've termed 'Mayan Templates', uses a coarse search skip increment equal to the width of the vessel template used in the search. I modified Markow's algorithm to test this concept. This modification allowed a separate skip increment for both the horizontal and vertical directions. I repeated the tests performed on the Markow algorithm. The success rate improved to approximately 67% for all images tested (enhanced fundus images, fluorescein angiogram images, and scanning laser ophthalmoscope images). The success rate was approximately 83% for enhanced fundus images. Although, this idea significantly improved the success rate. I felt that an 83% success rate was unacceptable for equipment used to control photocoagulation of the human retina.

Branch Point Tracking

Similar to the work of Markow is the work of Yu et al. This research team has developed a tracking algorithm based on detecting the movements of retinal vessel branch points. Their algorithm tracks retinal movement by detecting the location of the optic disk via thresholding and three predetermined vessel branch points. The orientation of the optic disk centroid to the three vessel branch points forms the complete tracking template. The calculated displacement in retinal drift provides the driving signal to a two-dimensional driving stage which controls the deflection mirror in a slit lamp microscope [66].

The system has been implemented on an Intel 30386 based personal computer operating at 33 MHz. With this computation power the whole eye-tracking process, including calculation of drift and deflection mirror adjustment, requires 1 second. A resolution of one pixel (20 microns) is reported [66].

Yu's description did not indicate how field of views not containing the optic disk are handled.

Dedicated Fast Fourier Transform (FFT) Processors

Considerable research is currently ongoing toward using dedicated, high speed reduced instruction set (RISC) processors to perform FFTs. These processors are being developed to provide tracking capability by performing template matching in the frequency domain. The tracking is performed by taking the two-dimensional FFT of the input image and multiplying it with a frequency domain template of the object to be tracked. The result of the multiplication is inversed transformed. The result is a peak response at the point of match between the image and the template. Current processors have the capability to provide a tracking update 15 times per second for a 256 x 256 input image [67]. This is similar to Ghaffari's optical correlation technique.

4.5 The Algorithm

This section details the tracking algorithm designed and implemented for this research. The section begins with a review of the key assumptions on which the tracking algorithm is based. A detailed description is then provided on the methodology and implementation of Spatially Distributed Normalized (SDN) templates. The section continues with a detailed description of the tracking algorithm and its features. The section concludes with a summary of results for the tracking algorithm.

4.5.1 Assumptions and Validity of Assumptions

The tracking algorithm is based on the following assumptions:

Exhaustive search required for 100% success rate To approach the desired 100% success rate, an exhaustive search of the image search area is required. An exhaustive search is defined as a pixel-by-pixel scan of the search area to find the match coordinate. Tests conducted using various skip increments indicates that the success rate increases as the skip increment decreases. Even at a skip increment of two pixels, errors caused by the coarse-fine search technique result.

Limiting Eye Movement With Fixation As mentioned in Chapter 2 of this document, the eye has a velocity of up to 800 degrees per second with saccadic eye movement. Eye movement may be minimized by having the patient fixate on a target with the conjugate eye while the other eye is being treated. Studies conducted by Kosnik et al. [18] indicate that fixation capability does not decrease significantly with age. This is important since diabetic retinopathy is predominant in the elderly population.

By using a fixation device eye movements are theoretically relegated to micro-saccades and micronystagmus since other types of eye movement are for acquiring a moving object, tracking a slowly moving object, and maintaining fixation on an object as the observer moves. Based on this concept the developmental tracking algorithm has been designed around a maximum eye velocity of 50 degrees per second. This velocity defines the size of the search area as follows:

- The posterior nodal distance of the eye is 16.7 mm[16].
- The velocity of retinal movement at 50 degrees per second may be converted to millimeters per second using an arc length calculation:

$$(50 \text{ degrees/s})(2\pi/360 \text{ degrees})(16.7\text{mm}) = 14.6 \text{ mm/s} \quad (4.10)$$

- The standard frame rate of 30 frames/second provides an image update every 33.3 milliseconds
- The distance that a point on the retina may move during 1 frame is then:

$$(14.6 \text{ mm/s})(33.3 \text{ ms}) = .48 \text{ mm/frame} \quad (4.11)$$

- At a 50 degree fundus camera field of view a single pixel displays a 46.4 micron (horizontal) by a 35.3 micron (vertical) area. This area has been measured with function `measure_displacement`. Function `measure_displacement` measures the displacement between two user placed cursors. The function is calibrated to the known dimensions of the optic disk.
- This equates to a movement of 14 pixels in any direction during a frame and a search area of 28 x 28 pixels. For safety the calculated area is expanded to a 40 x 40 pixel search area.

Minimization of rotational and scaling movements Since a fixation device is used, rotational and scaling movements are minimized. The only movement considered by the tracking algorithm is translation. The validity of this assumption has been tested by examining four different retinal movement

sequences in which fixation was used. A detailed description of the taped subjects is provided in Chapter 8. The subjects will be referred to as RCL, CSL, SBR, and ICR. A scattergram plotting the optic disk centroid for each sequence has been constructed using techniques similar to those of Kosnik et al. The centroid location was plotted over a 45 second period. Rotation was measured by comparing the orientation of three landmarks in each frame. Scaling was measured by measuring the optic disk image diameter with a caliper in each frame. No rotational or scaling movements have been observed. This is consistent with the findings of De Castro et al [68]. Also, no repeatable pattern has been observed in the translational movement.

To further substantiate the two previous assumptions a 40 x 40 pixel area was 'snapped' over a 3 minute period from subject SBR's retinal movement sequence. The results are illustrated in Figure 4.22. It was clear from this time record that rotation and scaling is minimized with fixation and the 40 x 40 search area calculation appears valid.

Conjugate Eye Movement The use of a fixation device to minimize eye movement in the conjugate eye while the other eye is being treated depends on the eyes moving as a conjugate pair. In most eye movements the eyes move together. All of the oculomotor control systems previously discussed in chapter 3 must move the eyes together precisely to maintain binocular vision. Misalignment, called heterotropia, is due to abnormalities of muscles or nerves [69]. The tracking system will continue to operate correctly in the event of misalignment if the patient is able to fixate. If the patient is not capable of holding fixation the system will continue to operate within the 50 degree per

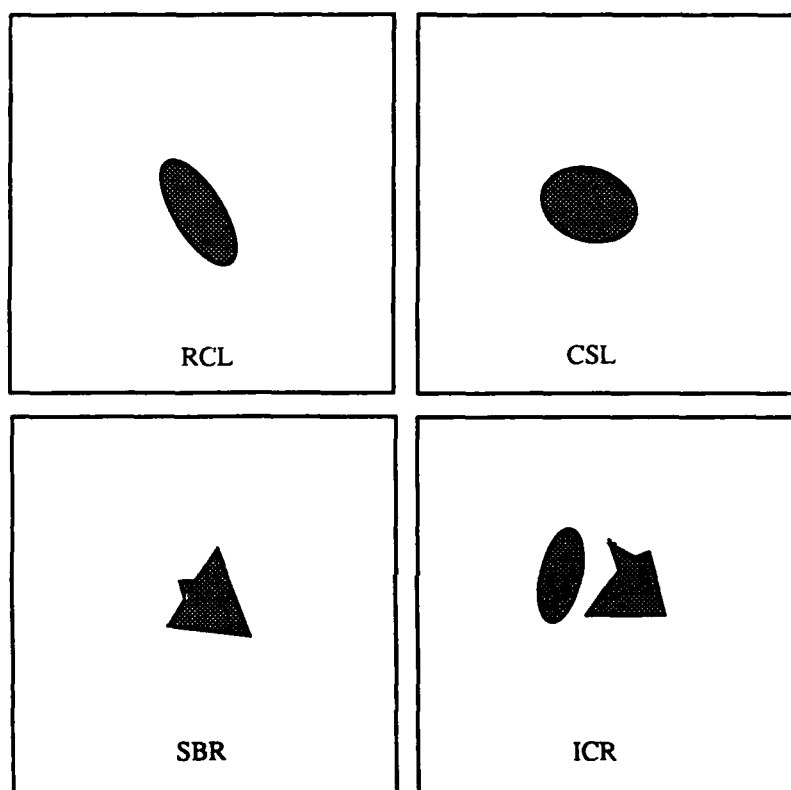


Figure 4.21: Scattergram of retinal movement for subjects RCL, CSL, SBR, and ICR. The shaded region demarcates the limit of movement for an arbitrarily chosen retinal landmark during a 45 second retinal movement sequence filmed using subject fixation. The diameter of the shaded region did not exceed 1.8 mm for subjects RCL, CSL, and SBR. Subject ICR's retinal movement was confined to two similarly sized regions. The fixation target was a small (.315 cm diameter), red light emitting diode. No rotational or scaling movements were observed in any of the sequences.

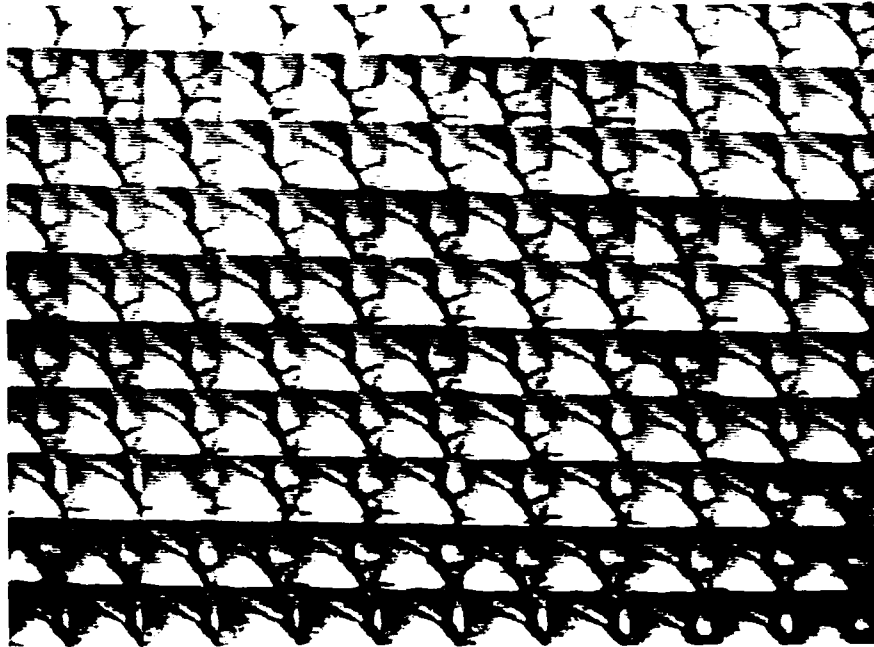


Figure 4.22: Time record of the 40 x 40 pixel search area. The same 40 x 40 pixel area was 'snapped' from a video sequence of subject SBR's retina.

second retinal velocity envelope. If this retinal velocity is exceeded the tracking algorithm will register a 'lost lock' condition and then attempt to re-establish lock.

Visible Tracking Features The tracking algorithm described in this section requires visible landmarks (i.e. vessels) to track the movement of the retina. Chapter 7 describes an algorithm to track the movement on a featureless retina.

Linearity of Retinal Reflectance The templates designed for the tracking algorithm depend on a linear relationship between the fundus illumination and the fundus reflectance. This assumption allows tracking to continue in the presence of an unstable illumination source. To test this assumption a video-

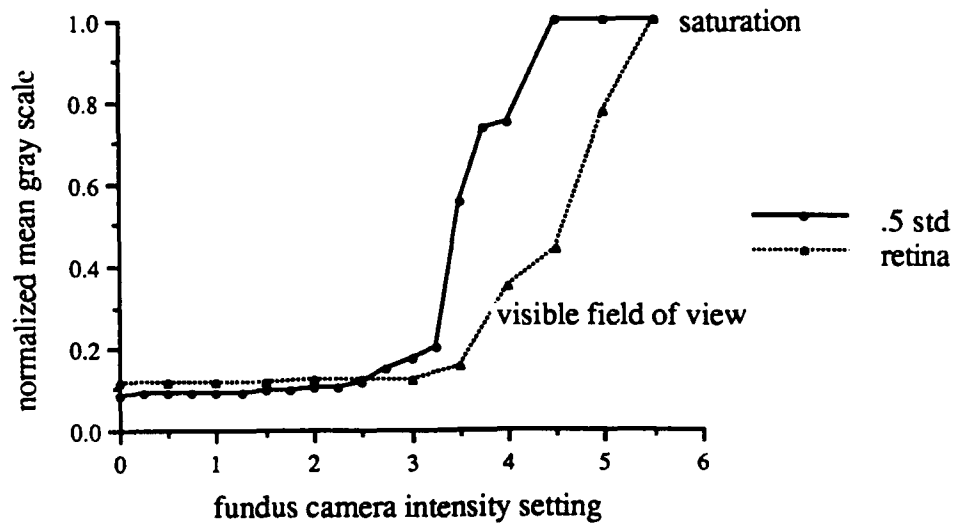


Figure 4.23: The linear relationship between average fundus reflectance and illumination

tape was produced of human retinal movement with fixation during different levels of fundus illumination. The average image gray level was measured over a 225 x 225 pixel area at different levels of illumination. The average gray level was measured over a large image area to minimize the effects of small retinal movement on the measurement. Also, the average gray level of a Labsphere .50 reflectance standard was measured. The average gray level was measured in a 25 x 25 pixel area. In both cases, a linear relationship was observed once a lower illumination threshold was exceeded. Slight deviations from the linear response are due to nonuniform CCD pixel response and slight retinal movement from frame-to-frame. The results are graphed in Figure 4.23.

4.5.2 Geographic Distributed Normalized Blood Vessel Templates

The first step in developing the tracking algorithm was designing an effective template methodology. The template developed for the tracking algorithm is illustrated in Figure 4.24.

This template has the following features:

- The template requires the use of only four pixel gray levels.
- The template has the flexibility of variable width. This idea was adapted from Markow's template [2].
- The template provides a positive response at only a single coordinate. This prevents the possibility of generating a false positive. Reference Figure 4.25.
- The template is normalized. Ideally, it should provide the same response under varying fundus illumination levels.

The template response

The template response is provided by:

$$\text{template response} = (p_1 - p_2 - p_3 + p_4) / (p_1 + p_2 + p_3 + p_4) \quad (4.12)$$

For an ideal edge (a black (0) vessel on a white (255) retinal background) the template response is:

$$\text{template response} = (255 - 0 - 0 + 255) / (255 + 0 + 0 + 255) = 1 \quad (4.13)$$

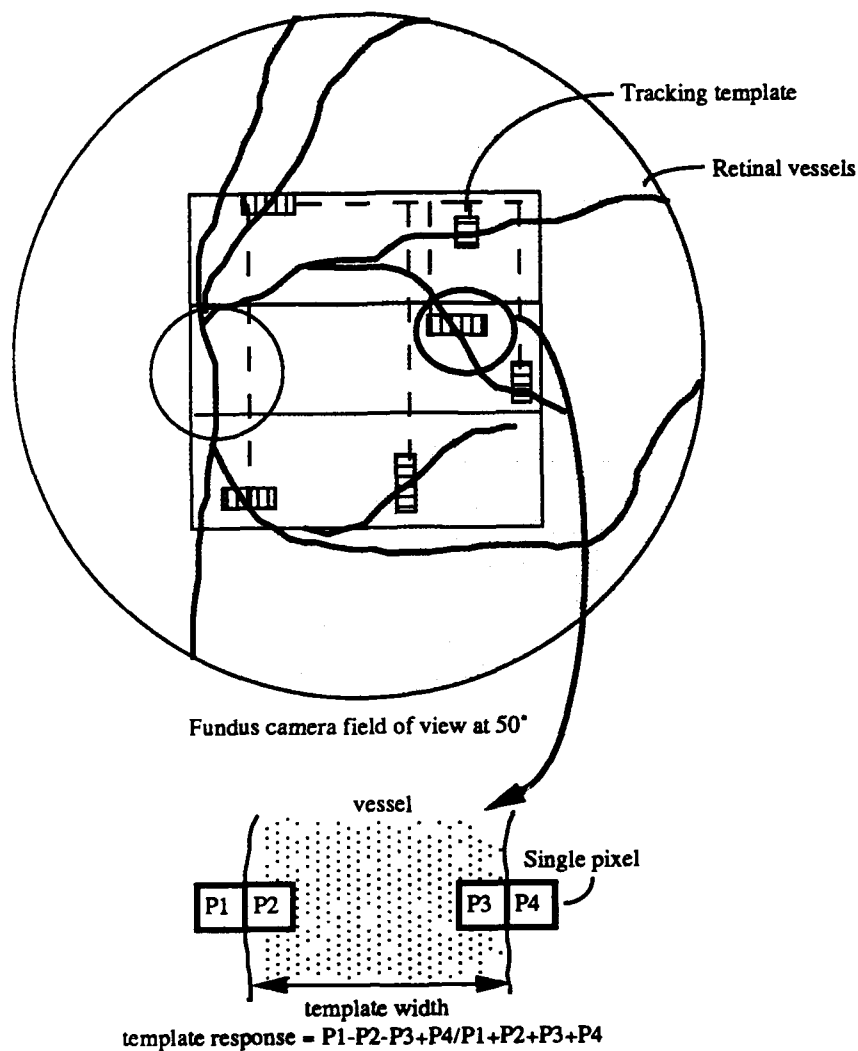


Figure 4.24: The tracking template. Six of the one-dimensional templates are used to build a single two-dimensional template. A pair of horizontal and vertical one-dimensional templates are selected from each third of the central portion of the reference image demarcated with heavy black lines above. The horizontal template chosen from the upper third of the reference image is designated the **first horizontal template**. All of the other five one-dimensional template locations are referenced to the first horizontal template's location. The response of each one-dimensional template is normalized as shown in the normalized template response equation.

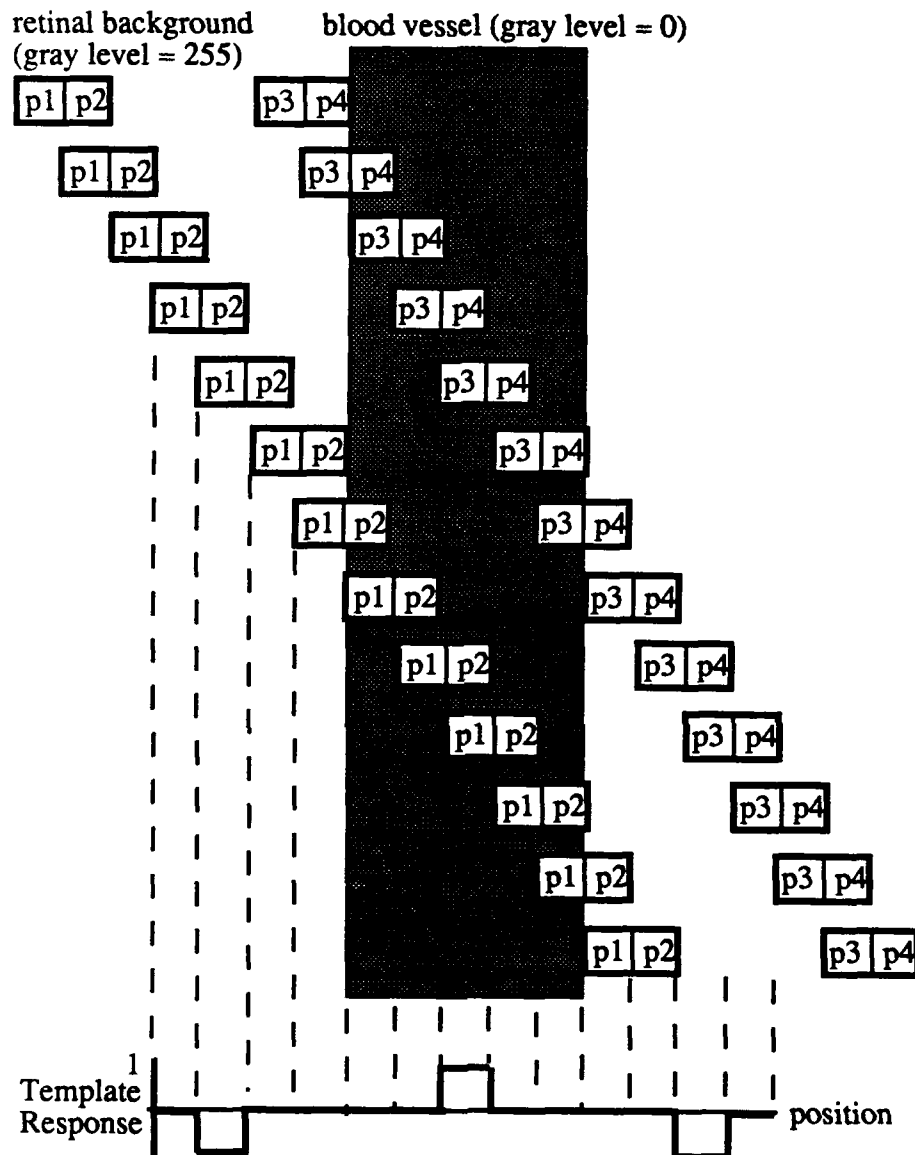


Figure 4.25: Normalized template response. Response of the normalized template in the vicinity of a blood vessel. This figure illustrates the response from a single template in the vicinity of a vertical blood vessel. The template is swept horizontally across the vessel. Different horizontal template positions are illustrated. The template response for an ideal vessel (a black (0) vessel on a white (255) retina) at each template position is provided on the template response plot.

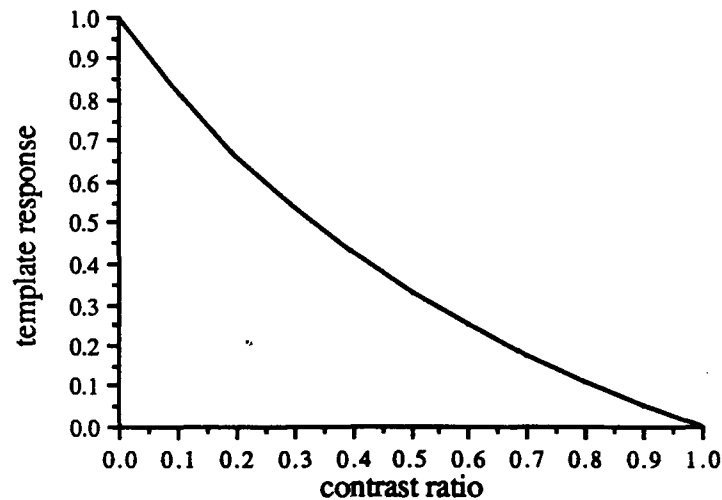


Figure 4.26: Theoretical template response. The contrast ratio is the ratio of vessel gray level to retinal background gray level.

Figure 4.26 provides the template response for all combinations of retinal vessel and background gray levels. Note that the peak response occurs for the highest degree of dissimilarity between retinal vessel and retinal background gray levels.

Automatic selection of the template pairs.

An algorithm was developed to automatically select the optimal pairs of templates from different areas of the reference image. The overall result of this template selection is a two dimensional template which has an optimal template pair chosen from each third of the central portion of the reference image. Reference Figure 4.24.

This spatial distribution of templates reduces false positives. If template pair selection is not spread across the reference image, all of the template pairs are clustered about the same small image area. This clustering of templates leads to false positives since nearby pixels have similar template response.

```

-----template_array-----
horizontal template | vertical template
[0] [1] [2] [3] [4] [5] [6] [7]
x_off y_off width x_cor x_off y_off width y_cor
[0] 0 0 3 17 -2 -12 11 24
[1] -5 43 3 18 37 68 3 23
[2] -26 87 3 27 -23 84 3 27
Total template correlation: 136

```

Figure 4.27: The template array.

Individual template pairs are found by scanning one dimensional horizontal and vertical templates within the partitioned reference image. The horizontal and vertical template providing the greatest numerical response is retained as the optimal pair. This scan is carried out in each third of the reference image. The three sets of optimal template pairs are then locked into a single two dimensional template as shown in Figure 4.24. All displacements are referenced to the horizontal template chosen from the upper one-third of the image. This template is designated the **first horizontal template**. The complete two-dimensional template is stored in an array as illustrated in Figure 4.27.

The template storage function allows templates for individual fields of view to be stored in the same patient file using a hashing function similar to that used by the Lesion Data Base storage function. Template offset values from the first horizontal template along with individual template response values are stored.

Implementation of a limited exhaustive search.

The key component of approaching a 100 percent success rate in the tracking algorithm is implementation of an exhaustive search. Due to the exorbitant

computation cost an exhaustive search of the entire image for each new frame is not feasible. However, a limited exhaustive search may be implemented at a significantly lower computation cost. The key idea of the limited search is to only search a 40 x 40 pixel region centered about the last known correct match. Based on previously presented calculations, the new correct match should be within this 40 x 40 pixel area. The new match coordinate becomes the center of the 40 x 40 pixel search area in the subsequent search. The x and y pixel displacement between subsequent match coordinates provides the amount of retinal movement. This information is interfaced to the Laser Positioning Subsystem to maintain the laser on the required lesion coordinate.

Since six separate spatially distributed templates (3 horizontal and 3 vertical) locked into a fixed two-dimensional orientation are used to track retinal movements, a separate 40 x 40 pixel search area is defined about each of the templates as diagrammed in Figure 4.28. The Matrox PIP-1024 frame grabber used in this project has the capability to efficiently transfer these six image windows directly into the host computer. Therefore, the computation of match location is performed in the host computer which has significant 'number crunching' capability. This window transfer mitigates the data bottleneck constraint identified by Markow [2].

Although the calculation of the match coordinate is the heart of the tracking algorithm, it is only one of the many tasks performed by the algorithm.

4.5.3 The tracking algorithm

Early in this chapter a flow chart of the tracking algorithm has been provided as an overview. In this section the entire algorithm will be revisited in much

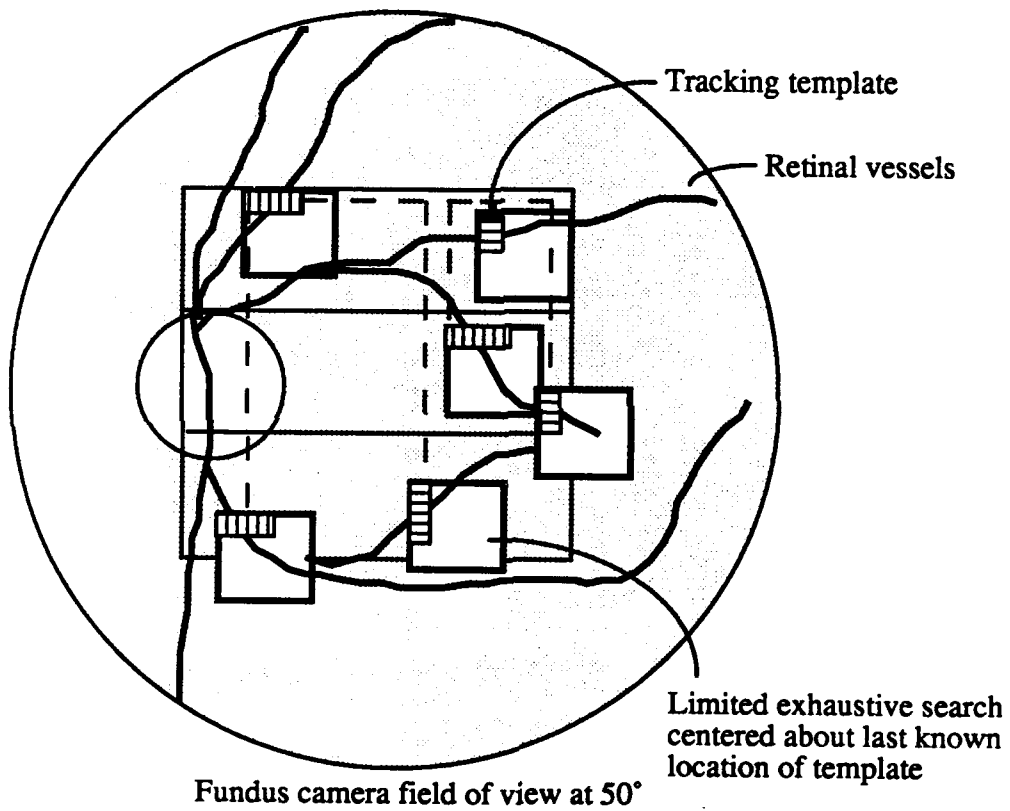


Figure 4.28: The limited exhaustive search

greater detail. A detailed flow chart of the tracking algorithm is provided in Figure 4.29. Reference to this chart during the following description may prove helpful.

System initialization

The RETINA Tracking Algorithm begins with several function calls to initialize the system. Function `initialize_system` initializes the Matrox PIP-1024 video frame grabber, the Data Translation DT2801A data acquisition board, and the RETINA Hardware/Software (HW/SW) Interface to a known state. Also, the following status flags are initialized: `lesion_complete` to one, `laser_point_error` to zero, `lost_lock` to zero, `patient_panic` to zero, `last_lesion` to zero, `first_lesion` to one, `snap_needed` to one, and the loop control variable `continue` to one.

Input look up table modification

In Chapter 3 a method of modifying the frame grabber's input look up table to enhance image contrast was discussed. Recall that the method described does not incur a time penalty. After system initialization the user is prompted for input look up table modification. Thresholds to modify the look up table may be automatically selected by the algorithm or be manually selected by the user. The automatic selection examines a reference image histogram for the first and last non-zero entry to define the current lower and upper thresholds. The new lower and upper thresholds are defined as 0 and 255 respectively.

RETINA Tracking Algorithm

• Initialize System
 • Matrox PIP-1024 frame grabber
 • Data Translation DT2801A
 • RETINA hw/sw interface
 • Initialize status flags:
 lesion_complete = 1
 laser_point_error = 0
 panic = 0
 last_lesion = 1
 first_lesion = 1
 snap_needed = 1
 continue = 1

modify ILUT?

yes → modify ilut
no → patient data available?

patient data available?

yes → select eye for treatment
no → modify ilut

select eye for treatment

I or L

• illuminate fixation lamp
 • load template
 • query for output file name
 • calculate field of view marker
 • open patient data file

prompt: Turn VCR on?

yes → set to external sync source
display frame grabber input

set to external sync source
display frame grabber input

continue?

no → close output file

close output file

last lesion?

yes → "field of view complete"

"field of view complete"

panic?

yes → "cause of panic?"

"cause of panic?"

no → internal sync
display camera

internal sync
display camera

STOP

Time critical tracking loop

print time to output file

lesion complete?

yes → reset patient and lesion status
lesion complete = 0
load next lesion coordinate
calculate lesion displacement from template
if (first lesion) establish lock
check reset
snap_needed = 1

reset patient and lesion status
lesion complete = 0
load next lesion coordinate
calculate lesion displacement from template
if (first lesion) establish lock
check reset
snap_needed = 1

end of lesion data?

yes → continue = 0
last_lesion = 1

continue = 0
last_lesion = 1

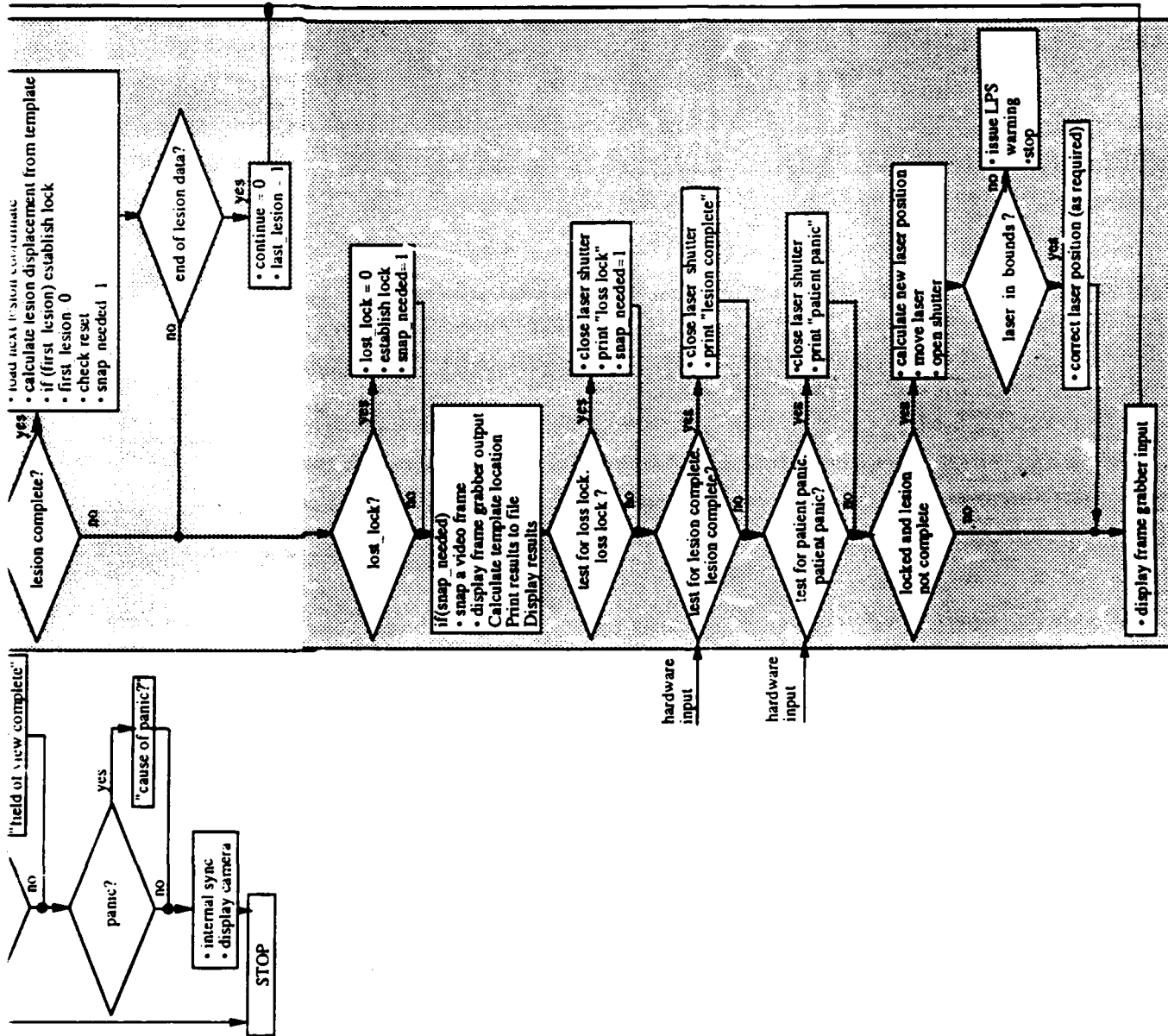


Figure 4.29: The tracking algorithm.

(2)

```

c:\sfb_0003 successfully opened.
-----
                LEFT EYE DATA:                RIGHT EYE DATA:
          Diabetic Detachment Template  Diabetic Detachment Template
1           0           0           0           1           1           1
2           0           0           0           0           0           0
3           0           0           0           0           0           0
4           0           0           0           0           0           0
5           0           0           0           0           0           0
6           0           0           0           0           0           0
7           0           0           0           0           0           0
8           0           0           0           0           0           0
9           0           0           0           0           0           0
10          0           0           0           0           0           0
11          0           0           0           0           0           0
12          0           0           0           0           0           0
13          0           0           0           0           0           0
14          0           0           0           0           0           0
15          0           0           0           0           0           0
16          0           0           0           0           0           0
-----
Choose a retinal field of view (fov) for treatment
with both lesion and template data present.
Select an eye with 'r' or 'l' or 'x' for exit. Press [Enter].

```

Figure 4.30: Patient data availability. A '1' entry in the matrix indicates the presence of a data base or template. In this example patient file sfb_0003 has a Lesion Data Base stored for the treatment of diabetic retinopathy in field of view 1 for the right eye. A two-dimensional tracking template is also stored for this field of view.

Availability of the patient file

After system initialization, the user is prompted for the patient's file designator. The designator consists of the patient's three initials followed by an underscore and the last four digits of the patient's social security number. For example, my patient file designator would be sfb_8253. The patient file may be resident on the hard drive, a floppy disk, or even a magnetic tape cartridge.

The program then searches through the specified patient file and provides a matrix of the available field of view data for treatment. An actual sample of this matrix is provided in Figure 4.30. A '1' indicates the presence of specific field of view data in the patient file.

The user is then prompted for the eye and specific field of view for

treatment. If the field of view the user wants to treat does not have both template and lesion data present, the user is given the opportunity to exit the tracking algorithm or select another field of view for treatment.

Once a field of view is selected for treatment, the RETINA HW/SW Interface automatically illuminates the proper fixation light emitting diode (LED) for the conjugate eye. A detailed description of this interface controller is provided later in this document.

After the appropriate fixation LED is illuminated, the required template for the specified field of view is loaded in the global variable `template_array`. The user is then prompted for the name of the output file to store results. This file is for algorithm development purposes only. It is not required for the clinical system.

Following specification of the output file, the lesion data portion of the patient file is accessed. Recall that access is accomplished using a hashing procedure. The user is then prompted to turn on the video cassette recorder. In the clinical system, this is the step where the patient would be instructed to fixate on the illuminated LED with the conjugate eye. As soon as the user depresses [Enter] the actual time critical tracking algorithm begins.

The time critical tracking loop

The first step of the time critical tracking loop is to print the local time (to the closest millisecond) to the outputfile. This is a developmental requirement only. It allows calculation of critical tracking loop execution time.

The `lesion_complete` flag is then checked. Recall that this flag was ini-

tially set to one so upon initial loop entry the lesion_complete steps are performed. If the lesion_complete flag is one, the patient and lesion status flags and status flip-flops within the RETINA HW/SW Interface are reset. The next lesion coordinate is then obtained from the patient file. If this is the first time through the tracking loop the first lesion coordinate is loaded. The x and y pixel displacement is then calculated between the coordinate of the first horizontal template and the lesion coordinate. Recall that all coordinates are referenced to the first horizontal template. Initial lock is then established by exhaustively searching a 100 x 100 pixel area around the coordinate of the first horizontal template. Lock is established using only a single template pair in an effort to conserve computation time expenditure.

After initial lock is established the lesion data just retrieved from the data file is compared to the hash markers signaling the end of lesion data. If the lesion data is complete, the last_lesion status flag is set to one and the loop control continue variable is set to zero. The loop is then exited.

If the lesion data is not complete, the lost_lock status flag is checked. If it is set one, the lost_lock flag is reset and the function establish_lock is called. This is the same function described above to establish initial lock. The function is provided the last known coordinate of the first horizontal template. The function returns the coordinate of the first horizontal template after lock is established. If the lost_lock flag is not set, the tracking algorithm continues.

The moving video sequence is then 'snapped' if the snap_needed flag is set. In other words a freeze frame is obtained to calculate the current template position. The function calculate_template_location calculates the current position of the first horizontal template using all three pairs of templates in a 40 x 40

pixel exhaustive search. This search is centered about the last known location of the first horizontal template. The function also updates the global variables for the correlation value obtained for each of the six individual templates. The results are then printed to the output file.

Loss of Lock

After the position of the first horizontal template is updated, the values of the six individual template correlations are examined for a loss of lock condition. Each of the individual template responses are normalized by the anticipated template value. This value is stored in the patient file during template construction. Any loss of lock conditions may be programmed. After studying several tracking sequences the following conditions are programmed to result in loss of lock status:

- If any four of the six templates respond with less than 15 percent of their anticipated value, or
- If any template responds with greater than 130 percent of its anticipated value.

If a loss of lock condition occurs the laser shutter is closed and the `lost_lock` flag is set.

Test for lesion complete and patient panic status

The Reflectance Based Feedback Control System will monitor lesion growth and issue a *lesion complete* signal at the appropriate time. To simulate this signal for system testing a pushbutton switch is provided on the RETINA HW/SW

Interface. When depressed the lesion complete flip-flop within the interface is set. The software function `check_lesion_status` checks the status of the flip-flop. If the flip-flop is set, the software flag `lesion_complete` is set. This condition causes the laser shutter to close. Patient panic is tested in a similar manner.

Laser Position Update

If the algorithm is in lock and the lesion is not complete the updated laser position is calculated and the laser is repositioned via the Laser Pointing Subsystem. The laser shutter is then opened (if not already opened).

Although the Laser Pointing Subsystem will have closed loop feedback control via mechanisms described in Chapter 6, the tracking algorithm also checks if the laser reached its intended coordinate. This check is accomplished by function `check_laser_position` by examining a 12 x 12 pixel region centered around the prescribed laser coordinate for the brightest pixel. The centroid of the laser spot is assumed to produce the brightest pixel. If the brightest pixel is found at the intended laser final destination coordinate no laser position update is required. However, if the brightest pixel is found within the 12 x 12 pixel region at a coordinate other than the intended laser final destination coordinate, a correction signal is provided to the Laser Pointing Subsystem via functions `move_laser_horizontally` and `move_laser_vertically`. If no pixel of laser spot brightness is found within the 12 x 12 pixel region, the laser shutter is closed, a Laser Pointing Subsystem malfunction warning is issued, and the tracking algorithm is aborted. These laser position correction activities are illustrated in Figure 4.31.

A Laser Pointing Subsystem malfunction could be caused by system

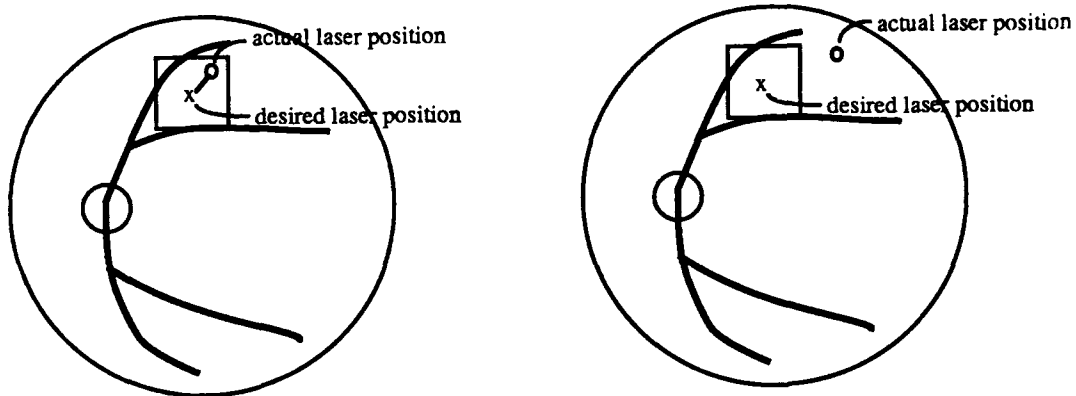


Figure 4.31: Laser position check. The tracking algorithm checks the final destination of the laser via function `check_laser_position`. This function examines a 12 x 12 pixel region centered around the prescribed laser coordinate for the brightest pixel. If the brightest pixel is found at the intended laser final destination coordinate no laser position update is required. However, if the brightest pixel is found within the 12 x 12 pixel region at a coordinate other than the intended laser final destination coordinate, a correction signal is provided to the Laser Pointing Subsystem (left). If no pixel of laser spot brightness is found within the 12 x 12 pixel region, the laser shutter is closed, a Laser Pointing Subsystem malfunction warning is issued, and the tracking algorithm is aborted.

misalignment which will be described in detail in Chapter 6, therapeutic laser failure, or failure of a component within the Laser Pointing Subsystem.

Continued Processing

The time critical loop is then continued until the lesion_complete flag is set, the patient panics, or the lesion coordinates for the field of view under treatment is exhausted.

Eye Blinks

When a patient blinks, the tracking algorithm must detect the condition and close the laser shutter. The system must return to tracking after the blink episode is complete. When a patient blinks, an image of the patient's eyelid is provided to the tracking algorithm. The eyelid is featureless and results in loss of lock. The loss of lock computation previously described handles the blink condition.

Fail Safe Mechanism

Fail safe mechanisms are provided by the patient panic switch and the internal protection provided with the laser shutter. In the event of a power failure the laser shutter closes and will not reopen until manually reset.

Chapter 5

The Laser Pointing Subsystem

5.1 Objective

The objective of the Laser Pointing Subsystem is to maintain the irradiating therapeutic laser on the prescribed lesion coordinate. This subsystem must have the capability to redirect the laser to correct for retinal movement detected by and compensated for by the Retinal Tracking Subsystem.

5.2 Ideal Laser Pointing Subsystem Characteristics

To accomplish this objective the Laser Pointing Subsystem must have the following capabilities:

- Be able to redirect the laser to within any coordinate within the visible fundus camera retinal field of view. The fundus camera will be used with the 50 degree field of view during the tracking operation. Therefore, the Laser Pointing Subsystem must be able to redirect the laser to within any point within a ± 25 degree field of view Cartesian coordinate system as illustrated in Figure 5.1,
- Have response characteristics to effectively compensate for eye movements,

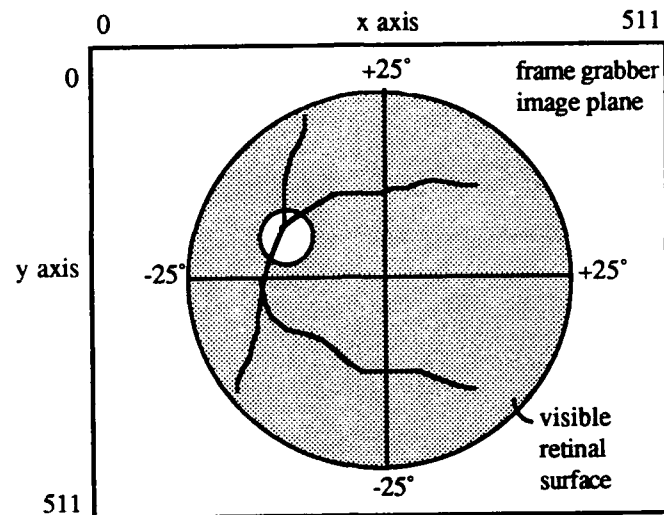


Figure 5.1: The Fundus Field of View Cartesian Coordinate System

- Have the capability to safely redirect laser energies at levels used to form therapeutic lesions,
- Have a feedback mechanism to allow for closed loop control,
- Have a linear response,
- Be reliable and easy to maintain and align, and
- Not hinder the operation of other system components.

5.3 Previous Work

Considerable work on a pointing system for precise laser positioning on the human retina has been accomplished by Mainster, Webb, Timberlake, Hughes, and Pomerantzeff in the development of the Scanning Laser Ophthalmoscope. A thorough review of their work was provided in Chapter 3. In their appli-

cation a raster scan was projected on the retina to map its physical features. Reflected light from the retina was captured and amplified to build an image of the retina. The laser delivery portion of their design may be modified to serve as the basis for the Laser Pointing Subsystem. The key components of this system include a set of galvanometers to steer the laser beam, a shutter for laser safety control, and optics to integrate the Laser Pointing Subsystem with the Reflectance Based Feedback Control System. No attempt is made to specify a final design for the Laser Pointing Subsystem. Final design decisions must be based on the actual implementation of the Reflectance Based Feedback Control System and the type of therapeutic laser system chosen. Work is ongoing to study the feasibility of substituting the argon laser with a solid-state laser diode. Instead, equipment considerations driven by Retinal Tracking Subsystem requirements are presented. Also, a developmental Laser Pointing Subsystem is provided. This system was used to test the closed loop tracking capability of the Retinal Tracking Subsystem and used for *in vivo* demonstrations. Information will be provided first on galvanometers and X-Y scanning systems followed by equipment specifications. Details of the Laser Pointing Subsystem modifications required for *in vivo* testing are deferred to Chapter 9.

5.4 Galvanometers

Galvanometers, also known as optical scanners, are an effective method of redirecting a laser beam. This section will provide a brief review of their theory of operation followed by detailed information for using a pair of galvanometers in a Cartesian coordinate scanning system.

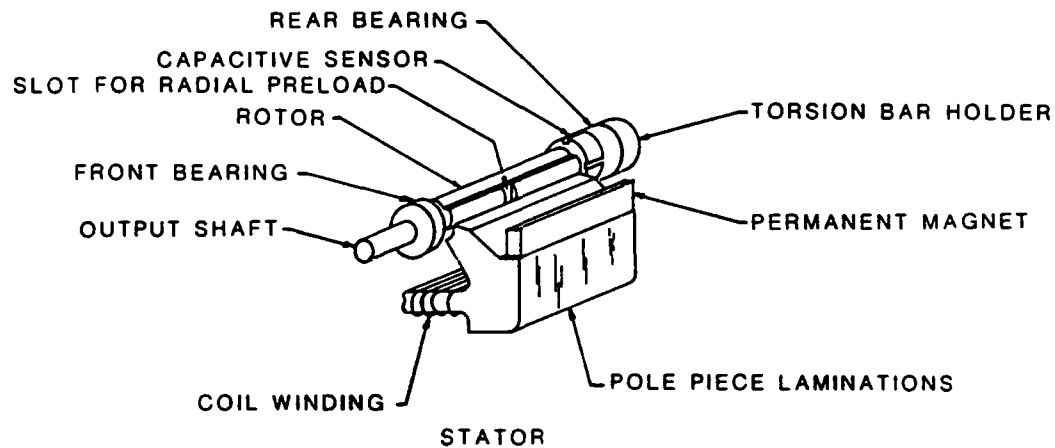


Figure 5.2: The galvanometer [76]

5.4.1 Theory of Operation

Galvanometers consist of an iron rotor suspended between a pair of front and rear bearings. Two permanent magnets and two drive coil windings provide for flux between the rotor and four stationary poles. The magnitude and direction of the drive coil flux determines the magnitude and direction of rotor torque. Feedback of rotor position is provided by a pair of capacitors formed by a stationary slotted metal ring attached to the electrically neutral rotor. The slotted ring forms four electrodes. Each pair of opposite electrodes forms a capacitor. The capacitance of the electrode pairs is determined by rotor position. The current (and hence rotor position) through each capacitor is monitored when the capacitor is excited with a high frequency oscillator [72, 73]. Reference Figure 5.2.

Galvanometers are driven by external driver amplifiers. Typically, these driver amplifiers are solid-state variable output impedance amplifiers. These drivers accept a DC voltage input in the range of ± 1.0 volt and provide a

galvanometer compatible drive current proportional to the input voltage. A stable input voltage is required for a reliable drive current. Also, the driver amplifier must be supplied with a stable supply voltage. Typically zero-offset and gain controls are provided to the user on the driver amplifier [74].

5.4.2 Characteristics

Galvanometer performance and characteristics are determined by a number of factors including armature (rotor) size, inertia of the mirror being driven, and the voltage limits of the external driver amplifier. Galvanometers are provided in an open loop mode with no position feedback or in a closed loop variety with position feedback using the capacitive mechanism described above [73]. Important galvanometer performance parameters include: load-free natural resonant frequency, peak-to-peak mechanical rotation, armature inertia, torque, linearity, and reliability.

Frequency Response

Frequency response is provided as a load-free natural resonant frequency rating. Derating curves are provided to determine the frequency response under a given load condition. Physically smaller galvanometers have a higher frequency response due to the lower armature inertia. However, these smaller galvanometers have lower torque capability. Galvanometers for laser beam steering are available with load-free natural resonant frequencies from 130 to 2,400 Hz [75].

The frequency response has an inverse relationship with the mirror size for a given galvanometer. Generally, the mirror inertia should be between .1 and 10 times the armature inertia. At larger mirror to armature inertia ratios the

frequency response degrades rapidly. Both mirror inertia and armature inertia are typically provided in $gm - cm^2$. Armature inertia ratings are available in ranges from 0.013 to 4.0 $gm - cm^2$ [75].

Peak-to-Peak Rotation

Another important characteristic of the galvanometer is peak-to-peak mechanical rotation. This is typically given in degrees. Rotation specifications are alternatively provided in optical scan angle. Galvanometers are available in optical scan angles ranging from 2 to 100 degrees [75].

Linearity

The linearity of a galvanometer is expressed as a percentage indicating the ratio of maximum position signal error to the peak-to-peak value of the position signal. Typical values range from ± 0.3 degrees to ± 1.0 degrees [73]. Galvanometers with lower linearity ratings (smaller percentage) are more expensive.

Failure Modes and Reliability Ratings

Galvanometers are susceptible to failure in two different areas: failure of electronic components and bearing wear. Reliability ratings are provided in the number of failures per 10^6 operating hours. Reliability for a commercial grade galvanometer operating at 25 degrees centigrade is 3.3 failures per 10^6 hours. The failure rate approximately doubles for an operating temperature of 125 degrees centigrade. Military specification (mil spec) galvanometers are available with failure rates an order of magnitude less than the commercial grade

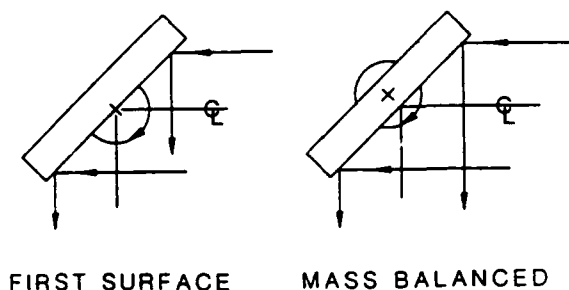


Figure 5.3: Scan head geometries. Left to right: first surface mirrors, mass balanced mirror [76]

galvanometer. However, their cost are approximately double compared to a similar commercial grade galvanometer [72].

5.4.3 Scan Heads

Galvanometers may be fitted with a variety of scan heads including mirrors or beam splitters. There are a number of variables which must be considered in choosing the appropriate scan head including: optical aperature, optical resolution, and speed. In general, larger aperatures provide better optical properties but lower speed capability [76].

The scan head aperature is the opening through which the optical system will image. Optical quality is specified via mirror flatness standards, scratch and dig specifications, and reflectivity parameters. Different mirror coatings are used to achieve required optical quality and power specifications. Mirrors with peak irradiance ratings up to 500 W/cm^2 are available [76].

There are two different types of scan head geometries: first surface mirrors and mass balanced mirrors. Reference Figure 5.3. A first surface mirror

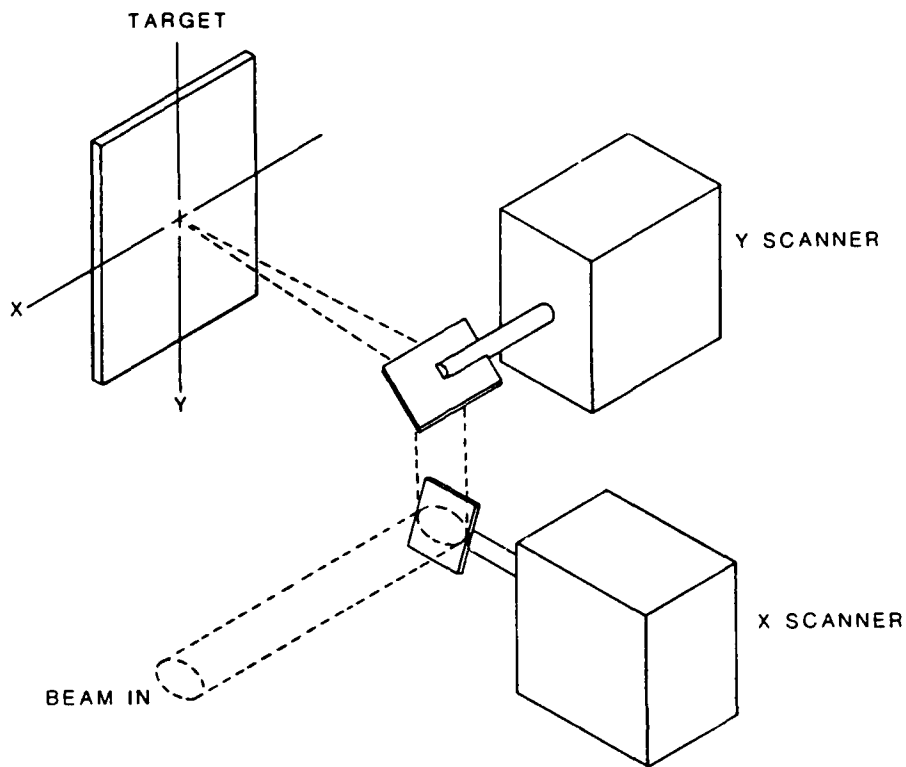


Figure 5.4: X-Y scanning system [76]

has the reflective surface on the axis of rotation. This geometry simplifies position calculations. However, it creates a lateral imbalance in the scanner when the mirror rotates. Mass balanced mirrors have mirror mass balanced about the axis of rotation. This type of geometry allows for less 'robust' mirrors. However, this configuration is more sensitive to alignment and linearity errors [76].

5.5 X-Y Scanning Systems

Manufacturer configured X-Y scanning systems are available. These systems use 2 mirrors and 2 galvanometers separately driven to provide an optical scan

in an X-Y plane. The mirrors are placed orthogonally with the smaller mirror mounted lower to provide the X scan and the larger mirror mounted above for the Y scan. The laser beam follows the path to the target as illustrated in Figure 5.4 [76].

5.5.1 Drive Signals

Drive signals are separately provided to the X and Y scanner drivers to position the laser at any point in the X-Y plane. These voltage drive signals may be of three different types: a raster signal, a step signal, or a vector signal [76].

A raster signal is used to scan the laser beam in a raster fashion in the X-Y plane. To generate a raster scan the X driver amplifier is provided a high frequency sawtooth wave to scan the raster across the X-Y plane. The Y driver amplifier is provided a slower signal to increment the laser scan a line at a time. This type of scan pattern was used with the Scanning Laser Ophthalmoscope [76].

The step signal allows positioning of the laser beam to any random position within the X-Y plane. This method of laser positioning has an inherently long settling time. This is the time required to settle within a small final area and compensate for any small position errors that might exist after 99 percent of the scanner motion is complete. Settling time increases with scan head diameters. A small 5 mm scan head has a settling time of 6.5 ms with a 1.0 ms travel time. A large 50 mm scan head has a 58.5 ms settling time with a 40.0 ms travel time [76].

Vector rotation is generated by the coordinated movement of both the

X and Y galvanometer. Vector rotation may use the point-to-point or the skywriting technique. In the point-to-point method vectors begin and end at drawn line endpoints. This is the fastest method of point-to-point transit. The skywriting method backs the scanner position up, scans across the vector start point, past the vector end point, and then stops beyond the end point. This method is slower than point-to-point vectoring but solves scanner acceleration and deceleration problems [76].

5.5.2 Sources of Error

Ideally, the laser should be precisely directed to any point in the X-Y plane. However, due to various sources of error this is not always the case. Sources of error include galvanometer errors and image distortion errors.

Galvanometer Errors

Galvanometer related errors include wobble, zero-drift, and repeatability errors. Wobble errors are rotations orthogonal to the axis of desired rotation. Wobble is caused primarily by mirror imbalance. It is caused to a lesser extent by asymmetrical forces on the galvanometer rotor or from worn bearings [73].

Zero-drift error is a slow variation of the X axis rest position with time. This error results from drive signal variation with temperature. This type of error may be minimized by applying temperature regulation to the galvanometer housing [73].

Repeatability errors is a variation of the X axis rest position from one scan to the next. Several noise sources contribute to the repeatability error.

The largest error source of this type is bearing noise. Bearing noise occurs as a random fluctuation in bearing performance. Performance is affected by rotor speed, bearing condition, bearing lubricant condition, and dust contamination [73].

Image Distortion Errors

Image distortion errors are of two types: optical path distortions (OPD) and cosine distortion. Optical path distortions are caused by mirror quality imperfections. This type of error is usually caused by mirror non-flatness. It results in the laser beam coming to a focus in an elongated or distorted spot [76].

Cosine distortion is caused by the geometry of the X-Y scan system. It is due primarily to the scanner pointing across a wide angular range from a single point. This results in an elongation of the incident laser beam at the far reaches of the scan field. Cosine distortion also results in an elongated laser spot. Cosine distortions are small for a laser pointing system due to the small laser spot size. Cosine distortion may be minimized by avoiding the far reaches of the image plane [76].

5.6 Retinal Tracking Subsystem Requirements

Only three Laser Positioning Subsystem parameters are driven by the Retinal Tracking Subsystem. These are: response time, position resolution, and the scan type employed.

5.6.1 Response Time

Retinal Tracking Subsystem real time specifications are provided in Chapter 10. These specifications indicate to track with 200 micron target radius at a retinal velocity of 50 *degrees/second* requires a position update approximately 120 times per second. This requires a galvanometer with a *loaded* frequency response of 120 Hz. Galvanometers with this capability are readily available.

5.6.2 Position Resolution

The resolution of the Retinal Tracking Subsystem is determined by the resolution of the CCD video camera coupled to the fundus camera. The developmental system configuration has an approximate retinal surface resolution of 40 microns. This is equivalent to .137 degrees. Galvanometers with this capability are readily available.

5.6.3 Maximum Displacement

The Retinal Tracking Subsystem employs a fundus camera with a 50 degree field of view. This requires a pair of X-Y galvanometers with a 50 degree peak-to-peak optical scan angle capability. Galvanometers with this capability are readily available. Galvanometers with an eight degree peak-to-peak optical scan angle were employed in the development system. Increasing the displacement from laser mirror to target countered the limited deflection.

5.6.4 Closed Loop Control

As previously mentioned, some galvanometers are equipped with position feedback capability using rotor position capacitive monitors. Specially configured driver amplifiers are equipped to process the feedback information from the galvanometer to ensure precise galvanometer positioning. Galvanometers and driver amplifiers of the closed loop type may be used with the Laser Positioning Subsystem to provide an additional level of safety beyond the check_laser_position function described in Chapter 4.

5.6.5 Scan Type Employed

To provide for timely movement of the therapeutic laser the vector point-to-point scan type will be used with the Laser Positioning Subsystem.

5.7 System Design

A X-Y scan system with the above specifications is readily available from General Scanning Incorporated for approximately four thousand dollars. The budget for the development system study did not allow purchase of this X-Y scan system. Instead, galvanometers and driver amplifiers already available within the laboratory were used to demonstrate the system concept.

5.8 Development System Implementation

A detailed description of the developmental system instrumentation is provided in Chapter 7 of this document. This system uses General Scanning Incorporated open loop galvanometers and driver amplifiers to demonstrate

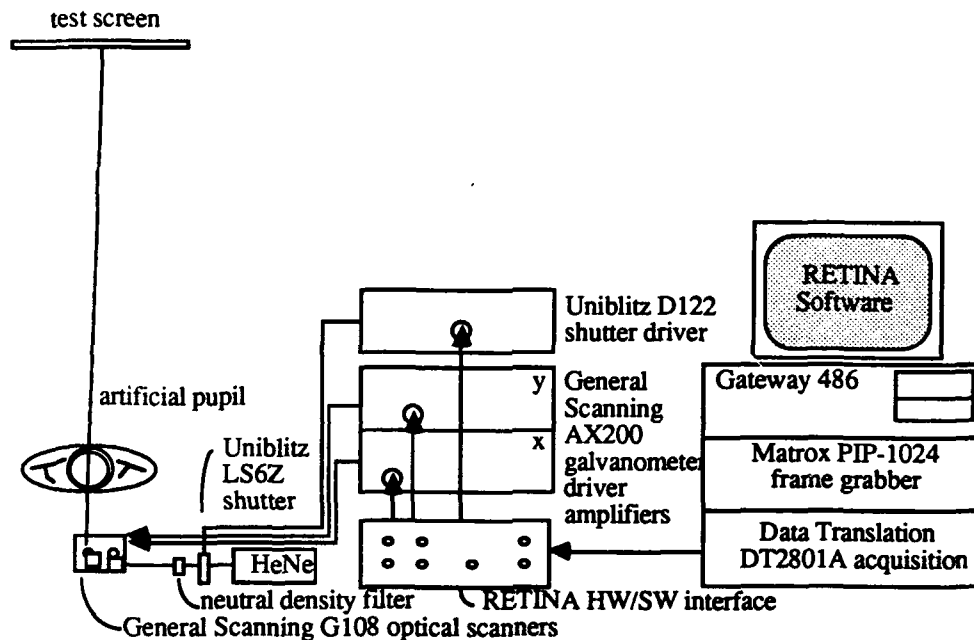


Figure 5.5: The developmental Laser Positioning Subsystem

the capabilities of the Retinal Tracking Subsystem. A HeNe laser is used as the simulated therapeutic laser. This laser is projected over two meters to a simulated retina to compensate for the limited 8 degree peak-to-peak deflection of the galvanometers. Reference Figure 5.5.

The simulated retina is simply a white cardboard screen. An image of an actual human retina taken through a fundus camera set at a 50 degree field of view is projected onto the screen. The screen is imaged with the CCD video camera of the Retinal Tracking Subsystem. Simulated retinal movement is accomplished by moving the retinal image in reference to the stationary screen. Further details of the testing apparatus is provided in Chapter 8.

5.8.1 System Alignment

Precise alignment is required between the Retinal Tracking Subsystem and the Laser Positioning Subsystem. This is accomplished by using a common coaligned coordinate system. The coordinate system of the frame grabber is a readily available common format. It has an X and Y axis each divided into 512 increments. To coalign the laser to the same coordinate system, the peak-to-peak drive voltage required by the driver-amplifier is divided into 512 separate increments. The two systems are then aligned by generating a 225 x 225 pixel test pattern with the Laser Pointing Subsystem and overlaying it with a 225 x 225 pixel test pattern within the image plane of the frame grabber. When the tracking algorithm computes an updated laser position coordinate, the updated coordinate from the tracking algorithm is simply passed to the functions `move_laser_horizontally` and `move_laser_vertically`. These functions provide the proper voltage to the driver-amplifiers via the data acquisition and control board to move the laser to the updated coordinate. It should be noted that this is easily modified for other configurations by modifying the software.

The drive signal used in the development system is a vector point-to-point scan. Correction signals for the X and Y galvanometers are provided virtually simultaneously by the data acquisition and control system. Although specifications for the real time system will include galvanometers equipped with position feedback mechanisms, an additional feedback mechanism provided by the tracking algorithm for redundancy is highly recommended. This mechanism which was described in Chapter 4 will be tested in Chapter 8.

5.9 Laser Pointing Subsystem Testing

Results of testing the Laser Pointing Subsystem are provided in Chapter 8 "Development System Testing".

Chapter 6

Tracking on a Featureless Retina

6.1 Alternate tracking mechanism requirement

Chapter 4 of this document provided a method to track and compensate for the movement of the retina using visible retinal landmarks as templates to derive position information. This method is effective in tracking retinal movement as long as visible retinal features are available. In retinal fields of view away from the optic disk the retinal vessels become less populous. Also, both horizontally and vertically oriented vessels necessary for effective vessel template construction may not be present in these peripheral fields of view.

This situation motivated research toward an alternate tracking method for peripheral fields of view using laser lesions as landmarks for deriving positional updates. It was also hoped that this alternate method might prove computationally less expensive and less susceptible to variations in the retinal illumination source than the vessel tracking algorithm.

6.2 Overview

This chapter describes an alternate tracking concept using therapeutic laser lesions as templates. The chapter begins with a description of a single lesion template and the two-dimensional lesion template. Two different methods of

implementing a lesion tracking algorithm are then discussed with their inherent advantages and disadvantages. These two methods are called: the Unique Template (UT) method and the Adaptive Template (AT) method. The chapter concludes with a description of the Lesion Tracking and Image Analyzer (LETINA) software developed to implement and test the lesion tracking methods.

6.3 The Lesion Template

The lesion template is very similar to the vessel template described in Chapter 4. The individual horizontal and vertical templates are normally oriented to one another and referenced to the center reference pixel. This template configuration forms a 'crosshair' over a lesion site. Reference Figure 6.1. Computation of the template response has been slightly modified to account for searching for a lighter laser lesion against a darker retinal background. The template response is given by:

$$\text{template response} = \frac{(p1 + p2 + p3 + p4) - (p5 + p6 + p7 + p8)}{(p1 + p2 + p3 + p4 + p5 + p6 + p7 + p8)} \quad (6.1)$$

This template provides a response of 1 to an ideal lesion. An ideal lesion is a white (255) lesion on a black background(0). Function `find_lesion_templates` was devised to search a user specified image search area for all occurrences of lesion templates. This function exhaustively searches all pixels in the specified search area for a lesion by testing templates of radius 1 pixel through 5 pixels for a fit. These radii correspond to lesion diameters of 150 to 500 microns respectively. A 50 x 50 pixel search area requires approximately 90 seconds of

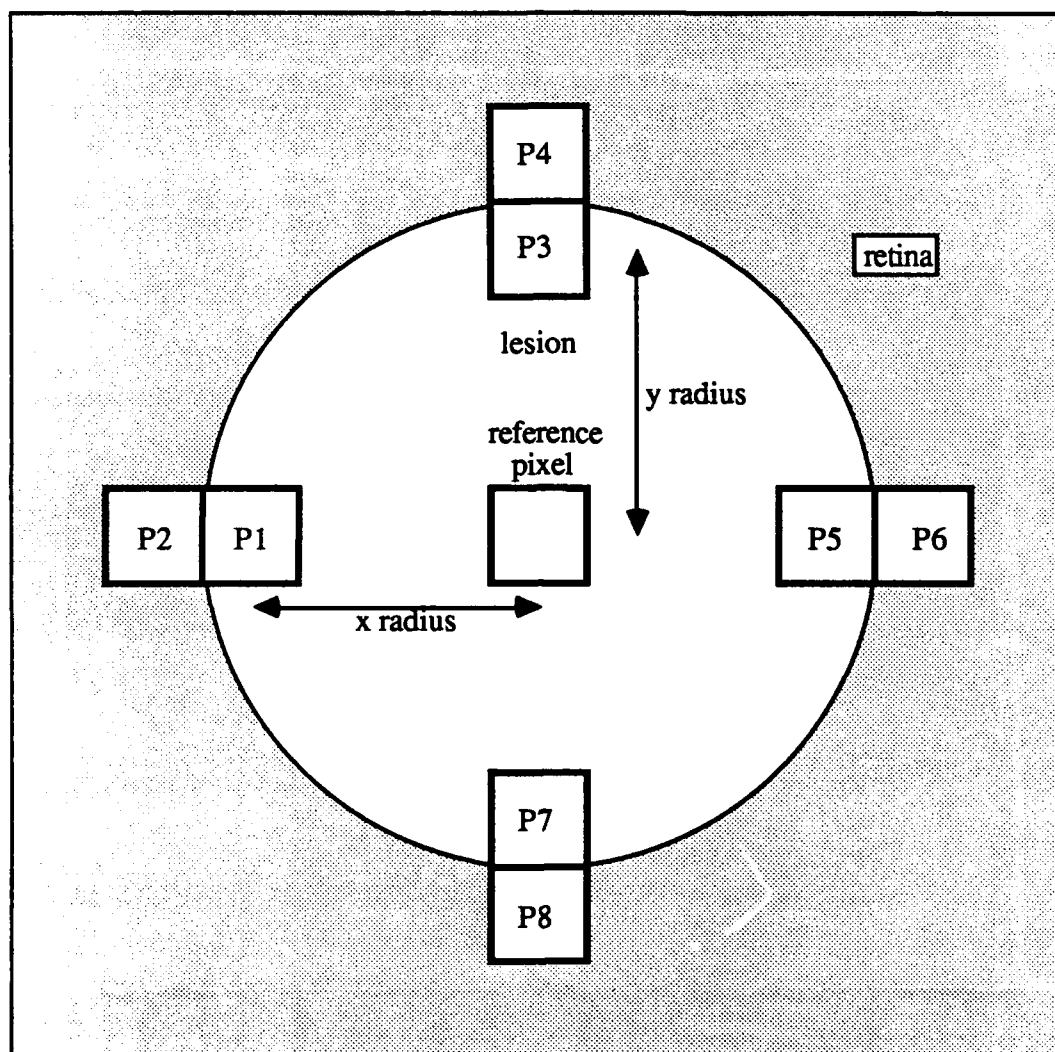


Figure 6.1: The lesion template. For a given reference pixel, values of radius from 1 to 5 pixels are tested for a lesion fit. The better the fit the higher the template response.

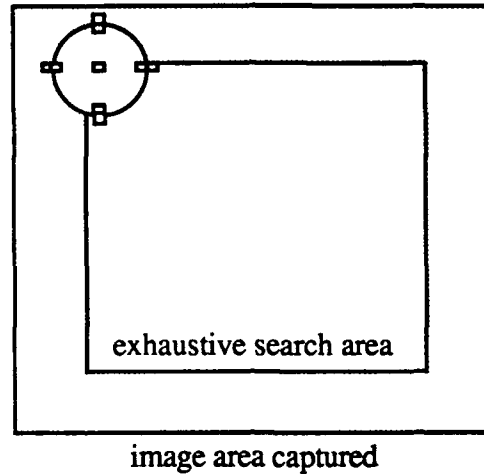


Figure 6.2: The lesion template search. The white region is the actual search area. The gray shaded region is provided as a pad to allow for the search of the entire white region.

processing (486-33) to locate all potential lesion locations. The function loads potential lesion templates into a linked list ordered from largest to smallest template response. The linked list insertion routine checks to ensure that a duplicate template is not inserted in the list and that only the lesions with the highest responses are retained for two-dimensional lesion template building. The lesion search is illustrated in Figure 6.2.

6.4 Two-dimensional lesion templates

Once potential lesion templates have been found, the user is prompted for the number of lesion templates desired for the two-dimensional lesion template. The function `auto_build_lesion_template` then constructs the two-dimensional lesion template. All individual lesion templates are referenced to the individual lesion template with the highest template response as illustrated in Figure

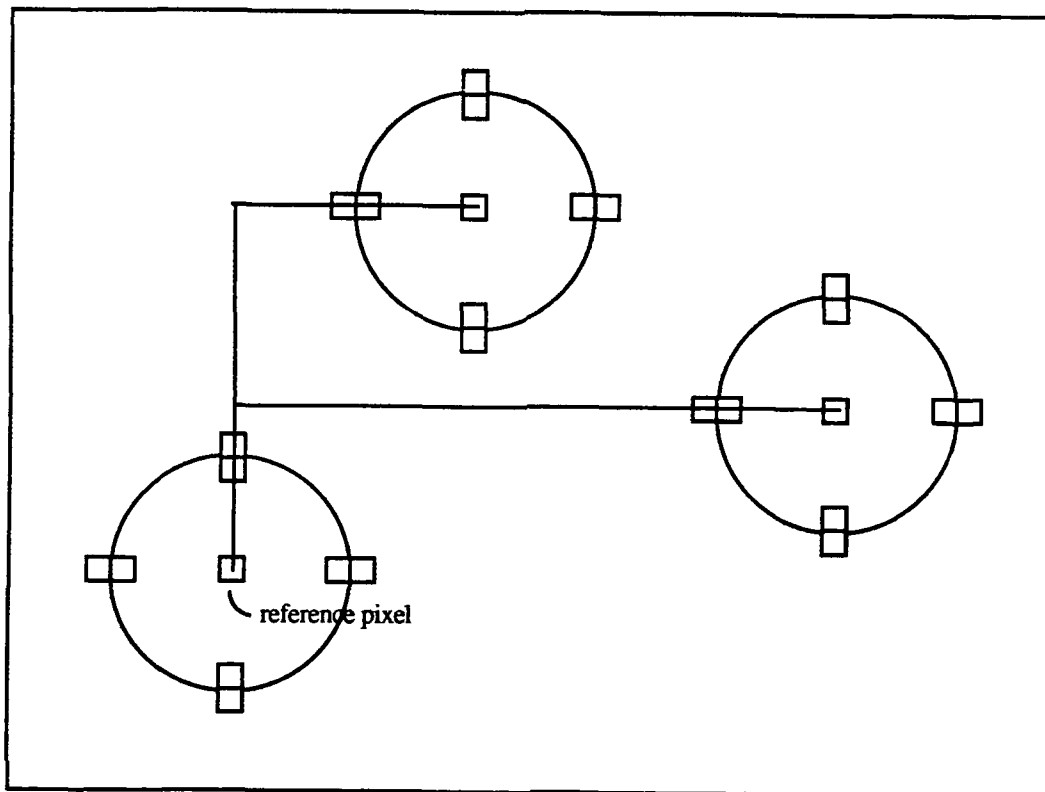


Figure 6.3: The two-dimensional lesion template formed by three separate lesion templates. All separate templates are referenced to the individual template with the highest template response. The lesion template on the left has the highest template response in this illustrative example.

6.3. The function superimposes a black cursor on the lesions used in the two-dimensional template. The two-dimensional template parameters are stored in the template array as illustrated in Figure 6.4.

6.5 Testing on ideal lesions

The template finding and automatic building functions were tested on a series of ideal lesions. A test pattern of three lesions was constructed using function `generate_test_pattern`. This function can generate any arbitrary user specified

```

-----template_array-----
      Template Constants      Lesion Constants
      [0]  [1]  [2]  [3]  [4]  [5]  [6]  [7]
      x_off y_off x_dm y_dm x_rad y_rad corr unused
[0]      0    0    11   14    5    7   100    0
[1]     -10  -10    9   12    4    5   100    0
[3]     -20  -20    7    9    3    4   100    0
Total template correlation:   300

```

Figure 6.4: The template array

lesion pattern. The finding and building functions correctly located and built a two-dimensional template. The results of this test are illustrated in Figure 6.5

6.6 Testing lesion templates on a rabbit retina

Dr. Maya Jerath performed *in vivo* tests on cross bred Californian and New Zealand rabbits in support of her research in real time control of laser induced retinal lesions. In these tests 3 kg rabbits were anesthetized intramuscularly with a combination of Ketamine (35 mg/kg) and Rompan (5.9 mg/kg). The rabbit's eye was then dilated with Atropine and a speculum inserted to open the eyelid. A suture was placed in the medial rectus muscle to allow eye movement. Controlled lesions were then placed on the rabbit's retina [4]. These experiments were filmed using a CCD video camera coupled to a fundus camera set a 50 degree field of view. No optical enhancement filters were used in the filming. These video tapes were used to test the efficacy of the lesion template concept. Several excerpts were selected from the tapes. Selection was based on the presence of multiple lesions within the central portion of the field of view.

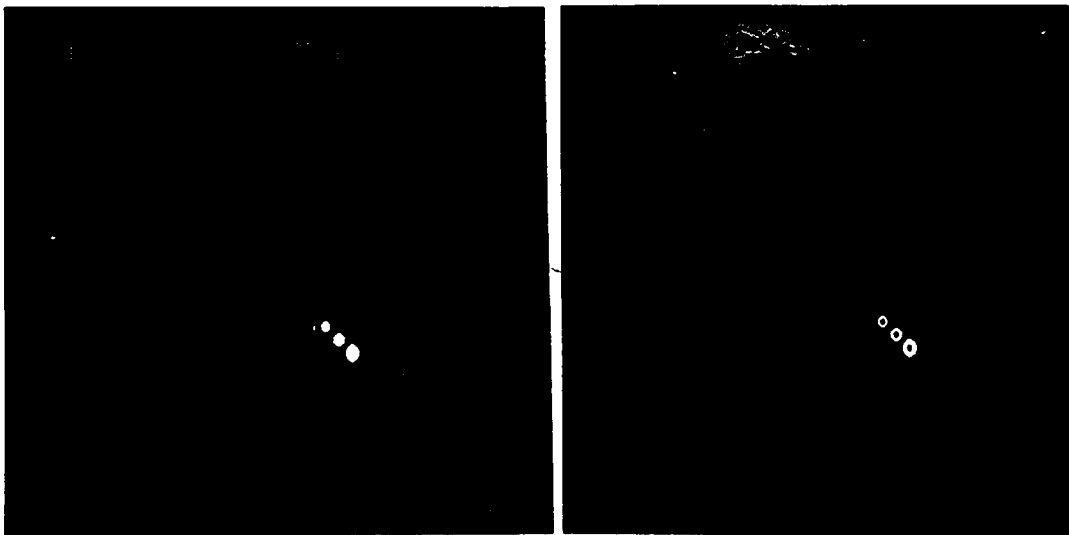


Figure 6.5: The function `generate_test_pattern` was used to generate three ideal (255) lesions of different diameters on a black (0) background. The functions `find_lesion_templates` and `auto_build_lesion_templates` correctly located the individual templates and constructed a two-dimensional template. The templates used in the two-dimensional template are highlighted with a black cursor.

Two excerpts were chosen from the video history of the experiment performed on rabbit RC. One excerpt had slow retinal movements of the anesthetized rabbit while the other excerpt had rapid suture induced retinal movement. Figure 6.6 illustrates the result of the lesion tracking tests. The figure on the top left is the original reference image used to construct the lesion template and the Lesion Data Base. The bright elongated object in the upper left portion of the image is the rabbit's optic disk. Four lesions are present in the center of the image. Function `find_lesion_templates` correctly found the three lesions with the highest template response. The highest actual template response was 0.05. Recall that an ideal lesion template has a response of 1. Function `auto_build_lesion_template` correctly assembled these three lesion templates into a single two-dimensional template. The three lesions chosen to build the template are highlighted with a black cursor in the top right image. Function `build_lesion_data_base` then plotted the coordinates of the desired therapeutic lesions. Results of tracking normal retinal movement are shown in the lower left image. Results of tracking the faster suture induced movement are shown in the bottom right image. The tracking algorithm was able to successfully track these faster movements for a 15 second span. When the eye was quickly pulled, the upper velocity limit of the tracking algorithm was exceeded. This occurred at an approximate retinal velocity of 20 degrees per second. Precise speed parameters of the tracking algorithm will be provided in Chapter 8. These experiments demonstrated the feasibility of using laser lesions as landmarks for tracking retinal movement.

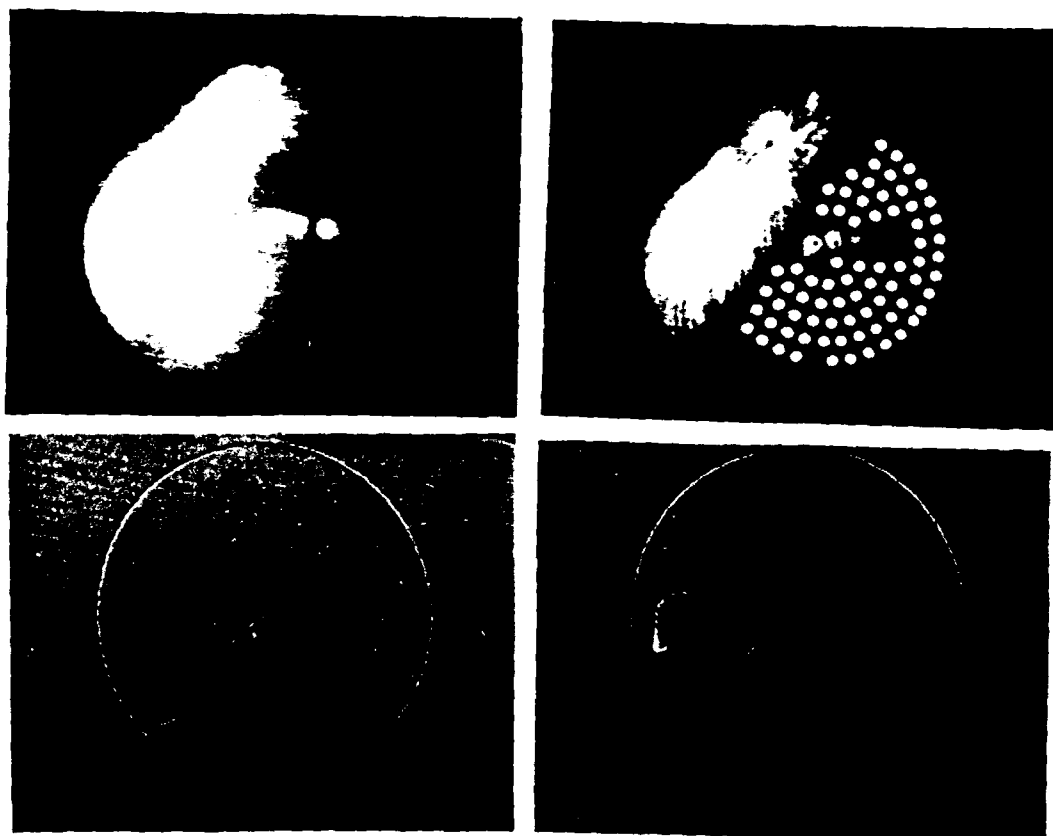


Figure 6.6: Results of the lesion tracking experiments conducted on anesthetized pigmented rabbits. Top left: reference image used to construct the lesion templates. Top right: results of building a two-dimensional lesion template and Lesion Data Building. Templates used in the two-dimensional template are highlighted with black cursors. Bottom left: results of tracking the movement of the anesthetized subject RC. Bottom right: results of tracking movement induced with a suture attached to the medial rectus muscle.

6.7 Template tracking methods

Two different methods have been devised to employ lesion templates as tracking landmarks. This section describes each method in turn with its associated advantages and disadvantages.

6.7.1 The Unique Template tracking method

The Unique Template tracking method uses a cluster of unique lesions to form a distinctive template. For the study described in this section, a triad of 200 micron lesions forming an isosceles triangle was used. Reference Figure 6.7. Any distinct lesion pattern may be used. The reference coordinate for the template is at the triangle center. Recall, from a previous chapter that the success of panretinal photocoagulation therapy is roughly proportional to the retinal area covered with a lesion. The triad covers approximately one-half the area of a 500 micron lesion.

The lesion triad template can be used to provide 'interlocking' templates between adjacent fields of view. For example, a series of lesion triad templates could be placed in a ring outside the normal therapeutic lesions as illustrated in Figure 6.8. These lesions could then be used by more peripheral fields of view as tracking templates while providing therapeutic value. This method of interlocking templates may be extended across the surface of the retina. This method has the advantage of simplicity. However, this simplicity is interrupted should a blood vessel cross an intended position of a lesion triad template. The function `build_lesion_data_base` required slight modifications to plot the outer ring of interlocking lesion triad templates. The result of these modifications are provided in Figure 6.9.

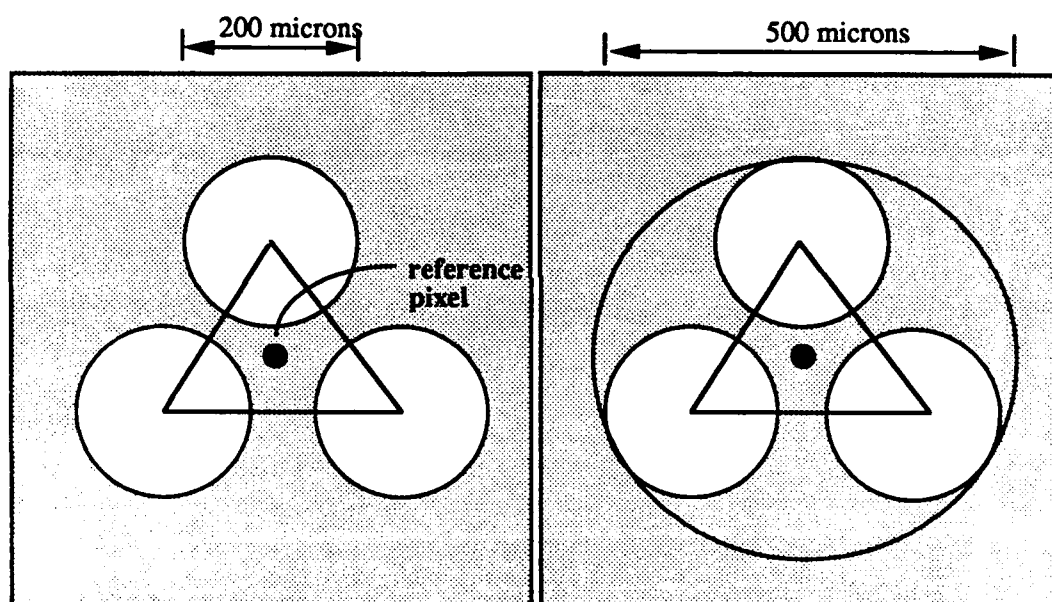


Figure 6.7: Left: the lesion triad template. Right: the lesion triad template illustrated to scale with a 500 micron lesion.

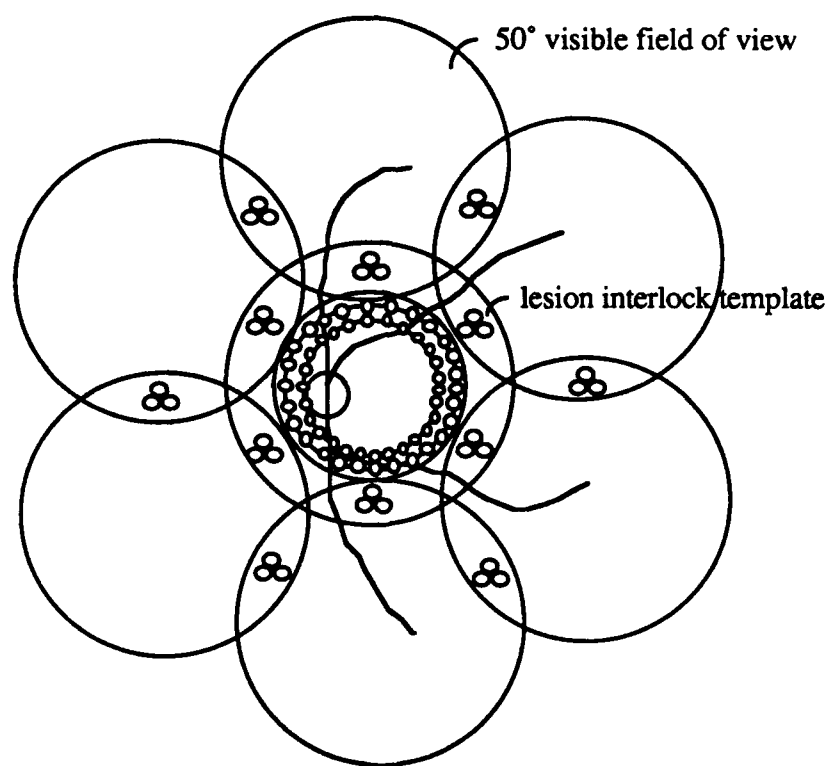


Figure 6.8: Interlocking triad lesion templates

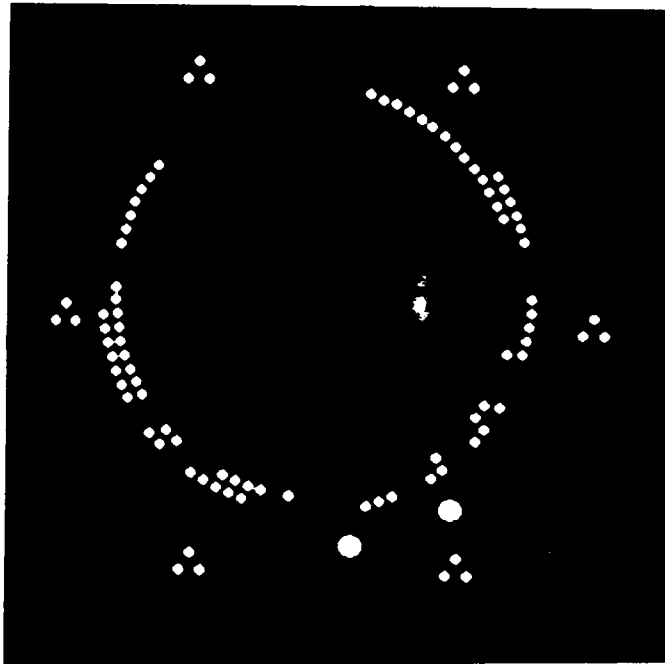


Figure 6.9: Results of adding interlocking lesion triad templates to the function `build_lesion_data_base`

6.7.2 The Adaptive Template tracking method

The Adaptive Template tracking method provides for the orderly placement of therapeutic lesions using predecessor lesions as a template to form current lesions. This method starts with a lesion in the center of the field of view for treatment. This first lesion serves as a template to form the second therapeutic lesion. The two therapeutic lesions are then used as a template to form the third lesion. Once the third therapeutic lesion is formed a triad template is used consisting of the first three lesions to form the fourth lesion. This process continues in a repeatable pattern radially outward from the center of the field of view. This therapeutic lesion formation process is illustrated in Figure 6.10. The completed pattern containing 61 therapeutic lesions is illustrated in Figure 6.11. A pattern of 61 500 micron lesions fills the central region of a 50 degree

retinal field of view. This tracking method is called the Adaptive Template method since the tracking triad template is updated for every new lesion.

This tracking method has inherent advantages and disadvantages. The triad template's component lesion template are local to one another is one advantage. Therefore, any variation in the retinal illumination source should effect the component lesion templates more evenly as compared to vessel templates. This advantage also applies to the UT method. The AT method also has the additional advantage of using therapeutic sized lesions as lesion templates. Recall that the UT method required lesions distinguishable from therapeutic sized lesions. This reduced the therapeutic value of the UT template lesions.

One disadvantage of the Adaptive Template tracking method is controlling the formation of the first lesion. All subsequent lesions use previous lesions as landmarks to stabilize the therapeutic laser. However, the first lesion must rely on some other method. This may be remedied by using some of the other tracking methods already presented in this document. Another disadvantage of the Adaptive Template tracking method is that each lesion template triad formed must provide a separate and distinct template from all other template triads in the array. Several methods may be used to provide lesion 'distinctness' in the array. Adjusting lesion diameter or depth would provide lesion variability; however, this method would defeat the purpose of the Reflectance Based Control System. Another method of providing variability is to provide a slight coordinate shift in lesion placement. A lesion could be shifted a pixel or two in a given direction to provide distinct lesions. This would provide the unique lesion template triads and provide only a slight modification in the lesion array. To study the impact of this disadvantage in detail, a simulation

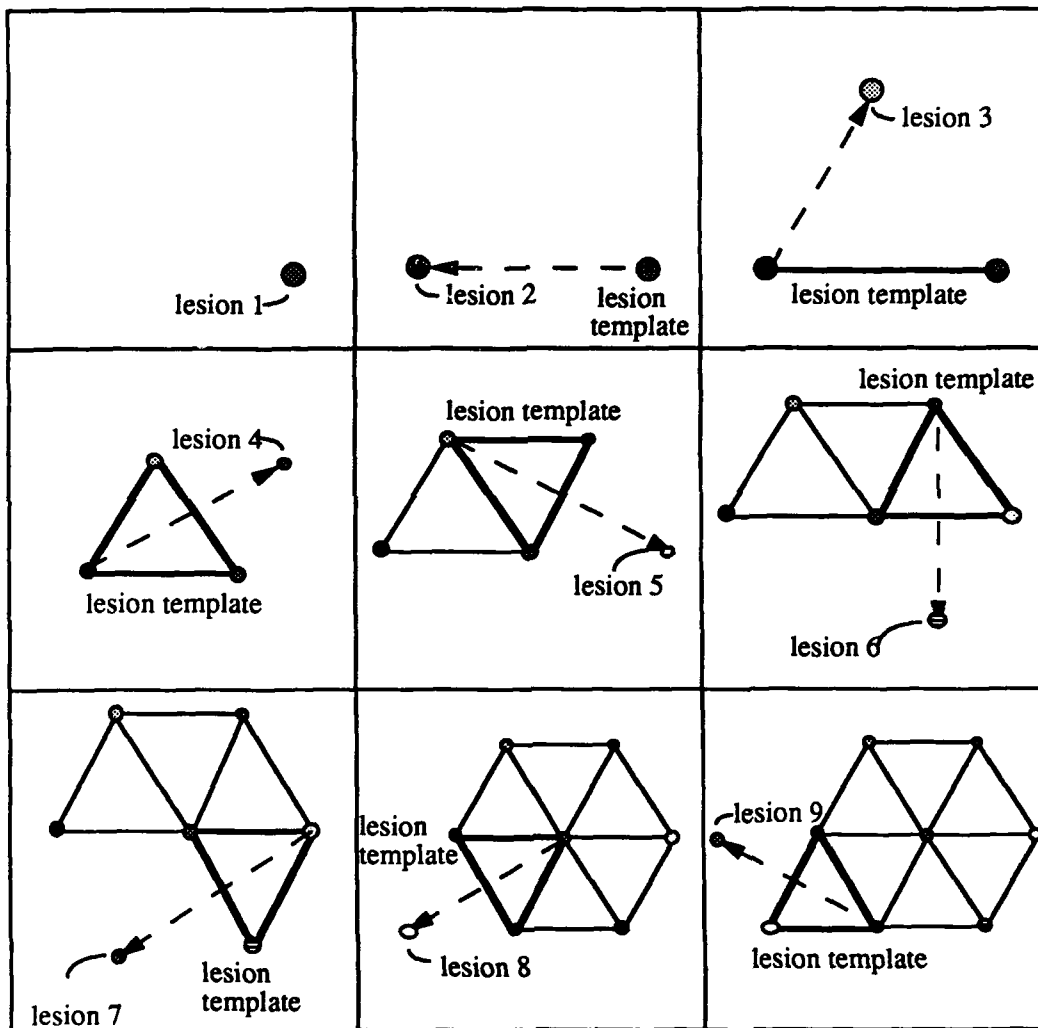


Figure 6.10: Therapeutic lesion formation using the Adaptive Template method

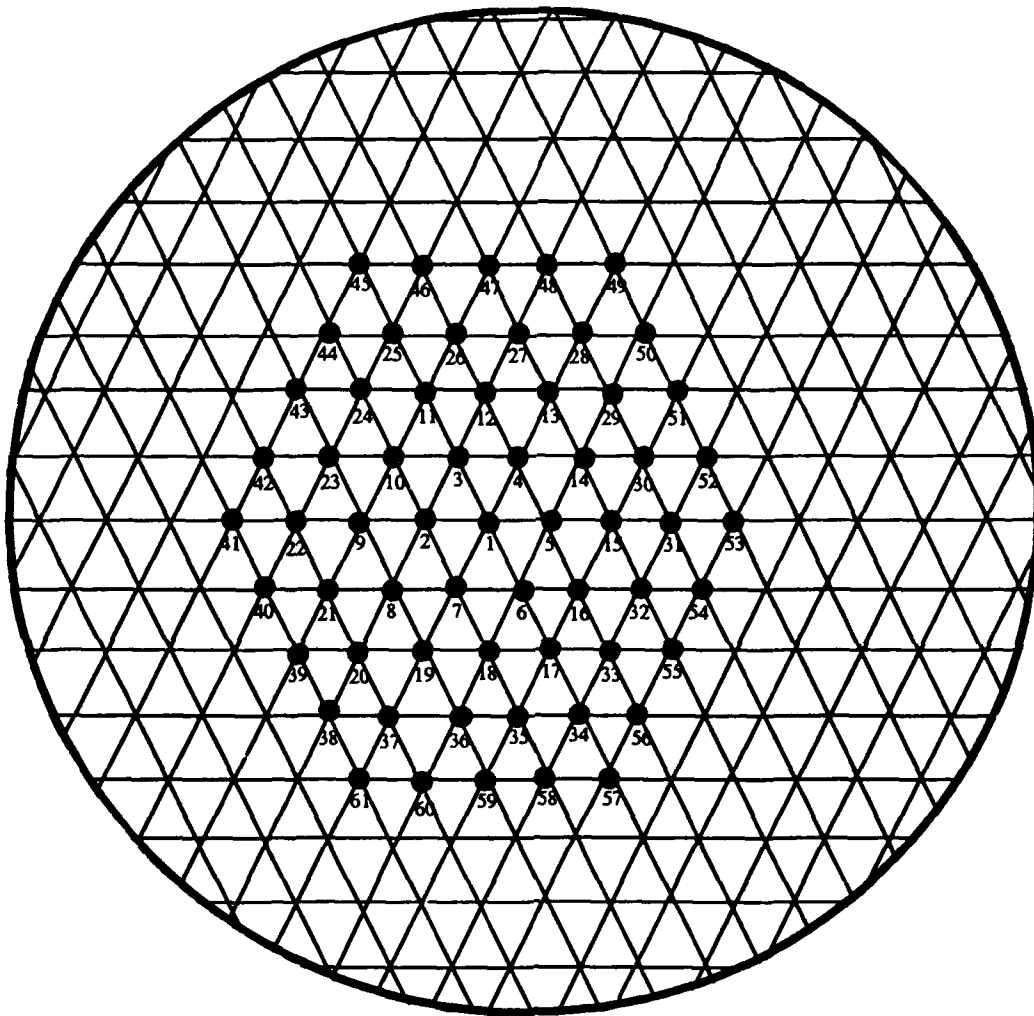


Figure 6.11: The complete pattern of 61 therapeutic lesions. The lesions are shown here in an orderly array of uniform size. To track retinal movement using lesions in a triad pattern, some method of 'distinctness' must be injected into the array pattern. Varying the diameter or depth of the lesion would provide the necessary distinctness but would contradict the goal of the Reflectance Based Feedback Control System. Instead, distinctness is introduced by randomly choosing one of twelve lesion offsets. These slight offsets provide the necessary distinctness without significantly altering the order of the array.

program was written to model lesion placement and triad template formation using the Adaptive Template method. The next several sections describe this study in detail.

Feasibility simulation testing

To model the efficacy of the Adaptive Template method, a simulation of the method was written. The first requirement for simulation development was to determine the number of distinct lesion types to form a therapeutic array of 61 lesions without forming any duplicate lesion triads. Second, it was necessary to show that an algorithm could be developed to form therapeutic lesions in an orderly method using predecessor lesions as templates to form the current lesion.

Determination of the distinct number of lesion types to form a therapeutic array To determine the number of distinct lesion types required to form an array of 61 lesions with no duplicate lesion triads, a program called RANDOM was written. RANDOM loads interconnect data on all lesion triads within a 61 lesion array. There are a total of 96 distinct lesion triads formed by the 61 lesions. The number of distinct lesion types (n) for simulation is then provided by the user. A random number generator then assigns each of the 61 lesions with a distinct type from 1 to n . The entire complement of 96 lesion triads are then tested for duplicates. Duplicate information is then provided.

The random number generator A random number generator was used to assign lesion types within the 61 lesion array to avoid duplicate triad

entries. A random number generator of the linear congruential generator type was used. This type of generator provides random numbers using the recurrence relation:

$$I_{j+1} = aI_j + c \pmod{m} \quad (6.2)$$

where a is the multiplier, c the increment, and m the modulus. The initial value of I_j is called the seed. The seed establishes the starting point of the repeating sequence. To break up the sequential correlation of the random stream, a shuffling routine is used. The shuffling routine uses the current random number to select a random number from an array of random numbers for output. The output random number is replaced in the array by the random number used to select its position in the array [71].

This random number generator was tested on various numbers of distinct lesion types. The results of using the random number to generate 32,000 random numbers between 1 and 12 are illustrated in Figure 6.12. Note the relatively equal assignment of lesion types.

Results of lesion assignment simulations A total of 16 simulations were performed for different numbers of distinct lesion types. The average of the 16 simulations are provided in Figure 6.13. As expected, when only one distinct lesion type is used 96 duplicate lesion triads result. The number of duplicate triads reduce as the number of distinct lesion types are increased. A total of 12 distinct lesion types were required to reduce the number of duplicate entries to less than 2.

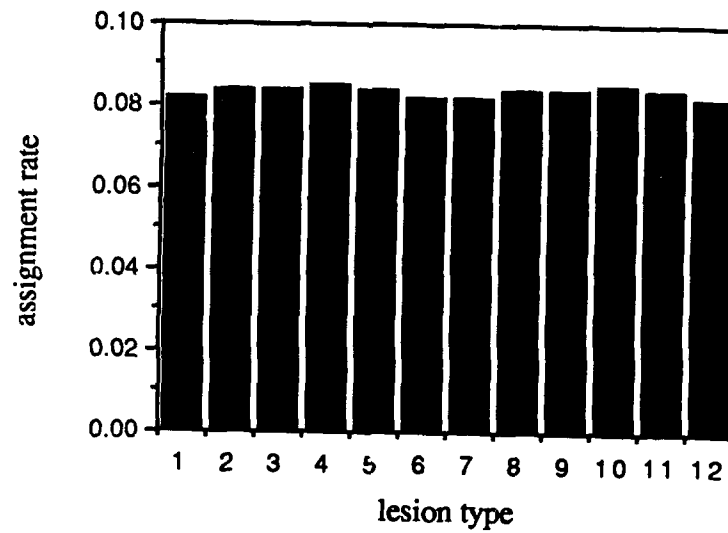


Figure 6.12: Random lesion type assignment

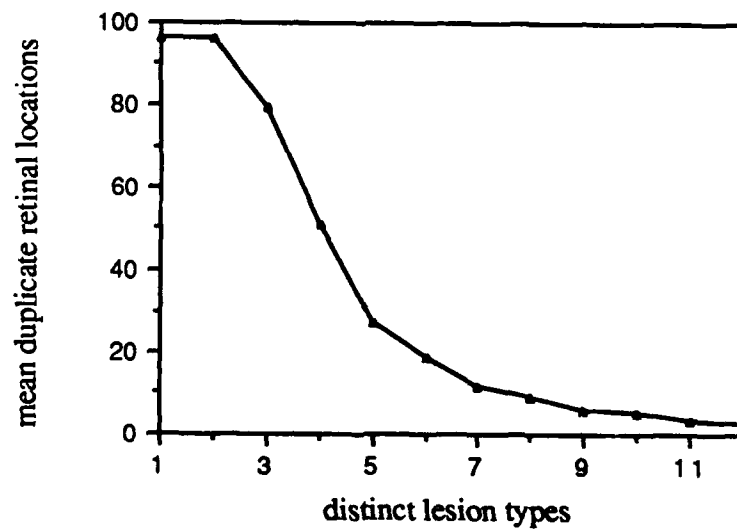


Figure 6.13: Results of distinct lesion type selection

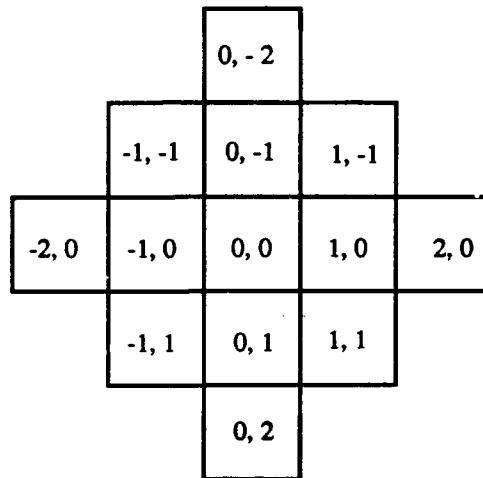


Figure 6.14: The pixel coordinate shift to provide distinct template triads. One of twelve available shifts are randomly chosen for lesion coordinate placement. These shifts provide the distinct template triads required for the Adaptive Template tracking algorithm without significantly altering the orderliness of the lesion template array.

Controlling the distinctness of a lesion To implement the Adaptive Template method some means of controlling the 'distinctiveness' of lesions is required. The above analysis indicated 12 distinct lesion types must be used to provide for nonduplicated lesion triads within a 61 lesion array. This required distinctiveness is obtained by varying the lesion coordinate by one or two pixels. This is easily implemented since a given pixel has eight neighboring pixels a single pixel away. The remaining four displacements are obtained two pixel displacements away. The pixel coordinate shift is illustrated in Figure 6.14.

The Adaptive Template Algorithm The final step in demonstrating the efficacy of the Adaptive Template method was developing an algorithm to place current lesions using the position of predecessor lesions as a location reference. This algorithm was developed to place these lesions on a still video frame. The

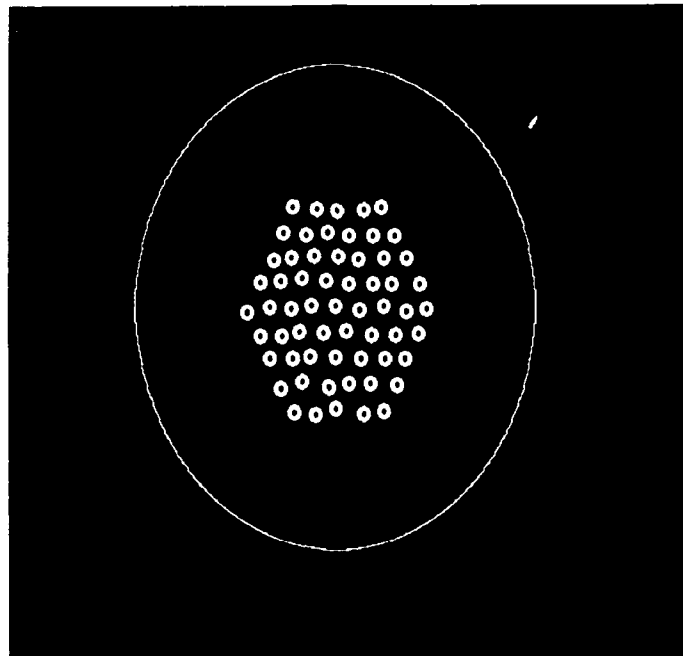


Figure 6.15: Adaptive Template results

algorithm developed to plot the results of the Adaptive Template method uses the first template to plot the second; the first and second to plot the third; the first, second, and third to form a triad and plot the fourth and so on. The results of this plot are provided in Figure 6.15.

6.8 Lesion Tracking and Image Analyzer software

The software developed to test the different concepts and methods for this chapter are found in programs Lesion Tracking and Image Analyzer (LETINA) and RANDOM. Structure charts for these programs are provided in Figures 6.16 and 6.17. Many of the support functions for program LETINA are identical to the support functions for program RETINA described in previous chapters. However, variations in template building functions, Lesion Data Base building

functions, and the actual tracking algorithms are different.

The lesion tracking algorithm uses a similar concept to that described for the tracking algorithm using vessels. The same limited exhaustive search technique is used. Figure 6.18 illustrates how this limited exhaustive search was implemented for lesion tracking.

Chapter 8 provides results of additional tests performed on the lesion tracking concept.

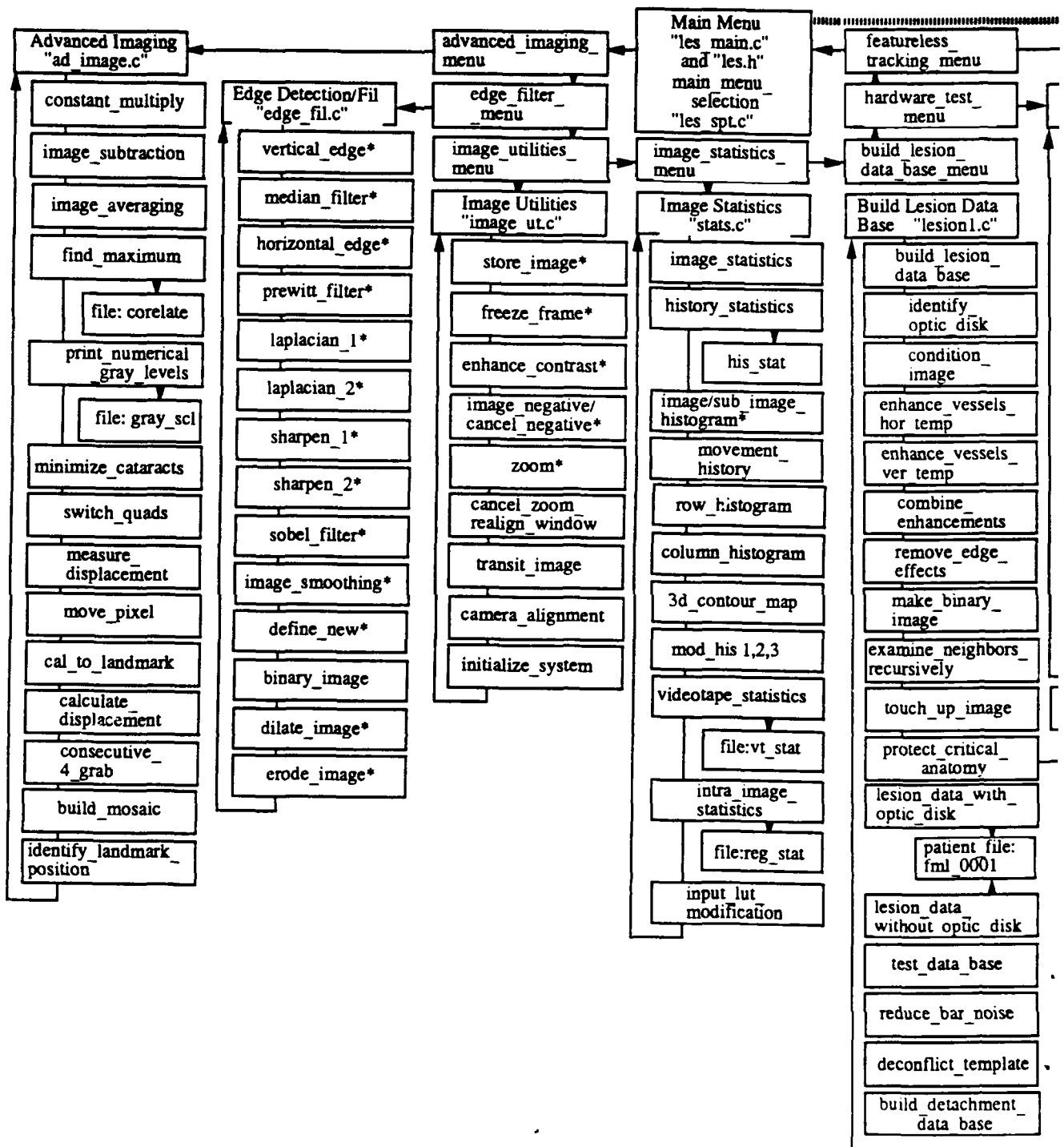
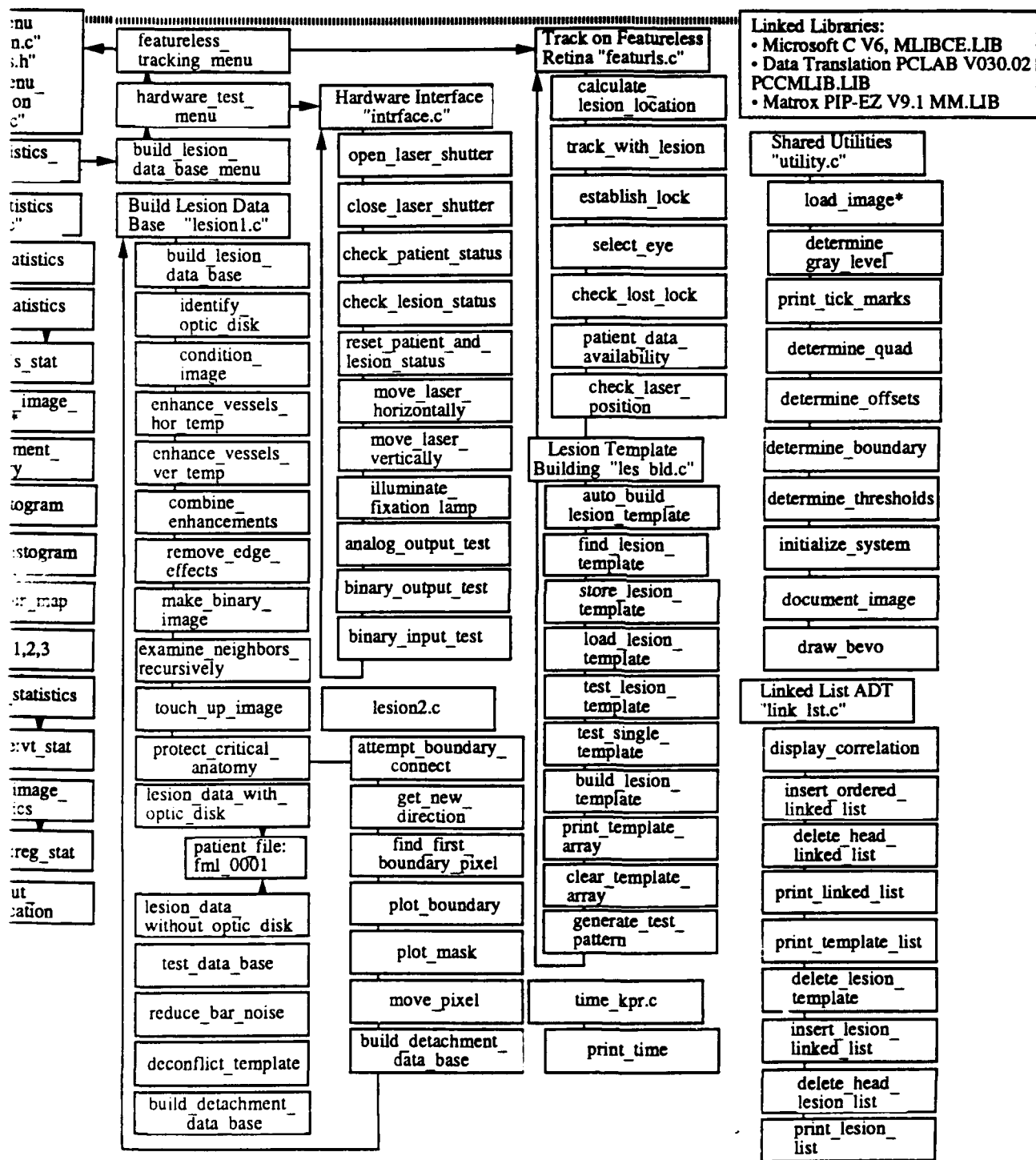


Figure 6.16: Lesion Tracking and Image Analyzer (LETINA)

(1)



Retinal Image Analyzer (LETINA) software

2

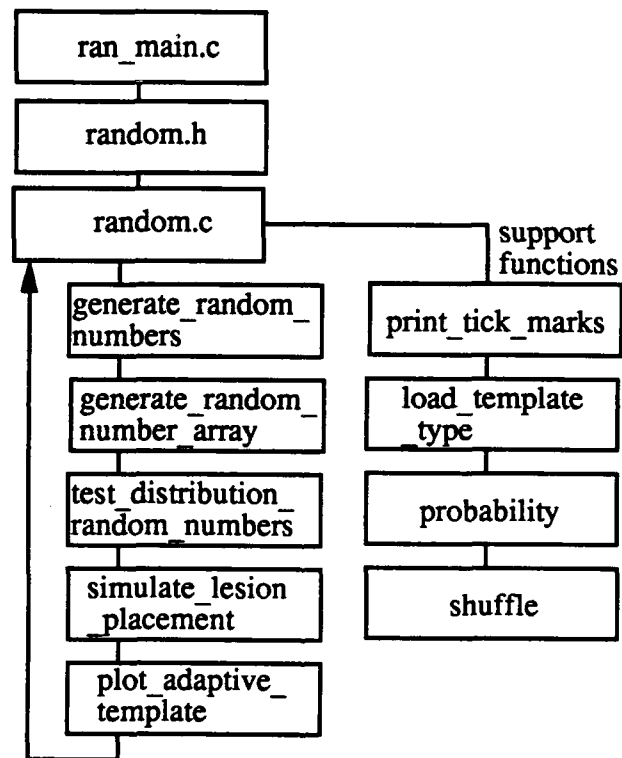


Figure 6.17: Program RANDOM

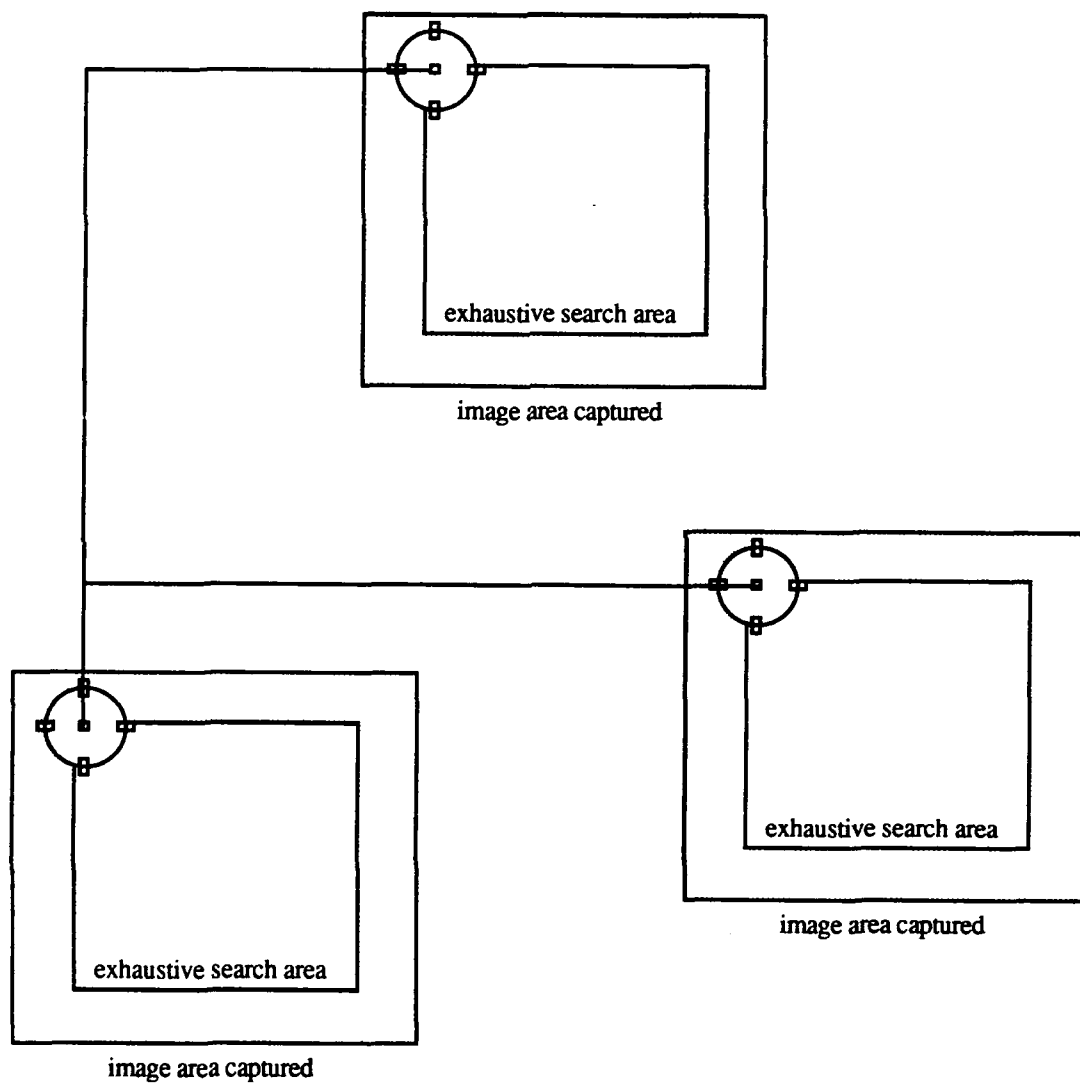


Figure 6.18: The limited exhaustive search using lesion templates

Chapter 7

Development System Instrumentation

7.1 Overview

This chapter describes the instrumentation used in the development system. Where pertinent, a description is provided on the theory of equipment operation.

The development system configuration is illustrated in Figure 7.1. This configuration operates in the following manner: The Olympus mydriatic fundus camera provides an optical image of the retina to the Panasonic charge coupled device (CCD) video camera. The video camera converts the optical image into a RS-170 video signal. This signal is recorded on standard VHS format video tape. The video signal is also routed to the Matrox PIP-1024 video frame grabber. The frame grabber converts the RS-170 video signal into a 512 x 512 array of integers. The integer magnitude corresponds to the gray level value of an individual pixel within a video frame. An image of the retina is now available for processing. The frame grabber is hosted on a Gateway 486 personal computer (PC) operating at 33 MHz. The PC executes the tracking algorithm using image data obtained from the frame grabber. An X and Y laser correction signal is derived from the tracking algorithm and provided to a pair of General Scanning AX-200 galvanometer driver amplifiers via the Data

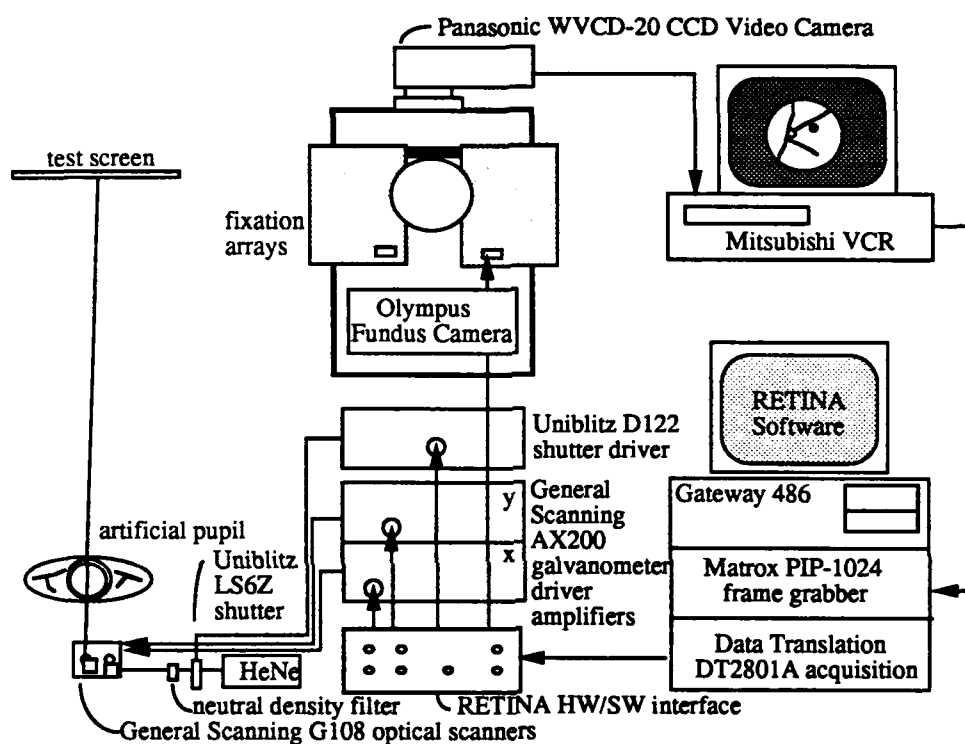


Figure 7.1: Developmental system instrumentation

Translation control board. These drivers provide the necessary signals to the General Scanning G108 optical scanners used to steer the laser beam. The surgical laser is simulated by a low power Helium Neon laser. This laser is projected through a neutral density filter and a Uniblitz LS6Z laser shutter. The interface between the PC and the shutter and driver amplifiers is provided by the RETINA HW/SW Interface designed by the author. More information is now provided on each component.

7.2 The Fundus Camera

The fundus camera is an optical camera used to image the surface of the retina. There are two basic types of fundus cameras: the contact type and the non-contact type. With a contact fundus camera, an ophthalmoscopic lens touches the patient's cornea. This type of fundus camera affords a field of view up to 85 degrees. The noncontact type fundus camera does not use a contact lens and has a maximum field of view of 60 degrees[77].

For this study an Olympus mydriatic fundus camera model GRC-W was used to image the retina. The Olympus GRC-W requires dilation of the patient's pupil (mydriatic) to view the retina. With the pupil dilated, the eye's interior is illuminated via a halogen source axially aligned with the camera's objective lens. Light reflected from the fundus is captured by the objective lens and is provided to an eyepiece, to a video camera port equipped with a C mount, and to several still photography ports.

For effective fundus imaging the optics of the fundus camera must obey the Gullstrand Principle. This principle indicates the ray bundles used for illumination and observation must be separated on the cornea and on the first surface of the crystalline lens. This is accomplished by having the illumination source form a bright, luminous ring on the cornea. This light ring also forms a ring on the anterior portion of the crystalline lens. The area inside the ring is called the corneal window and it is used for observation of the retinal image [77]. This prevents the bright reflections from the cornea from overwhelming the dim reflections from the retinal surface [78].

A real aerial image of the retina is formed by the ophthalmoscopic lens. This lens forms a blurred image of the retina. This blurring is caused by bundles

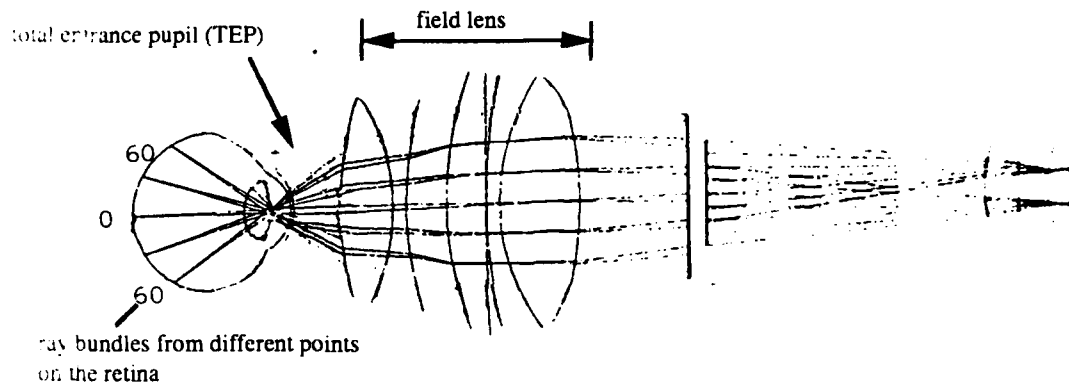


Figure 7.2: Noncontact fundus camera optics [77]

of rays originating from different points on the retina not coming to a sharp focus. Each of the bundles has an individual entrance pupil (IEP) to the eye. Anterior to the eye's pupil plane is a common waist of all IEPs called the total entrance pupil (TEP). Ideally the image bundles' IEPs are equal and concentric at the TEP. This is possible when the field of view is limited to values below 60 degrees and the pupil is widely dilated [77]. Typically, pupil dilation is limited to eight millimeters [79]. At fields of view greater than 60 degrees the image bundle's IEP cause the TEP to exceed the size of the corneal window allotted for imaging [77].

The curvature of the retinal surface must also be considered to obtain a sharp image. An additional requirement is for a comfortable, safe level of retinal illumination. This illumination requirement calls for a fundus camera objective lens that is as fast (short focal length) as possible. This further complicates the curvature problem since the individual entrance pupils for the different image bundles will not converge to a single point as required by the discussion above. These conflicting requirements call for a large aperture lens with a corresponding small depth of field. The lens must focus both paraxial

and peripheral fields in the same plane despite the curvature of the retinal surface. Through careful choice of the ophthalmoscopic lens's refractive index, thickness, and curvature the individual entrance pupils may come to focus at a single total entrance pupil[77].

Following the ophthalmoscopic lens is a set of field lens whose purpose is to bend all of the individual image bundles into the entrance pupil of the recording device [77].

7.2.1 Fundus Camera Filters

The fundus camera may be used with various inline filters to enhance certain portions of the retinal image. Early in this study an Olympus GRCW-FGE green filter was employed to enhance the retinal vessel network. This is a green bandpass filter with a maximum transmittance wavelength of 530 nm. The spectral response of the filter was obtained with a Varian 2300 spectrophotometer.

A 568 nm interference filter (Edmund Scientific J43,127) was also used inline with the fundus camera illumination lamp. This filter was chosen based on the work of Delori et al. described in Chapter 3 of this document. As expected, vessel contrast enhancement was superior to that obtained with the Olympus filter. The spectral response of this filter was also obtained with the Varian 2300 spectrophotometer. Use of this inline interference filter also reduces the level of illumination reaching the surface of the patient's retina.

7.3 The CCD Video Camera

A Panasonic WV-CD20 charge coupled device video camera was connected to the Olympus fundus camera via a standard C mount. This is a 510 x 492 pixel camera with 256 distinct gray levels. The camera operates at a standard 30 frames per second. The camera has a peak sensitivity of .07 footcandles at 530 nm. This camera provides a resolution of approximately 40 microns on the retinal surface. A high resolution is required when forming lesions on the order of 200 microns and to obtain a detailed retinal diagnostic map.

7.4 The Video Frame Grabber

The video frame grabber chosen for the development system was the Matrox PIP-1024. This video digitizer provides a 1024 x 1024 pixel image plane which may be partitioned in various configurations. For this research effort the frame grabber was partitioned into four 512 x 512 image planes.

The frame grabber's primary purpose is to provide a 'snapshot' of eye movement. Correction information for the Laser Pointing System is then derived from the still image. Many other frame grabber functions provided within the PIP-EZ MS DOS Software Library were used in this project. The interested reader is referred to [80].

7.4.1 Theory of Operation

A block diagram of the PIP-1024 is provided in Figure 7.3. The PIP-1024 is equipped with three separate video input sources. One of these sources is selected via software. The video functions of the PIP-1024 are driven by the

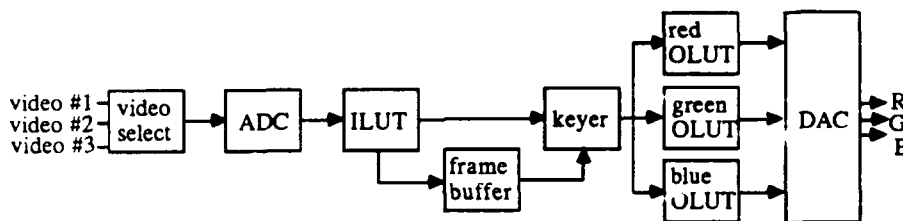


Figure 7.3: The Matrox PIP-1024 video frame grabber [81]

timing from the selected input video source. A stable internal video source may also be selected [81].

The video source signal is provided to a sync separator where the image data is extracted. The data is then passed to an analog to digital converter (ADC). The user has control over the gain and offset control of the converter via software. This allows the user to center the incoming signal in any portion of the ADC's range. These controls are similar in function to the brightness and contrast controls on a standard monitor. The ADC converts the analog video signal into an 8 bit digital integer. The output of the ADC is routed to the input look-up table (ILUT) [81].

The ILUT consists of 8 separate 256-byte maps. The ILUT maps the input data to values established by the user. As previously described, the ILUT has been employed in this project to dramatically increase the contrast of the retinal vessels against the retinal background. The output of the ILUT is provided to the frame buffer [81].

The frame buffer is a 1 Mbyte random access memory (RAM) module. The frame buffer may be accessed for reading and writing using a Cartesian coordinate system. A video frame is stored in the frame buffer when frame

grabbing is active. For this project the snapshot grabbing mode was used. In this mode a single frame is grabbed and stored in the frame buffer [81].

The output section of the frame grabber consists of a keyer and output look up tables (OLUT). The video keyer allows selection of either the incoming video signal for output or the output may be obtained from the frame buffer. The output selected is routed through three separate OLUTs (red, green, blue). These three OLUTs may be adjusted to provide a pseudo-color output or the green OLUT may be used to provide monochrome output. The frame grabber was used in the monochrome mode. The OLUTs are routed to Digital to Analog Converters (DAC) for reformatting into a video output [81].

7.5 Laser Pointing Hardware

The laser pointing hardware consists of galvanometer driver amplifiers and optical scanners manufactured by General Scanning Incorporated. The AX-200 driver amplifiers and the G-108 optical scanners were chosen for the development system due to their ready availability.

7.5.1 Driver Amplifiers

A separate AX-200 driver amplifier is provided for the X and Y optical scanners. The AX-200 is a solid-state variable output impedance amplifier. The variable output impedance permits adjusting the amplifier response to step changes in the input. The AX-200 has a maximum input range of ± 1 vdc with a maximum output current of ± 1 amp [74]. The required input signal to direct the laser is derived from the tracking algorithm and provided via the RETINA Hardware/Software Interface. This driver provides open loop control of the

optical scanners since no feedback signal is provided back to the driver.

7.5.2 Optical Scanners

The optical scanners employed in the development system are a set of G108 galvanometers. These scanners do not include a position sensor to provide feedback for precise positioning. These scanners may be driven sinusoidally at up to 1,275 Hz. The scanners have a mechanical peak-to-peak rotation of 8 degrees and a torque rating of 80 gm-cm. A mirror is attached to a separate mount attached to the output shaft of the scanner. Mirror deflection is proportional to drive current [75].

7.6 The Laser Shutter

The laser shutter chosen for the development system is a self contained laser shutter and drive unit manufactured by Vincent Associates. The shutter is a Uniblitz LS6Z driven by a Uniblitz D122 driver.

The shutter has a 6 mm opening for the laser. The shutter blades are coated with Aluminum Silicon Oxide and .001 Beryllium Copper which withstands laser energy upto $5 W/mm^2$ in the visible wavelengths. The shutter rapidly responds to input signals. The shutter only requires 1.8 msec to open and 0.8 msec to close [82].

The Uniblitz D122 driver may be used in many different modes. For this application, the driver was configured in the 'Pulse In' mode. This mode provides an active high input to control shutter exposure for the duration of a positive pulse applied to the driver. The shutter follows the pulse applied to the

driver. The driving signal was provided via the RETINA HW/SW Interface from the tracking algorithm [83].

The D122 driver also has a built-in safety feature to guard against power failure. In the event of an AC power failure to the driver, the laser shutter remains closed after power is restored until manually reset by the user [83].

7.7 The Computer

The computer selected for this project was a Gateway 486-33 computer. This computer serves as the host for the video frame grabber hardware board and the data acquisition and control board. This computer is equipped with an Industry Standard Architecture (ISA) bus. This bus configuration allows compatibility with the hardware boards. The ISA architecture contains two buses: a separate 16 bit input/output bus and a 32 bit memory bus [84].

7.7.1 Specifications

The Gateway 486-33 is equipped with an Intel 33 MHz 80486DX central processing unit. This 'chip' is equipped with a 8 KB cache controller and an on-chip floating point unit. The input/output bus operates at 8.3 MHz [85].

7.7.2 Specifications

The tracking algorithm was also tested on a Gateway 486-50 computer. This computer is equipped with an Intel 80486DX2/50 central processing unit. This processor is also equipped with a 8 KB cache controller and an on-chip floating point unit. The input/output bus on this computer also operates at 8.3 MHz

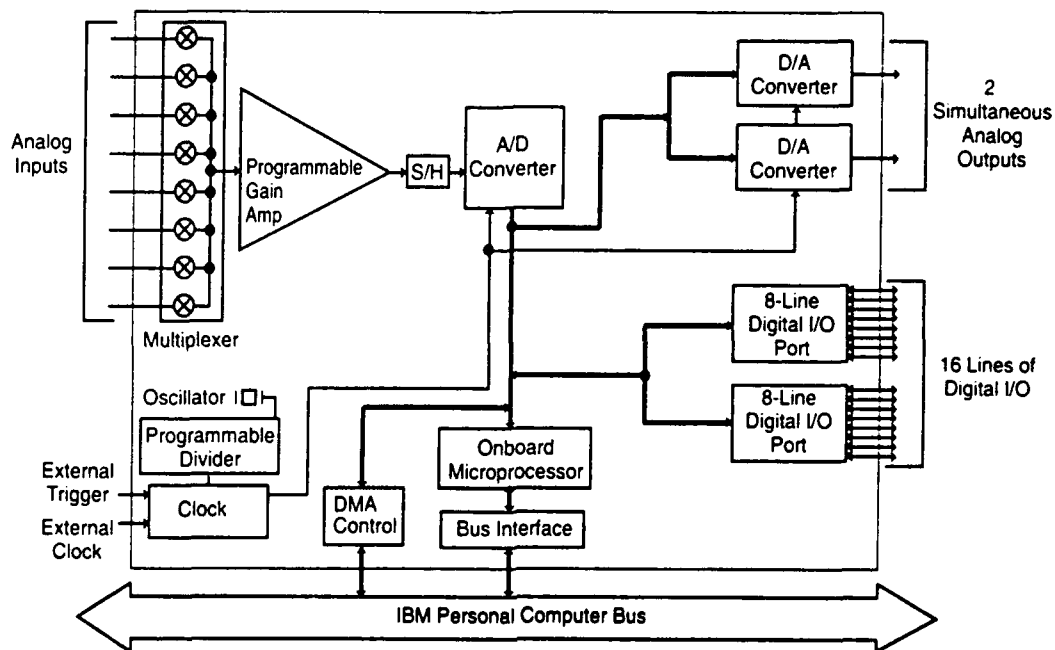


Figure 7.4: The Data Translation DT2801A I/O board [88]

[86].

7.8 Data Acquisition and Control Hardware

Considerable information is transferred into and out of the tracking algorithm. The main interface between the tracking algorithm and the external hardware is the Data Translation DT2801A analog and digital input/output (I/O) board. This board contains its own resident microprocessor and software library to perform data transfer operations. The board is configured with a programmable analog input channel, two analog output channels, and a 16 bit digital input/output port. A block diagram of the board is provided in Figure 7.4 [88].

The DT2801A board is controlled by a number of high order programming languages. For this project, the board was accessed via C functions resident in the Data Translation PC Lab software library. This library is linked with the compiled tracking algorithm just prior to program execution. Use of software version V03.02 (or later) allows full compatibility with the 486 PC operating at 33 and 50 MHz [88].

7.9 The RETINA HW/SW Interface

The RETINA HW/SW Interface is a self developed hardware 'black box' to fully integrate all PC hosted boards, external drivers, and peripheral hardware. The interface also simulates signals that would be provided by the Reflectance Based Feedback Control System. A schematic of this interface is provided in Figure 7.5.

Specifically, the RETINA HW/SW Interface provides the following functions:

- Provides an interface between the Data Translation DT2801A I/O board and all external circuitry. The DT2801A is linked to the RETINA HW/SW Interface circuit board via a 50 conductor ribbon cable.
- Simulates the 'Lesion Complete' signal from the Reflectance Based Feedback Control System (RFS). The RFS provides a signal when a lesion has reached its prescribed size. This signal is simulated via a pushbutton on the front panel of the RETINA HW/SW Interface. When depressed a bounceless pulse provided by the cross-coupled NAND gates (7400) sets a JK flip-flop (7476). A status indicator on the front panel is also set.

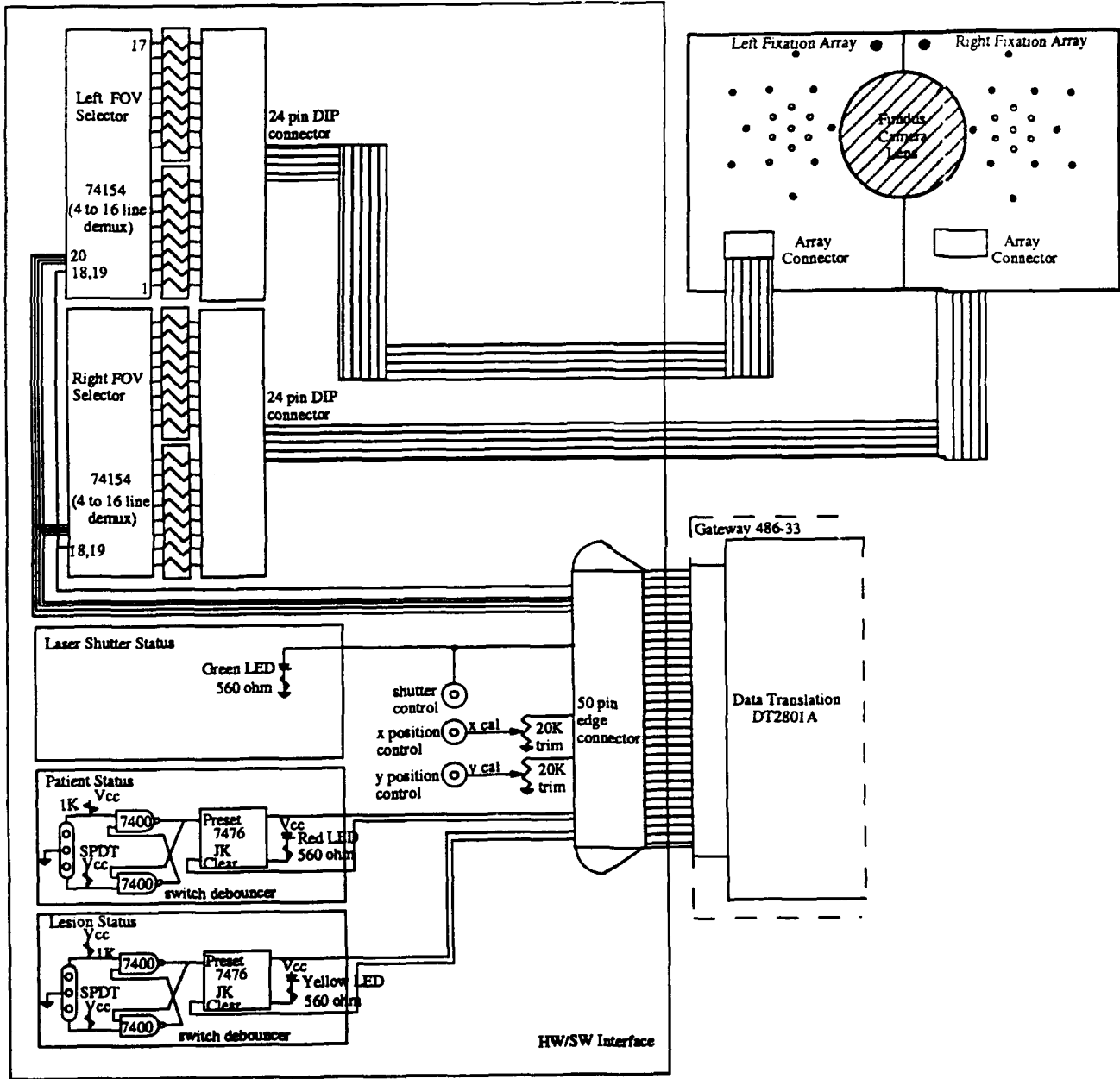


Figure 7.5: The RETINA HW/SW Interface

The tracking algorithm reads the status of the flip-flop via the function `check_lesion_status`.

- Provides a 'Patient Status' control. This control is also provided on the front panel of the RETINA HW/SW Interface. This allows the patient to halt the laser surgery. When depressed a JK flip-flop is set as previously described. A status indicator is also set. The tracking algorithm monitors the status of the flip-flop via the function `check_patient_status`. When the tracking algorithm detects a set flip-flop the laser shutter is closed and the laser surgery is brought to an orderly halt.
- Provides for laser shutter control. The actual laser shutter control signal is generated within the tracking algorithm and the DT2801A I/O board. The RETINA HW/SW Interface routes the laser control signal from the DT2801A to the Uniblitz D122 shutter driver.
- Provides the laser correction signals. The actual laser correction signal is derived within the tracking algorithm and output via the DT2801A in analog form. However, the peak-to-peak swing of the laser correction signal is ± 10 volts. The maximum allowable input to the AX-200 galvanometer driver amplifiers is ± 1 volts. The RETINA HW/SW Interface provides 20 K ohm trim potentiometers to reduce the signal from the DT2801A for AX-200 compatibility. These 'trimmers' are also used to calibrate the Laser Pointing System.
- Provides the decoding circuitry necessary to illuminate the proper light emitting diode (LED) on the Left and Right Fixation Arrays. Recall, that each field of view data is stored separately within the Patient File.

When a given field of view's lesion data is retrieved for treatment, the field of view designator is decoded from the hashing function code. This code is converted into the addressing necessary to drive the 4 to 16 line demultiplexers (74154). The output of the demultiplexers illuminate the proper LED on the fixation arrays. For example: if field of view 5 of the left eye is being readied for treatment, the LED corresponding to field of view 5 in the right eye is illuminated.

7.9.1 The Fixation Device

The purpose of the fixation arrays are to minimize eye movement during laser irradiation. By fixating on an object the patient is able to minimize movement in the conjugate eye. Fixation array design assumptions are based on the work of Cornsweet and Steinman.

Cornsweet [87] proposed a saccadic correction mechanism for fixation based on an optimal locus centered on the fovea. This optimal locus is assumed to be the origin of an error-signal system guiding corrective eye movements. Studies have shown the standard deviation of a fixating eye is on the order of 5 minutes of arc. Steinman's work demonstrated that the optimal locus described by Cornsweet is small and invariant in position on a given retina [89].

Steinman studied various fixation device variables including size, color, and luminance using subjects experienced in maintaining fixation. The following findings from Cornsweet's and Steinman's work were used to design the fixation targets for this study:

- Saccadic eye movements are reduced with the use of a fixation target.

- The primary stimulus for involuntary saccadic eye movements is displacement of the retinal image on the retina.
- Retinal drift movements are the result of instability in the oculomotor system.
- Even when a subject tries to fixate on a target the eyes are in constant motion.
- The dispersion of subject fixation increases monotonically with target size.
- No significant differences occur in fixation stability between red, blue, and white targets. However, all subjects tested had the least fixation dispersion with the red target and the most with the white target.
- Increasing target luminance reduces the variability of eye position.

Using these findings as a guideline, small (.315 cm diameter), red light emitting diodes biased to operate at a safe current load were used as the fixation target. Sixteen diodes were arranged in three concentric rings as illustrated in Figure 7.6. The three rings had axial displacements of 14.3 degrees, 28.6 degrees, and 44.6 degrees. Each ring contained six LEDs staggered at 60 degree intervals. A target LED was also provided in the center of the array.

The fixation background was painted matte (flat) black. Each target background was mounted to a sliding bracket that was fixed to the fundus camera. The fixation background was mounted 6.5 cm from the corneal surface (7.2 cm from the nodal point of the eye). The sliding apparatus allows

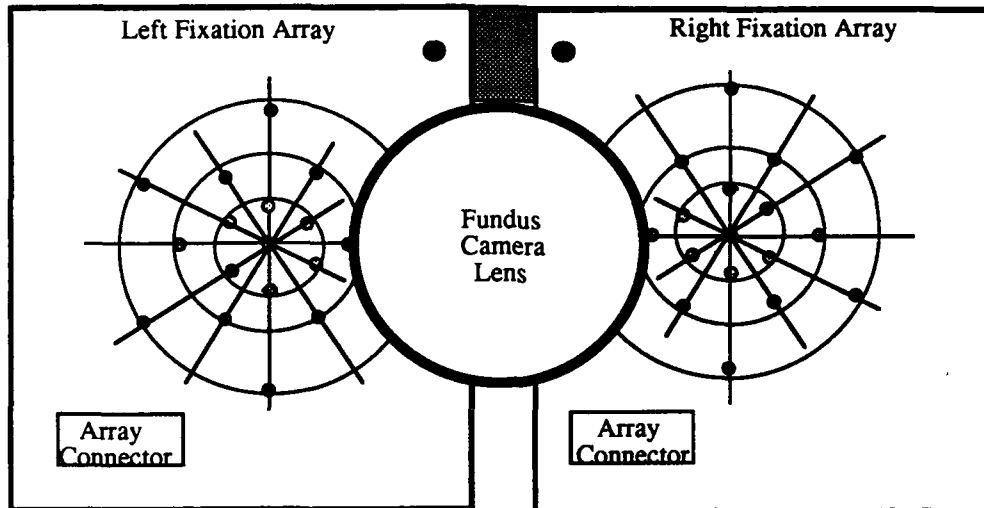


Figure 7.6: The fixation device

adjustment for different displacements between the eyes. As mentioned previously, the entire array is controlled via the tracking algorithm and the RETINA HW/SW Interface.

Chapter 8

Development System Testing

This chapter contains test descriptions, results, and analysis of test results performed on the developmental Retinal Tracking Subsystem. The chapter begins with a description of the testing configuration followed by sections on tracking using blood vessel template methods, timing test, and lesion template methods. Background information is provided throughout the chapter as needed.

8.1 Retinal Tracking Subsystem testing using blood vessel templates

This section begins with an equipment configuration description used for testing the tracking algorithm based on blood vessel templates. Following the equipment description, the testing protocol is described with test results and analysis. Algorithm timing results are then provided with methods of reducing algorithm execution time.

8.1.1 Test system configuration

Figure 8.1 illustrates the test configuration used to test the tracking algorithm based on blood vessel templates. Note that the Laser Pointing Subsystem is not part of this test. Results of testing the Laser Pointing Subsystem are provided

separately in this chapter.

Each piece of equipment was described in Chapter 7. In this configuration the Olympus fundus camera is equipped with a Panasonic WVCD-20 CCD video camera to record patient eye movement on the Mitsubishi video cassette recorder (VCR). The fundus camera is also equipped with a 568 nm interference filter (Edmund Scientific J43,127) to enhance the retinal vessels. The recordings were completed on several subjects over a period spanning 10 months. The recordings formed the data base for testing the tracking algorithm.

The fundus camera was not used during tracking algorithm testing. The Mitsubishi VCR provided the video record of the subject's retinal eye movement for analysis. The VCR's video output was provided to a Panasonic monitor for viewing and to the Matrox PIP-1024 frame grabber hosted on the Gateway 486-33 personal computer (PC). The video output of the frame grabber was displayed on a second Panasonic monitor. The PC also hosted the Data Translation DT2801A acquisition board. The RETINA HW/SW Interface provided a link from the DT2801A to the fixation array mounted to the fundus camera during the filming experiment.

8.1.2 Test description

This section describes the test protocol used to film the subjects' retinal eye movement and then to test the tracking algorithm.

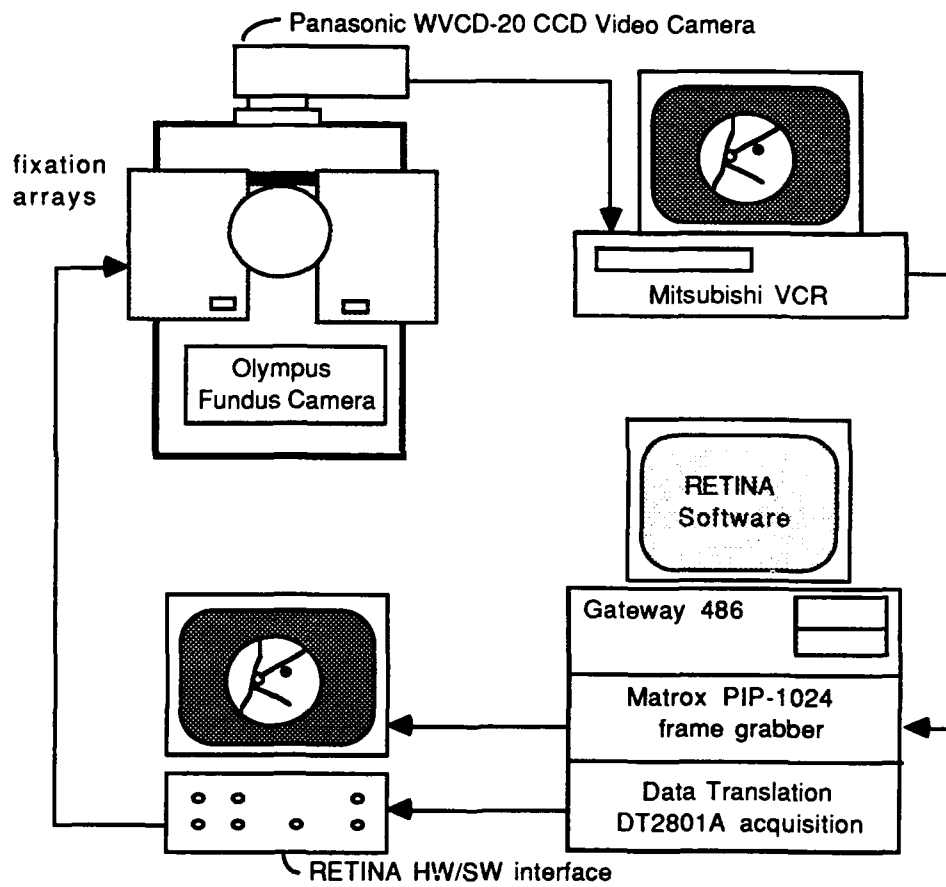


Figure 8.1: Tracking algorithm test configuration

Test subject description

Subjects were chosen for this test to obtain a variety of age, sex, and nationality. All subjects were unpaid volunteers familiar with this ongoing research effort. None of the subjects had fixation experience except for subject SBR.

- Subject RCL is a 21 year old male of Indian descent. RCL's left eye was filmed at a 50 degree fundus camera field of view using a 568 nm interference filter.
- Subject CSL is a 27 year old Caucasian female. CSL's left eye was filmed at a 50 degree fundus camera field of view using a 568 nm interference filter.
- Subject SBR is a 34 year old Caucasian male. SBR's right eye was filmed at a 50 degree fundus camera field of view using a 568 nm interference filter. SBR had participated in two filming exercises with fixation prior to this filming test.
- Subject ICR is a 28 year old female. ICR's right eye was filmed at a 50 degree fundus camera field of view using a 568 nm interference filter.

Test protocol for filming retinal movement

Each subject had their eye dilated 30 minutes prior to the filming experiment. The subjects were briefed on test procedure and the use of test results. The subjects were asked to fixate on the illuminated light emitting diode on the fixation array. The subject's were told to close their eyes if any discomfort was experienced. Total exposure to the fundus camera illumination source was

90 seconds or less during the filming of the fixation sequence. The subject's forehead and chin were stabilized using the rests provided on the fundus camera. Results of the filming were recorded on standard one-half inch VHS format video tape with the VCR set to standard play speed.

Test protocol for testing the tracking algorithm

Each video tape of retinal eye movement was processed through a test battery culminating with the tracking algorithm test. The test battery consisted of the following steps:

1. A reference image was arbitrarily selected from the video sequence. The reference image was 'snapped' to a still frame from the video tape and stored for further processing on the PC's hard disk.
2. The position of the optic disk centroid was then determined using function `find_optic_disk`. This function had the user align a cursor over the center of the optic disk. The coordinate of the optic disk center was retained for later use.
3. A histogram was then plotted of the central 225 x 225 reference image pixels. This histogram provided a method of comparing the reference image before and after histogram modification.
4. The histogram of the reference image was then modified using function `mod_hist`. This function was described earlier in this document. The histogram thresholds were automatically determined by function `determine_thresholds`. This function examined the histogram for the first and

last non-zero entry to determine the lower and upper thresholds prior to histogram modification. The new upper and lower histogram thresholds were preset to 0 and 255. A measure of histogram expansion was defined to compare histogram modifications as:

$$\text{expansion ratio} = \frac{\text{new upper threshold} - \text{new lower threshold}}{\text{current upper threshold} - \text{current lower threshold}} \quad (8.1)$$

5. The reference image with histogram modification was then used to build a two-dimensional vessel tracking template using the template building process described in Chapter 4.
6. After the template was built a Lesion Data Base was built (assuming a typical treatment for diabetic retinopathy) using the process described in Chapter 4. The template and the Lesion Data Base were both stored in a 'patient file' for each subject.
7. A 45 second retinal movement sequence was then used to test the tracking algorithm. The 45 second interval corresponded to the estimated amount of time required to treat a single retinal field of view. The tracking algorithm was tested using two different versions. The first version plotted the movement of the retina by tracking and plotting the position of the two-dimensional template. The plotting commands artificially slowed the tracking algorithm. The second version of the tracking algorithm had all print and plot commands removed. This version provided code timing status of the tracking algorithm.

8.1.3 Test results

The results of the test battery for each subject are provided in Figures 8.2, 8.3, 8.4 and 8.5. In each of these figures a reference histogram is provided before and after histogram modification. Also, results of building a Lesion Data Base for the treatment of diabetic retinopathy is provided for each subject. Finally, a plot of the position of the first horizontal template is provided over a 45 second test sequence. Figure 8.6 provides a summary of results for the test battery. The total reference template response provided in the figure is the sum of the six individual template responses multiplied by 100.

8.1.4 Analysis of test results

Overall, the template building, Lesion Data Base building, and tracking functions performed correctly for these four subject sequences. Subject RCL had excellent contrast between the retinal vessels and retinal background even *without* histogram modification. Histogram modification further enhanced the vessel network. The histogram expansion ratio was 2 for subject RCL. Seven blinks were detected during the test. The tracking algorithm correctly registered a loss of lock condition, re-established lock in approximately 330 ms, and continued with the tracking sequence. The tracking sequence was halted after the 45 second period using the Patient Panic switch on the HW/SW Interface.

Subject CSL also had an expansion ratio of 2. The span of the reference image histogram prior to modification was 0 to 155. The histogram was truncated to 0 to 127 prior to expansion to 0 to 255. CSL blinked once during the test. The tracking algorithm correctly registered a loss of lock condition, re-established lock, and continued with the tracking sequence. The tracking

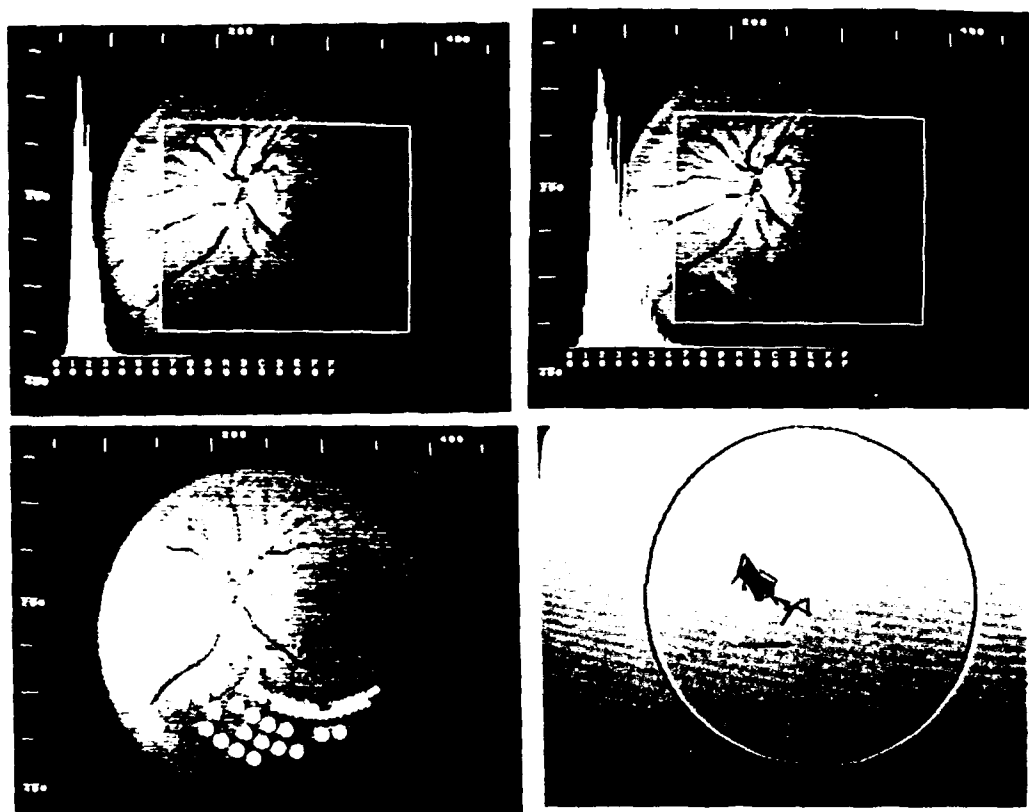


Figure 8.2: Results of testing subject RCL. Upper left: histogram of the reference image. Upper right: histogram of the reference image after histogram modification. Lower left: results of Lesion Data Base building. Lower right: results of the tracking sequence. A 40 pixel (approximately 1.86 mm) reference line is provided.

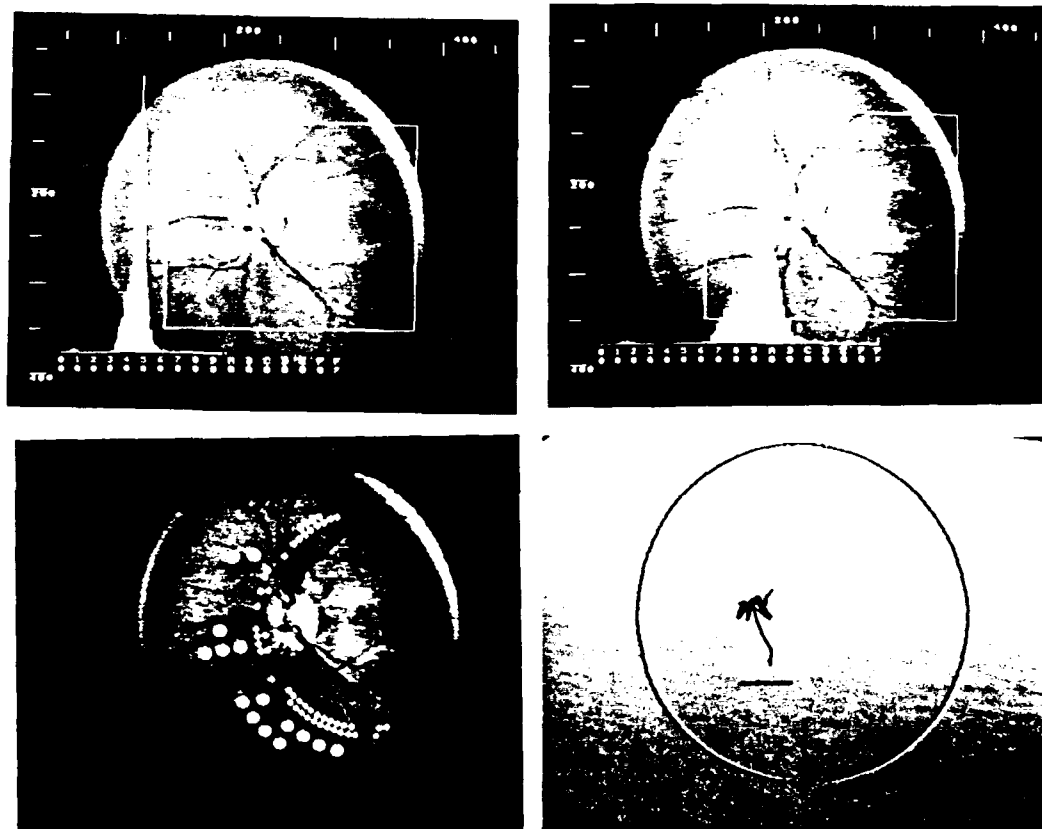


Figure 8.3: Results of testing subject CSL. Upper left: histogram of the reference image. Upper right: histogram of the reference image after histogram modification. Lower left: results of Lesion Data Base building. Lower right: results of the tracking sequence. A 40 pixel (approximately 1.86 mm) reference line is provided.

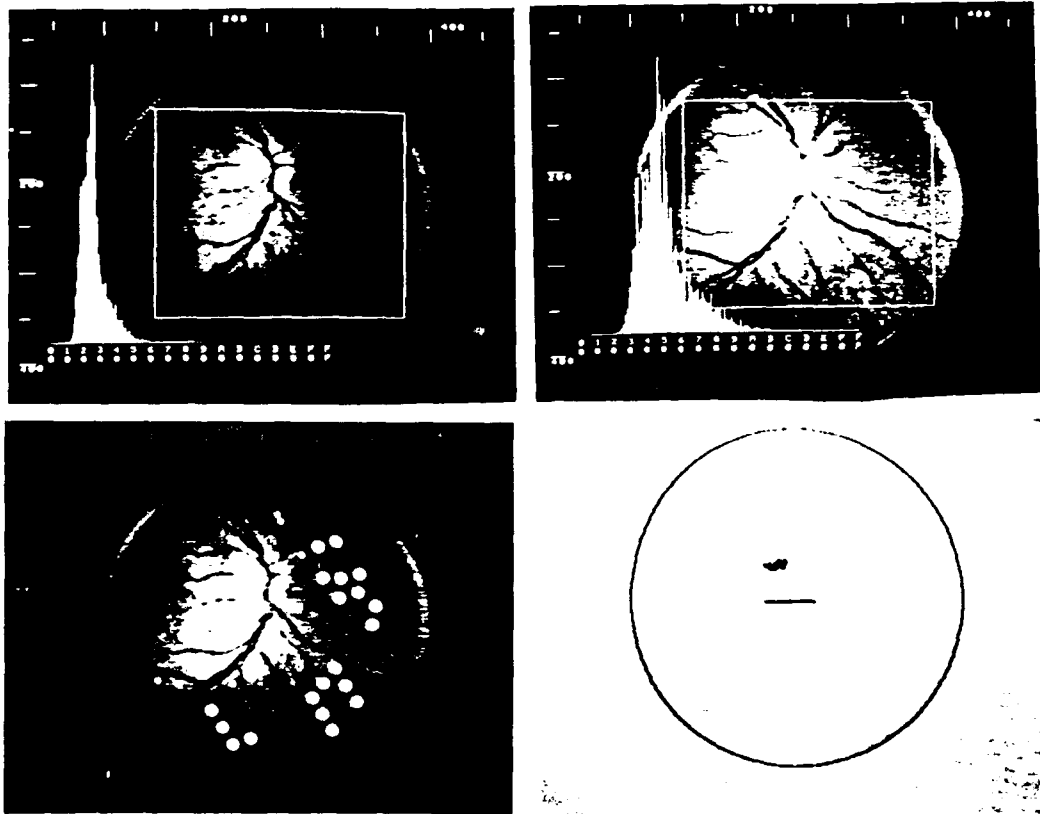


Figure 8.4: Results of testing subject SBR. Upper left: histogram of the reference image. Upper right: histogram of the reference image after histogram modification. Lower left: results of Lesion Data Base building. Lower right: results of the tracking sequence. A 40 pixel (approximately 1.86 mm) reference line is provided.

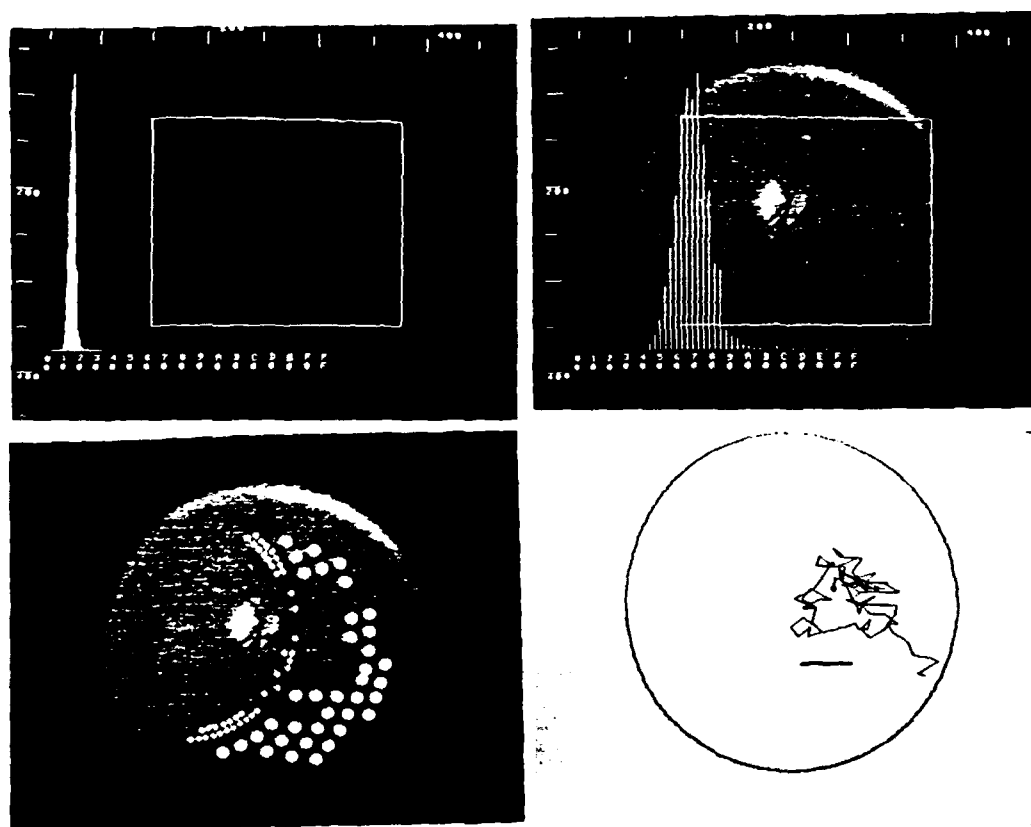


Figure 8.5: Results of testing subject ICR. Upper left: histogram of the reference image. Upper right: histogram of the reference image after histogram modification. Lower left: results of Lesion Data Base building. Lower right: results of the tracking sequence. A 40 pixel (approximately 1.86 mm) reference line is provided.

	Subject			
	RCL	CSL	SBR*	ICR
sex, age, eye	m, 21, l	f, 27, l	m, 34, r	f, 28, r
histogram expansion ratio	2	2**	2**	5
lost lock/ blink detected	7	1	0	0
total reference template response	232	55	170	143
average update time (ms)***	220	220	220	220
total tracking area (sq mm)****	4.39	1.31	.482	*****

* Two previous fixation experiences

** Reference histogram was truncated to allow histogram expansion.

*** 40 x 40 search area

**** 45 second test sequence

***** Algorithm did not track

Figure 8.6: Summary of results for tracking tests performed on subjects RCL, CSL, SBR, and ICR.

sequence was halted after the 45 second period using the Patient Panic switch on the HW/SW Interface.

Subject SBR's histogram (0 to 140) was also truncated to allow a histogram expansion ratio of 2. Note the small movement of SBR's retina during the 45 second sequence. Recall that subject SBR had completed two filming sequences prior to this filming. The 'tight' movement pattern may indicate a benefit to having patients practice fixation prior to a treatment session. The tracking sequence was halted after the 45 second period using the Patient Panic switch on the HW/SW Interface.

Subject ICR sequence 'stress' tested the tracking algorithm. ICR had a difficult time maintaining fixation during the filming sequence due to discomfort with the retinal field illumination source. The field illumination was reduced to comfortable level. The reduction in field intensity dramatically reduced the contrast of the retinal vessels against the retinal background. Histogram modification did not significantly improve the situation; nevertheless, I elected to test the tracking algorithm with this sequence to see how the algorithm would respond. Several problems were encountered. First, the template building algorithm correctly chose vessel templates as required for 3 of the 6 templates. However, the 3 other template locations did not correspond to any discernible retinal feature. This was due to the absence of discernible features in certain portions of the image. The tracking algorithm also had difficulty tracking a specific coordinate on the retina. A loss of lock condition was not registered because the template response did not fall outside the preset loss of lock conditions. This indicated that the templates chosen did not differentiate between a correct match coordinate and an incorrect coordinate. This was an antici-

pated result due to the poor template selection already described. The video sequence was also examined frame-by-frame to determine other possible reasons for this situation. It was found that retinal features used to track retinal movement were not visible in certain video frames due to poor image contrast. Although the tracking algorithm would not be used under such conditions, this test provided insight into the limitations of the tracker. A more sensitive CCD camera would allow a lower retinal field illumination and hence allow tracking for subject ICR.

Wide variation of template response

During the testing of the tracking algorithm a wide variation of the individual tracking templates was noted. Individual templates' response could vary from 0.15 to 1.3 while maintaining lock. Recall from Chapter 4 an ideal template response is 1.0. This indicates a duplicate response to the reference template. A response less than 1.0 indicates a template response less than the reference template while a response greater than 1.0 indicates a response greater than the reference template. The templates were designed to be normalized against a uniform change in field illumination intensity due to fluctuations in the illumination lamp. Thus the wide variation in the template response was a puzzle. A non-uniform field illumination pattern was hypothesized as the cause of this variation. To test this theory, the fundus camera illumination source was projected through a lens ($f = 25 \text{ mm}$) to approximate the focusing power of the eye onto a Labsphere 0.5 reflectance standard. The standard had a planar surface. The reflectance standard used a barium-sulfate-based coating called Spectrafect to provide a uniform reflectance surface over a wide wave-

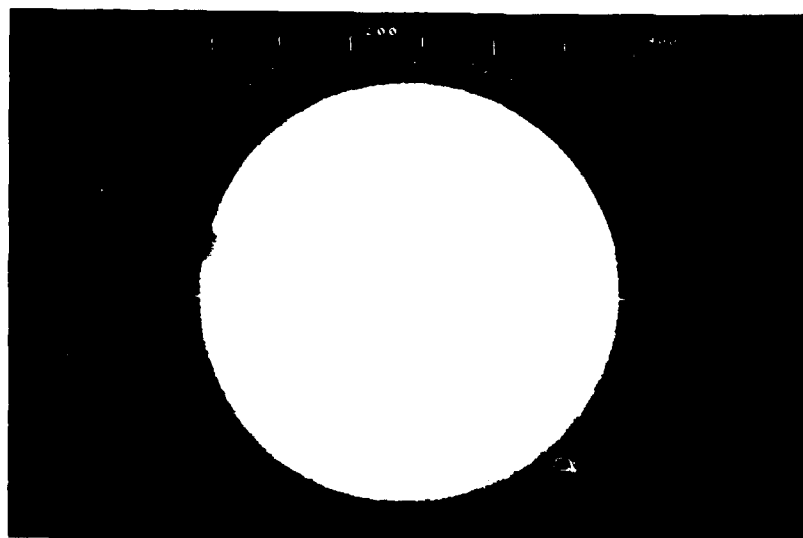


Figure 8.7: The fundus camera illumination source projected onto a 0.5 reflectance standard

length range [90]. An image of the standard was 'snapped' and a histogram was plotted through the center of the standard using function `row_histogram`.

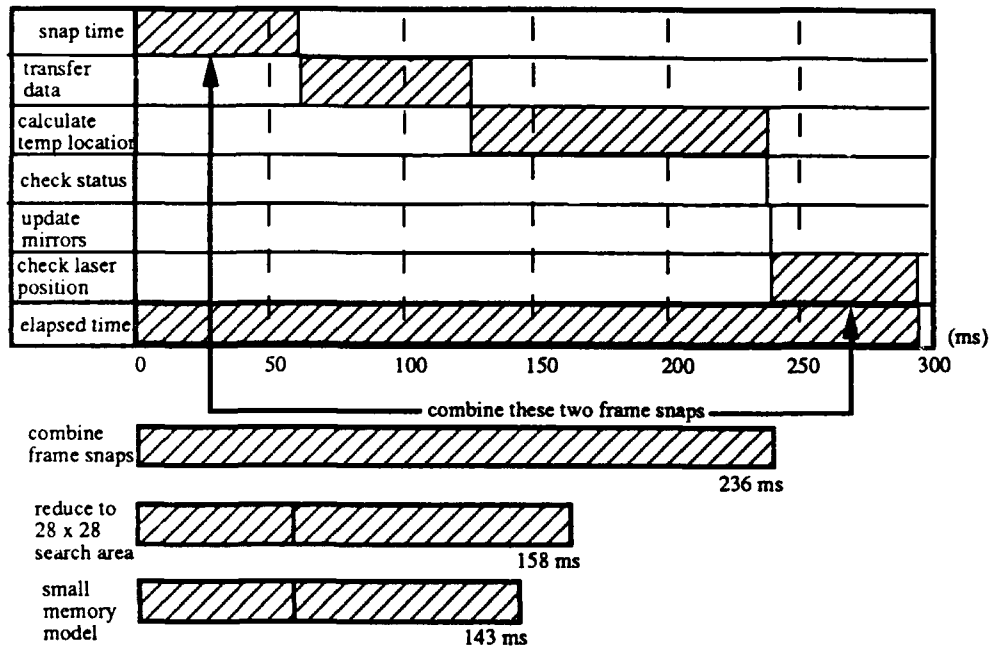
The results are provided in Figure 8.7. Note the wide variation of field intensity as a function of radial position within the image. The variation in gray level from the edge of the image to the center of the image is 50 gray levels. A similar variation pattern occurs in actual retinal images. This variation produces a position dependent template response and explains the wide variation of measured template response.

Timing Tests

The tracking algorithm was timed using the function `print_time`. This function derives a time 'hack' from the computer clock and prints time to the nearest millisecond.

The tracking algorithm was hosted on a 486 PC operating at 33 MHz. With this host the algorithm required 330 ms to establish initial lock. Once initial lock was established a position update was provided every 290 ms. A portion of this increment (55 ms on average) was required to 'snap' a still frame and 165 ms was required to transfer data from the frame grabber to the computer and compute a position update. Approximately one-third of the 165 ms was used transferring the image data from the frame grabber to the PC. The remaining two-thirds were used to calculate the new position update. Finally, 55 ms was required to recheck the laser position after laser position update. Most of this 55 ms is used to 'snap' a still frame. This timing distribution is illustrated in Figure 8.8. The algorithm was also tested on a 486 PC operating at 50 MHz. With this host initial lock was provided in 280 ms and a position update every 210 ms.

To further reduce processing time the frame grab used to check the terminal laser position was combined with the frame grab for the subsequent position update. This combined two frame grabs that occurred back-to-back. This trimmed 55 ms from the update cycle. Also the 10 pixel pad added to the search area as a safety pad was removed such that the search area was 28 x 28 pixels. This represented a fifty percent decrease in data transfer from the frame grabber to the host computer and a fifty percent decrease in total pixel calculations. These time reduction steps are summarized in Figure 8.8. The reduction of search area reduced the upper velocity tracking capability of the tracking algorithm to 10 degrees per second but improved the capability of the tracking algorithm to maintain the laser within a given target radius. These trade-offs will be discussed in detail in Chapter 10.



Processor: Intel 33 MHz
80486DX

Figure 8.8: Position update timing distribution

Memory model selection and testing

When using a Microsoft C compiler a memory model size must be specified. These models include the Tiny-Model, Small-Model, Medium-Model, Compact-Model, Large-Model, and Huge-Model. The Tiny-Model is for programs which can be contained in a single memory segment of 64 kilobytes. This restriction includes both code and data. The Small-Model allows 64 kilobytes for code and 64 kilobytes for data. The Small-Model programs (along with the Tiny-Model) are faster than the other memory model programs because all memory addressing is performed within a given memory segment using near calls (intra-segment) [91].

The Medium-Model provides a trade-off between program execution speed and program size. Data is limited to a single 64 kilobyte segment while the program may contain multiple segments. Data is accessed with near addresses while code is accessed using far (inter-segment) addresses [91].

The Compact-Model provides for multiple data segments and a single code segment. The Large-Model provides for multiple code and data segments and the Huge-Model should be used if arrays larger than 64 kilobytes are required in a program [91].

Program RETINA was compiled and executed using the Medium-Model. Also, the medium memory model for the Matrox PIP-1024 frame grabber and the Data Translation DT2801A were linked to the program. Based on the information above, the tracking algorithm should perform faster using the Small-Model [91].

A separate program called `main_trk.c` was written that contained only

the tracking algorithm. Template and Lesion Data Base functions were not included. This program was hosted on a 486 PC operating at 33 MHz. This change of memory model 'trimmed' approximately five percent from the update time of the Medium-Model. Additional methods of reducing the update time are presented in Chapter 9.

8.2 Laser Pointing Subsystem testing

8.2.1 Testing the Laser Pointing Subsystem with simulated retinal movement

The Laser Pointing Subsystem was tested using the test configuration illustrated in Figure 8.9. This is the same configuration illustrated in Figure 8.1 with the addition of the Laser Pointing Subsystem described in Chapter 5. A 35 mm slide projector was used to project a retinal image onto a 14 cm diameter circular silicon wafer. The silicon wafer served as a light weight, ultra-flat, rigid mirror. The wafer was attached to a General Scanning G330 galvanometer driven by a General Scanning AX-200 driver amplifier via an aluminum coupling post. The total moment of inertia for the mirror and post assembly was $216.3 \text{ gm} - \text{cm}^2$. The armature inertia of the G330 galvanometer was $4 \text{ gm} - \text{cm}^2$. The ratio of the two were 54.1 which allowed the mirror to be used at 13 percent (estimated from the frequency response derating curve provided with the galvanometer) of the galvanometer's unloaded frequency response or 16.9 Hz.

A 1 Hz triangular wave was provided to the AX-200 driver amplifier controlling the G330 optical scanner. The triangular wave amplitude was varied to provide equivalent retinal velocities of 1.0, 2.0, 3.2, 5.0, 6.4, 10.0, 12.8 and

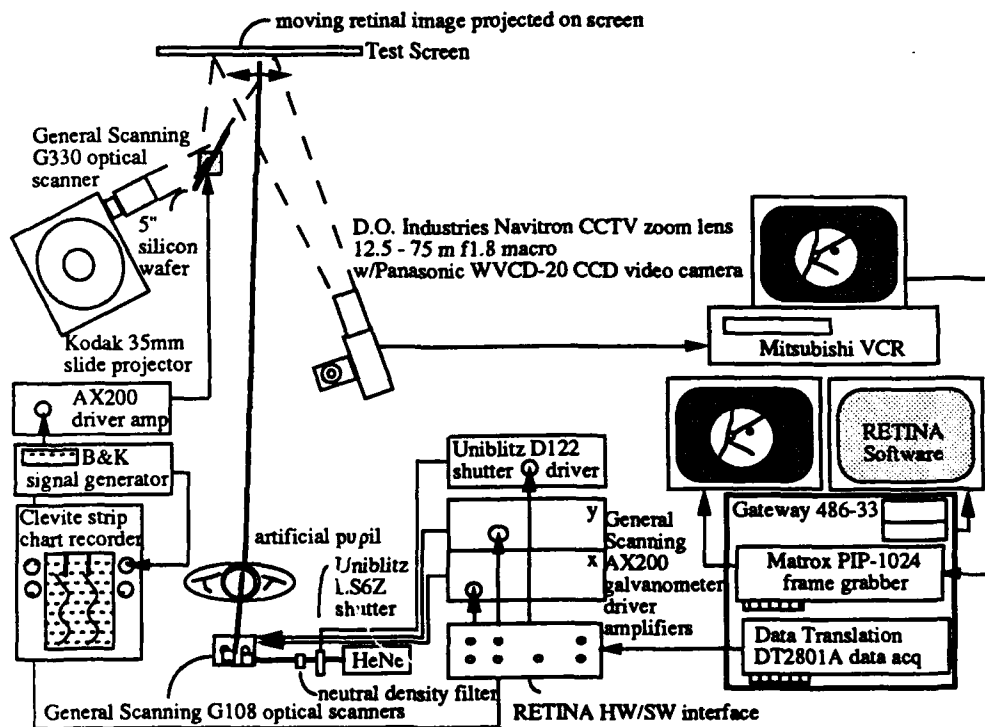


Figure 8.9: Laser Pointing Subsystem test configuration. A retinal image is projected onto a test screen via a silicon wafer acting as a mirror. The mirror is attached to a G330 optical scanner via an aluminum coupling post. The mirror is deflected to provide equivalent retinal velocities of 1.0, 2.0, 3.2, 5.0, 6.4, 10.0, 12.8, and 16.0 degrees per second. The CCD provides video of the moving 'retina' to the tracking algorithm which calculates laser position updates. The position updates drive the G108 optical scanners via the AX200 driver amplifiers to maintain the laser on the prescribed retinal coordinate.

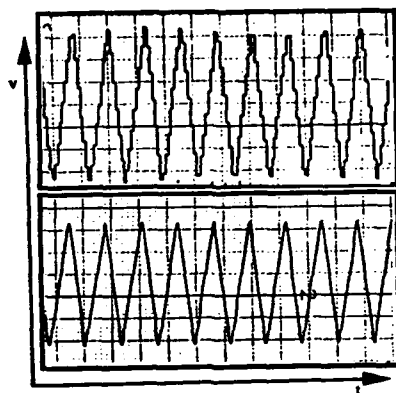


Figure 8.10: Results of testing subject RCL's retinal image at a retinal velocity of 12.8 degrees per second. The lower trace is the deflection signal provided to the AX-200 driver amplifier controlling the G330 image deflection galvanometer. The upper trace is the correction signal calculated by the tracking algorithm and provided to the AX-200 driver amplifier controlling the X (horizontal) mirror of the Laser Pointing Subsystem. Chart speed was 125 mm per minute.

16.0 degrees per second. The tracker consistently lost lock at 16.0 degrees per second. The signal provided to the deflection mirror and the correction signal provided by the tracking algorithm to the X galvanometer were plotted with a strip chart recorder for each retinal velocity.

The tracking algorithm was first tested without function check_laser_position. This test demonstrated the capability of the tracking algorithm to correctly calculate a position update. Results of this test for subject RCL at a retinal velocity of 12.8 degrees per second are provided in Figure 8.10. The same test was then accomplished at a retinal velocity of 16 degrees per second. The tracking algorithm lost lock at this velocity due to retinal features going outside the search area. The results of this test are provided in Figure 8.11.

The tracking algorithm was then tested with function check_laser_position. This function corrects for minor misalignment between the frame grabber co-

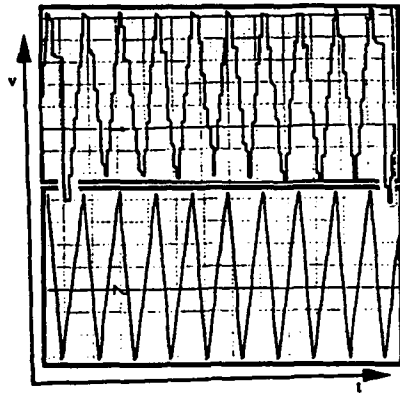


Figure 8.11: Results of testing subject RCL's retinal image at a retinal velocity of 16.0 degrees per second. The lower trace is the deflection signal provided to the AX-200 driver amplifier controlling the G330 image deflection galvanometer. The upper trace is the correction signal calculated by the tracking algorithm and provided to the AX-200 driver amplifier controlling the X (horizontal) mirror of the Laser Pointing Subsystem. Chart speed was 125 mm per minute.

ordinate system and the Laser Pointing Subsystem coordinate system as described in Chapter 7. The results are provided in Figures 8.12, 8.13, 8.14, 8.15, 8.16, and 8.17 for subjects RCL, CSL, and SBR respectively. Note the minor corrective signals in the upper trace in each of these figures as compared to Figures 8.10 and 8.11. During these tests, the tracking algorithm calculated laser position updates and projected the simulated therapeutic laser (HeNe) onto the retinal image. Thus, the entire system was demonstrated. Results were recorded on video tape.

8.2.2 Testing the Laser Pointing Subsystem with lesion templates

The Laser Pointing Subsystem was also tested using lesion templates. The same equipment configuration used to test vessel templates (reference Figure 8.9) was used to test lesion templates. For this test a 35 mm slide of a human

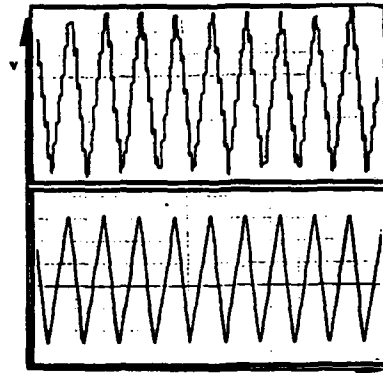


Figure 8.12: Results of testing subject RCL's retinal image at a retinal velocity of 12.8 degrees per second. The lower trace is the deflection signal provided to the AX-200 driver amplifier controlling the G330 image deflection galvanometer. The upper trace is the correction signal calculated by the tracking algorithm and provided to the AX-200 driver amplifier controlling the X (horizontal) mirror of the Laser Pointing Subsystem. Note the minor corrective signals provided by the function check_laser_position. Chart speed was 125 mm per minute.

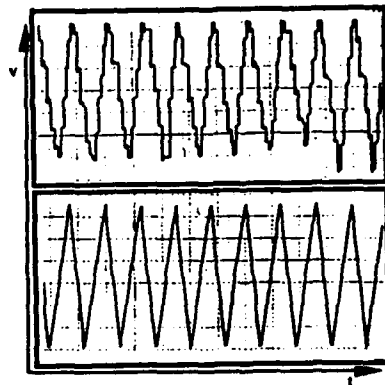


Figure 8.13: Results of testing subject RCL's retinal image at a retinal velocity of 16.0 degrees per second. The lower trace is the deflection signal provided to the AX-200 driver amplifier controlling the G330 image deflection galvanometer. The upper trace is the correction signal calculated by the tracking algorithm and provided to the AX-200 driver amplifier controlling the X (horizontal) mirror of the Laser Pointing Subsystem. Note the minor corrective signals provided by the function check_laser_position. Chart speed was 125 mm per minute.

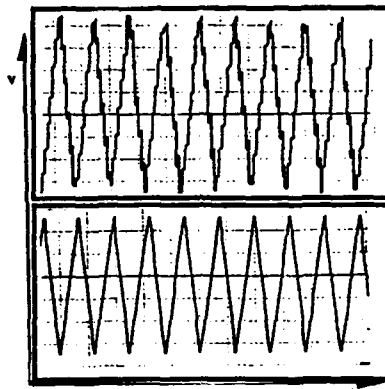


Figure 8.14: Results of testing subject CSL's retinal image at a retinal velocity of 12.8 degrees per second. The lower trace is the deflection signal provided to the AX-200 driver amplifier controlling the G330 image deflection galvanometer. The upper trace is the correction signal calculated by the tracking algorithm and provided to the AX-200 driver amplifier controlling the X (horizontal) mirror of the Laser Pointing Subsystem. Note the minor corrective signals provided by the function check_laser_position. Chart speed was 125 mm per minute.

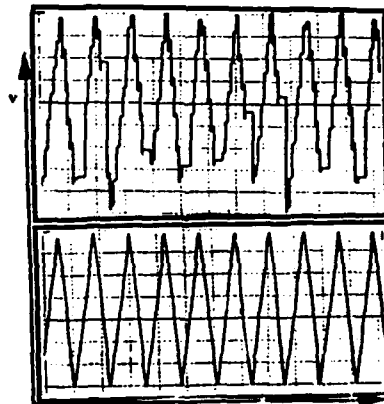


Figure 8.15: Results of testing subject CSL's retinal image at a retinal velocity of 16.0 degrees per second. The lower trace is the deflection signal provided to the AX-200 driver amplifier controlling the G330 image deflection galvanometer. The upper trace is the correction signal calculated by the tracking algorithm and provided to the AX-200 driver amplifier controlling the X (horizontal) mirror of the Laser Pointing Subsystem. Note the minor corrective signals provided by the function check_laser_position. Chart speed was 125 mm per minute.

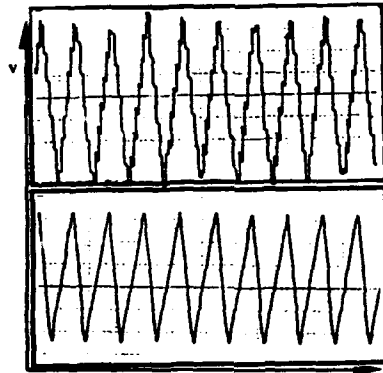


Figure 8.16: Results of testing subject SBR's retinal image at a retinal velocity of 12.8 degrees per second. The lower trace is the deflection signal provided to the AX-200 driver amplifier controlling the G330 image deflection galvanometer. The upper trace is the correction signal calculated by the tracking algorithm and provided to the AX-200 driver amplifier controlling the X (horizontal) mirror of the Laser Pointing Subsystem. Note the minor corrective signals provided by the function check_laser_position. Chart speed was 125 mm per minute.

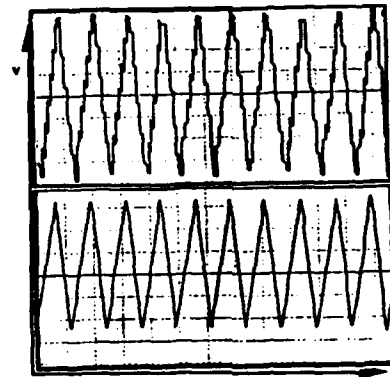


Figure 8.17: Results of testing subject SBR's retinal image at a retinal velocity of 14.0 degrees per second. The lower trace is the deflection signal provided to the AX-200 driver amplifier controlling the G330 image deflection galvanometer. The upper trace is the correction signal calculated by the tracking algorithm and provided to the AX-200 driver amplifier controlling the X (horizontal) mirror of the Laser Pointing Subsystem. Note the minor corrective signals provided by the function check_laser_position. Chart speed was 125 mm per minute.



Figure 8.18: Subject DL. This subject was treated for diabetic retinopathy using an argon laser. Note the irregular shaped lesions. Histogram modification was performed on the image via input look-up table modification to increase contrast. The lesions used for tracking are highlighted by three black cursors in the central portion of the image.

retina with actual argon laser lesions was tested. This color 35 mm slide of photocoagulative treatment for diabetic retinopathy was provided by Dr. H. Grady Rylander. The subject was designated DL. As before, the images were moved at equivalent retinal velocities. A maximum retinal velocity of 6.7 degrees per second was tested. Higher retinal velocities were attempted but the tracker lost lock. This was due to a reference template response of only 9.

A photograph of the retinal image is provided in Figure 8.18. The signal provided to the image deflecting mirror and the correction signal to the horizontal mirror driver is provided in Figure 8.19 for a retinal velocity of 6.7 degrees per second.

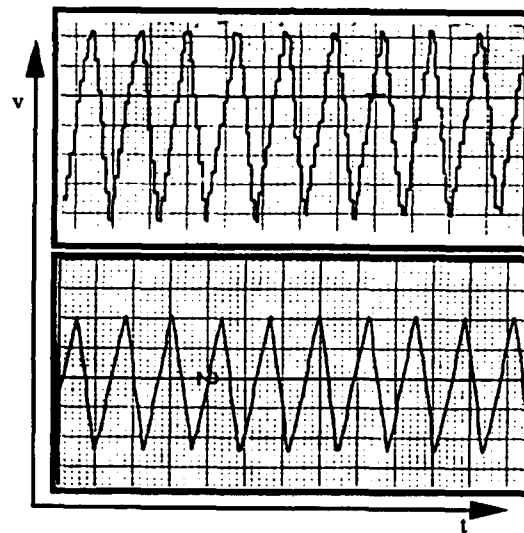


Figure 8.19: Results of testing a human retinal image with actual argon lesions using the lesion template tracking algorithm at a retinal velocity of 6.7 degrees per second. The lower trace is the deflection signal provided to the AX-200 driver amplifier controlling the G330 image deflection galvanometer. The upper trace is the correction signal calculated by the tracking algorithm and provided to the AX-200 driver amplifier controlling the X (horizontal) mirror of the Laser Pointing Subsystem. Note the minor corrective signals provided by the function check_laser_position. Chart speed was 125 mm per minute.

8.2.3 Analysis of results

The following observations were based on the results of testing the Laser Pointing Subsystem with the vessel template tracking algorithm and the lesion template tracking algorithm:

- The tracking algorithm using vessel templates successfully tracked retinal movements up to 16 degrees per second. At 16 degrees per second the algorithm lost lock for subject SBR because portions of the two-dimensional vessel template went outside the fundus camera field of view.
- The tracking algorithm using vessel templates and a 28 x 28 pixel search area was able to constrain the laser within a 100 micron target radius for retinal velocities less than two degrees per second.
- At retinal velocities greater than two degrees per second but less than ten degrees per second the tracking algorithm maintained lock on the moving retina. Due to the 143 ms position update processing time, the position update lagged behind the intended target coordinate. The lag was proportional to the retinal velocity. Figure 8.20 provides a representative sample of the relationship between lag and retinal velocity. The tracker lost lock at retinal velocities greater than ten degrees per second because retinal vessel landmarks passed outside the 28 x 28 pixel search area.
- Cycles of the X (horizontal) mirror correction signal for a subject were similar but not identical. Slight variations in the correction signal over a cycle were due to different reference frames being 'snapped' for update calculations.

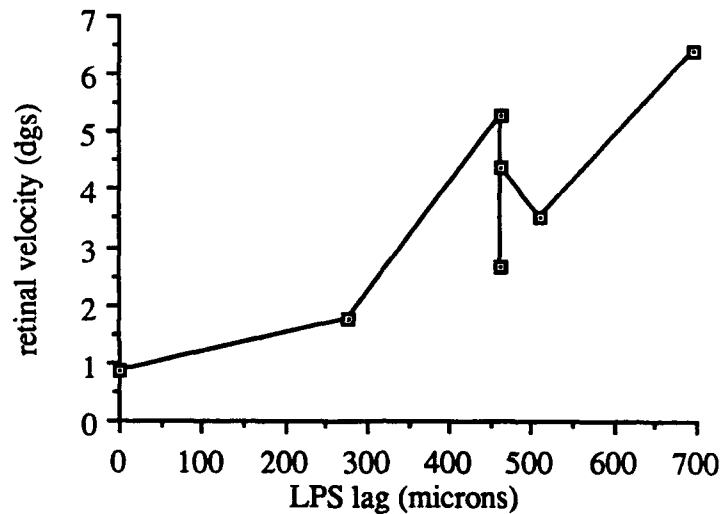


Figure 8.20: Laser Position Subsystem lag versus retinal velocity. This is a representative sample of the relationship between retinal velocity and the lag of the Laser Positioning Subsystem from the intended coordinate. The lag was measured from the center of the laser spot to the intended coordinate. The center of the laser spot did not always correspond to the brightest pixel in the laser spot. This accounts for the odd shape of the graph.

- Although the video camera was capable of providing 30 frames per second, only seven frames were examined per second due to position update processing time delay.
- Function `check_laser_position` provided slight positional updates for minor misalignments between the frame grabber coordinate system and the Laser Pointing Subsystem coordinate system. This was evident as slight correcting traces in the X (horizontal) mirror correction signal.
- Precise coalignment of the Retinal Tracking Subsystem with the Laser Pointing Subsystem is essential for successful tracking and laser placement.

- The tracking algorithm using lesion templates tracked videotaped circular lesions on the rabbit retina quite well; however, when tested on actual human lesions the tracking algorithm consistently lost lock. The function to find lesion templates `find_lesion_templates` was adjusted to search for circular as well as noncircular lesions. When tested against the retinal slide for subject DL the lesion templates used were for noncircular lesions.
- The tracking algorithm using lesion templates successfully tracked retinal velocities up to 6.7 degrees per second. The poorer response of the lesion templates was attributed to low values of total template response. The total template response for vessel templates were on the order of 40. The total template response for lesion templates was 4.

This concludes the chapter on testing the Developmental System. The next chapter describes *in vivo* testing and results.

Chapter 9

In vivo Development System Testing in Pigmented Rabbits

9.1 Overview

This chapter details the *in vivo* testing performed with the Retinal Tracking Subsystem and the Laser Pointing Subsystem on pigmented cross bred Californian and New Zealand rabbits. The chapter begins with a discussion of the optics required to place a laser on a specified coordinate within the fundus camera field of view. Safety considerations are then discussed in detail. Safe levels of maximum permissible exposure are derived for the Laser Pointing Subsystem. The *in vivo* preparation of the rabbit is then discussed with the equipment configuration. The chapter concludes with testing results and demonstrations of panretinal photocoagulation treatment, repair of retinal breaks or tears, and a lesion matrix experiment.

9.2 Optical configuration for *in vivo* testing

The Laser Pointing Subsystem was described in detail in Chapter 5 of this document. This subsystem was then tested in Chapter 8 with the Retinal Tracking Subsystem. The subsystems were tested by projecting a retinal image moving at a calibrated retinal velocity onto a screen and testing the closed loop

feedback mechanism of the tracking algorithm. To test this closed loop feedback mechanism *in vivo* requires the addition of a plano-convex lens in the laser path. The purpose of the lens is to bring the laser to a focus at the pupil such that the laser passes through the center of the pupil. This allows the laser access to the retina without modifying the optics of the fundus camera. A beam splitter is provided between the fundus camera and the pupil to allow coalignment of the fundus camera field of view and the Laser Pointing Subsystem field of view. A neutral density filter is required to reduce the 8 mW HeNe laser output to a safe level. Reference Figure 9.1. This optical configuration was adapted from similar systems designed for the scanning laser ophthalmoscope [31]. The optical configuration was tested on a model eye prior to *in vivo* testing. The model eye was constructed from a 31.75 mm table tennis ball which had the first 6.35 mm removed. A biconvex lens ($f = 25.4 \text{ mm}$) was affixed to the front of the ball to simulate eye optics. Simulated vessels were drawn inside the ball. The ball was attached to a ring stand and used to align the optical arrangement. Reference Figure 9.1.

9.3 Safety considerations for *in vivo* testing

It is imperative that test rabbits be protected from harmful levels of laser irradiation. American National Standards (ANSI Z136.1) provides guidance for the safe use of lasers and laser systems. Guidance provided in this document was used to derive safe levels of laser irradiation for use in *in vivo* testing. Safe levels are specified for laser use based on laser wavelength, laser viewing configuration, laser type, and exposure duration. It was assumed that safe viewing levels derived for humans would also be safe for rabbits. For this

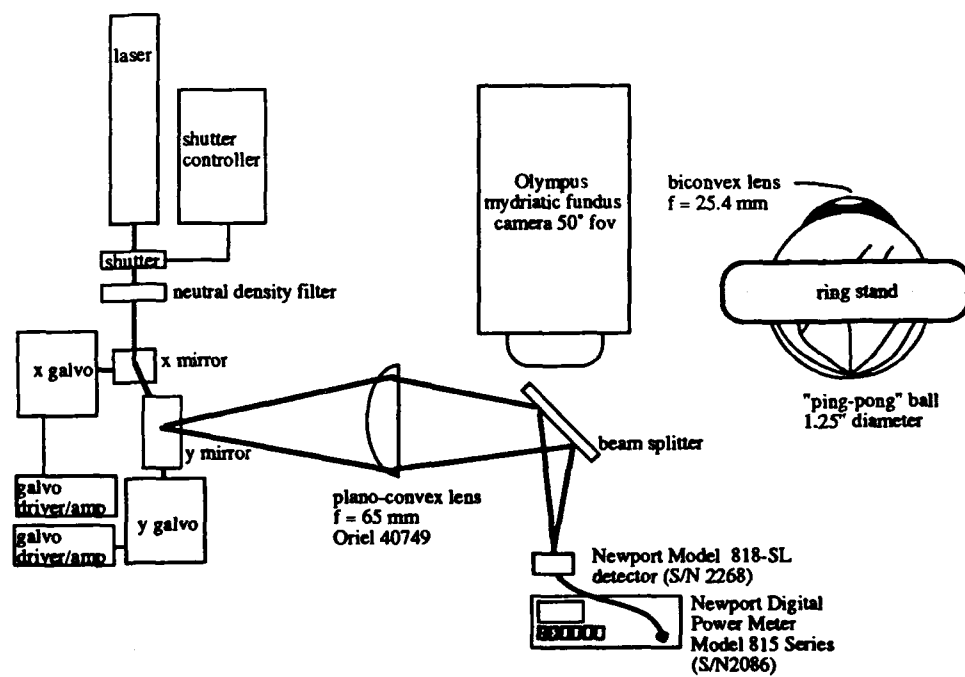


Figure 9.1: Left: optical configuration for *in vivo* testing and Right: model eye used to align system prior to *in vivo* testing.

experiment an eight mW HeNe laser operating in a continuous wave mode at 633 nm for experiments of 300 second duration was used to simulate a therapeutic laser. The laser was projected into the rabbit's eye via the pupil. This is defined as intrabeam viewing. The laser output was reduced to 3.5 microwatts at the rabbit's pupil with a spot size of 1.0 mm by employing a neutral density filter of optical density 3 (OD3). Optical density is given as [92]:

$$\text{optical density} = \log(1/\text{transmittance}) \quad (9.1)$$

or,

$$\text{transmittance} \approx 10^{-\text{optical density}} \quad (9.2)$$

Therefore, an OD3 neutral density filter has a transmittance of 0.001.

Maximum permissible exposure levels for the *in vivo* experiment were derived in the following way:

ANSI Z136.1 provides an equation for exposure duration for a continuous wave laser operating in the visible region as [93]:

$$T_1 = 10 \times 10^{20(\lambda - 0.550)} \quad (9.3)$$

For a wavelength of 633 nm (0.633 microns) T_1 equals 457 seconds. This value of exposure duration specifies an equation for maximum permissible exposure as [93]:

$$MPE = 1.8 t^{3/4} \times 10^{-3} J cm^{-2} \quad (9.4)$$

For an experiment duration of 5 minutes ($t = 300$ seconds) MPE is calculated as:

$$MPE = 1.8 \times 300^{3/4} \times 10^{-3} J cm^{-2} = 129.8 \times 10^{-3} J cm^{-2} \quad (9.5)$$

This may be converted to $W cm^{-2}$ using [93]:

$$MPE = 129.8 \times 10^{-3} J cm^{-2} / 300 s = 433 \times 10^{-6} W cm^{-2} \quad (9.6)$$

The beam diameter at the rabbit's pupil was measured as 1.0 mm. This equates to an area of $7.85 \times 10^{-3} cm^2$. To maintain a safe operating condition the laser power at the pupil must be under 3.4 microwatts by:

$$433 \times 10^{-6} W cm^{-2} \times 7.85 \times 10^{-3} cm^2 = 3.4 \times 10^{-6} W \quad (9.7)$$

This safe operating condition is maintained with the inline neutral density filter with optical density OD3.

9.4 *In vivo* experimental method

The rabbit subjects were handled in accordance with Animal Resource Center protocol T02880906. Humane treatment of the rabbits was of paramount importance. The experimental configuration of Figure 9.2 was used. A photograph of the optical equipment configuration is provided in Figure 9.3.

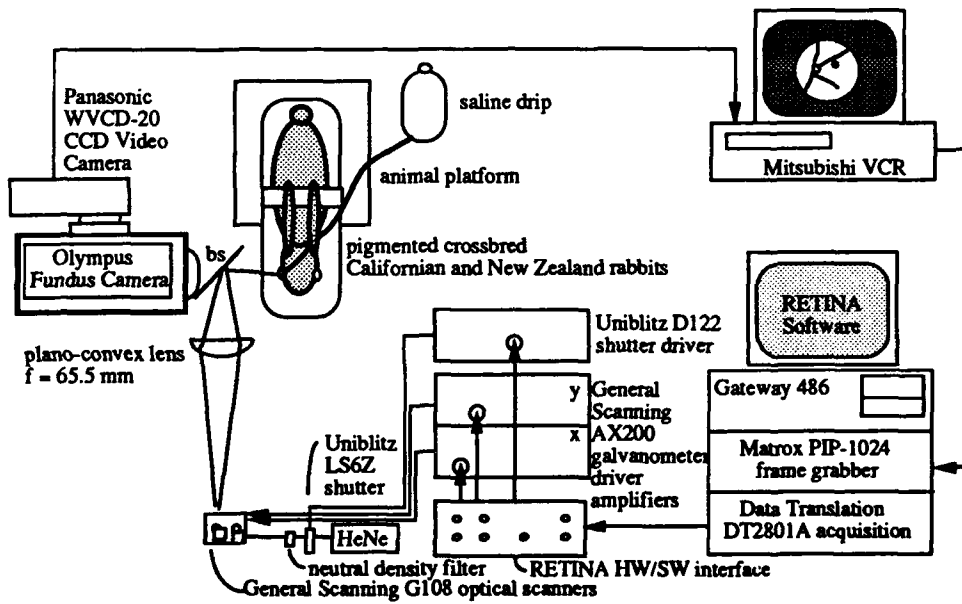


Figure 9.2: *In vivo* experimental configuration

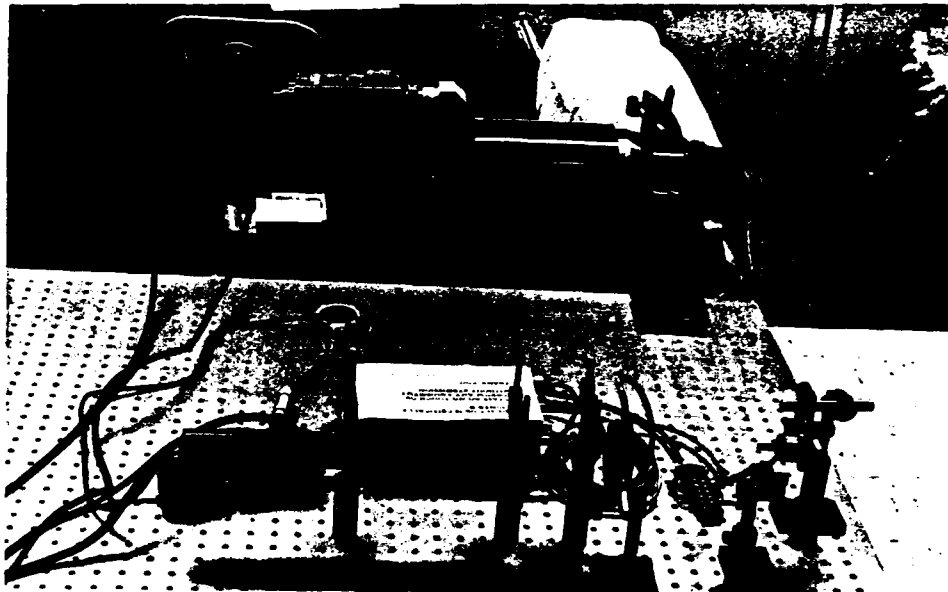


Figure 9.3: Equipment configuration for *in vivo* tracking.

A pigmented cross bred Californian and New Zealand rabbit was anaesthetized intramuscularly with a combination of Ketamine (ketamine hydrochloride 35 mg/kg) and Rompun (xylazine hydrochloride 5.9 mg/kg). Following injection the rabbit's right pupil was dilated with Mydriacyl 1% (Tropicamide 1% ophthalmic solution). Several drops of Alcaine were placed in the eye as a local anaesthetic. A speculum (Sontec Instruments 10-1000 Barraquer wire speculum, small) was then inserted to hold the eyelids in an open position. Sutures were then placed in the four recti (superior, inferior, medial, and lateral) muscles to facilitate retinal movement. The rabbit was then secured to an animal platform via a safety belt. A 0.9 percent saline drip was used periodically to irrigate the cornea to maintain moistness. The depth of anaesthesia was checked at five minute intervals using the toe pinch method. Reference Figure 9.4. Following the experiment Ocumycin salve (Bacitracin Zinc and Polymyxin B Sulfate ophthalmic ointment) was applied to the eye under the lid. Also, 1

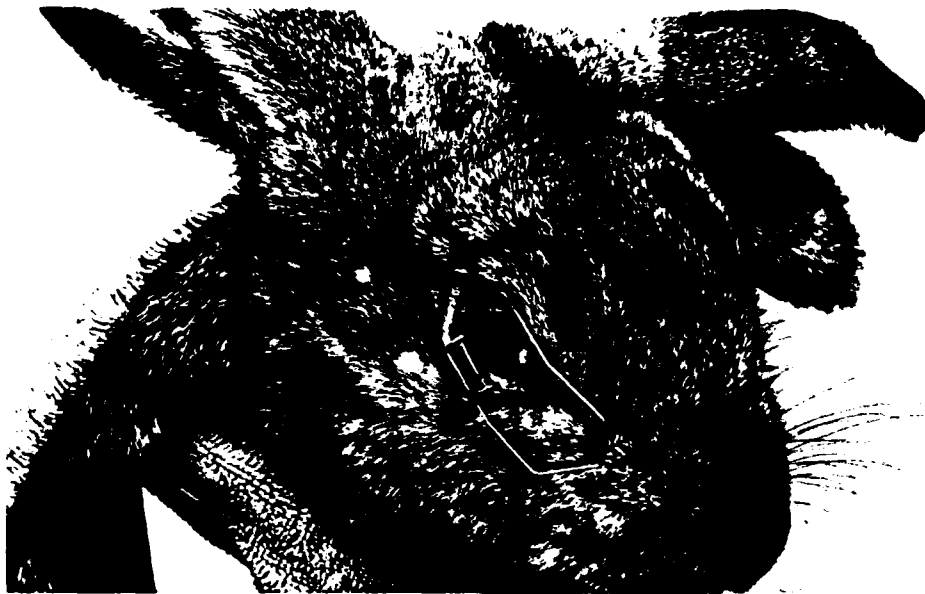


Figure 9.4: Rabbit preparation for *in vivo* experiments. Note the speculum in place. A suture is shown in the medial rectus muscle.

cc of Pen BP-48 (Penicillin G Benzathine and Penicillin G Procaine in aqueous suspension antibiotic) was injected intramuscularly.

With the rabbit preparation complete, final coalignment of the Retinal Observation Subsystem and the Laser Pointing Subsystem was accomplished. This step is the most critical for a successful *in vivo* experiment. To properly coalign the two systems the Laser Pointing Subsystem is programmed to trace a rectangular pattern. However, the subsystem's optics are adjusted such that the rectangular pattern comes to a **point** focus at the corneal surface. This point focus is adjusted such that it passes through the center of the fundus camera illuminating ring. This method allows projection of the rectangular pattern onto the retina without interfering with the fundus camera's imaging optics. Once past the pupil point focus, the rectangular pattern rediverges and forms a rectangular pattern on the retina. Reference Figure 9.5. The

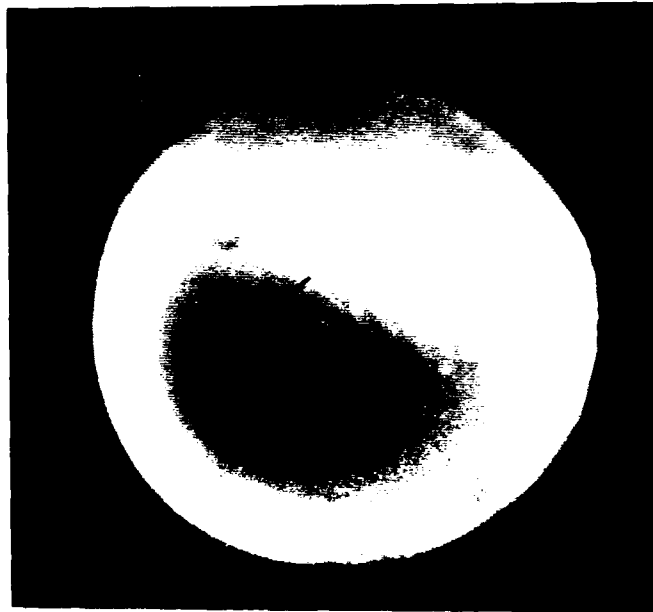


Figure 9.5: Rectangular laser pattern on the retina.

rectangular pattern is then coaligned with the identical rectangular coordinates of the frame grabber. This alignment process is illustrated in Figure 9.6.

After subsystem coalignment a reference image of the rabbit's retina was 'snapped'. The recti muscle sutures were gently pulled to ensure the optic disk with the accompanying retinal vessels were in the fundus camera field of view. Histogram modification was not used to improve image contrast since the gray levels present in the rabbit retinal image covered much of the available gray level spectrum. A tracking template was then built along with a Lesion Data Base using techniques described in Chapter 8. Results of these steps are provided in Figure 9.7.

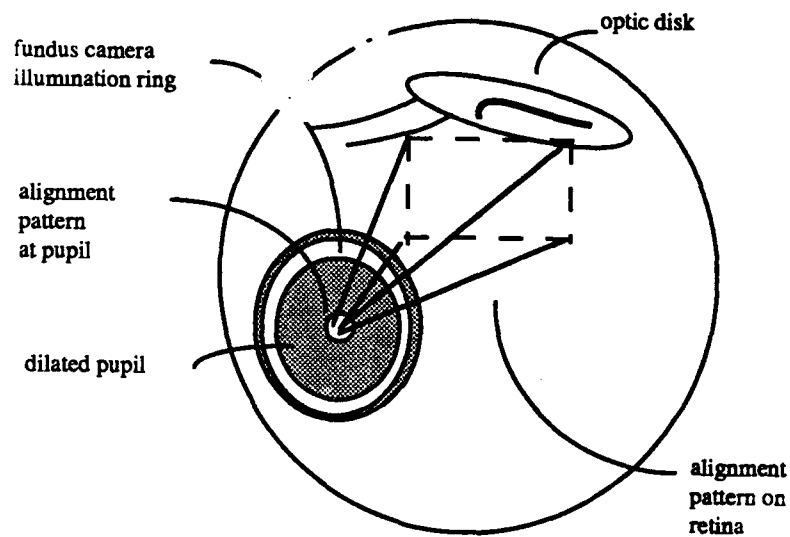


Figure 9.6: *In vivo* alignment of the Laser Pointing Subsystem. A rectangular pattern is traced by the Laser Pointing Subsystem. The rectangular pattern is brought to a point focus at the rabbit's corneal surface. The point focus is adjusted such that it passes through the center of the fundus camera illuminating ring. Once past the pupil focus, the rectangular pattern rediverges and forms a rectangular pattern on the retina. The rectangular pattern is then coaligned with the identical rectangular coordinates of the frame grabber.

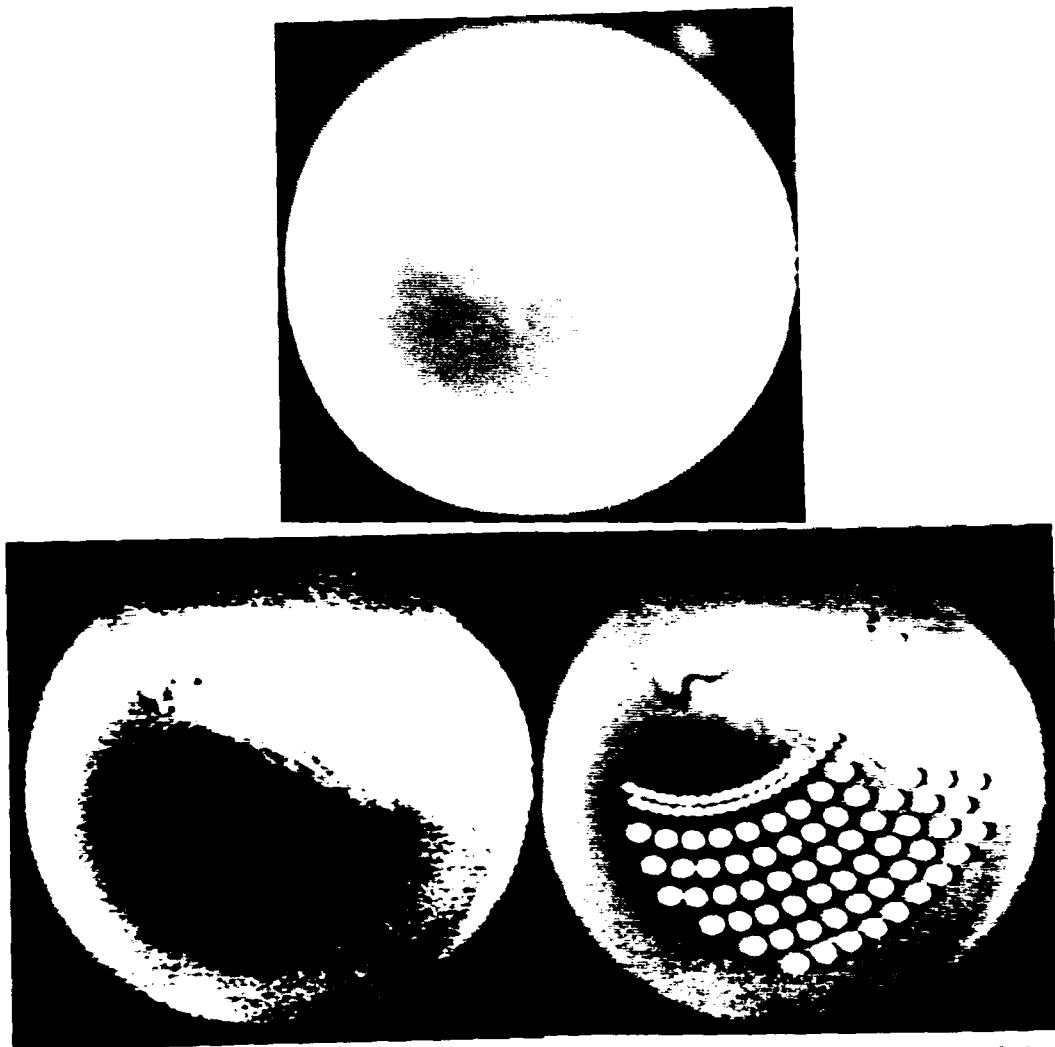


Figure 9.7: Preparation for the *in vivo* experiment. Top: reference image of the rabbit retina. The optic disk is oblong in shape. Retinal vessels are confined to regions near the optic disk. Bottom left: results of building a tracking template. Bottom right: results of building a Lesion Data Base.

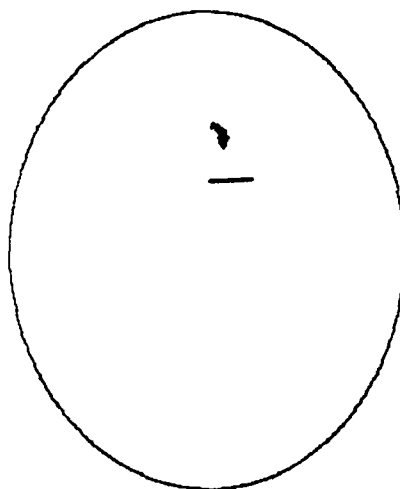


Figure 9.8: Plot of laser position during a four minute tracking experiment conducted on an anesthetized cross bred pigmented rabbit. A 40 pixel (approximately 1.86 mm) reference line is provided.

9.5 *In vivo* experimental results

The Retinal Observation and Tracking System was successful in simultaneously tracking slight retinal movement in an anaesthetized pigmented rabbit retina and maintaining a laser on a prescribed target coordinate. Precise coalignment of the Retinal Tracking Subsystem with the Laser Pointing Subsystem contributed to successful tracking and laser placement.

To demonstrate the *in vivo* tracking ability the rabbit's retina was video taped during a four minute tracking sequence. During the four minute test the rabbit's retina was moved using the recti sutures. The plot of laser position during the four minute test is provided in Figure 9.8. Also, a video summary of the target area over the four minute period is provided in Figure 9.9.

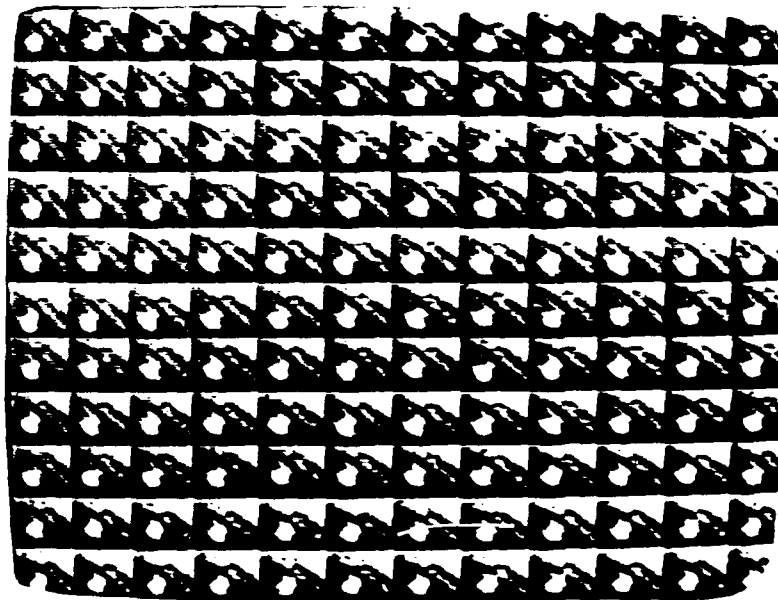


Figure 9.9: Video results of *in vivo* tracking.

9.6 *In vivo* panretinal photocoagulation and retinal tear demonstration

9.6.1 Objectives

Since the Robotic Laser System is under development for the photocoagulative treatment of diabetic retinopathy, macular degeneration, and retinal break or tear repair; demonstration of these techniques *in vivo* using the Retinal Tracking and Observation System would prove useful. To transition from tracking using a lower power HeNe laser to an argon ophthalmic laser required several modifications to the Laser Pointing Subsystem. This section begins with a description of these required modifications followed by a description of preliminary testing completed prior to the actual *in vivo* experiment. This section concludes with a description of the protocol used to demonstrate panretinal photocoagulation and retinal tear treatment *in vivo* and the results of this

demonstration.

9.6.2 Equipment Configuration

The ophthalmic laser used initially for this demonstration was a Coherent System 900 Argon Laser Photocoagulator. This is an all lines argon laser rated at 5.0 watts. The actual output from the laser fiber was approximately 1.4 watts. To use the argon laser in place of the low power HeNe laser required several modifications to the laser delivery optics of the Laser Positioning Subsystem. The optics of the delivery system were adapted from those developed for the scanning laser ophthalmoscope [95]. The modified Laser Positioning Subsystem is provided in Figure 9.10.

Lenses L1 and L2 are biconvex lens ($f = 12.7 \text{ mm}$) configured as a beam collimator. These are required since the fiber delivered beam from the photocoagulator is highly divergent. Lenses L3 and L4 are plano-convex lenses configured as a laser beam expander [94]. The beam expander is followed by an aperture iris to reduce beam radius. Lens L5 has the dual purpose of focusing the expanded beam to a spot and collimating the laser scan. In other words, it converts the angular deflection of the galvanometer driven mirrors into a beam displacement referenced from the undeflected beam path [95]. Lens L6 brings the laser raster to a point focus at the pupil so that the laser can pass through the center of the illuminating ring from the fundus camera. Once past the pupil, the beam scan rediverges such that any retinal coordinate within the fundus camera field of view may be targeted by the Laser Positioning Subsystem. The beam splitter between the fundus camera and the rabbit's eye allows coalignment of the frame grabber's image plane as viewed through the

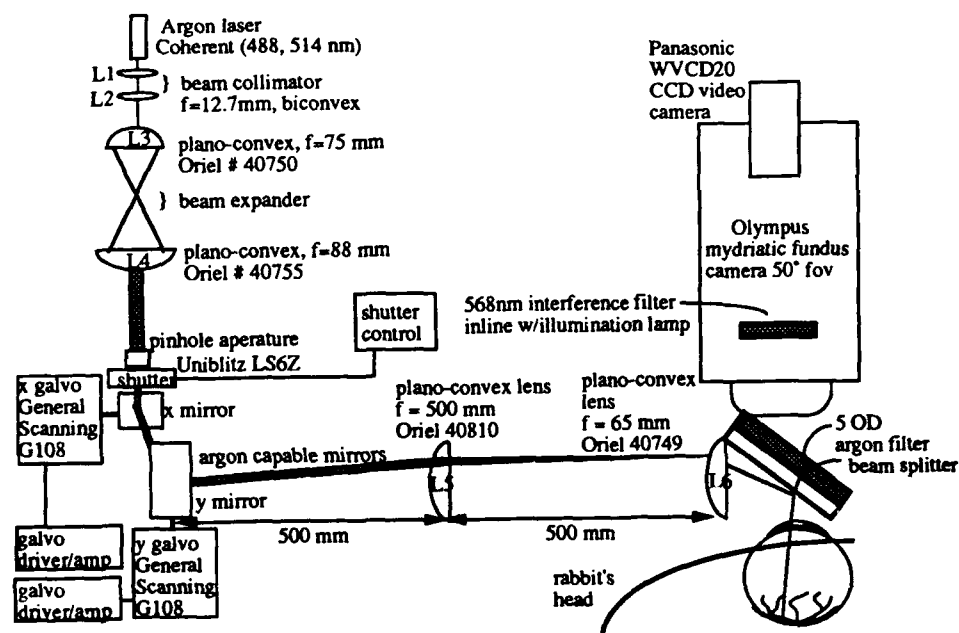


Figure 9.10: Modifications required to the Laser Positioning Subsystem for argon laser delivery using a Coherent System 900 Argon Laser Photocoagulator.

fundus camera with the coordinate system of the Laser Positioning Subsystem. A removable 5 OD argon filter is mounted between the beam splitter and the fundus camera to protect the CCD camera from the argon beam. The filter is removed for aligning the system with a low power argon beam. After alignment the filter is dropped in place to protect the CCD array from damage and avoid image saturation. The filter is set at an angle to cast the reflection from the filter out of the fundus camera field of view.

This optical configuration allowed precise beam placement on the rabbit's retina. However, due to the low (1.4 W) source power and the losses within the optical system the power delivered to the cornea was only 20.8 mW. At least 100 mW was desired. The major source of power loss was the beam shaping optics (lenses L1 to L4 and the aperture iris).

To remedy this situation the Coherent System 900 was replaced with a Coherent Innova 100 Argon Ion Laser. This laser can deliver up to 20 watts of argon laser power. Also, the laser may be delivered without a fiber. Use of this laser allowed the removal of lenses L1 to L4. For ease of laser coupling the plano-convex lens (L1 in Figure 9.11) was changed to $f = 750 \text{ mm}$. Also, a laser shield of flat black (matte) aluminum foil was added between the fundus camera body and the edge of the beam splitter. This shield serves the dual purpose of increasing the quality of the fundus camera image and blocking the laser beam passing through the beam splitter. The modified configuration is shown in Figure 9.11.

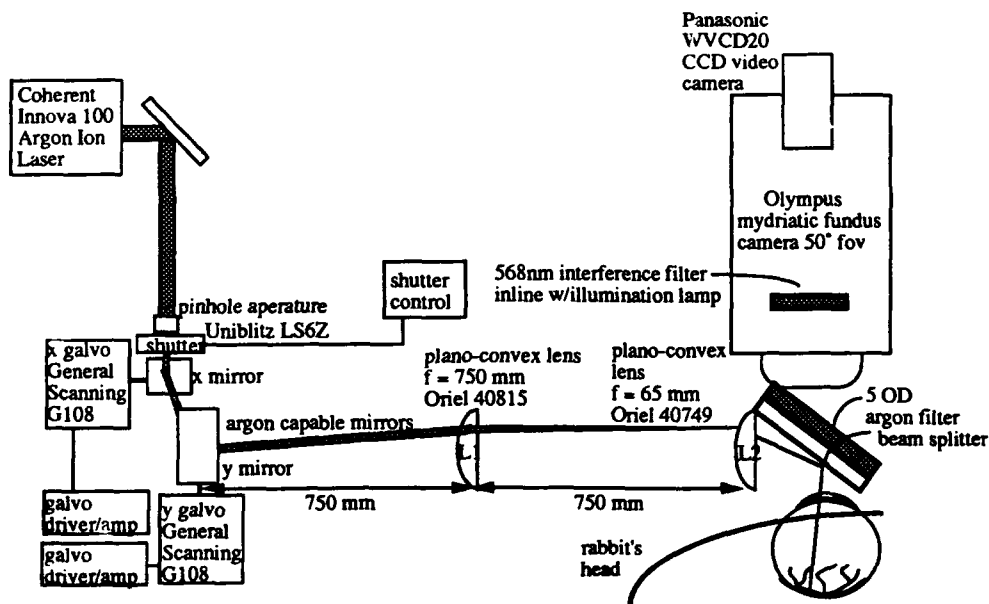


Figure 9.11: Modifications to the optical delivery system for using the Innova 100 Argon Ion Laser.

9.6.3 Preliminary Testing

Prior to performing a panretinal and retinal tear repair photocoagulation demonstration preliminary system tests were performed to verify system operation. The tests included a computer simulation of panretinal photocoagulation while tracking actual human retinal movement, performing panretinal photocoagulation on a stationary paper target 'retina', and demonstrating treatment of retinal tear repair on a stationary paper target 'retina'.

To provide a simulation of panretinal photocoagulation on actual human retinal movement, a Lesion Data Base for the treatment of panretinal photocoagulation was built from a representative frame from the videotape of subject SBR (34 year old caucasian male, right eye, filmed with a 568 nm interference filter, histogram expansion ratio 2). A tracking template was also

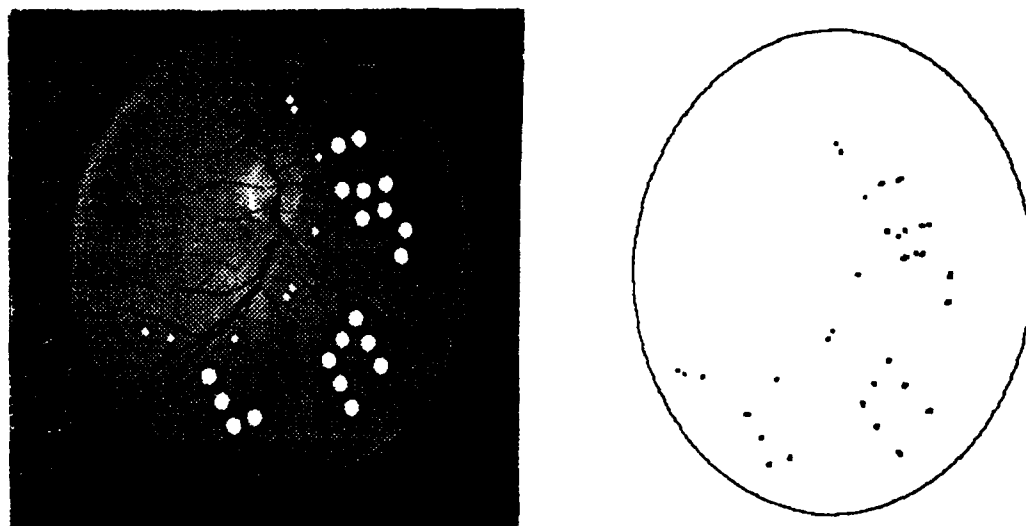


Figure 9.12: Panretinal photocoagulation simulation on human retinal movement. Left: desired lesion pattern and Right: laser position plot on a **moving** retinal image. If the target retina had been stationary, the right plot would be an exact duplicate of the left illustration.

built using procedures previously described in Chapter 4. The position of the laser coordinate was plotted on one of the frame grabber's imaging planes during the tracking sequence. The results are illustrated in Figure 9.12. The left illustration is the desired lesion pattern while the right illustration shows the laser plot. The right plot is for a **moving** retinal image. If the target had been stationary, the right plot would be an exact duplicate of the left illustration. The laser time on lesion target was controlled to simulate actual irradiation time for a 100 mW laser power at the cornea. The entire panretinal irradiation procedure required 21.4 seconds.

The tracking algorithm was slightly modified due to lessons learned from this simulation. Prior to the simulation, initial tracker lock was reestablished

every time a new lesion coordinate was initiated. This was not required since tracker lock is not tied to the laser target coordinate. This slight change in the tracking algorithm saved considerable time in the panretinal photocoagulation sequence and provided a more accurate lesion placement.

The second stage of the preliminary testing involved placing actual laser lesions on stationary paper target 'retinas'. A retinal vessel pattern was drawn on a white thermal paper target background. A Lesion Data Base was then built for the treatment of diabetic retinopathy and retinal tear repair. The system was aligned and the lesions were placed as prescribed by the data base. The results are illustrated in Figure 9.13.

These simulation exercises on thermal paper targets allowed fine tuning of the *in vivo* experimental procedure. Specifically, the following lessons were learned:

- Templates selected for retinal tracking should not be close to an intended lesion target coordinate. If the laser illuminates the retina within approximately one lesion diameter of a tracking template the tracker loses lock. This does not constrain tracking algorithm operation since blood vessels used as tracking templates are not viable lesion target coordinates. This restriction may be lifted with the inclusion of additional argon wavelength blocking filters placed between the fundus camera and the CCD video imaging camera. Specifically, an Andover Corporation OG-550 sharp-cut filter (550FG05-25) [96] would serve this purpose. This optical filter passes wavelengths above 550 nm and blocks those below 550 nm. The characteristics of this filter was measured with a Hitachi U3300 spectrophotometer. Results are provided in Figure 9.14.

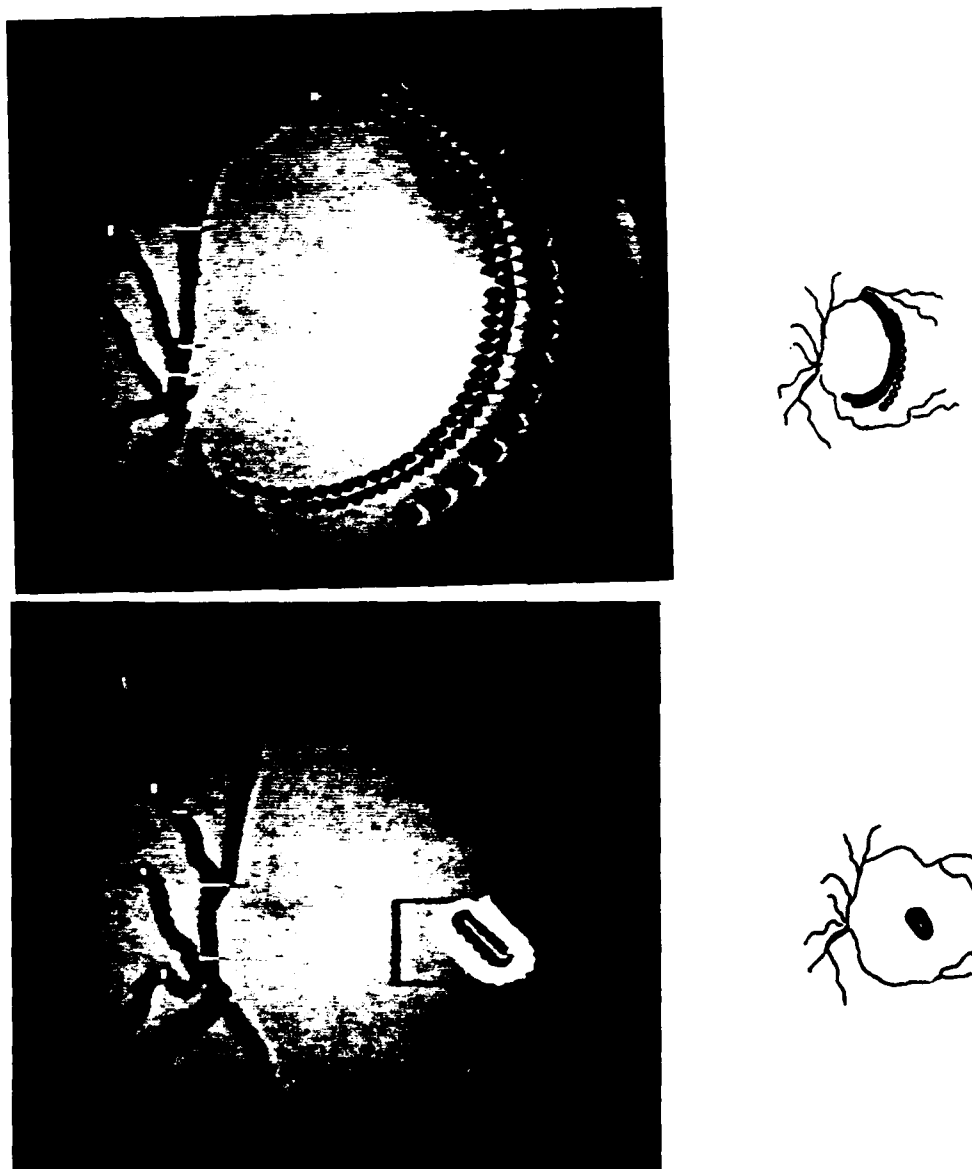


Figure 9.13: Results of photocoagulation on paper retina targets. Top left: desired lesion placement for panretinal photocoagulation as viewed through the fundus camera, Top right: lesion placement shown actual size, Bottom left: desired lesion placement for retinal tear repair as viewed through the fundus camera, Bottom right: lesion placement shown actual size.

- Templates should not be chosen close to the edge of the fundus camera field of view. The field of view edge provides a strong template response which overwhelms the correct template response. Proper choice of template thresholds will allow discrimination between the correct template response and a false template response.
- Careful alignment of the laser delivery optics and coalignment with the video frame grabber imaging plane is **critical** for correct laser placement. Also, care should be taken to use the paraxial regions of the lenses within the laser delivery system to avoid Seidel (monochromatic) aberration affects [10]. If marginal portions of the lenses are used the alignment rectangle appears distorted and lesions will not be placed in prescribed locations.

9.6.4 *In vivo* demonstrations

Based upon lessons learned from testing on the paper targets, several slight modifications were made to the system optical configuration. Specifically, the 5 OD filter was removed from the optical path between the fundus camera and the beam splitter. Although the filter optically worked quite well, mechanically it was large and hampered precise alignment of the system. An Andover OG-550 filter was placed inline between the fundus camera and the CCD video camera as shown in Figure 9.15.

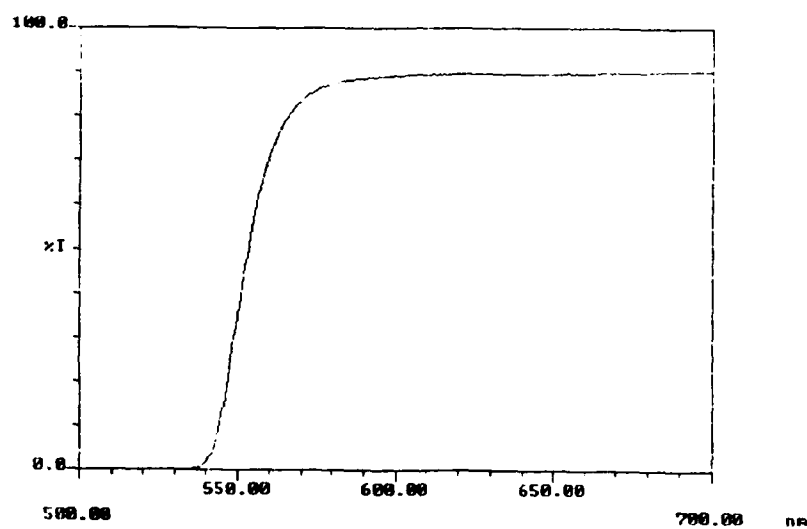


Figure 9.14: Transmission characteristics of an Andover Corporation OG-550 sharp-cut filter measured with a Hitachi U3300 spectrophotometer. This filter prevents the argon laser from saturating the CCD video camera. The argon laser when used in the all lines mode provides laser output at specific wavelengths between 454.4 nm and 528.7 nm [97].

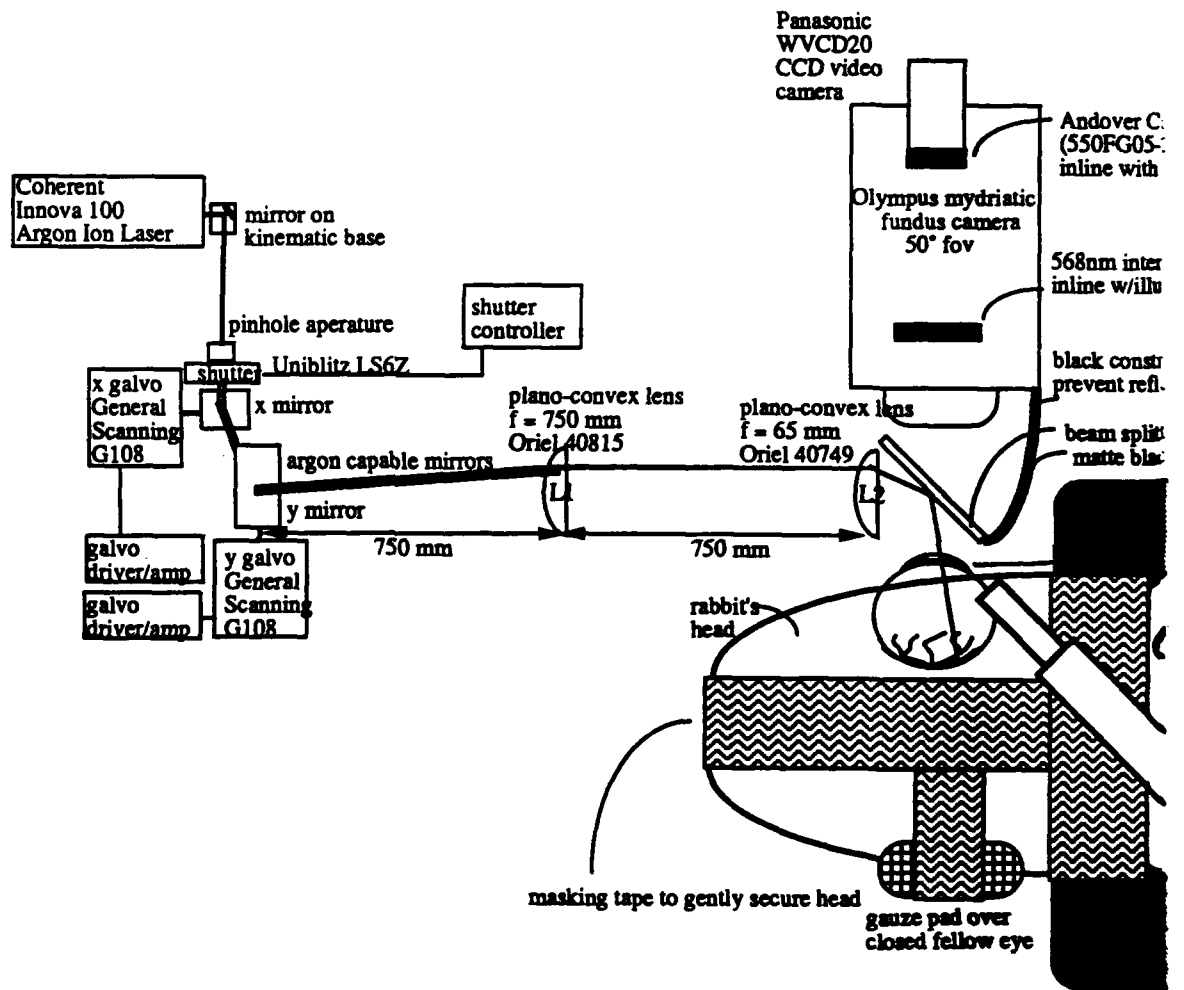


Figure 9.15: *In vivo* experin

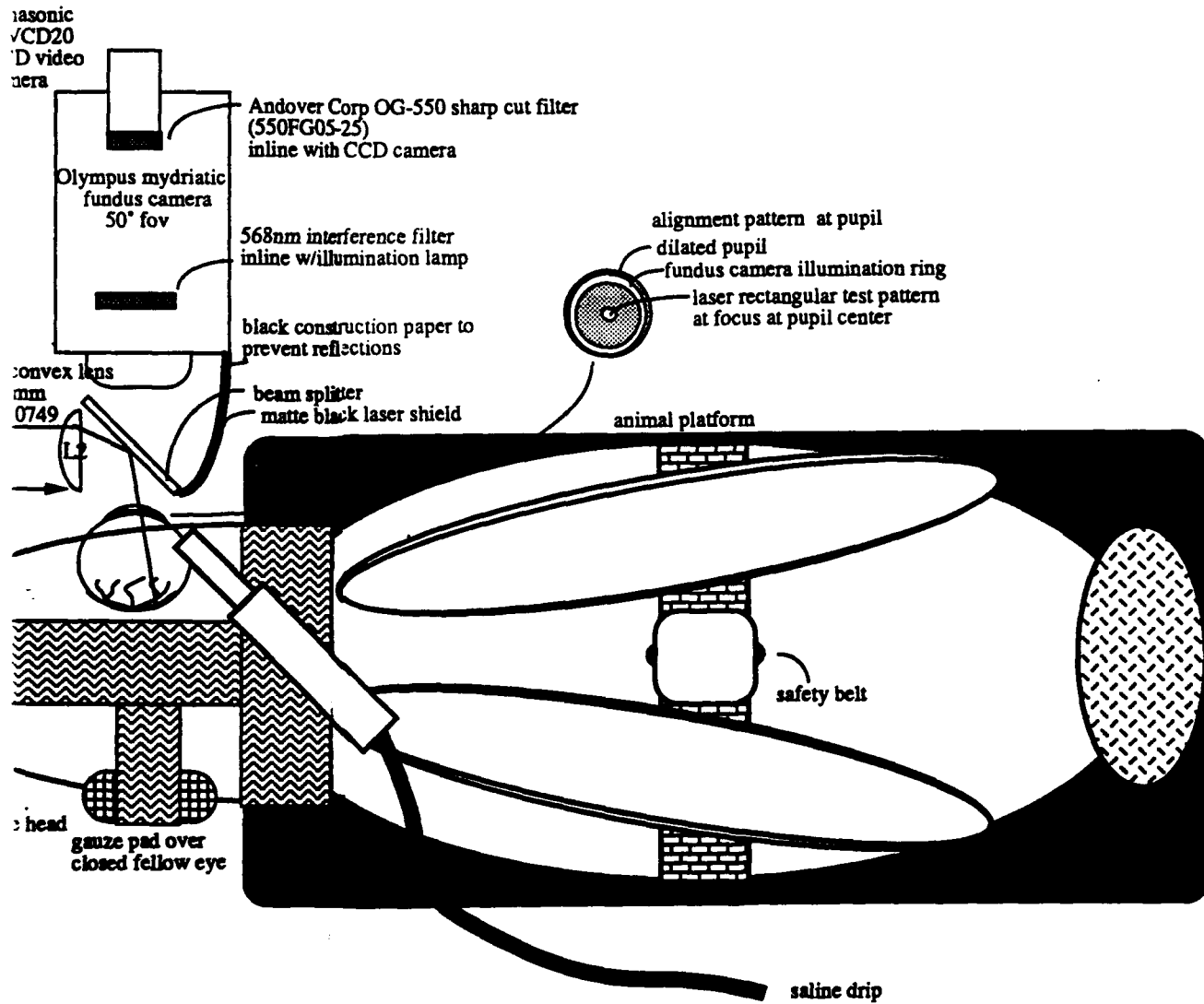


Figure 9.15: *In vivo* experimental configuration

(2)

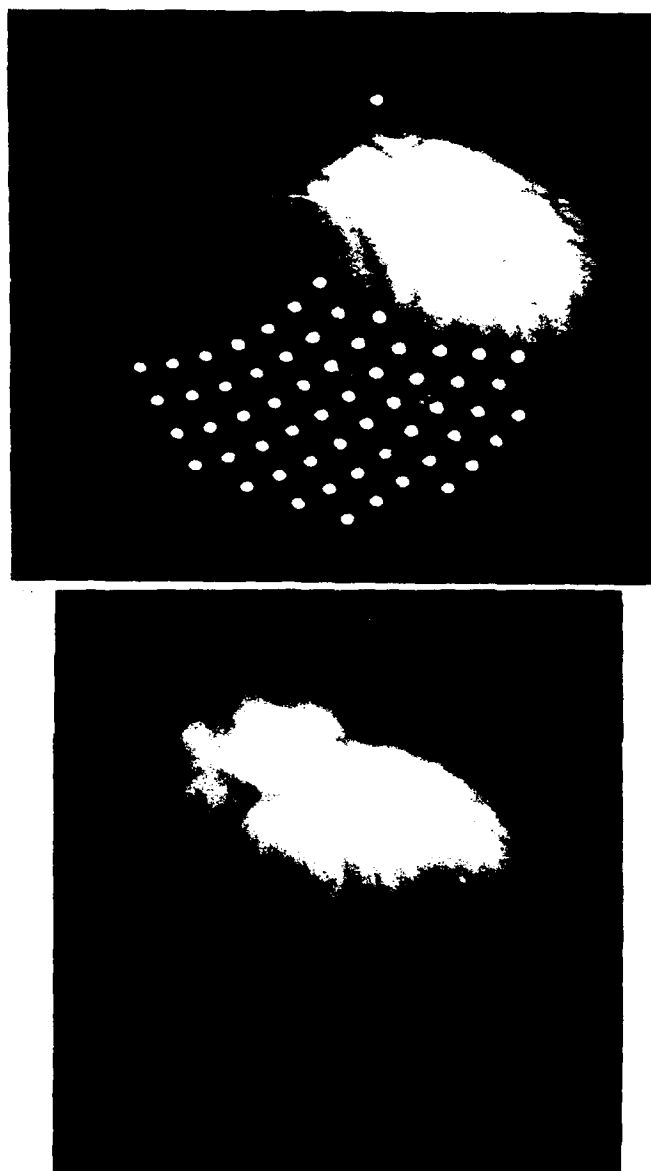


Figure 9.16: *In vivo* test results for diabetic retinopathy treatment. A Coherent Innova 100 laser operating at 514 nm was set to deliver 100 mW to the cornea. This power setting was increased to 145 mW at the cornea to provide visible lesions. The tracking algorithm maintained an average irradiation time per lesion of 267.3 ms. These parameters were chosen to provide a shallow but visible lesion on the subject retina. Top: retinal map illustrating the tracking template and the intended lesion coordinates. Bottom: photograph of actual lesion placement.

Figure 9.17 provides results of the *in vivo* test for treating retinal tear. Figure 9.17 top provides a retinal map illustrating the tracking template and the intended lesion coordinates. Figure 9.17 bottom is a photograph of the actual lesion placement on the subject's retina taken immediately following lesion placement.

Analysis of results

The *in vivo* treatment for diabetic retinopathy and retinal tear repair demonstrated the capability of the Retinal Tracking and Observation System. Many lessons were learned from these two demonstrations including:

- Precision placement of lesions on the retina for the treatment of eye diseases is possible with the prototype system. For precise lesion placement the Retinal Observation Subsystem must be precisely coaligned with the Laser Positioning Subsystem. The result of misalignment is evidenced by a displacement between desired and actual lesion placement in the demonstration of treatment for retinal tear. In the demonstration lesions were placed in correct orientation to one another but the lesion pattern was displaced from its intended position. Displacement was approximately 1500 microns.
- The prototype system is very effective in efficiently placing lesions for treatment. Each lesion required (on average) 267.3 ms for placement. To determine total treatment time the number of lesions is multiplied by the time required per lesion. For example the treatment of retinal tear repair required approximately 6 seconds while the treatment of diabetic

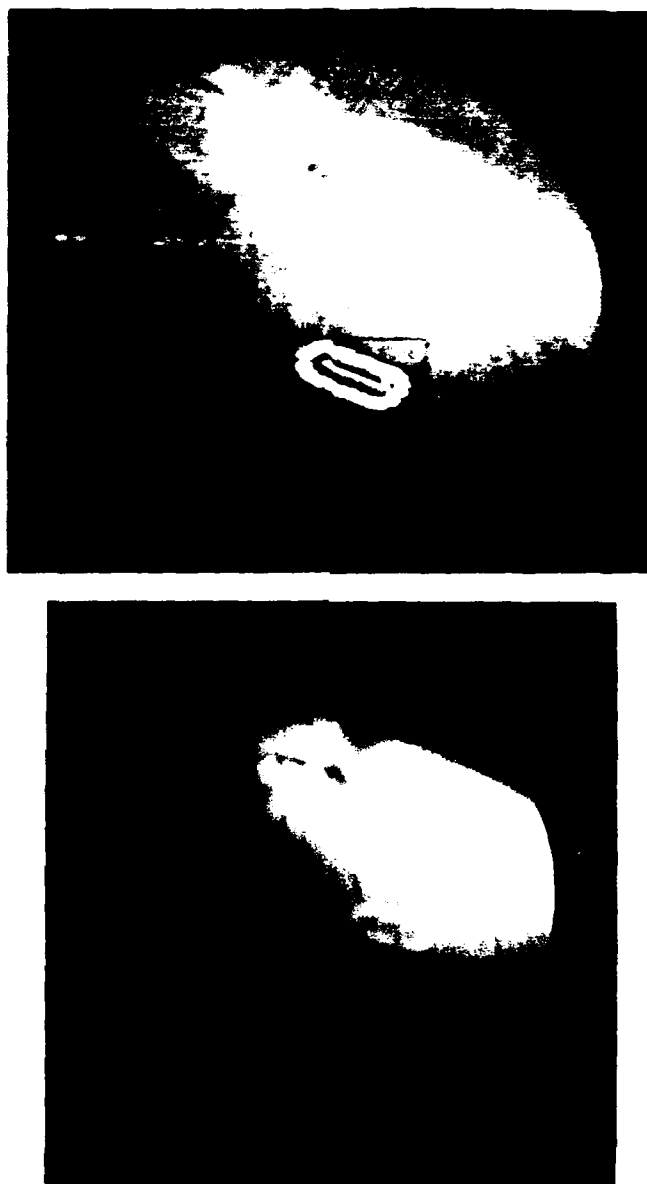


Figure 9.17: *In vivo* test results for retinal tear repair treatment. A Coherent Innova 100 laser operating at 514 nm was set to deliver 230 mW to the cornea. The tracking algorithm maintained an average irradiation time per lesion of 267.3 ms. These parameters were chosen to provide a shallow but visible lesion on the subject retina. Top: retinal map illustrating the tracking template and the intended lesion coordinates. Bottom: photograph of actual lesion placement.

retinopathy required approximately 16 seconds.

- A Reflectance Based Feedback Control System is required to control lesion depth during irradiation. Although, laser parameters were fixed for a given treatment demonstration, a visible lesion was not always rendered on the retina. This was due to retinal tissue inhomogenities and variation in laser approach angle in reference to system optics. A depth control system would compensate for these variations.
- A wide variation in laser parameters were noted among subject rabbits. The retinal tear repair demonstration was accomplished first. The laser was set for 514 nm and 230 mW at the cornea. These parameters provided visible lesions on the retina. These same parameters with the same spot size and irradiation time was then used on the same rabbit for demonstrating diabetic retinopathy. The Retinal Observation and Tracking System correctly placed lesions at the required coordinates. However, retinal hemorrhage occurred during the formation of two lesions. Reference Figure 9.18. The hemorrhage indicated penetration of the choroidal layer. This observation again attested for the need of a depth control system. The diabetic retinopathy demonstration was successfully demonstrated at a corneal power of 145 mW.
- To maintain alignment during the duration of the experiment a surgical table is needed which contains both the fundus camera and the animal platform. This platform must has the capability to be locked into a stationary position. For both the retinal tear repair demonstration and the diabetic retinopathy demonstration the fundus camera and the animal



Figure 9.18: Retinal hemorrhage due to penetration of the choroidal retinal layer. The dark mass is fresh blood from the third lesion formed. The blood is obscuring lesions formed. Note blood is also evident on two lesions in the outer lesion ring.

platform were on separate tables. These tables were on moveable casters for equipment portability. Once the overall system was aligned the slightest movement would cause system misalignment and misplaced lesions.

Lesion matrix experiment

Several *in vivo* experiments were accomplished to demonstrate lesion placement in a matrix pattern. A matrix pattern allowed documentation of system characteristics. Prior to accomplishing this experiment a slit lamp microscope table with lockable casters was redesigned to support the fundus camera and the animal platform on the same stable stand.

The placement of lesions was modified such that lesions were arranged in a matrix pattern with 750 micron spacing between lesion rows and columns. The subject rabbits were prepared as described earlier in this chapter. The Innova laser was set for 514 nm irradiation and various corneal powers.

Results

Figure 9.19 shows the desired lesion matrix and the actual lesion matrix placement achieved with the Retinal Tracking and Observation System. In this first lesion experiment corneal power was set for 155 mW. The laser exposure time of 267 ms per lesion was controlled by the update cycle of the tracking algorithm. The irradiating laser produced severe glare along the field of view edges which often obliterated the tracking templates.

Figure 9.20 shows the desired lesion matrix and the actual lesion matrix placement achieved with the Retinal Tracking and Observation System for the second lesion experiment. In this second experiment the size of the matrix was reduced to avoid some of the edge effects experienced during the first matrix experiment. Two OG-550 filters were mounted inline between the fundus camera and the CCD video camera to further reduce glaring effects from the irradiating laser. Corneal power was set for 165 mW. Laser exposure time was again 267 ms.

Figure 9.21 shows the lesion matrix placement achieved with the Retinal Tracking and Observation System immediately post-operative (top) and ten minutes post-operative (bottom). In this third matrix experiment a five column four row matrix was placed at a corneal power of 55 mW. Row 1 had a laser exposure time of 267 ms, Row 2 534 ms, Row 3 801 ms, and Row 4 1068

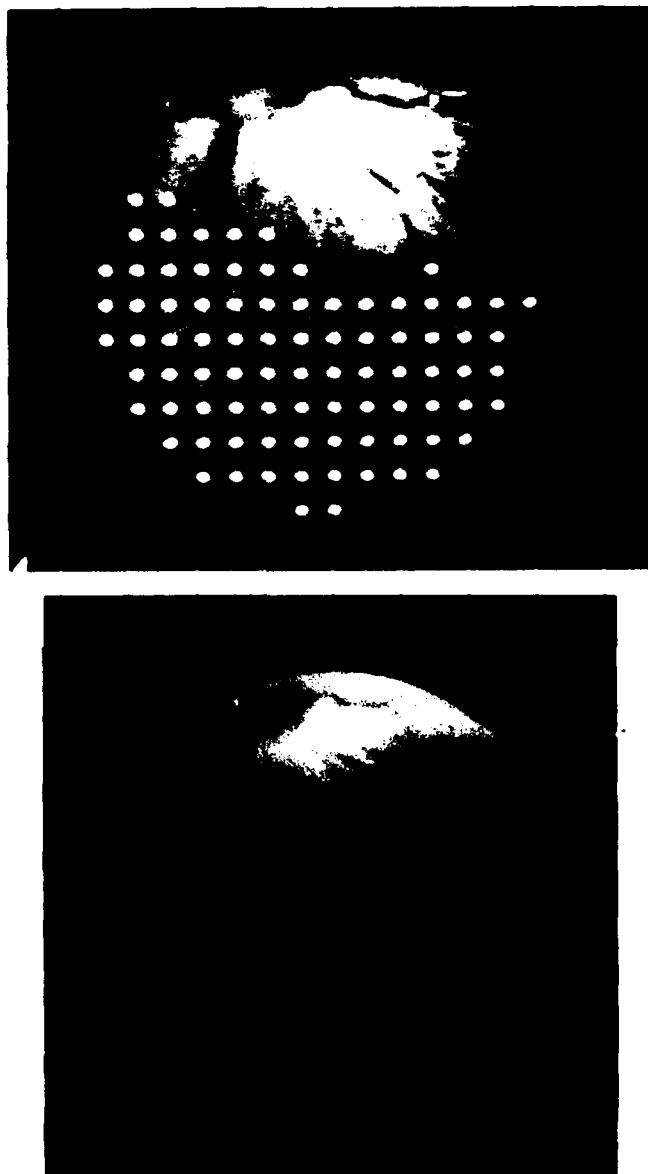


Figure 9.19: First matrix experiment results. Top: desired lesion placement as viewed through the fundus camera. Bottom: actual lesion placement.

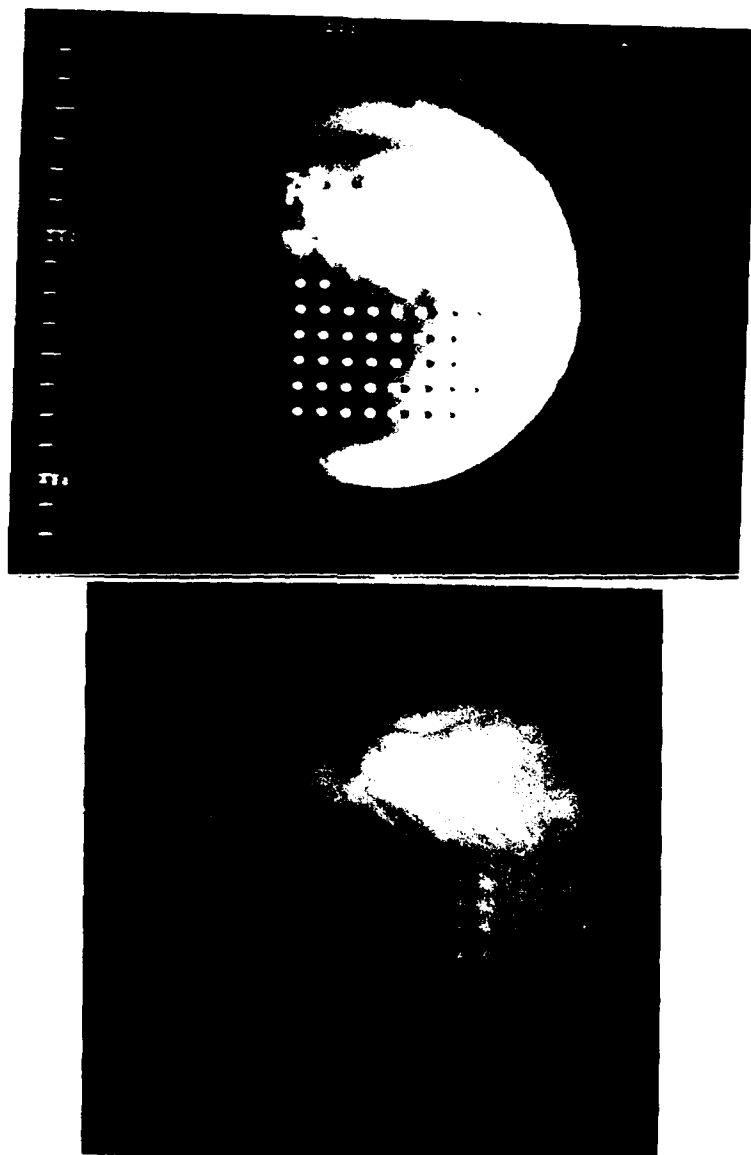


Figure 9.20: Second matrix experiment results. Top: desired lesion placement as viewed through the fundus camera. Bottom: actual lesion placement.

ms. The purpose of this experiment was to demonstrate the capability of the tracking algorithm to maintain the laser on a specific lesion coordinate during multiple position updates.

Summary of results

Results of the *in vivo* experiments are summarized in Figure 9.22.

Analysis of results

The lesion matrix experiments demonstrated the capability to precisely place lesions on the retina. However, several necessary system improvements were noted:

- The requirement for precise coalignment between the Laser Positioning Subsystem and the Retinal Observation Subsystem is again evident. Although the modified animal platform allowed improved alignment, greater precision is desired. This can be achieved by mounting the Laser Positioning Subsystem to the same stable platform as the Retinal Observation Subsystem. The galvanometers currently available do not allow this modification.
- The `check_laser_position` function could correct some of the misalignment errors. This function was turned off during the *in vivo* experiments. The prototype system is not fast enough to simultaneously use this function and several other documentation functions required during *in vivo* testing.
- The irradiating laser sometimes produced severe glare which obliterated the tracking templates. This situation can be remedied with the inclusion

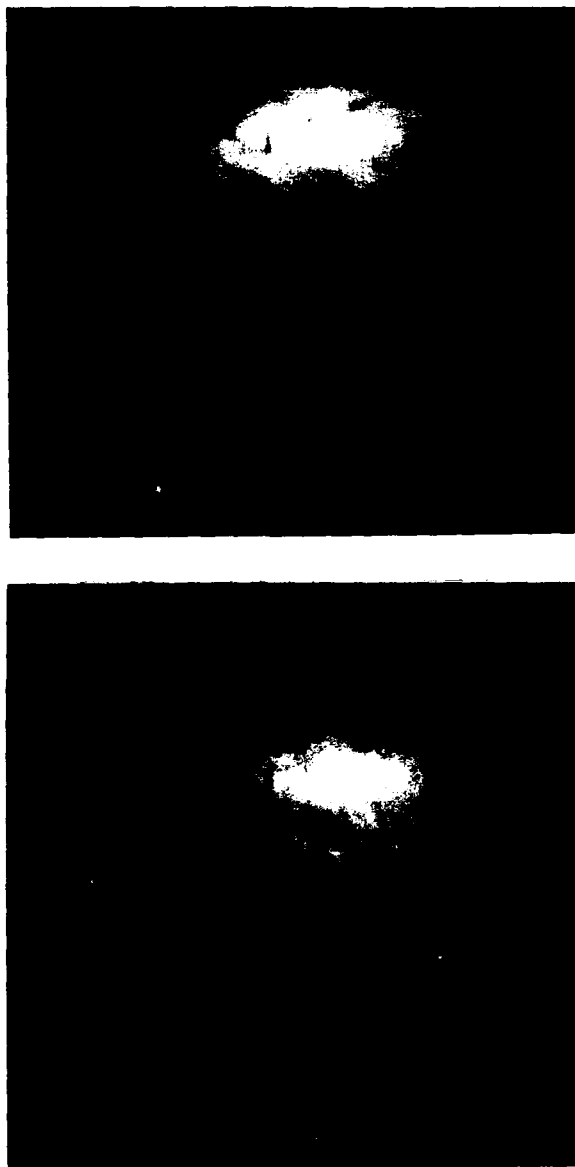


Figure 9.21: Third matrix experiment results. Top: A lesion matrix of five columns and 4 rows were placed such that Row 1 had a laser exposure time of 267 ms, Row 2 534 ms, Row 3 801 ms, and Row 4 1068 ms. Corneal power was set for 55 mW. Note the variation in lesion characteristics for a given row. (Top) Immediately post-operative and (Bottom) ten minute post-operative.

Description	Rabbit	Laser parameters: λ (nm), corneal power (mW), spot size (μm), exposure time (ms)	lesions placed/lesions attempted
diabetic retinopathy	1888	514 nm, 145 mW, 325 μm , 267.3 ms	33/59
retinal tear	1887	514 nm, 230 mW, 325 μm , 267.3 ms	23/25
large matrix	1944	514 nm, 155 mW, 460 μm , 267.3 ms	77/86
small matrix	1989	514 nm, 165 mW, 420 μm , 267.3 ms	42/42
4 row x 5 column matrix	1675	514 nm, 55 mW, 325 μm Row 1: 267 ms Row 2: 534 ms Row 3: 801 ms Row 4: 1,068 ms	19/20

* worst case error reported, open loop mode, error due primarily to misalignment between Retinal Observation Subsystem and Laser Pointing Subsystem

Figure 9.22: Summary of *in vivo* experiments

corneal power (mW), pulse (ms)	lesions placed/ lesions attempted	laydown time (s)	retinal movement (mm ²)	approximate* error (microns)
, 267.3 ms	33/59	15.7 s	1 mm ²	300 um
, 267.3 ms	23/25	6.7 s	0.1 mm ²	1,500 um
, 267.3 ms	77/86	23.0 s	0.48 mm ²	500 um
, 267.3 ms	42/42	11.2 s	0.16 mm ²	1,000 um
34 ms 068 ms	19/20	13.4 s	0.1 mm ²	750 um

ie primarily to misalignment between
; Subsystem

Figure 9.22: Summary of *in vivo* experiments.

(2)

of more OG-550 filters inline between the fundus camera and the CCD. Also, the use of a anti-reflection coating on the plano-convex lenses will further reduce glare. The current matching connector between the fundus camera and the CCD video camera only allows two OG-550 filters. A modified design is under investigation.

- Lesion placement errors and glaring were pronounced at the edges of the image in lesion experiment 1. Also, at the extreme edge of the field of view the laser did not reach the retina because of physical limitations imposed by the size of the Laser Positioning System lenses. To remedy these problems the software was modified to avoid the field of view edges on lesion experiments 2 and 3.
- On average each lesion required 267 ms to form on matrix experiments 1 and 2. To complete the matrix of 86 lesions for experiment 1 only required 23 seconds.

In vivo lesion tracking experiment

The final *in vivo* experiment was designed to demonstrate the capability of the system to track using lesion templates. In this experiment a triad of lesions were first placed using retinal vessels as a tracking template. The lesion triad was then used as a tracking template to place another lesion triad.

Results

Figure 9.23 illustrates the result of this experiment. The lesion triad on the left was placed using vessel templates while the lesion triad on the right was placed



Figure 9.23: *In vivo* lesion template tracking. The lesion triad on the left was placed using vessel templates while the lesion triad on the right was placed using the left lesion triad as a template. The laser was set for 514 nm and 150 mW at the cornea. The mean irradiation time for the lesions in the left triad was 267 ms while the mean irradiation time for the right triad was 330 ms. The laser fired at the apex of the right triangle but did not leave a visible lesion.

using the left lesion triad as a template. This experiment demonstrated the feasibility of using lesions as templates to place other lesions using techniques described in Chapter 6.

Chapter 10

The Real Time System

10.1 Overview

This chapter analyzes equipment requirements, specifies actual hardware components and costs, and provides a design for a real time tracking algorithm. The chapter begins with trade-off analysis of interrelated factors which influence the performance of a real time system. This analysis forms the basis for selection of actual hardware which follows. A complete real time system is then specified.

10.2 Sensitivity Analysis

In Chapter 2, graphs were provided which illustrated the relationship between retinal eye movement velocities, desired laser target radius, and the number of position updates required per second. This analysis will now be revisited in much greater detail and used to specify real time system components. This section begins with definitions of factors influencing the performance of the Retinal Tracking Subsystem. A detailed analysis of the interrelationship of these factors then follows.

10.2.1 Factors influencing Retinal Tracking Subsystem performance

The following factors influence the performance of the Retinal Tracking Subsystem:

- Desired laser **target radius** is defined as the radius of a circle which contains the laser spot's centroid movement as illustrated in Figure 10.1. Forty microns was arbitrarily chosen as the lower target radius bound used in the trade-off analysis because this is the approximate pixel length of the development system. The upper bound was chosen to be 520 microns because this is close to the desired diameter of therapeutic lesions. Ideally, laser target radius should be zero. At the other extreme, as the target radius becomes greater the control of therapeutic lesion size degrades. These two extremes are also illustrated in Figure 10.1.
- Different types of **retinal movement** were discussed in Chapter 2. Intuitively, there is a direct correlation between the velocity of retinal movement and the required performance of the tracking algorithm. As the retinal velocity increases the tracking algorithm must provide positional updates at a faster rate to maintain a given laser target radius. At faster retinal velocities, the tracker may be able to maintain lock on the moving retina but the updated laser position will lag behind the intended target coordinate. By employing visual fixation retinal velocities may be theoretically reduced to micro-saccades and micronystagmus. However, for safety purposes the real time system will be designed to track at retinal velocities up to 50 degrees per second.

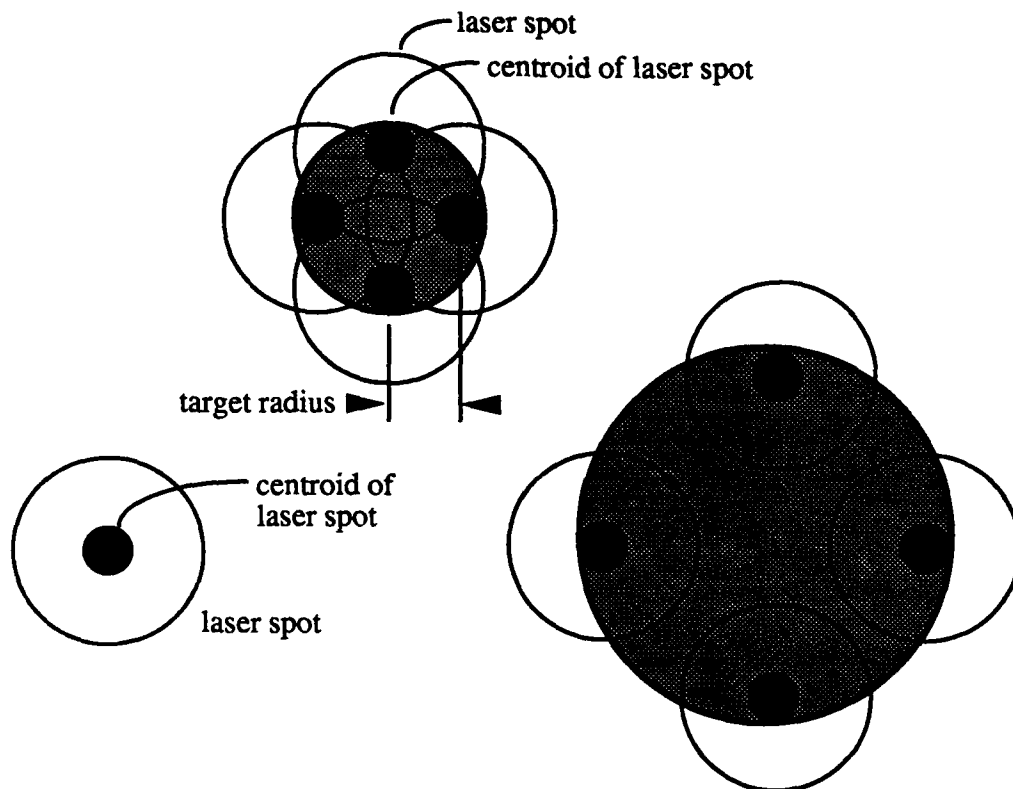


Figure 10.1: Target radius of the laser. Top: Target radius is defined as the radius of a circle which contains the laser spot's centroid movement. Bottom left: Ideally the target radius should be zero. Zero radius allows laser placement directly on target. Bottom right: As the target radius becomes larger the control of therapeutic lesion size degrades.

- The number of **laser position updates** required per second are directly driven by the desired laser target radius and the upper bound of retinal velocity that the algorithm must track. As the target radius becomes smaller the number of position updates required per second increases. Also, as the upper bound of retinal velocity increases the number of position updates required to maintain a given target radius increases.
- The tracking algorithm uses a limited exhaustive search to derive laser position updates. To calculate a position update requires a finite amount of computer **processing time**. Intuitively, as the number of position updates per second increase the amount of retinal movement that may occur between position updates decreases for a fixed retinal velocity. Hence, the required processing time for a given position update also decreases.

10.2.2 System specification trade-offs

To clearly demonstrate the interrelationship and trade-offs between the factors influencing tracking algorithm performance, the following analysis uses techniques described in Chapter 4 for different retinal velocities. Arc length calculations are used to determine the number of laser position updates required per second for a given laser target radius at a given retinal velocity. The number of laser position updates required per second may also be used to determine the total number of template calculations required per second. This analysis is independent of system implementation. A specific system may then be analyzed by converting the total number of template calculations required per second to the amount of time required by the system processor to complete these required calculations.

Figure 10.2 illustrates the relationship between parameters influencing tracking algorithm performance. To reduce target radius for a given retinal velocity the number of position updates must be increased (upper left). An increase in the position update rate decreases the time the retina may move between updates. The potential search area size decreases as the position update rate increases (upper right) due to limited eye movement between updates. The number of computations required per second increase with the size of the search area (lower left). The computations required per second decrease as the position update rate is increased (lower right). This reduction is due to the reduced search area size and hence fewer computations as the position update rate increases. The double ordinate graphs of Figure 10.3 (bottom) ties these interrelated factors together for various retinal velocities. Required position updates per second is provided on the left y axis. The right y axis provides the total number of template calculations required per second. Both y axis share the desired laser target radius on the x axis (in microns). Program `sensitiv.c` was used to compute the number of updates required per second and the amount of processing time (for a 486-33 PC) required to calculate a position update for a given retinal velocity and laser target radius. The results are provided in Figure 10.3 for system independent implementation and for implementation on a 486-33 in Figure 10.4.

10.2.3 Interpretation and analysis of results

A double ordinate graph is used to plot the interrelationship of factors influencing tracking algorithm performance. Required position updates per second is provided on the left y axis. The right y axis provides the total number of

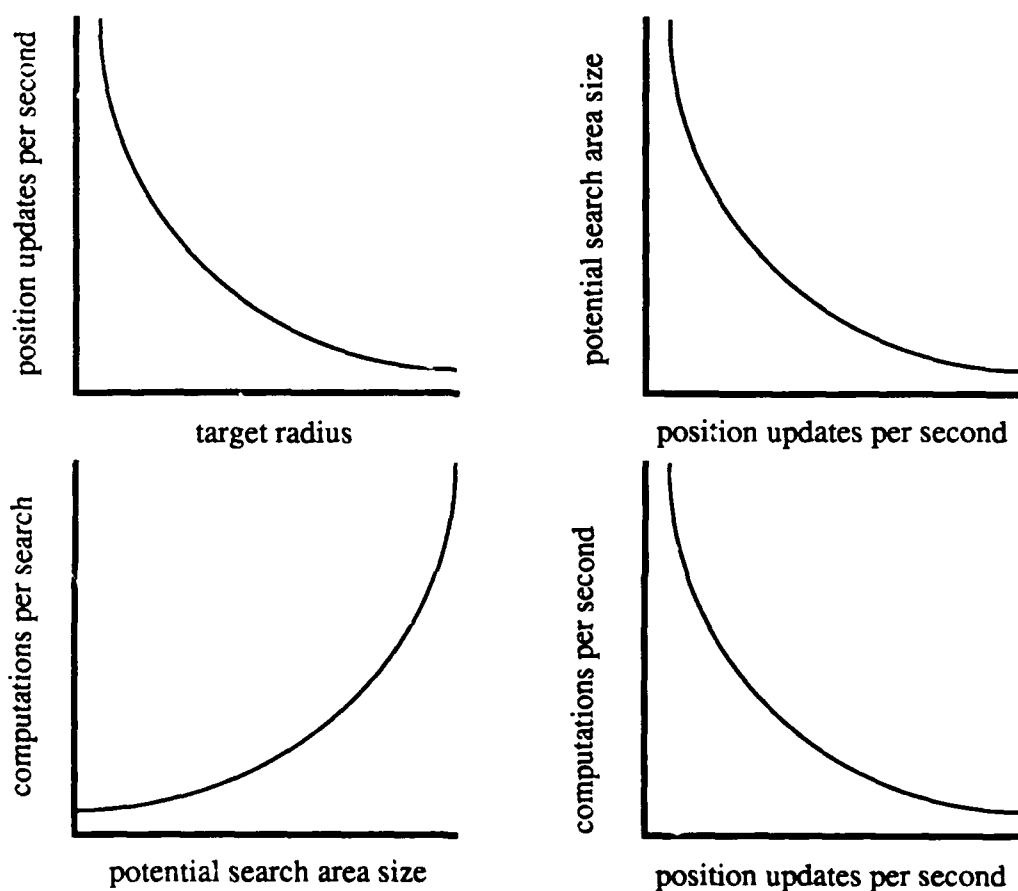


Figure 10.2: Relationship between parameters influencing tracking algorithm performance. To reduce target radius for a given retinal velocity the number of position updates must be increased (upper left). An increase in the position update rate decreases the time the retina may move between updates. The potential search area size decreases as the position update rate increases (upper right) due to limited eye movement between updates. The number of computations required per second increase with the size of the search area (bottom left). The computations required per second decrease as the position update rate is increased (bottom right). This reduction is due to the reduced search area size and hence few computations as the position update rate increases.

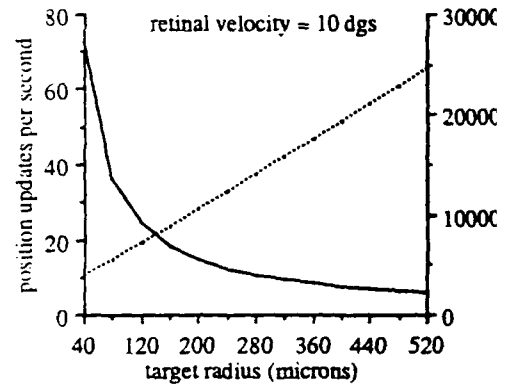
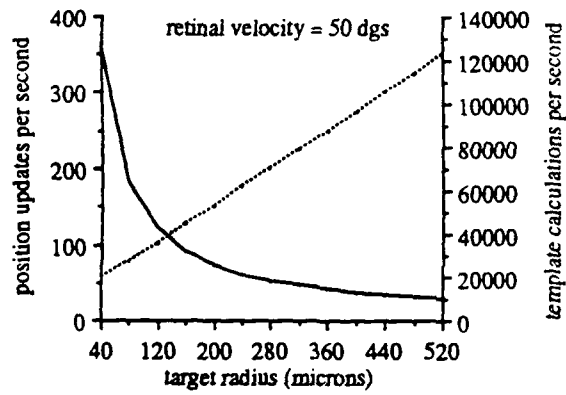
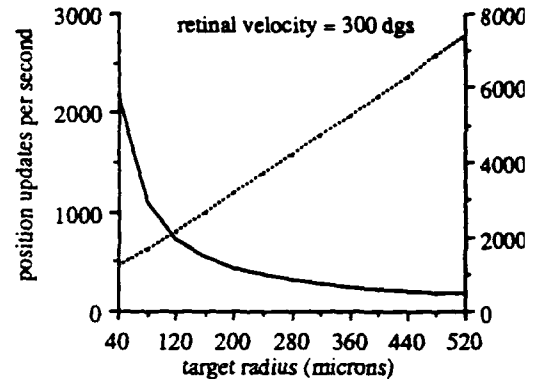
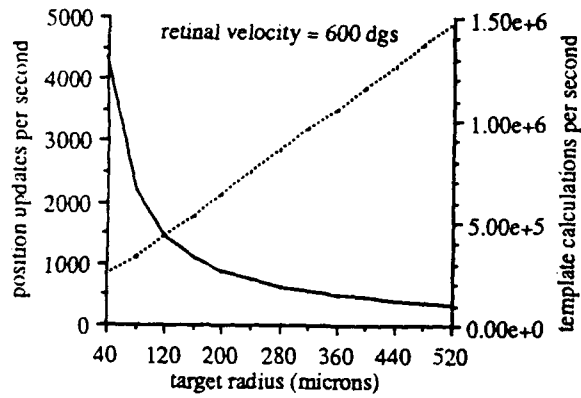
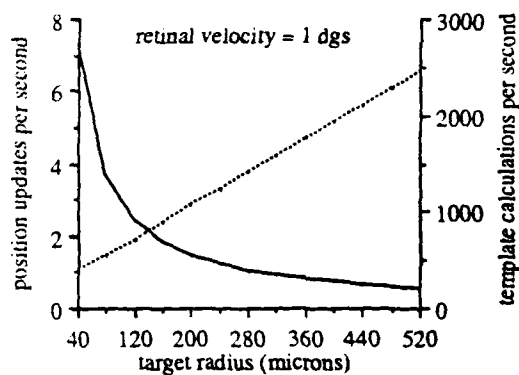
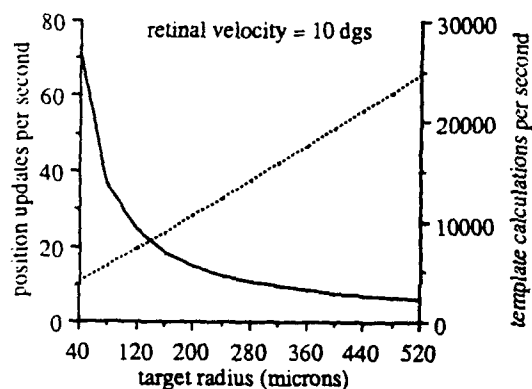
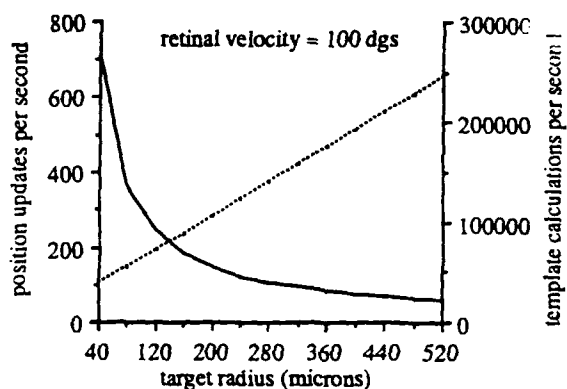
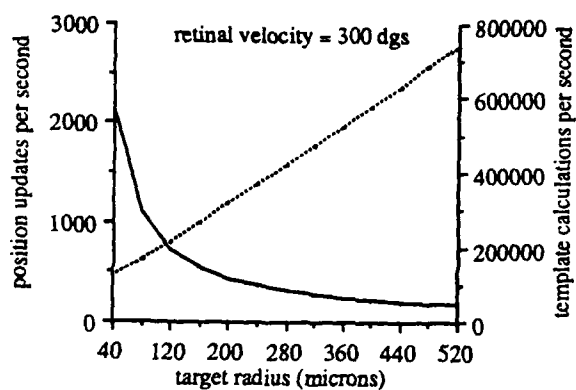


Figure 10.3: Trade-off analysis results based upon the performance of a tracking algorithm. These graphs describe the interrelationship between the number of position updates and the number of template calculations required as a function of retinal velocity and target radius. The number of position updates (solid line) and the number of template calculations (dotted line) are graphed as a function of retinal velocity and target radius. The operating parameters (retinal velocity and target radius) are obtained by drawing a vertical line through the graphs. The number of position updates and template calculations are provided on the respective plots.



Trade-off analysis results based upon template calculations per graphs describe the interrelationship between factors influencing ce of a tracking algorithm. The number of laser position updates phed as a function of retinal velocity and desired laser target umber of template calculations required per second (dashed) are he right ordinate. The operating parameters for a given retinal arget aradius are obtained by drawing a vertical line up from the radius on the appropriate retinal velocity graph. The number of tes and template calculations are provided at the intersection of ne and the respective plots.

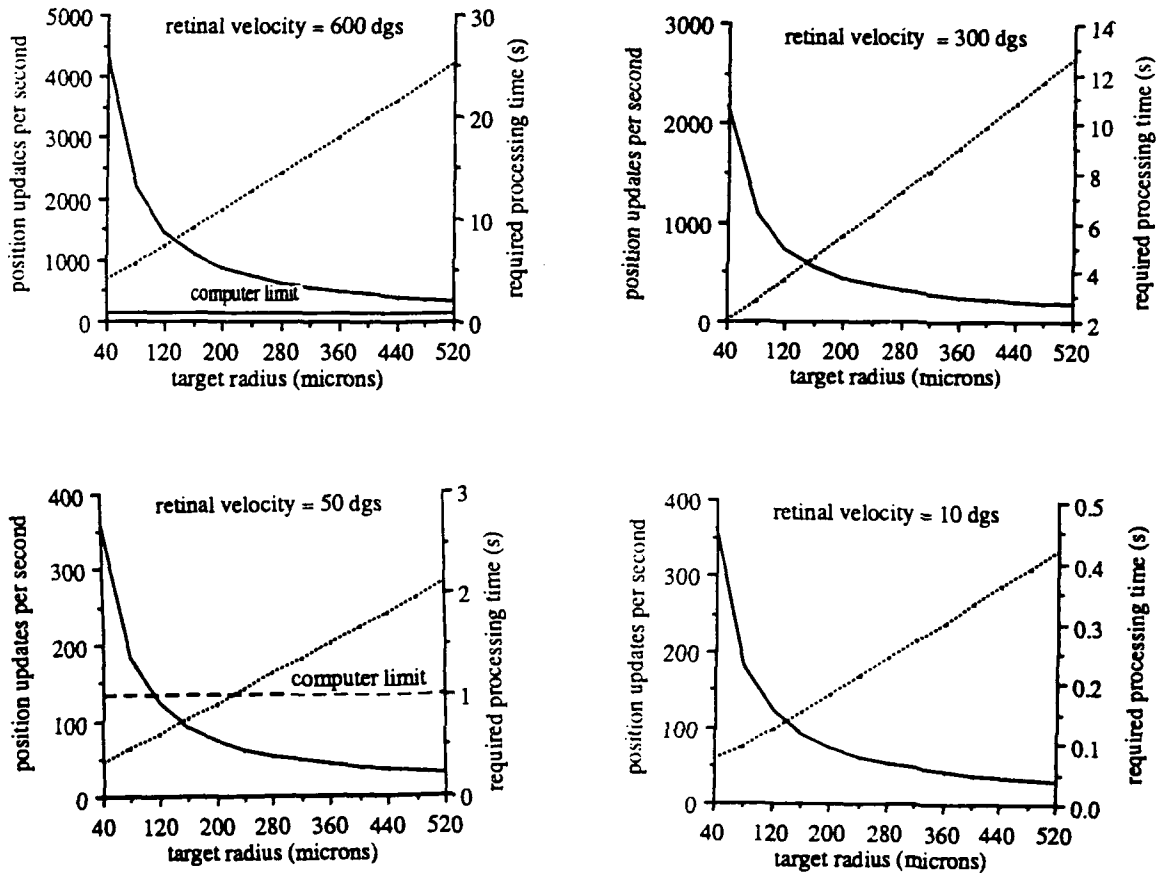
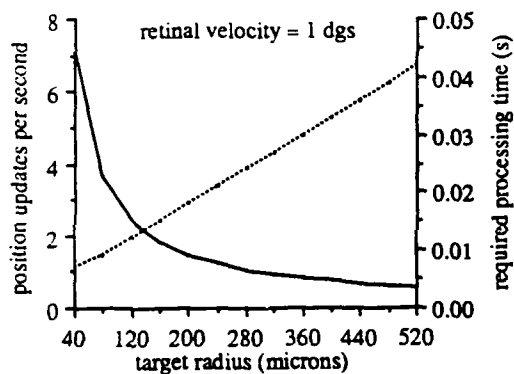
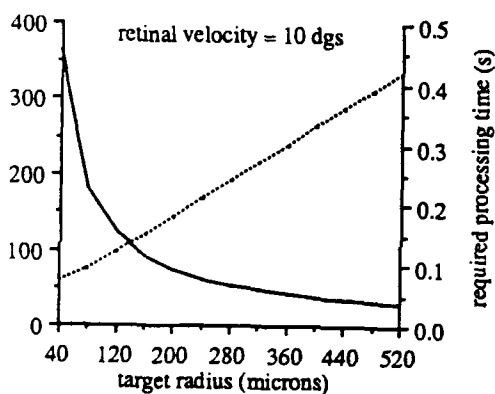
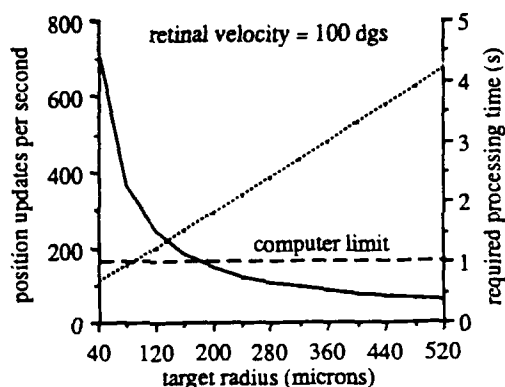
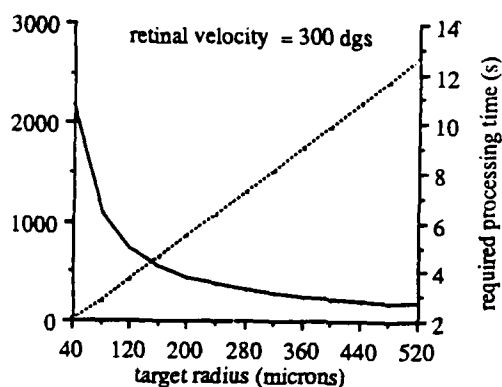


Figure 10.4: Trade-off analysis results based on an Intel 33 M processing time. These graphs describe the interrelationship between the performance of a tracking algorithm. The number of updates (solid) are graphed as a function of retinal velocity and target radius. The amount of processor time required to complete the calculations required per second (dashed) are provided on the right y-axis. The processor is too slow for a given retinal velocity and target radius combination if the processor requires more than one second to complete the template calculations required every second.



off analysis results based on an Intel 33 MHz 80486DX processor. The graphs describe the interrelationship between factors influencing the performance of a tracking algorithm. The number of laser position updates per second (dashed) are graphed as a function of retinal velocity and desired laser target radius. The amount of processor time required to complete the template matching algorithm (solid) is also graphed. A horizontal dashed line indicates the computer limit of one second per second. If the processor requires more than one second to process a given target, the system is too slow for a given retinal velocity and laser position target radius. The number of position updates required every second.

template calculations required per second. Both y axis share the desired laser target radius on the x axis (in microns). A separate graph is provided for the following retinal velocities: 600 degrees per second, 300 degrees per second, 100 degrees per second, 50 degrees per second, 10 degrees per second, and 1 degree per second. A common graph containing all retinal velocities is too 'busy' to be useful.

These graphs may be used to determine the number of position updates required per second and the accompanying total number of pixel calculations required per second for a given laser target radius for a given retinal velocity. For example: for a laser target radius of 160 microns and a retinal velocity of 50 degrees per second, 90 position updates are required per second. These 90 position updates require approximately 44,000 total template calculations per second (see Figure 10.3). Figure 10.4 indicate that 0.76 seconds of 486-33 processing time is required to compute the 44,000 total pixel calculations. This type of data can be determined for any combination of retinal velocity and desired target radius.

These graphs may also be used to examine the capability of an existing system. If the number of position updates a given system can complete in a second is known its tracking capability for a given retinal velocity at a given target radius may be measured. Several trends may be noted from the graphs:

- To obtain laser target radius less than 120 microns requires a substantial increase in position updates per second.
- Only a slight increase in position updates per second is required to improve laser target radius from 500 to 200 microns.

- At faster retinal velocities and smaller laser target radii the number of template calculations required per second exceed the processing capacity of the computer. This is most evident in Figure 10.4 for retinal velocities of 600, 300, and 100 degrees per second. For these graphs the 486-33 requires tens of seconds of processing power to perform the number of template calculations required every second. Methods of mitigating this situation will be discussed later in this chapter.
- A faster processor will shift the required processing times graph (dashed line) down.

10.3 Real Time Equipment Specification

The analysis in the previous section may be used to determine component requirements for the real time Retinal Tracking Subsystem and Laser Pointing Subsystem. This section will establish these requirements and then describe the components required to construct a real time system. This section concludes with the cost of the real time system.

10.3.1 Real time system parameters

The speed and processing power of the real time system may be determined by specifying an upper bound for retinal velocity and desired laser target radius. In Chapter 2 retinal velocity parameters were described in detail. If patient visual fixation is used an upper bound of retinal velocity may be safely specified at 50 degrees per second. The tracking algorithm will register a loss of lock condition should retinal velocity exceed this upper bound. A laser target radius

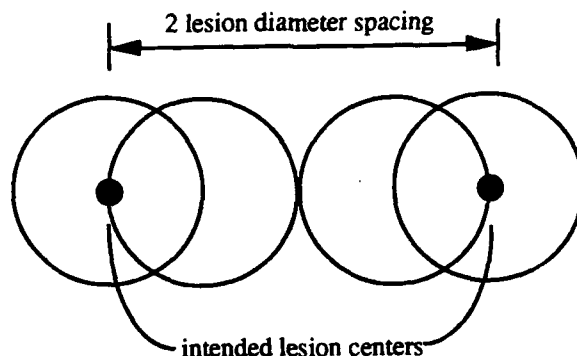


Figure 10.5: Resolution of adjacent lesions. A laser target radius of 100 microns as a lower bound for lesions 2 lesion diameters apart will prevent the overlap of adjacent 200 micron lesions.

of 100 microns as a lower bound for lesions 2 lesion diameters apart will prevent the overlap of adjacent 200 micron lesions. In a worst case situation at this target radius two adjacent 200 micron lesions would just touch. Reference Figure 10.5.

The 50 degree per second graph of Figure 10.3 indicates approximately 150 position updates are required per second. Figure 10.4 indicates that a 486-33 processor has about the required processing power to perform the necessary calculations. With these parameters established system components will now be described for the real time system.

To transition from a prototype system to a real time system requires an increase in the number of position updates per second. An increase in position updates may be accomplished by using a faster frame rate camera and a faster processor. The number of position updates does not directly equate to a required camera frame rate. The camera frame rate must be faster than the number of position updates required per second to allow for position update calculations to occur between subsequent images. For example: in

the prototype system a camera with a 30 frame per second rate was used ;however, only 7 frames per second were used. More efficient use of available camera frames is possible if position updates can be calculated in minimal time. The position processing time may be minimized by hosting the tracking algorithm on a faster processor. For example: the current prototype system could provide 10 position updates per second if hosted on a 486-66 processor. To further reduce position update processing time a frame grabber with an onboard arithmetic logic unit could be used.

10.3.2 The camera

The preceding analysis indicates a camera with a frame rate of at least 150 frames per second is required to provide for position updates. Ideally, a camera resolution of 512 x 512 pixels with 256 gray levels is required. A video camera with this resolution and frame rate combination is not readily available. A 256 x 256 pixel camera may be used; however, a lens system between the fundus camera and the video camera is required to focus the central portion of the fundus camera field of view on the video camera's active sensing array. Dalsa Incorporated of Waterloo, Ontario manufactures a 256 x 256 CCD camera that operates at up to 200 frames per second. This camera, the Dalsa CA-D1-0256, is compatible with other high speed imaging equipment to be discussed [99]. Dalsa application engineers indicate the sensitivity of the camera at 30 frames per second is comparable to other CCD cameras at 30 frames per second. Due to a linear decrease in integration time at higher camera speeds, the image quality will also degrade linearly. **Some** of this image degradation may be offset with input look-up table modifications in the frame grabber.

10.3.3 The frame grabber

The desired features of the real time system frame grabber is compatibility with the high speed CCD camera, an on-board processor to speed template calculations, and compatibility with a personal computer host. The choice of a PC host helps to contain overall system cost.

Imaging Technology Incorporated of Woburn, Massachusetts manufactures an entire product line of high-performance modular image processing subsystems. In particular, their Series 150/151 modular processors provide some of the required capability for this system. The Series 150/151 is a module family to perform real time image operations and image analysis. The Retinal Tracking Subsystem would require the following Series 150/151 components: VSI-150 Variable Scan Interface, FB-150 Frame Buffer, and ALU-150 Pipeline Processor [100].

The VSI-150 allows the Series 150/151 system interface to a variety of nonstandard video sensors. This feature will allow use of the Dalsa high speed CCD video camera. The VSI-150 is also equipped with a programmable input look-up table which allows real time histogram modification for image contrast enhancement. Histogram modification techniques were described in Chapter 3 of this document. The FB-150 contains the frame storage for the system. It is equipped with a single 512 x 512 by 16 bit frame buffer to store intermediate results and two 512 x 512 by 8 bit frame buffers. The ALU-150 has pipelined architecture which allows simple operations on data passing through the module to be performed in minimal time [100].

Two additional system requirements are the interface to the host computer and the ITI system software library. An AT to VME bus interface is

required for the ITI system to work with a PC host computer. This interface may be ordered as an option with the system. The ITI system is supported by the ITEX 150/151 software library of image processing functions. This software is directly compatible with Microsoft C and contains a wide variety of image acquisition and processing functions [100].

10.3.4 The Computer

Previous analysis indicates the 486-33 processor almost has enough computation power for the real time system configuration. A prudent choice would be a 486-50 processor or the recently released 486-66 processors. Intel has just released a faster processor, the Pentium. This processor will be able to run all the software developed for X86 processors [114]. The Pentium theoretically has a peak performances rating of 112 million instructions per second (mips) while the 486-66 processor is rated at 54 mips [115]. More computation power will allow for system refinement and additional features.

10.3.5 Galvanometers and driver amplifiers

As discussed in Chapter 5 of this document, galvanometers and drivers with feedback control are required in the real time system. Also, galvanometers with MIL STD levels of reliability will provide an additional measure of safety to the real time system. A pre-configured X-Y scan head package is further recommended. These products are available from General Scanning Incorporated. The X-Y scan head package may be equipped with mirrors specially matched to argon wavelengths. These mirrors have 98.5 percent minimum reflectance between 480 and 514 nm. They are rated at 100 W/cm^2 for 100 ns pulses

(model XY2026A). The AE1000 controller board provides the necessary closed loop control for the X-Y scan head package [101].

10.3.6 Data acquisition system

The Data Translation DT2801A data acquisition board described in Chapter 7 of this document has the required capability to support the real time system configuration.

10.3.7 Laser Shutter

The Uniblitz LS6Z2 shutter and the D122 shutter driver described in Chapter 7 of this document has the required capability to support the real time system configuration.

10.3.8 System Description

Figure 10.6 provides the configuration of the real time system. The intent is not to specify a final system design but to specify a design to demonstrate that the necessary technology now exists to implement a real time tracking algorithm.

10.3.9 Real time system cost

The system configuration illustrated in Figure 10.6 costs 26,955 dollars. This is a breakdown for equipment costs:

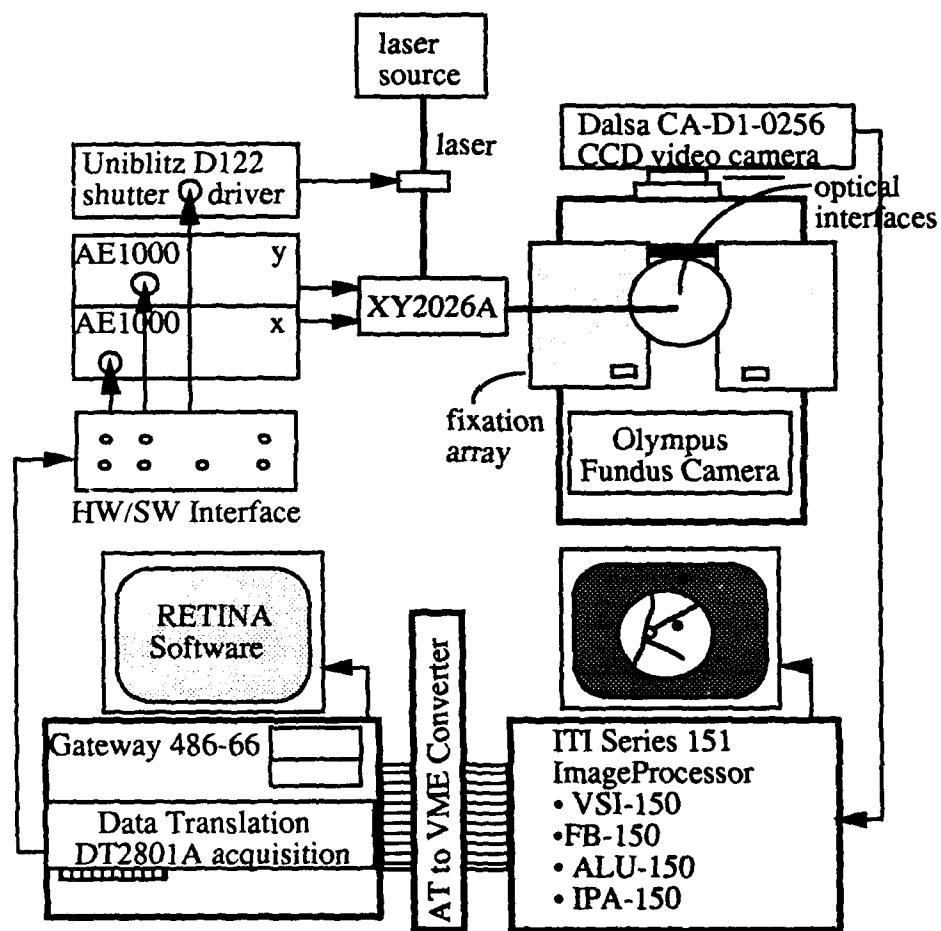


Figure 10.6: The real time system configuration.

Description	Price
Dalsa CA-D1-0256 CCD video camera	2550.00
ITI Series 150/151 Image Processor (88 price)	14485.00
486-XX computer configured with an AT bus	3000.00
X-Y scan head with closed loop controllers	4200.00
DT2801A acquisition board with PC-LAB software	1660.00
Uniblitz LS6Z2 shutter and D122 shutter driver	710.00
Microsoft C version 7	350.00
Total	26955.00

10.3.10 Technical concerns

Several technical concerns exist with the real time system implementation. First, at faster frame rates image quality degrades due to a shorter camera element integration time. The rate of image degradation is proportional to camera frame rate. Second, to study a real time system, an inexpensive image storage capability for nonstandard frame rates is required. Finally, although frame grabbers are available with onboard arithmetic logic units, the instructions sets are quite limited. Care must be taken to select a frame grabber with the required instructions.

This completes the description of the real time system. Chapter 11 describes related research work required to complete the design of the Robotic Laser System.

Chapter 11

Conclusions

11.1 Conclusions

This research demonstrated the feasibility of tracking human retinal movement to stabilize laser positioning during photocoagulation therapy. A development system was built and tested. This system incorporated automatic Lesion Data Base building, template building using blood vessel and lesion templates, a tracking algorithm to compensate for retinal movement, and a Laser Pointing System. Closed loop feedback laser control using the tracking algorithm was demonstrated with the development system. Also, panretinal treatment for diabetic retinopathy and the repair technique for treating detached tears and breaks were demonstrated *in vivo*. The requirements and equipment necessary to implement a real time system was provided.

A real time system is required for clinical use. However, several areas of research need further investigation prior to implementation of a real time system. This chapter reviews these areas of further research followed by a summary of significant findings from this research study. The chapter concludes with suggestions for using results of this research effort in other related research efforts.

11.2 Future Improvements and Further Research

11.2.1 *In vivo* testing on *Macaca mulatta* monkeys

The *in vivo* testing on pigmented rabbits provided valuable insights on system performance and limitations. Although the tissue properties of the rabbit's retina is similar to the human's, its physical features are quite different. An *in vivo* test on a human similar subject would prove beneficial. A *Macaca mulatta* (rhesus monkey) was chosen as the test subject.

Only minor modifications are required to the prototype system for the *in vivo* monkey experiment. The subject animal will be oriented such that the forehead is facing the fundus camera as illustrated in Figure 11.1.

A cooperative experiment between the University of Texas at Austin's Biomedical Engineering Program, the Air Force's Laser Biophysics Research Branch at Armstrong Laboratories, Brooks Air Force Base, San Antonio, Texas, and the United States Air Force Academy (USAFA) at Colorado Springs, Colorado is tentatively planned for Summer 1993. Due to the high cost of the animal subject (\$1000), only one experiment is planned using two monkey subjects. This experiment will demonstrate the treatment of diabetic retinopathy in one eye and the treatment for retinal tears in the fellow eye for one subject monkey. The other monkey will be used to demonstrate lesion matrix placement as a feasibility study to use the Retinal Observation and Tracking System in conjunction with ultrashort pulse laser tissue studies. Results will be presented in the literature. The following people will participate in this joint experiment: Major Steven F. Barrett (USAFA); Dr. A.J. Welch (UT), Dr. H. Grady Rylander (UT), M.D.; Captain Cameron Wright (UT); Dr. (Lt Col)

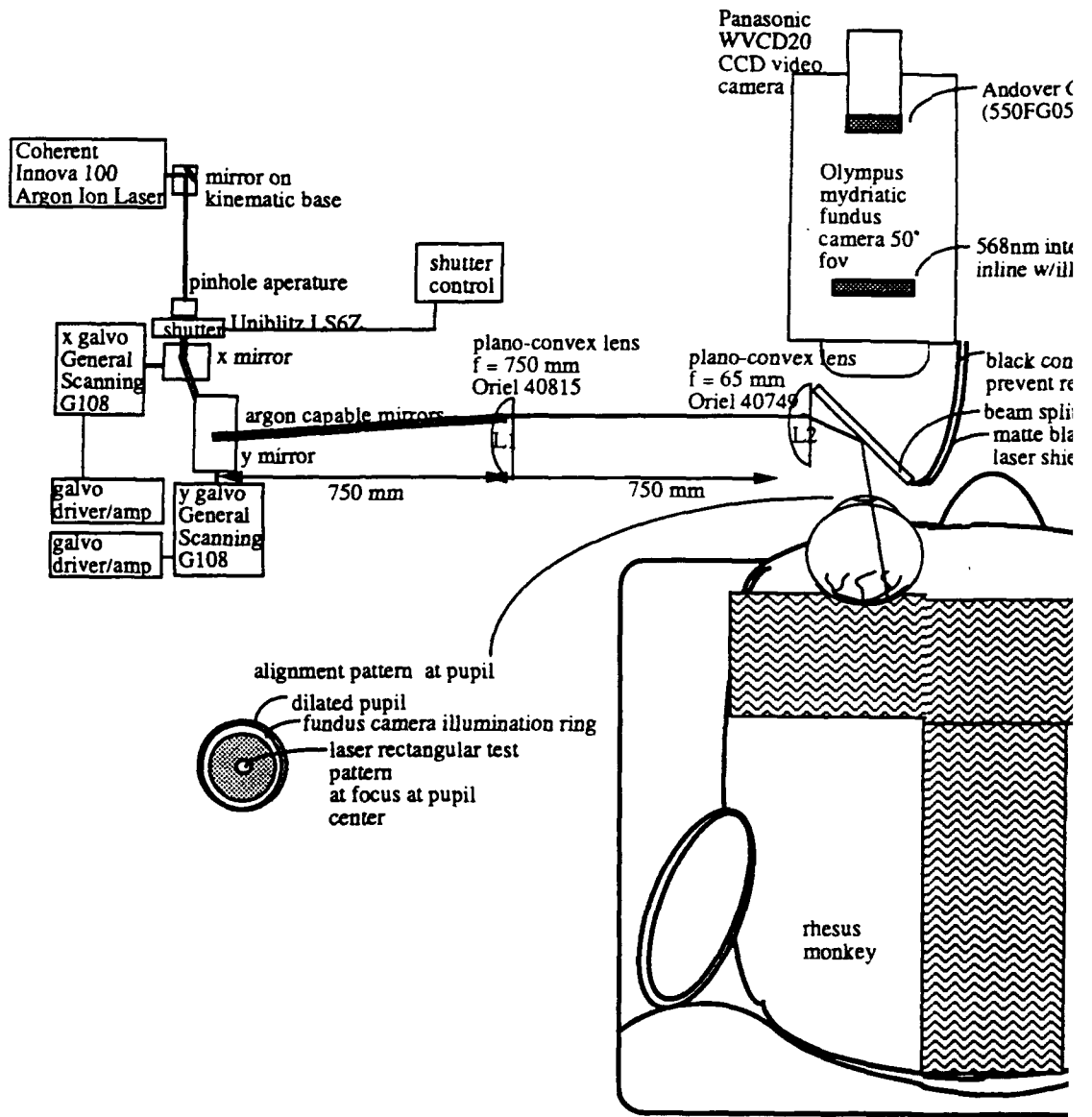


Figure 11.1: Equipment configuration for *in vivo* *Macaca mulatta*. Use of a monkey test subject requires orientation of the subject that the forehead is facing the fundus camera.

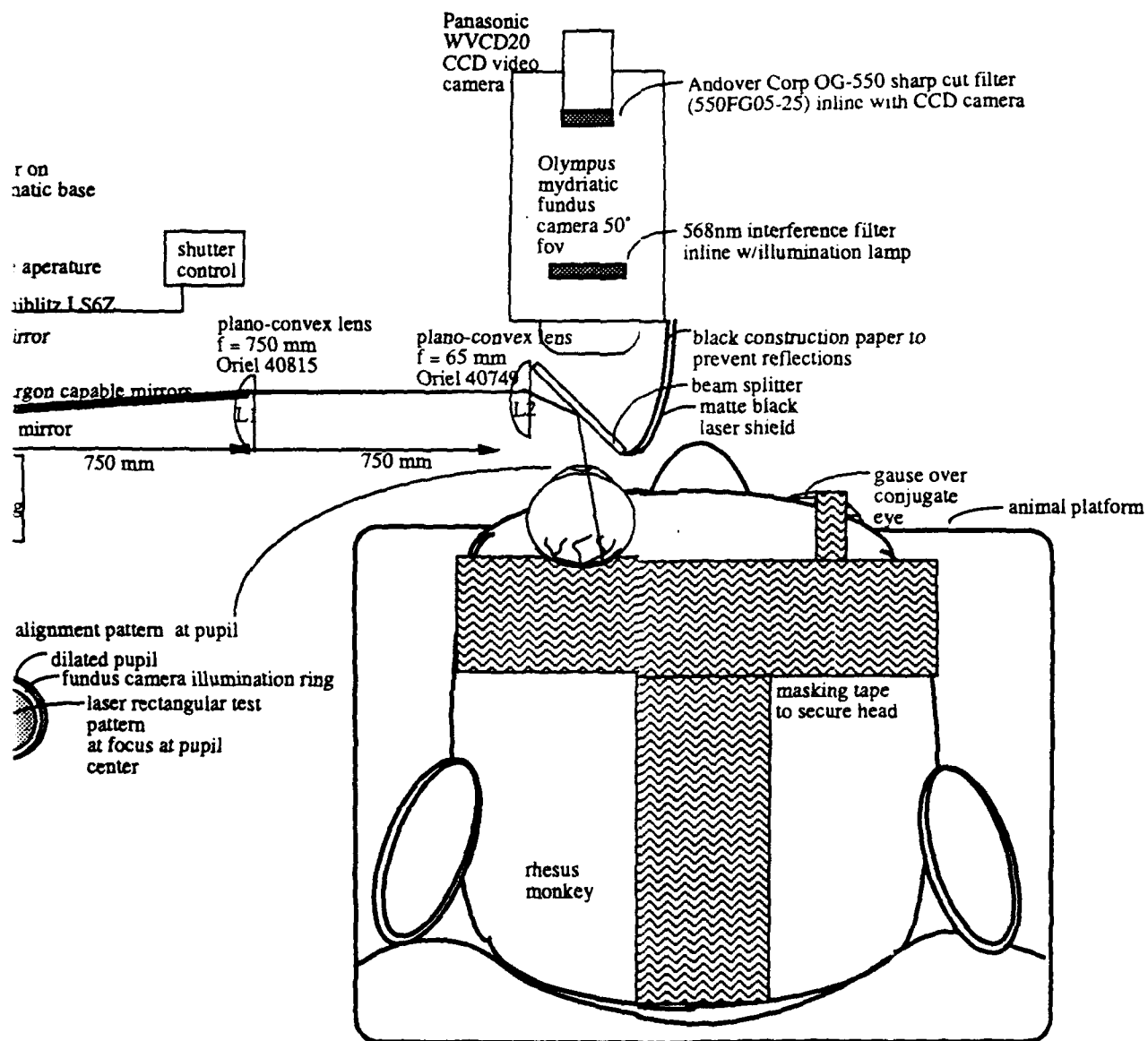


Figure 11.1: Equipment configuration for *in vivo* *Macaca mulatta* experiments. Use of a monkey test subject requires orientation of the subject's head such that the forehead is facing the fundus camera.

Mark E. Rogers (AL), Dr. (Major) Cynthia Toth, M.D. (AL), Dr. Clarence Cain (AL), Dr. (Capt) Pat Roach (AL), and Lt. Stein (AL).

11.2.2 Solid-state laser diode therapeutic laser

Dr. Maya Jerath used an argon laser (488 and 514 nm) for her research on the Reflectance Based Feedback Control System. This has been the therapeutic laser of choice for many ophthalmological based treatments. Although this laser has proved extremely effective, it has some significant disadvantages. These disadvantages include:

- The laser is quite large. Although the laser is conveniently delivered via an optical fiber, the actual lasing equipment is housed in a large cabinet.
- A 3 to 5 watt argon laser requires an external cooling system to maintain the lasing mechanism at a non-destructive temperature. This is typically provided by a water cooling loop. This loop creates a significant mess when it leaks (experienced first hand).
- The laser requires special power requirements. For example the Coherent System 900 Argon Laser Photocoagulator used in this study required 208 VAC, 3 phase, 30 amp power. The Innova 100 Argon Ion Laser required 480 VAC, 3 phase, 60 amp power.
- Since the all lines argon laser beam has several wavelengths it is difficult to completely filter out the laser with a single filter. To protect the imaging camera from the argon laser source, Dr. Jerath used a chopper wheel. This mechanism was quite effective; however, it required critical

alignment and a feedback speed control mechanism on the chopper wheel motor. Use of a single wavelength laser source can reduce the complexity of the Reflectance Based Feedback Control System.

Some of these disadvantages may soon be of historical interest. A 1.5 W argon photocoagulator using forced air cooling and operating at 120 VAC, 20 amp power is now available from Coherent Incorporated. This portable system, designated the Ultima 2000 Argon Laser System, has been FDA approved for all photocoagulator clinical applications [102].

Solid state laser diodes

Solid state laser diodes are recent technological developments which may remedy the disadvantages of the argon laser source. Solid state laser diodes offer the advantages of compact size, long operating life, reduced power requirements, and air cooling [103]. However, a possible disadvantage is pain associated with heating of the choroid and a narrow therapeutic power window [1].

Solid state laser diodes consist of a semiconductor junction similar to those found in a rectifying diode. In standard Ge and Si rectifying diodes, energy is released predominantly as heat during the recombination of holes and electrons at the semiconductor junction. In III-V and II-VI compound materials, energy is released as photons with energies approximately equal to the bandgap of the material. When reflective facets are included on these diodes a laser diode results. The facets reflect the light energy back and forth through the semiconductor junction to further stimulate emission. When the current within the junction reaches a certain threshold, internal losses are overcome by

the stimulated emission and a laser output results. At lower junction currents the laser diode acts as a light emitting diode [109].

Current technology

Currently solid state laser diodes are not available in shorter (close to argon wavelengths). Shorter wavelength diodes have been produced by increasing the aluminum content of InGaAlP diodes. This increase in aluminum has the disadvantage of decreasing the diode's lifetime. Recent work by Masselink and Zachau of IBM's Watson Research Center have produced **incoherent** emissions at wavelengths as short as 585 nm at room temperature [110, 111] using InGaP. Active research in this area continues.

Experimental work using the diode laser

Currently solid state laser diodes are readily available from 810 to 850 nm at peak power of 10 watts [108]. Sato et al. have compared the effects of such a diode (810 nm) to the argon (488 and 514 nm) laser for retinal endophotocoagulation. Sato examined the blood-retinal barrier (BRB) breakdown within rabbit eyes using magnetic resonance imaging. He hypothesized that the possible adverse effect of BRB breakdown related to retinal photocoagulation may be different for the diode laser as compared to the argon laser. Sato suggests that evidence "supports the notion that BRB breakdown can promote the development of proliferative vitreoretinopathy [103]".

Sato tested the hypothesis on rabbits. Clinically similar lesions using the diode laser were placed in one of the rabbits' eye. The other eye received lesions from the argon laser. The lesions and degree of BRB breakdown was then ex-

aminated two days and seven days after treatment. Sato noted that two days after treatment the argon treated eyes showed greater leakage than the diode treated eyes. Furthermore, the diode lesions displayed mild cellular displacement in the pigment epithelium and extensive thrombosis of the choriocapillaris and larger choroidal vessels. The argon lesions displayed severe cellular displacement in the pigment epithelium and fewer occlusions of the choriocapillaris and large choroidal vessels. Sato cautioned against extrapolating these results to humans because of a fully developed retinal vasculature in the human eye [103]. Related work has been accomplished by various researchers [104, 105, 106, 107].

The use of diode lasers especially at argon similar wavelengths appear promising. Additional research in this area is required.

11.2.3 System integration study

Dr. A.J. Welch, Dr. H.G. Rylander III, Dr. W.S. Weinberg, Dr. M.S. Markow, Dr. Y. Yang, Dr. S. Ghaffari, Dr. A.J. Seltzer, Dr. M.R. Jerath, and the author have spent considerable time developing the Robotic Laser System for the treatment of ophthalmologic diseases and disorders. Their related research efforts have included studies on basic laser tissue interactions, theoretical basis of lesion reflectance, lesion reflectance feedback daemons, conceptual design of the Robotic Laser System, optical tracking mechanisms, real time feedback control systems, reflectance based feedback control algorithms, and digital tracking mechanisms. Much of this work has been cited in this document. An integration study between the Reflectance Based Feedback Control System and the Retinal Observation and Tracking System is required. The goal of this study would be the design and implementation of the complete Robotic Laser System.

A preliminary discussion of an integrated system is provided here.

This discussion begins with a listing of the key equipment requirements for the Reflectance Based Feedback Control System and the Retinal Observation and Tracking System. Alternative methods for implementing an integrated system are then presented with associated advantages and disadvantages.

Individual system requirements

This section describes the special equipment and algorithmic requirements of the Reflectance Based Feedback Control Subsystem and the Retinal Observation and Tracking Subsystem.

Implementation details of the Reflectance Based Feedback Control Subsystem are provided in [4]. Careful study of this document reveals the following equipment requirements for this subsystem:

- A high resolution CCD video camera is required to image the forming lesion. Jerath used a 512 x 512 pixel camera. The camera should have the capability to shut off automatic gain control (AGC). The AGC feature adversely affects lesion reflectance measurements.
- The lesion imaging CCD video camera must have enough pixel resolution to adequately measure central reflectance. Jerath's system monitored the central 5 pixels of the lesion in real time. These 5 pixels represented 0.05% of the total lesion area.
- The argon source must be **completely** blocked during reflectance measurements. Any argon irradiation adversely affects lesion reflectance measurements.

The equipment requirements for the Retinal Observation and Tracking Subsystem have been carefully detailed throughout this document. The only requirement that may conflict with the Reflectance Based Feedback Control System is the need for a visible laser beam on the retina to recheck terminal laser position after position update.

Alternative solutions

There are several different methods of integrating these two subsystems. Alternatives include but are not limited to:

- **Method 1:** Implement two distinct subsystems to control lesion placement and depth. These subsystems would be implemented on separate computer hosts using separate but coaligned imaging systems. This technique was proposed by Markow [2].
- **Method 2:** Implement a single system to accomplish lesion placement and depth control using a semiconductor diode laser.
- **Method 3:** Implement a single system to accomplish lesion placement and depth control using an argon diode laser.

Method 1 provides the advantage of system speed. Implementing separate subsystems allows parallel control of lesion depth and placement. However, this method has inherent disadvantages including: 1) duplication of expensive hardware (high speed camera, frame grabber, and computer), 2) the need for a separate master controller to interface the two systems, and 3) precision optical alignment of the two systems.

Method 2 uses a single system to control both lesion placement and depth. This method solves the duplication of hardware and the optical alignment problems of **Method 1**. The diode wavelength (810 to 850 nm) is visible to a standard CCD video camera and would thus interfere with reflectance measurements. Use of a single system to control lesion placement and depth would slow overall system performance since these two tasks would be performed serially.

Method 3 also solves the duplication of hardware and the optical alignment problems of **Method 1**. This method has the same disadvantages of **Method 2**.

A single integrated system appears to be an attractive answer. However, several key questions require answers prior to implementing an integrated system. These questions include:

- **Question 1:** Does the Retinal Tracking and Observation Subsystem have the required resolution to monitor lesion growth?
- **Question 2:** Are camera requirements for each subsystem compatible such that they may be combined in a single camera?
- **Question 3:** How much time is required to check the reflectance response?
- **Question 4:** Can the laser irradiation be effectively blocked during reflectance measurements?
- **Question 5:** Can lesions be formed at slower rates to allow testing of an integrated prototype system?

Both Dr. Jerath and I believe a detailed integrated system study is the next logical step in system development. The goal of this study would be answering the above questions and implementing a single Robotic Laser System to precisely control both lesion depth and position.

11.2.4 Neural nets to learn match conditions

Currently loss of lock is determined in the tracking algorithm by comparing the tracking templates' response to predetermined upper and lower thresholds. These thresholds are determined by studying template response from both correct and incorrect match conditions. As described in Chapter 4 the lower bound was set at 0.15 of the expected template response and the upper bound was set at 1.3 of the expected template response. The determination of these thresholds is time intensive.

Artificial neural networks may be used to determine the loss of lock thresholds. Neural networks are computer models of the behavior of real neurons. These networks are made up of three types of units: input units, output units, and the hidden units. The hidden units link the input to the output units via weighted links. A given set of inputs will provide an output should the threshold of the hidden unit be exceeded. Any logic function may be modeled with neural networks by proper selection of weights and thresholds. The weights are determined by the neural network using a learning set of inputs and outputs [113].

The response of the six templates used in the tracking algorithm could be provided as inputs to a neural net. Proper match conditions could then be learned by the net. The output of the net would be a lock/loss_of_lock signal.

This interesting concept requires further work.

11.3 Summary of significant findings

This research effort has carefully explored the use of digital tracking mechanisms to correct for retinal movement during laser photocoagulation. The following is a summary of significant findings and accomplishments:

- The contrast of a retinal image may be significantly enhanced by combining optical filtering techniques with frame grabber input look-up table modifications. The overall effect is a dramatic increase in retinal vessel contrast against the retinal background. This contrast enhancement may be implemented without an associated time penalty.
- Image processing techniques were conceptualized and developed to build lesion data bases for the treatment of diabetic retinopathy, macular degeneration, and retinal breaks and tears.
- A method of storing multiple retinal fields of view tracking templates and lesion data bases was conceptualized and developed.
- An image acquisition, storage, documentation, and enhancement system was developed to support this research effort. This system has already been used to support other research efforts.
- A tracking algorithm based on retinal vessel templates has been implemented which uses a limited exhaustive search to determine match conditions.

- A development system was designed and implemented. This development system includes a retinal imaging system, a retinal tracking system, a patient interface, and a laser pointing subsystem.
- Two tracking concepts using lesion templates were developed, modeled, and tested.
- Closed loop feedback control of laser position was demonstrated using the tracking algorithm implemented on the development system. This capability was demonstrated with calibrated retinal velocities and *in vivo* using a rabbit model.
- Panretinal photocoagulation and the repair technique for retinal tears and breaks were demonstrated *in vivo*.
- Tracking with lesion templates was demonstrated *in vivo*.
- A trade-off study was completed to determine the interrelationship between the factors influencing the performance of the tracking algorithm.
- Results of the trade-off analysis were used to design and specify the requirements for the real time system.

11.3.1 Application of tracking algorithm to other laser stabilization systems

As previously mentioned, some of the imaging software developed for this project has already been used to support other research efforts. In response to this need a general purpose imaging software package based on the Matrox PIP-1024 and the Gateway 486-33 was implemented for use by fellow researchers.

A laser stabilized against subject movement is a common problem in retinal photocoagulation, corneal thermokeratoplasty, and laser tissue and vessel welding. Many of the techniques described in this document may be used in these other related areas with slight modifications.

11.4 Acknowledgements

This research was sponsored in part by the Texas Coordinating Board and in part by the Office of Naval Research under grant N00014-91-J-1564.

Results of this study have been documented in [116, 117, 118, 119].

Bibliography

- [1] Rylander, H. Grady, M.D. and Professor of Electrical Engineering, The University of Texas at Austin, Austin, TX, technical conversation.
- [2] Markow, M.S., "The Preliminary Development of a Robotic Laser System Used for Ophthalmic Surgery", Ph.D. Dissertation, The University of Texas at Austin, Austin, TX, August 1987.
- [3] Markow, M.S., Y. Yang, A.J. Welch, H.G. Rylander III, and W.S. Weingerg, "An Automated Laser System for Eye Surgery", *IEEE Engineering in Medicine and Biology Magazine*, December 1989, 24 - 29.
- [4] Jerath, M.R., "Real Time Control of Laser Induced Retinal Lesions", Ph.D. Dissertation, The University of Texas at Austin, Austin, TX, December 1992.
- [5] Jerath, M.R., "A Software Package for the Analysis of Laser Induced Retinal Lesions", Master's Thesis, The University of Texas at Austin, Austin, Texas, August 1989.
- [6] Jerath, M.R., C. Gardner, H.G. Rylander III, and A.J. Welch, "Dynamic Optical Property Changes: Implications for Reflectance Feedback Control of Photocoagulation", *J. Photochem. Photobio.*, Volume 16, pp 113 - 116, 1992.

- [7] Jerath, M.R., R. Chundru, S.F. Barrett, H.G. Rylander III, and A.J. Welch, "Reflectance Feedback Control of Photocoagulation *In Vivo*", *Archives of Ophthalmology*, submitted for publication.
- [8] Jerath, M.R., R. Chundru, S.F. Barrett, H.G. Rylander III, and A.J. Welch, "Preliminary Results of Reflectance Feedback Control of Photocoagulation *In Vivo*", *IEEE Transactions on Biomedical Engineering*, submitted for publication.
- [9] Ganong, W.F., *Review of Medical Physiology*, Appleton and Lange, Norwalk, CN, 1989.
- [10] Hecht, E., *Optics*, Addison-Wesley Publishing Company, MA, 1987.
- [11] Quigley, H.A., A.E. Brown, J.D. Morrison, and S.M. Drance, "The Size and Shape of the Optic Disk in Normal Human Eyes", *Arch Ophthalmol*, Volume 108, January 1990, pp 51 - 57.
- [12] Mansour, A.M., "Measuring Fundus Landmarks", *Investigative Ophthalmology and Visual Science*, Volume 31, Number 1, January 1990, pp 41 - 42.
- [13] Straatsma, B.R., M.B. Landers, A.E. Krieger, and L. Apt, "Topography of the Human Retina", *The RETINA Morphology, Function, and Clinical Characteristics*, University of California Press, Berkeley and Los Angeles, 1969, pp 379 - 410.
- [14] Eaton, A. M. and D.L. Hatchell, "Measurement of Retinal Blood Vessel Width Using Computerized Image Analysis", *Investigative Ophthalmology and Visual Science*, Volume 29, Number 8, August 1988, pp 1258 - 1264.

- [15] Engelken, E.J. , "Influence of Visual and Auditory Stimuli on Saccadic Eye Movement", Ph.D. Thesis, The University of Texas at Austin, May 1987.
- [16] Barlow, H.B. and J.D. Mollon, *The Senses*, Cambridge University Press, London, 1984.
- [17] Guyton, A.C., *Textbook of Medical Physiology*, W.B. Saunders Company, Philadelphia, PA, 1986.
- [18] Kosnik, W., J. Fikre, and R. Sekuler, "Visual Fixation Stability in Older Adults", *Investigative Ophthalmology and Visual Science*, Volume 27, Number 12, December 1986, pp.1720 - 1725.
- [19] Wise, G.N., Retinal Neovascularization, *Transactions American Ophthalmol Society*, Volume 54, 1956, pp 729.
- [20] Stefansson, E., R. Machemer, E. de Juan, B.W. McCuen, and J. Peterson, "Retinal Oxygenation and Laser Treatment in Patients with Diabetic Retinopathy", *American Journal of Ophthalmology*, Volume 113, January 1992, pp 36 - 38.
- [21] Wolbarsht, M.L. and M.B. Landers, "The Rationale of Photocoagulation Therapy for Proliferative Diabetic Retinopathy: A Review and Model", *Ophthalmic Surgery*, Volume 11, Number 4, April 1980, pp 235 - 245.
- [22] Dickman, I.R., "A Vision Impairment in Later Years:Macular Degeneration", *Public Affairs Pamphlet No. 610*, Public Affairs Committee Inc., 1982.

- [23] Weale, R.A., *The Aging Eye*, Harper and Row Publishers, 1963, pp 9 - 23.
- [24] *Dorland's Pocket Medical Dictionary*, W.B. Saunders Company, Philadelphia, PA, 1977.
- [25] West, S.S., A.M. Potts, and J.R. Shearer, "Television Ophthalmoscopy", *IRE Transactions on Biomedical Electronics*, April 1962, pp 162.
- [26] Delori, F.C., E.S. Evangelos, S. Gragoudas, R. Francisco, and R.C. Pruett, "Monochromatic Ophthalmoscopy and Fundus Photography", *Arch Ophthalmol*, May 1977, pp 861 - 863.
- [27] van Gemert, M.J.C., A.J. Welch, and A.P. Amin, "Is There An Optimal Laser Treatment for Port Wine Stains ?", *Lasers in Surgery and Medicine*, Volume 6, 1986, pp 76 - 83.
- [28] Nielsen, N.V., "The Normal Fundus Fluorescein Angiogram and the Normal Fundus Photograph", *Acta Ophthalmologica*, Supplement 180, Volume 64, 1986, pp 7.
- [29] Novotny, H.R. and D.L. Alvis, "A Method of Photographing Fluorescence in Circulating Blood in the Human Retina", *Circulation*, Volume XXIX, July 1961, pp 82 - 86.
- [30] Webb, R.H. and G.W. Hughes, "Scanning Laser Ophthalmoscope", *IEEE Transactions on Biomedical Engineering*, Volume BME-28, Number 7, July 1981, pp 488 - 489.
- [31] Timberlake, G.T., M.A. Mainster, E. Peli, R.A. Augliere, E.A. Essock, and L.E. Arend, "Reading with a Macular Scotoma - I. Retinal Location

- of Scotoma and Fixation Area”, *Invest Oph and Vis Sci*, Volume 27, July 1986, pp 1137 - 1139.
- [32] Mainster, M.A., G.T. Timberlake, R.H. Webb, and G.H. Hughes, “Scanning Laser Ophthalmoscopy - Clinical Applications”, *American Academy of Ophthalmology*, Volume 89, Number 7, July 1982, pp 852 - 857.
- [33] Elsner, A.E., A.H. Jalkh, and J.J. Weiter, “Retinal Imaging and Function Evaluation”, *Practical Atlas of Retinal Disease and Therapy*, W. Freeman editor, Raven Press, NY, in press.
- [34] Rosenfeld, A. and A.C. Kak, *Digital Picture Processing - Volume 1,2*, Academic Press Inc, Orlando, Fl, 1982.
- [35] “C2400 Series Cameras for Video Microscopy” Hamamatsu Photonic Systems Inc.
- [36] Galbiati, L., *Machine Vision and Digital Image Processing Fundamentals*, Prentice-Hall Inc, Englewood Cliffs, NJ, 1990.
- [37] Wilson, J. and J.F.B. Hawkins, *Optoelectronics - An Introduction*, Prentice Hall International Ltd, New York, NY, 1989.
- [38] “ISG Series Cameras for High Performance Electronic Imaging”, Xybion Electronic Systems, San Diego, CA.
- [39] Zimmerman, J.B., S.W. Pizer, E.V. Staab, J.R. Perry, W. McCartney, and B.C. Brenton, “An Evaluation of the Effectiveness of Adaptive Histogram Equalization for Contrast Enhancement”, *IEEE Transactions on Medical Imaging*, Volume 7, Number 4, December 1988, pp. 304 - 312.

- [40] Harris, M.W., "DAT Magnetic Storage and Imaging: Beyond Backup", *Advanced Imaging*, Volume 7, Number 2, February 1992, pp 59 - 61.
- [41] Whiteside, S., S. Mitra, T. Krile, and Z. Shihab, "Microcomputer Based Fundus Imaging in RNFL Assessment", *Investigative Ophthalmology and Visual Science*, ARVO Supplement, Volume 27, March 1986, pp 160.
- [42] Ward, N.P., S. Tomlinson, and C.J. Taylor, "Image Analysis of Fundus Photographs - The Detection and Measurement of Exudates Associated with Diabetic Retinopathy", *Ophthalmology*, Volume 96, Number 1, January 1989, pp 81 - 86.
- [43] Varma, R. and G.L. Spaeth, "The PAR IS 2000: A New System for Retinal Digital Image Analysis", *Ophthalmic Surgery*, Volume 19, Number 3, March 1988, pp 183 - 192.
- [44] Tanaka, M. and K. Tanaka, "An Automatic Technique for Fundus-Photograph Mosaic and Vascular Net Reconstruction", *MEDINFO 80*, North-Holland Publishing Co, 1980, pp 116 -120.
- [45] Gilchrist, J. , "Computer Processing of Ocular Photographs - A Review", *Ophthal Physiol Opt*, Volume 7, Number 4, 1987, pp 379 - 386.
- [46] Akita, K., and H. Kuga, "A Computer Method of Understanding Ocular Fundus Images", *Pattern Recognition*, Volume 15, Number 6, 1982, pp 431 - 443.
- [47] Makes, D.J., "Digital Fundus Camera", Ophthalmic Imaging Systems, Inc., Sacramento, CA, 95815.

- [48] *USAF RM 2000 Process*, Headquarters, United States Air Force, Office of Special Assistant for R and M, Washington, D.C., October 1988.
- [49] Ghaffari, S. , "The Design of a 2-Dimensional Optical Image Correlator and Its Application in Image Tracking", Ph.D. Dissertation, The University of Texas at Austin, Austin, TX, May 1990.
- [50] Parks, M., *Ocular Motility and Strabismus*, Harper and Row Publishers, Hagerstown, Maryland, 1975, pp 1 - 3.
- [51] D'Anna, S.A. and T.W. George, "Retinal Fundus Cameras" *Ophthalmology - Instrument and Book Supplement 1984*, 1984, pp 94 - 119.
- [52] Dale, N. and S.C. Lilly, *Pascal Plus Data Structures*, D.C. Heath and Company, Lexington, MA. 1988, pp 560 - 570.
- [53] Spaeth, G.L., *Ophthalmic Surgery*, W.B. Saunders Co., Philadelphia, PA, 1982, pp 402-408.
- [54] Ballard, D. H. and C.M. Brown, *Computer Vision*, Prentice-Hall Inc, Englewood Cliffs, NJ. 1982, pp 65 - 70.
- [55] Bovik, A.C., "Lecture Notes for Computer Vision", Fall 1990, pp 36 - 39c.
- [56] West, D. C., "Positional Control of Laser Photocoagulator Lesions Near the Fovea", *British Journal of Ophthalmology*, Volume 52, 1968, pp 938 - 939.
- [57] Timberlake, G.T. , letter to Steven Barrett, 3 February 1993.

- [58] Kelly, D.H. and H.D. Crane, "Research Study of a Fundus Tracker for Experiments in Stabilized Vision", National Aeronautics and Space Administration, Washington D.C., September 1968.
- [59] Crane, H.D. and C.M. Steele, "Accurate Three- Dimensional Eyetracker", *Applied Optics*, Volume 17, Number 5, 1 March 1978, pp 691 - 704.
- [60] Snodderly, D.M., W.P. Leung, G.T. Timberlake, and D.P.B. Smith, "Mapping Retinal Features in a Freely Moving Eye With Precise Control of Retinal Stimulus Position", pp 79 - 91.
- [61] Okuyama, F. and T. Tokoro, "Eye-Tracking Infra- Red Optometer".
- [62] Barnea, D.I. and H.F. Silverman, "A Class of Algorithms for Fast Digital Image Registration", *IEEE Transactions on Computers*, Volume C-21, Number 2, February 1972, pp 179 - 186.
- [63] Peli, E., R.A. Augliere, and G.T. Timberlake, "Feature-Based Registration of Retinal Images", *IEEE Transactions on Medical Imaging*, Volume MI-6, Number 3, September 1987, pp 272 - 278.
- [64] Ott, D. and M. Lades, "Measurement of Eye Rotations in Three Dimensions and the Retinal Stimulus Projection Using Scanning Laser Ophthalmoscopy", *Ophthal Physiol Opt*, Volume 10, 1990, pp 67 -71.
- [65] Bantel, T., D. Ott, and M. Rueff, "Global Tracking of the Ocular Fundus Pattern Imaged By Scanning Laser Ophthalmoscopy", *Int J Biomed Comput*, Volume 27, 1990, pp 59 -69.

- [66] Yu, J.J., Y.H. Ho, L. Ko, M. Kao, "Eye-Tracking System for Computer-Assisted Photocoagulation", Volume 22, Number 5, May 1991, pp 260 - 265.
- [67] Hose, M. , "FFT Chips for Transform-Based Image Processing", *Advanced Imaging*, June 1992, pp 56 - 59.
- [68] De Castro, E., G. Cristini, A. Martelli, C. Morandi, and M. Vascotto, "Compensation of Random Eye Motion in Television Ophthalmoscopy: Preliminary Results", *IEEE Transactions on Medical Imaging*, Volume MI-6, Number 1, March 1987, pp 74 - 81.
- [69] Kandel, E.R. and J.H. Schwartz, *Principles of Neural Science*, Elsevier Science Publishing Co. 1985.
- [70] Larsen, H., *The Ocular Fundus A Color Atlas*, W.B. Saunders Company, Philadelphia, PA.,1976, pp 11.
- [71] Press, W.H., B.P. Flannery, S.A. Teukolsky, and W.T. Vetterling, *Numerical Recipes The Art of Scientific Computing*, Cambridge University Press, London, UK, 1986, pp 191 - 195.
- [72] "User's Manual Galvanometer Scanners", General Scanning Incorporated, Watertown, MA., March 1989.
- [73] Brosens, P. "Scanning Accuracy of the Moving Iron Galvanometer Scanner", *Optical Engineering*, Volume 15, Number 2, March - April 1976, pp 95 -98.

- [74] "A-102 and AX200 Driver Amplifiers Operating Manual", General Scanning, 500 Arsenal Street, P.O. Box 307, Watertown, MA 02272.
- [75] "Series G Optical Scanners", General Scanning, 500 Arsenal Street, P.O. Box 307, Watertown, MA 02272.
- [76] "XY Scan Head Series: X-Y Scan Head", General Scanning, 500 Arsenal Street, P.O. Box 307, Watertown, MA 02272.
- [77] Pomerantzeff, O., R.H. Webb, and F.C. Delori, "Image Formation in Fundus Cameras", *Investigative Ophthalmology and the Visual Science*, Volume 18, Number 6, June 1979, pp 630 - 637.
- [78] Webb, R.H. "Manipulating Laser Light for Ophthalmology", *IEEE Engineering in Medicine and Biology Magazine*, December 1985, pp 12 - 16.
- [79] Ducrey, N., O. Pomerantzeff, C.L. Schepens, F.C. Delori, J. Schneider, "Clinical Trials With the Equator-Plus Camera", *American Journal of Ophthalmology*, Volume 84, Number 6, December 1977, pp 840 - 846.
- [80] "PIP-EZ MS DOS Software Library for the PIP Video Digitizer, User Manual", 238-MU-00, Revision 7, March 23, 1989, Matrox Electronic Systems Limited, 1055 St Regis Blvd, Dorval, Quebec, Canada H9P2T4.
- [81] "PIP Video Digitizer Board for the IBM PC, XT, and AT Hardware Manual 289-MH-00, Revision 5, October 11, 1989, Matrox Electronic Systems Limited, 1055 St Regis Blvd, Dorval, Quebec, Canada H9P2T4.
- [82] "Uniblitz LS2, LS3, and LS6 Shutter Series Specifications", Vincent Associates, 1255 University Avenue, Rochester, NY 14607.

- [83] "Instruction Manual for Uniblitz Models D122, T132 Shutter Driver, Shutter Driver", Vincent Associates, 1255 University Avenue, Rochester, NY 14607.
- [84] Eggebrecht, L.C. *Interfacing to the IBM Personal Computer*, SAMS, Carmel, IN, 1990.
- [85] "Gateway 2000 Computer System - 486/33 ISA User's Guide". Part 070-00402 Revision 1.2, November 1991, 610 Gateway Drive, N. Sioux City, SD 57048
- [86] "Gateway 2000 Computer System - 486DX2/50 User's Guide", Part 070-00816 Revision 1.00, 610 Gateway Drive, N. Sioux City, SD 57048.
- [87] Cornsweet, T.N. "Determination of the Stimuli for Involuntary Drifts and Saccadic Eye Movements", *Journal of the Optical Society of America*, Volume 46, Number 11, November 1956, pp 987 - 993.
- [88] "Data Translation 1992 Product Handbook", Data Translation, Marlboro, MA, 1992.
- [89] Steinman, R.M. "Effect of Target Size, Luminance , and Color on Monocular Fixation", *Journal of the Optical Society of America*, Volume 55, Number 9, September 1965, pp 1158 - 1165.
- [90] "Comparative Properties of Reflective Materials and Coatings", Lab-sphere, Incorporated, North Sutton, NH.
- [91] *Microsoft QuickC Compiler Toolkit, Version 2.5*, Microsoft Corporation, 1990, pp 196 - 203.

- [92] "Melles Griot Optics Guide 5", 1770 Kettering Street, Irvine, CA 92714-5670, pp 11-18, 11-19.
- [93] "American National Standard Z136.1 - American National Standard for the Safe Use for Lasers", American National Standards Institute, 1430 Broadway, New York, NY, 10018.
- [94] "Newport Catalog", Newport Corporation, Fountain Valley, CA, 92728-8020.
- [95] Webb, R.H. "Optics for Laser Rasters", *Applied Optics*, Volume 23, Number 20, 15 October 1984, pp 3680 - 3683.
- [96] "Optical Filter Guide", Andover Corporation, 4 Commercial Drive, Salem, NH 02379, 1989.
- [97] "Innova 100 Series Ion Lasers", Coherent Laser Products Division, 3210 Porter Drive, P.O. Box 10321, Palo Alto, CA 1986.
- [98] James L. Letchworth, Animal Resources Manager, Animal Resources Center, The University of Texas at Austin, Austin, TX, technical conversation.
- [99] "Dalsa Incorporated CCD Image Sensors", Dalsa Inc., Waterloo, Ontario, Canada, pp 161 - 171.
- [100] "Series 150/151 Product Brief High-Performance Modular Image Processing Subsystem", Imaging Technology Inc., 600 West Cummings Park, Woburn, MA., pp 4 - 26.
- [101] "G100 and G300 Series Galvanometer Optical Scanners", General Scanning Incorporated, 500 Arsenal St., P.O. Box 307, Watertown, MA.

- [102] "1993 Medical Laser Buyers Guide", 1421 S. Sheridan, P.O. Box 180, Tulsa, OK, 74101-9949, pp. 23.
- [103] Sato, Y., B. Berkowitz, C. Wilson, and E. de Juan, "Blood-Retinal Barrier Breakdown Caused by Diode vs Argon Laser Endophotocoagulation", *Arch Ophthalmol*, Volume 110, February 1992, pp 277 - 281.
- [104] Puliafito, C.A., T.F. Deutsch, J. Boll, K. To, "Semiconductor Laser Endophotocoagulation of the Retina", *Archives of Ophthalmology*, Volume 105, March 1987, pp 424 - 427.
- [105] Sliney, D.H. and J. Marshall, "Tissue Specific Damage to the Retinal Pigment Epithelium: Mechanisms and Therapeutic Implications", *Lasers and Light in Ophthalmology*, Volume 5, Number 1, 1992, pp 17 - 28.
- [106] Smiddy, W.E. and E. Hernandez, "Histopathologic Results of Retinal Diode Laser Photocoagulation in Rabbit Eyes", *Archives of Ophthalmology*, Volume 110, May 1992, pp 693 - 698.
- [107] Wallow, I.H., W. Sponsel, and T.S. Stevens, "Clinicopathologic Correlation of Diode Laser Burns in Monkeys", *Archives of Ophthalmology*, Volume 109, May 1991, pp 648 - 653.
- [108] "EG&G Optoelectronics Short Form Catalog Emitters and Detectors", EG&G Solid State Products Group, 35 Congress St., P.O. Box 5006, Salem, MA.
- [109] Hecht, J., "Diode-laser Performance Rises as Structures Shrink", *Laser Focus World*, May 1992, pp 127 -143.

- [110] "Shorter Wavelength Diodes", *Laser and Optronics*, Volume 11, Number 9, September 1992, pp 7.
- [111] Masselink, W. and M. Zachau, " $In_{0.35}Ga_{0.65}P$ Light-Emitting Diodes Grown by Gas-Source Molecular Beam Epitaxy", *Applied Physics Letters*, Volume 61, Number1, 6 July 1992, pp 58 - 60.
- [112] *The Student Edition of MATLAB for MS-DOS Personal Computers*, The Math Works Inc., Englewood Cliffs, NJ 07632.
- [113] van Camp, D., "Neurons for Computers", *Scientific American*, September 1992, pp 170 -172.
- [114] Robinson, P., "Follow the Trends When Buying PC", *Austin American Statesman*, January 11, 1993.
- [115] Lewis, P., "Pentium may be a revolution - or not", *Austin American Statesman*, April 5, 1993.
- [116] S.F. Barrett, M.R. Jerath, H.G. Rylander III, A.J. Welch, "Digital Tracking and Control of Retinal Images", *SPIE - The International Society for Optical Engineering Biomedical Optics Proceedings 1993*, session 1877, Bellingham, WA.
- [117] S.F. Barrett, M.R. Jerath, H.G. Rylander III, A.J. Welch, "Instrumentation for Feedback Controlled Retinal Photocoagulation", *SPIE - The International Society for Optical Engineering Biomedical Optics Proceedings 1993*, session 1892, Bellingham, WA.

- [118] S.F. Barrett, M.R. Jerath, H.G. Rylander III, and A.J. Welch, "Automated Feedback Control of Lesion Placement *In Vivo*", *Archives of Ophthalmology*, submitted for publication.
- [119] S.F. Barrett, M.R. Jerath, H.G. Rylander III, and A.J. Welch, "Digital Tracking and Control of Retinal Images", *Optical Engineering*, accepted for publication.

Vita

Steven Frank Barrett was born on 30 January 1957 in Warner Robins, Georgia to Eleanore Olga Barrett and Frank John Barrett. He is married to Cynthia Sue Barrett. They have three children: Heather (13), Jonathan (11), and Graham (7).

Steven graduated from Bellevue High School, Bellevue, Nebraska in May, 1975. He attended the University of Nebraska at Omaha under the AFROTC Scholarship program. He graduated in May 1979 Magna Cum Laude with a Bachelor of Science Degree in Engineering Technology. He was commissioned as a Second Lieutenant in the United States Air Force. He then was assigned to Malstrom AFB, Montana as a Missile Combat Crew Member. He was promoted to First Lieutenant and Captain while there. He was reassigned to Vandenberg AFB, California as a Missile Combat Crew Instructor in May 1983. He was then assigned to Strategic Air Command Headquarters at Offutt AFB, Nebraska as a Missile Staff Officer working on the employment of the PEACEKEEPER intercontinental ballistic missile system. He obtained the Master of Engineering degree in Electrical Engineering from the University of Idaho in August of 1986. He served as an adjunct faculty member at the University of Nebraska at Omaha during the Fall 1986 semester. Captain Barrett was assigned to the United States Air Force Academy as an Electrical Engineering instructor in June 1988. While at the Academy, he taught courses

in semiconductor theory and design, communication theory, and biomedical engineering. Captain Barrett was selected for Air Force Institute of Technology (AFIT) sponsorship to obtain the PhD degree. He entered the Graduate School of the University of Texas in August 1990. He was also promoted to Major that same month. He will return to the Academy as an Assistant Professor of Electrical Engineering in June 1993.

Permanent address: 1608 Lincoln Rd
Bellevue, NE 68005

This dissertation was typeset with \LaTeX [†] by the author.

[†] \LaTeX is a document preparation system developed by Leslie Lamport as a special version of Donald Knuth's \TeX Program.